AD-A053 735 LICHT (L) SAN MATEO CA F/G 13/9
FOIL BEARINGS FOR AXIAL AND RADIAL SUPPORT OF HIGH SPEED ROTORS--ETC(U)
JAN 78 L LICHT N00014-76-C-0191
UNCLASSIFIED NASA-CR-2940 NL

AD No.
DDC FILE COPY

AD A053735

(2)

NASA Contractor Report 2940

Foil Bearings for Axial and Radial Support of High Speed Rotors - Design, Development, and Determination of Operating Characteristics

L. Licht

Engineering Consultant
San Mateo, California

DDC
RECEIVED
MAY 10 1978
F

Prepared for
Office of Naval Research
ONR Contract N00014-76-C-0191
and
Lewis Research Center
NASA Purchase Request C-75012-C

NASA
National Aeronautics
and Space Administration

Scientific and Technical
Information Office

1978

This document has been approved for public release and sale; its distribution is unlimited.

See 1473

PRECEDING PAGE NOT FILMED
BLANK

FOREWORD

This experimental study was performed in the Federal Republic of Germany, during the tenure by the author of an award by the Alexander von Humboldt Foundation, in cooperation with the Technical University of München, Motoren und Turbinen Union (MTU) GMBH, München, the NASA Lewis Research Center, Cleveland, Ohio, and the Office of Naval Research, Arlington, Virginia.

The author wishes to express his gratitude and appreciation to Dr. H. Pfeiffer and Dr. H. Hanle of the Alexander von Humboldt Foundation, Bonn, for their unreserved support and for the most friendly reception in Germany.

The design, construction, and instrumentation of experimental apparatus were performed largely while the author was a guest of the Institut für Feingerätebau und Getriebelehre (Institute of Precision Mechanisms and Drives) of the Technical University of München. The author is indebted to Professor R. Unterberger for his generous and enthusiastic support of this project and his faith in the successful outcome of the undertaking. He is grateful for the assistance and friendship extended to him by the members of the Institute.

The experiments were conducted in the Development Laboratories of Motoren and Turbinen Union (Department EVBG), and this brief acknowledgement cannot possibly suffice and do justice to the efficient, purposeful, and highly productive support and assistance given to this project by MTU. In thanking Dr. W. Heilmann, Mr. J. Schmidt, Mr. H. Raudies, and Mr. B. Hoffmann, the author wishes to express his appreciation to all at MTU who contributed to the success of this undertaking.

Mr. W. J. Anderson of the NASA Lewis Research Center and Mr. S. W. Doroff of the Office of Naval Research lent their full and wholehearted support to this international venture, were instrumental in formulating the program, provided highly useful, technical suggestions in the course of this study, and kept the writer abreast of related research activities.

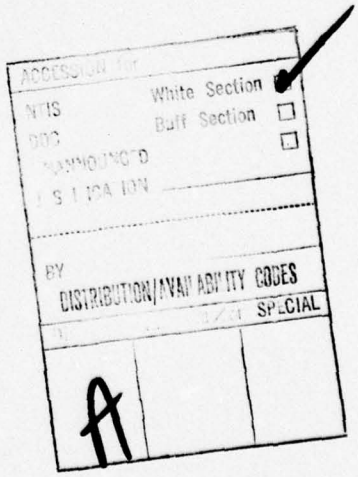

PRECEDING PAGE NOT FILMED
BLANK

TABLE OF CONTENTS

TABLE OF CONTENTS (CONTINUED)

ILLUSTRATIONS

ILLUSTRATIONS (CONTINUED)

ILLUSTRATIONS (CONTINUED)

ILLUSTRATIONS (CONTINUED)

ILLUSTRATIONS (CONTINUED)

ILLUSTRATIONS (CONTINUED)

LIST OF SYMBOLS

a_n	Effective radius of circular plate-spring of n-th array
A	Thrust-bearing area; $A = \pi(R_o^2 - R_i^2)$
b_n	Width of flexure element in n-th array of spider spring
c	Radial clearance (rigid journal-bearing)
$\bar{c}$	Maximum radial clearance of journal foil-bearing LLF-1J; $\bar{c} \approx R_c - nt_f$
e	Eccentricity of journal
E	Modulus of elasticity
f_n	Fraction of thrust load supported on n-th annulus of bearing area; n = 1, 2, 3, 4, 5, 6
F	Thrust (axial) load
$\bar{F}$	Dimensionless load; $\bar{F} = F/p_a A$
F_∞	Thrust load of spiral-groove bearing with very large number of grooves
h	Thrust-bearing clearance; $h = h(R, \theta)$
h_o	Parallel clearance of ideal, spiral-groove bearing
$\bar{h}$	Mean clearance of spiral-groove thrust bearing
$\tilde{h}$	A measure of clearance; $\tilde{h} = H_{ROT} - H_{STA}$ (see Section 2.3)
H_{ROT}	Mean displacement of rotating runner at outer periphery relative to arbitrary datum for H_{STA}
H_{STA}	Mean displacement of nonrotating runner at outer periphery relative to arbitrary datum
j	Ordering integer (number of polygon vertex)
k_m	Stiffness of m-th element (in n-th array)
K_s	Overall stiffness of membrane support; $K_s = dF/d\delta$
l	Distance of center of rotor mass to midplane of runner-end bearing
l_s	Length of flexure element of spider spring
L	Bearing span (midplane to midplane of journal bearings)
m	Number of spring elements in n-th array (m = 3 in LLF-1T thrust bearing, and m = 12 in LLF-2T thrust bearing)
M	Friction moment (torque) of spiral-groove thrust bearing

$\overline{M}$	Dimensionless moment of spiral-groove thrust bearing; $\overline{M} = 6M/p_a \pi (R_o^2 + R_i^2) . \Lambda . h_o$
n	Integer denoting an annulus of the thrust-bearing area and corresponding array of spring elements; n = 1, 2, 3, 4, 5, 6
n	Number of layers along radius of foil bearing (also number of complete turns of foil coil, if the number is an integer)
n	Number of sides of open polygon
N	Rotational speed in rps or rpm
p_a	Atmospheric or ambient pressure, absolute
p_g	Mean pressure at boundary of grooved and plane regions of thrust bearing, absolute
Δp_g	Pressure rise; $\Delta p_g = p_g - p_a$
r_p	Polar radius of gyration of rotor
r_t	Transverse radius of gyration of rotor
r_v	Radius of rounded vertex of quasi-polygonal support section of foil
R_c	Bore radius of foil-retaining cartridge
R_j	Radius of journal
R_g	Radius at boundary of grooved and plane regions of thrust bearing
R_i	Inner radius at boundary of active thrust-bearing area
R_o	Outer radius at boundary of active thrust-bearing area
t_f	Foil thickness
t_m	Thickness of membrane
t_p	Overall thickness of spider spring
t_s	Thickness of flexure element of spider spring, or thickness of plate spring
$\overline{t}_s$	Mean thickness of 72 flexure elements of spider spring
$u_{1,2}$	Residual rotor unbalance referred to balancing planes 1 and 2
$U_{1,2}$	Added unbalance in planes 1 and 2
W	Rotor weight ($W_{1,2}$ are components of rotor weight supported by bearings 1 and 2)
XYZ	Cartesian coordinates
Z	Relative axial displacement of runner and stator (referred to point on stator 45 mm from rotor axis)

$(XY)_{1,2}$ –	Refer to monitoring planes of capacitance probes at the runner (1) and at the turbine (2) journal bearings
$X_{1,2}$ and $Y_{1,2}$	Refer to components of amplitude of journal motion in monitoring planes of capacitance probes
(X_1X_2) –	Refers to the horizontal plane through the axis of journal bearings (plane of X-probes)
(Y_1Y_2) –	Refers to the vertical plane through the axis of journal bearings (plane of Y-probes)
α_v	Angle subtended between sides of quasi-polygonal foil section
β	Spiral angle of thrust-bearing grooves
δ	Deflection of flexible support; $\delta = H_c - H_{STA}$ (H_c corresponds to arbitrary offset of capacitance probe)
Δ	Depth of spiral groove
Δ	Denotes an increment (e.g., ΔF) or peak-to-peak amplitude (e.g., ΔY_1)
ϵ	Apparent eccentricity (see Section 6.1); $\epsilon = e/\bar{c}$
$(\epsilon_{X,Y})_{1,2}$	Components of apparent eccentricity in monitoring planes 1 and 2
ϵ	Deviation from flatness
ϵ	Deviation of clearance from $\bar{h}$ or $\tilde{h}$ (see Section 2.3); $\epsilon = \lvert h - \bar{h} \rvert$ or $\epsilon \approx \lvert h - \tilde{h} \rvert$
θ	Angular coordinate (arbitrary origin)
θ_g	Angle subtended by spiral groove along arc of constant radius
θ_r	Angle subtended by spiral ridge along arc of constant radius
Λ	Bearing number (spiral-groove bearing); $\Lambda = 3\mu\omega(R_o^2 - R_i^2)/p_a h_o^2$
μ	Viscosity
υ	Poisson's ratio
ω	Angular speed; $\omega = 2\pi N$

1.0 INTRODUCTION

The rigid bearing is a useful, if abstract concept, and provides an adequate approximation as a mathematical model for the solution of many lubrication problems. In many fluid film and rolling-element bearings, deformations and deflections under load may be negligible in comparison with the clearance, but in other situations elasticity modifies, or governs the operational characteristics [1 to 5] *. Although elasticity plays a dominant role in foil bearings, the subject of this report does not fall into the category of classical problems generally dealt with in elastohydrodynamics [6, 7, 8].

Nor does this experimental investigation involve bearings which are rigid, but are flexibly mounted [9 to 16], except that the remedies sought and the objectives of applications may overlap. The distinction between foil bearings and flexibly mounted, rigid bearings is not only due to the degree of surface compliance, but also to the much smaller mass and inertia of foils, membranes and their support elements, in comparison with pivoted sliders, flexure-mounted plates, and gimbals.

Lastly, foil and elastomer-lined bearings [17 to 21] have much in common, both functionally and physically. The objective in both types of support is to purposefully provide conformable bearing surfaces, but while elastomer-lined bearings appear to be more suitable for lubrication with liquids and are limited to lower operating temperatures, the gas-lubricated metal foil-bearings considered in this report are capable of operating at higher temperatures and can equally well be designed for lubrication with liquids.

The preceding paragraphs define the aspect of foil bearings in regard to elastohydrodynamics and to functionally related rotor supports, and it is appropriate at this point to provide additional background relevant to foil bearings as such.

There are two classes of foil bearings; the classical foil bearing, in which the dominant mode of elastic deformation is extension, and the flexible-surface bearing, in which compliance is effected mainly through bending. The foregoing classification is approximate and is intended to convey the distinction in a qualitative manner, rather than in a strict sense.

Although Blok and Van Rossum [22] are credited with being first to provide experimental and analytical data of tension-type foil bearings, in 1953, the concept was lucidly described in a patent issued in 1928 [23] **, and the inventor correctly inferred that both pressure and clearance would be sensibly constant in the region of wrap. The classical foil bearing did not become a widely used method of rotor support, but its utility was rediscovered by mechanical engineers in the computer industry as means of support and guidance of the flexible recording media in magnetic

---

*Numbers within brackets designate references

**The applicants were the British Thomson-Houston Company, Ltd. and A.A. Pollock, presumably the inventor.

tape and card transports [24]. The rediscovery gave impetus to sponsorship of many analytical and several experimental studies [25 to 36], which were related primarily to the transport of flexible films, but proved also useful in the development of tension-type foil bearings, endowed with attractive operational characteristics when used as means of support of high-speed rotors [37 to 41]. The tension-type foil bearing referred to in the foregoing references has three foil sectors, disposed around the journal and preloaded against it. A lubricating gas-film is established at relatively low speed, whereupon the device transforms from a slippery band-brake to a foil bearing. The classical foil bearing shares many attractive performance characteristics with other types of journal foil-bearings; it is superior in some respects, and deficient in others. It has no complementary thrust-bearing embodiment, except when externally pressurized [42], because unlike the sling-like configuration of the journal foil-bearing, in which the component of tension opposing the radial force is considerable, a stretched and transversely unsupported membrane can accommodate no substantial load. Furthermore, while pressure generation between a rotating journal and a tensioned foil is a self-sustaining process inherent in the cylindrical configuration, the juxtaposition of a runner and a stretched, unsupported membrane is not conducive to the formation of a load-supporting fluid film.

Turning now to the subject of foil bearings dominated by flexure, rather than by tension, it would appear that their progenitors and precursors date back to the beginning of this century [43, 44, 45], and that many of the more recent journal-bearing configurations bear a rather striking family resemblance to their ancestors. The patents of D. J. Marley [46 to 49], however, contained many novel concepts, which provided a foundation for the successful development of flexure-type journal and thrust bearings. The journal bearings contain arrays of overlapping flexible reeds, anchored within the bore of a retainer, and the thrust bearings utilize foil sectors, spot-welded to an annular membrane supported by radially oriented and strategically placed spring elements [50 to 53].

An intensively advertised foil-bearing type employs a corrugated support, both in the journal and thrust-bearing versions [53, 54, 55]. The corrugated backing, which resembles the spring elements described in references [43] and [45], is spot-welded to the foil and to the retaining cartridge. The journal bearings provide a greater margin of stability than rigid bearings, but the corrugations are prone to buckling under impact, and wear along the lines of support corresponding to the ridges of the corrugations can be severe [53]. The thrust bearing has undergone several metamorphoses [54, 55], but adequate load capacity at a safe clearance has not been demonstrated with gaseous lubricants. The difficulty is due to the absence of control in this compliant thrust bearing over the formation of a lubricating wedge for efficient pressure generation [53]. Also, since the corrugated backing and foil sector of each shoe are welded to a rigid support-plate along the leading edges, the compliance is greatly reduced and the ability to accommodate the runout of the thrust runner diminished. As an air-lubricated support the utility is marginal, and the thrust bearing has now been relegated to lubrication with oil [55].

A very simple journal foil-bearing and preliminary test results obtained with a small, high-speed rotor were described in reference [56]. The bearing consists of a spirally-wound strip of foil, contained within a cartridge, or retainer. The coiled foil has flexibility, and damping is provided through friction between foil layers and squeezing of fluid in interstitial clearances of the coil. It is probably the simplest foil bearing in existence, and since its whirl-suppressing and amplitude attenuating characteristics appeared to be very promising, the study of this journal bearing was pursued further in the course of this investigation. Brief reference was also made in this paper to experimental results with coiled foil-strips, in which the first turn had six sharp creases. While these preliminary results were very promising, creasing of foils causes the inception and propagation of cracks during fabrication and operation. This deficiency was eliminated in a new journal-bearing design, reduced to practice in the course of this investigation.

Potential and sometimes current applications of foil bearings, their advantages and - less frequently - disadvantages are discussed in many references quoted in this report. The discerning reader will make allowance for the exuberance of researchers and innovators and distinguish between natural bias and commercialism. It is also assumed that most readers interested in the content of this report will have sufficient familiarity with bearings and rotor dynamics, possibly also with foil bearings, to provide their own lists of advantages, disadvantages and areas of application. It would be useful, however, to point up the relationship of this activity in regard to the state of the art of foil bearings as a whole.

The weakest link in the application of foil-supports to turbomachinery was always the thrust bearing. Some of the difficulties were due to exacting and conflicting requirements, such as supporting a large load with a small bearing, yet at an adequate (safe) clearance. Many applications were doomed to failure, because pitching amplitudes of the runner, due to excessive unbalance, or angular deflection under the influence of gyroscopic couples could not be accommodated despite compliance [51].

On the other hand, while rigid thrust bearings of optimized goemetry rarely perform in concert with predictions based on idealized models, the foil bearings never matched their rigid progenitors in load capacity realized at a given minimum clearance. Nor is this surprising, since the topography of clearance between the runner and the flexible surface has been casual, rather than controlled with deliberation.

In a rigid bearing, the approximation of optimal geometry (within limits of deviations) is effected by machining of the surface contour by mechanical, electrical or chemical means. In a flexible-surface bearing, in which the surface-displacement and pressure fields are coupled, a very special support system is required to approximate an optimal clearance topography.

The existing thrust bearings [51, 53, 55] are simply provided with means of inducing a nondescript lubricating wedge between the runner and the deformed surface, the shape of which is generally unknown, much less optimal. Similar

remarks apply to journal foil-bearings, although the requirements of thrust and journal bearings coincide only in part. This does not detract from the fact that these bearings, developed by trial and error over a period of fifteen years, may function well within the framework of several turbomachines [50].

The writer, who was instrumental in developing several types of journal foil-bearings, was always acutely aware of the need of an efficient, flexible-surface thrust bearing. An opportunity finally presented itself in 1975 to reduce to practice two out of several concepts of such bearings, both incorporating the spiral-groove geometry known for efficient pressure-generation and superior load capacity [57 to 61].

The literature relevant to the theory of spiral-groove thrust bearings is very extensive, and much effort has been expended to analyze the response and stability of these bearings [59], to account for the effect of thermal distortion [62], to refine the analysis [63, 64], and even to consider the stability of a gimbaled system comprising a spiral-groove bearing [65]. The abundance of theoretical contributions, only a very small fraction of which is quoted in the list of references, must be contrasted with the paucity of published experimental data and correlations of theoretical with experimental results. Also, while the segmented thrust bearings with inclined (or curved) rigid sliders have corresponding embodiments with flexible surfaces, the two methods of incorporating the spiral-groove geometry in a fully flexible thrust-bearing are new.

The objective was to combine the superiority of high load-capacity of rigid, spiral-groove bearings with the advantage of surface compliance. The prerequisite for the realization of this objective was a support system for a flexible membrane, which would permit maintenance of a parallel clearance between the runner and the compliant surface, at least approximately. Furthermore, the realization of this objective implied also that a deliberate method of clearance control would be furnished, however imperfect, so that the formation of the lubricating film and the generation of pressure could at least approach an optimal condition. One also hoped that secondary benefits would ensue, and that the designs would lend themselves to further changes and ameliorations. For example, the support would provide partial compensation for crowning of the runner, the grooves could be placed on the runner, rather than on the membrane, and the cost of etched and plain membranes and other components would be small.

The approach in the study of journal foil-bearings could be best described as "mechanical breadboarding". No analytical background exists for the bearings studied and developed in the course of this investigation, but judging from the relevance of mathematical models and analyses to previously discussed foil bearings and related rotor dynamics, the unavailability of similar design guides and predictors could not be considered a serious handicap in this undertaking.

Simple as the construction of these foil bearings may be (and it is difficult to visualize anything less complicated than a plane foil, or one integral with a quasi-polygonal

section, coiled within a simple bushing), the mathematical modeling is difficult, because the elastohydrodymic and frictional processes involving the main and the interstitial clearances cannot be described with certainty. The experimental results illustrate the intricacy of amplitude response of a rotor supported by these bearings and indicate that a veracious mathematical model would be highly complex, assuming one could be constructed.

On the other hand, a well designed test rig permits rapid changes of foils, bushings, and even rotors, so that a skilled experimentalist can literally "breadboard" a rotor support-system. This method was practiced by the writer and produced results which speak for themselves.

2.0 DESIGN OF TEST APPARATUS

Although the test rig was designed primarily with the objective of determining the performance characteristics of flexible-surface thrust bearings, provision was made for the replacement of externally-pressurized journal bearings with foil-bearing cartridges, in order to provide means of mounting the rotor on fully flexible supports, both axially and radially.

2.1 Description of Test Rig

Referring to the assembly drawing in Figure 1 and to the legend listing the main components of the test rig, it is noted that the thrust-bearing assembly (1) is located opposite the thrust runner (2), secured to the rotor (3) and is mounted on one end of the stator shaft (4), the other end of the shaft serving as an air piston for applying an axial load by means of the loading cylinder (5).

The rotor is driven by a double-bucket impulse air-turbine (6). The stator shaft and the rotor are supported by externally pressurized journal bearings (7), but the rotor can also be supported on foil journal-bearings described in Section 4.0 of this report.

The force applied to the flexible thrust bearing by means of the loading cylinder is balanced by an externally-pressurized thrust bearing, the inboard thrust-pad (8) of which is integral with one journal bearing. The outboard thrust-pad (9) balances the applied load. The rotating surfaces of this thrust bearing are provided by the flat and parallel faces of the turbine wheel, and the supply pressure to each pad can be varied independently. The total axial clearance can be adjusted by shims placed at the rear of the rotor housing (11), between the pad and the face of the nozzle ring (17).

The lapped surfaces of the runner and of the support plate of the thrust-bearing assembly must be parallel and axially aligned. To this effect, the stator housing (10) can be rotated about trunnions and moved laterally in the adjustable support (12), as well as rotated about the pivot (13). The manipulation is accomplished by sets of alignment screws (14), after loosely bolting the stator and rotor housings to the base plate (15). The final alignment (as some readers may know from experience) is

ERKLÄRUNG	
1	AXIALSTUFE AXIALLAGER
2	TRAGRING
3	ROTOR
4	WELLE
5	ANPRESSZYLINDER
6	LUFTTURBINE
7	RADIALLAGER
8	RADIAL- U. AXIALLAGER
9	AXIALDRUCKLAGER
10	STATORGEHÄUSE
11	ROTORGEHÄUSE
12	JUSTIERBARER LAGERBOCK
13	GRENZZAPFEN
14	JUSTIERSCHRAUBE
15	GRUNDPLATTE
16	LUFTZUFUHR TURBINE
17	DÜSENRING
18	LUFTZUFUHR LAGER
19	LUFTZUFUHR ANPRESSZYLINDER
20	KAPAZITIVER AUFNEHMER
21	DREHMOMENTENAUFNEHMER

LEGEND	
1	THRUST BEARING ASSEMBLY
2	THRUST RUNNER
3	ROTOR
4	SHAFT
5	LOADING CYLINDER
6	AIR TURBINE
7	JOURNAL BEARING
8	JOURNAL BEARING & THRUST PAD
9	THRUST PAD
10	HOUSING, STATOR
11	HOUSING, ROTOR
12	ADJUSTABLE SUPPORT
13	PIVOT
14	ADJUSMENT SCREW
15	BASE PLATE
16	TURBINE AIR SUPPLY
17	NOZZLE RING
18	BEARING AIR SUPPLY
19	CYLINDER AIR SUPPLY
20	CAPACITANCE PROBE
21	TORQUE SENSOR

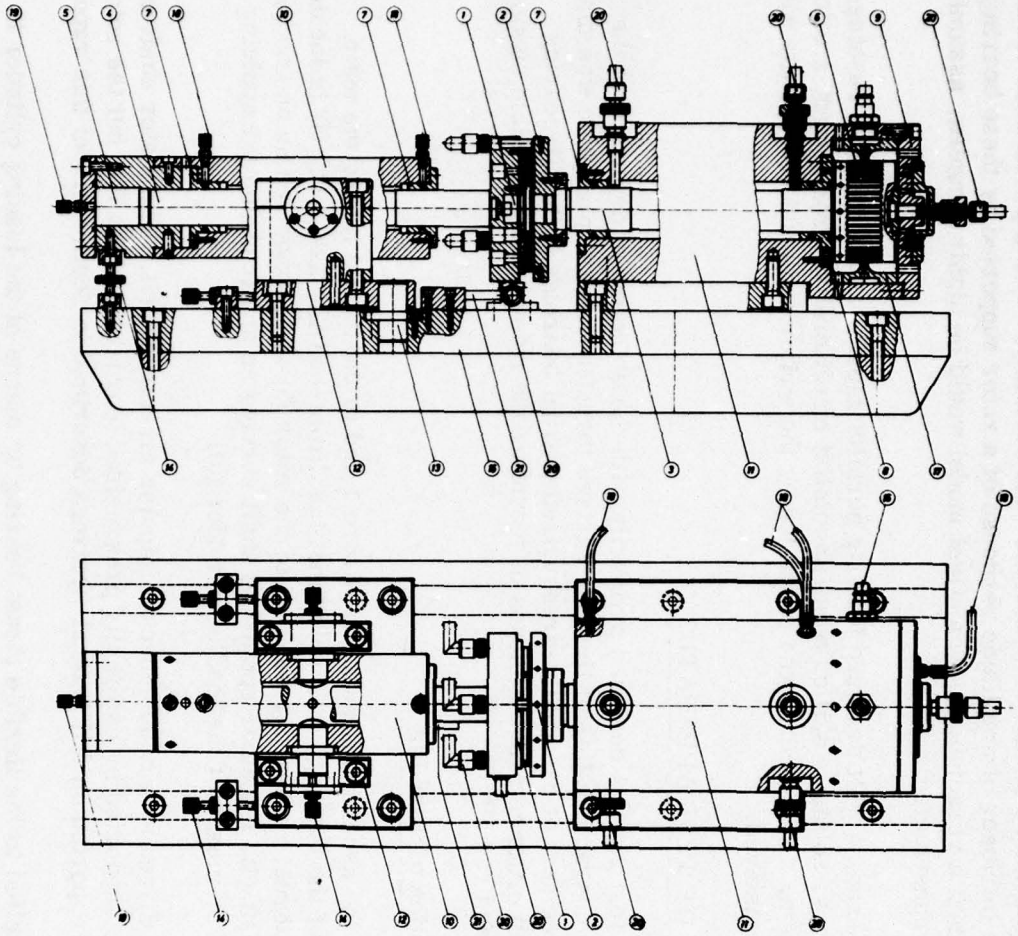

FIGURE 1. ASSEMBLY DRAWING OF TEST RIG

achieved by preferential tightening of bolts securing the housings to the base and to the adjustable support. Axial alignment, which is less critical than parallelism, is achieved by means of a plug gauge, placed in the central bores of the stator plate and of the runner and having diametral clearance of approximately 0.05 mm in each bore.

In addition to the turbine air-supply (16), there are six independent air supplies (18) for the externally pressurized bearings, and one (19) for the loading cylinder. Provision is made also for mounting and securing nine capacitance probes (20); two pairs to monitor the motion of the rotor axis in two planes, one axial probe at the turbine end of the rotor, three probes in the support plate of the thrust bearing facing the extension of the active surface of the thrust runner, and one probe monitoring the deflection of the torque-sensing cantilever (21).

The partly assembled test rig is shown in the view of Figure 2, with the rotor assembly placed along the base, opposite the rotor housing. The lapped support-plate for one type of a flexible thrust bearing is mounted on the stator shaft, above the torque sensor. The nozzle ring, with one sealing O-ring visible, protrudes from the rear of the rotor housing. A view of the rotor and housing is shown in Figure 3. The rotor has been placed on two capacitance probes, in a position directly above that which it would occupy in the housing. On the right side of the photograph is the nozzle ring and the rear cover-plate, integral with the load-balancing pad. Twelve holes in the cover plate and a corresponding number along the periphery of the housing provide for sensibly unobstructed discharge of turbine air from the housing and lower noise to an acceptable level.

A view of the inboard (unloaded) thrust-pad, integral with a pressurized journal bearing, but supplied with independently regulated air, is seen through the turbine enclosure of the housing in Figure 4. The turbine wheel (48 milled, penny-slot double buckets) is illustrated in Figure 5. The faces of the wheel, which serve as bearing surfaces, are flame-plated with Nickel-Chromium bonded Cr_2O_3 and ground and lapped parallel and flat. The 3 mm socket set-screws are for balancing, or for adding unbalance, and are accessible through the 12 air-discharge holes in the housing. Turbine wheels made of both steel and aluminum were manufactured and used. The turbine is also shown in Figure 6, together with the nozzle ring. There are 18 nozzles, discharging at an angle designed to produce at high torque in the speed range centered at approximately 720 rps. The outside of the nozzle ring shows the circumferential plenum chamber between the O-rings, supplied through two liberally sized fittings and air lines.

The rotor assembly in Figure 7 shows the shaft which was used with externally-pressurized journal bearings only. The journals are Cr_2O_3-plated over a length limited to approximately 20 mm. In a nearly identical shaft, used later in conjunction with foil bearings, each journal was provided with two 20 mm, flame-plated sections, separated by an unplated band of metal opposite the monitoring capacitance probes. A number of these probes are shown in the foreground of Figure 8, in front of a calibration fixture and a six-channel displacement meter. A close-up view of probe tips in Figure 9

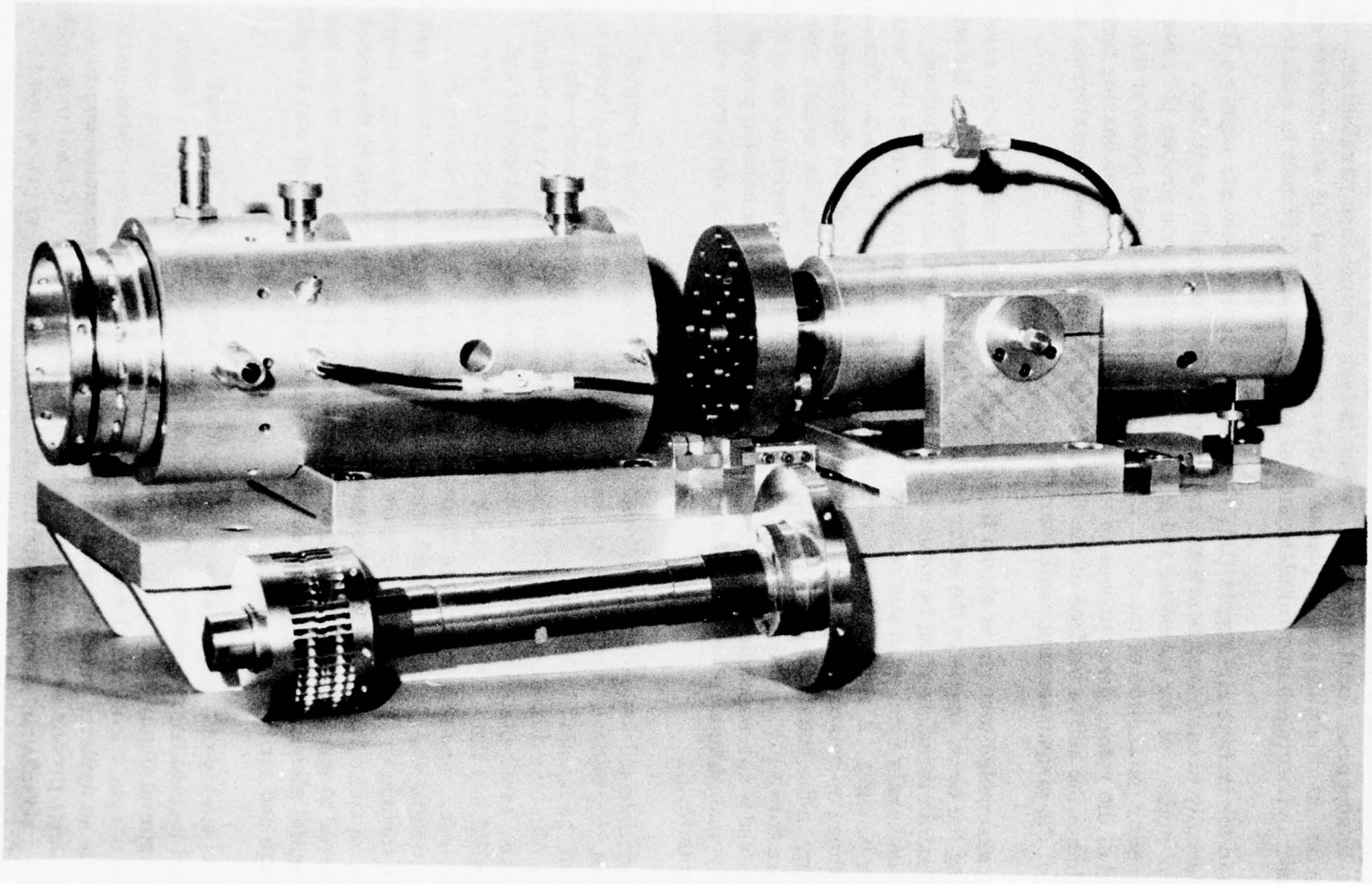

FIGURE 2. VIEW OF PARTLY ASSEMBLED TEST RIG

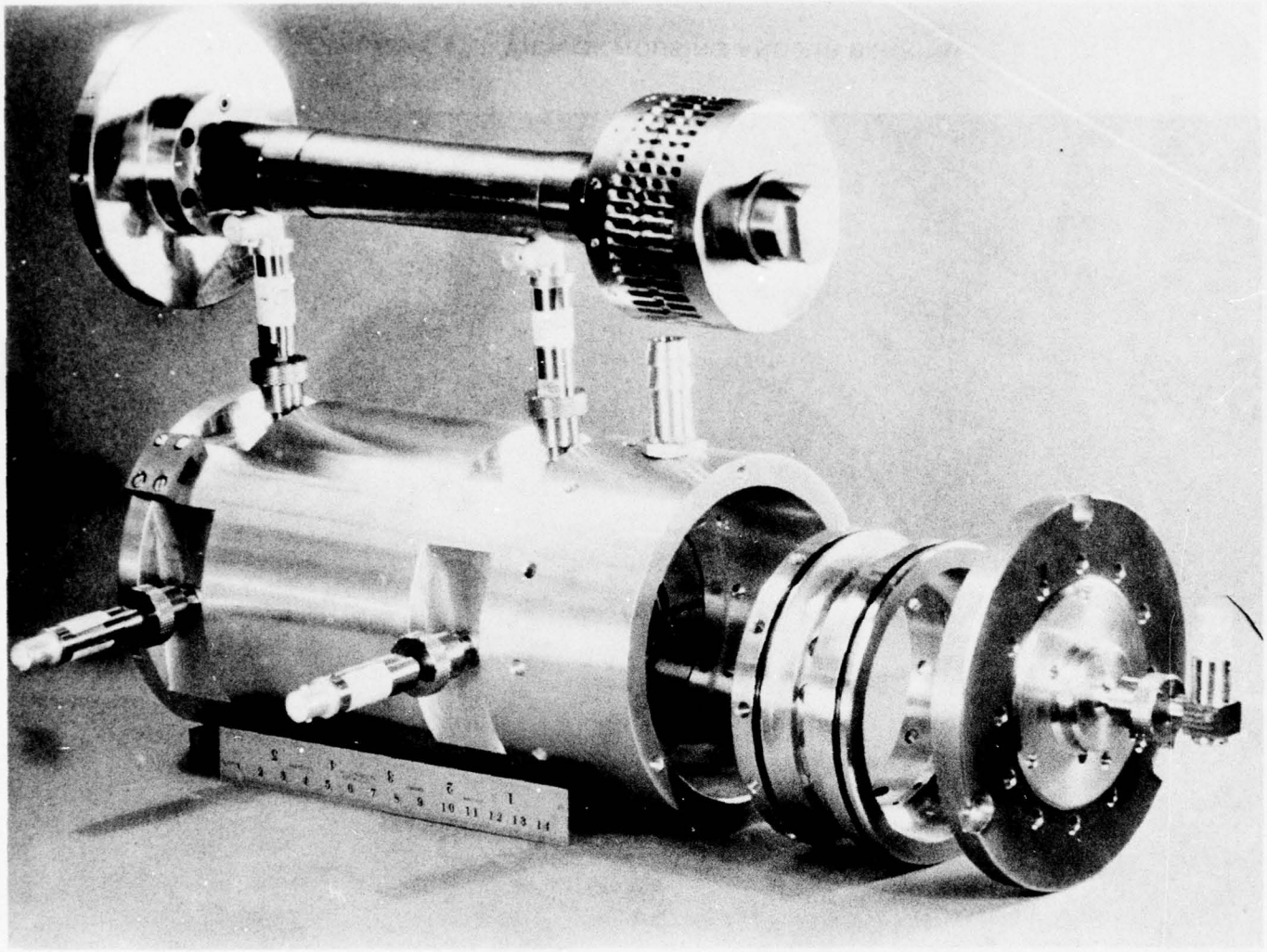

FIGURE 3. VIEW OF ROTOR AND HOUSING

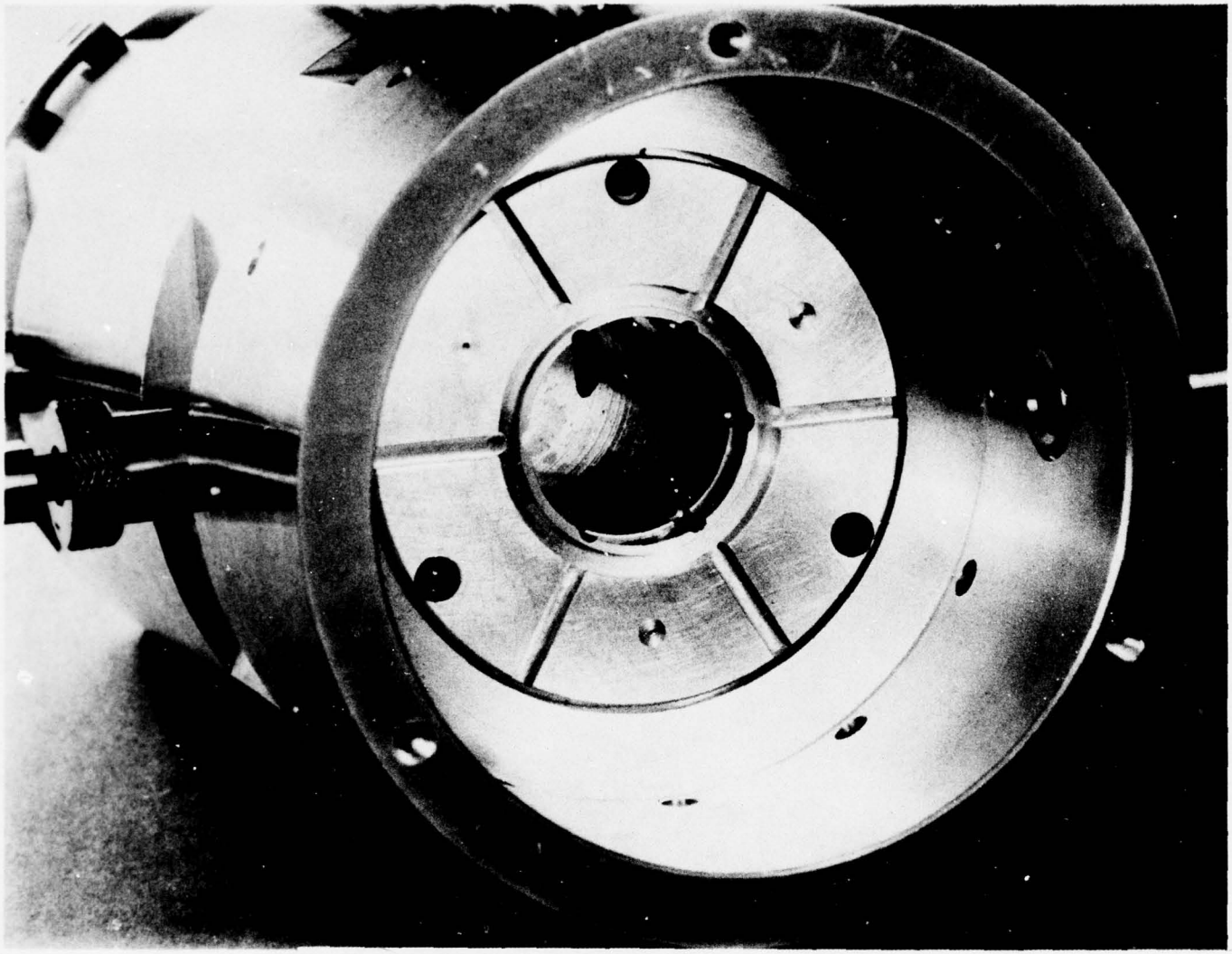

FIGURE 4. VIEW OF HOUSING AND AIR BEARING

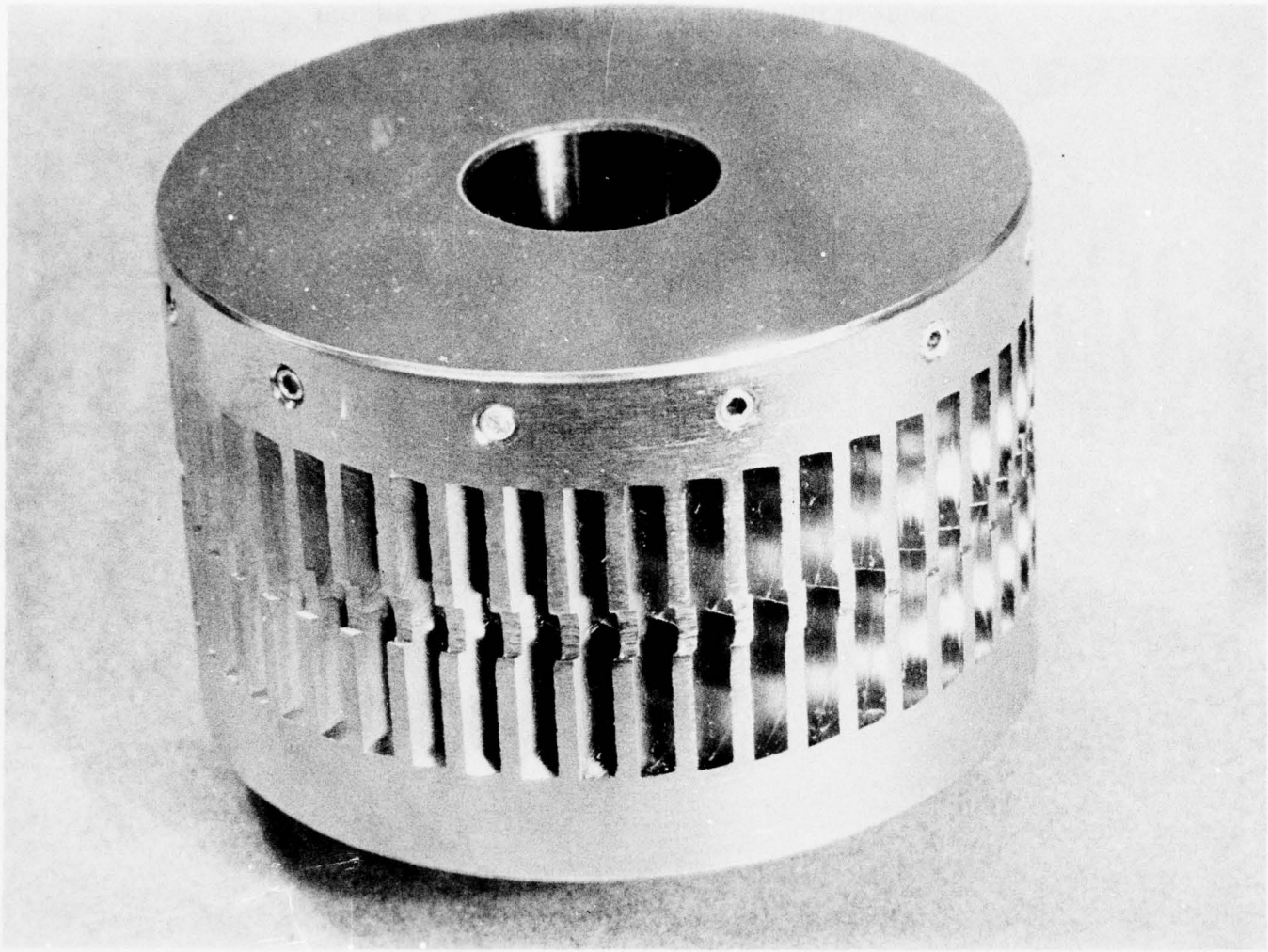

FIGURE 5. VIEW OF TURBINE

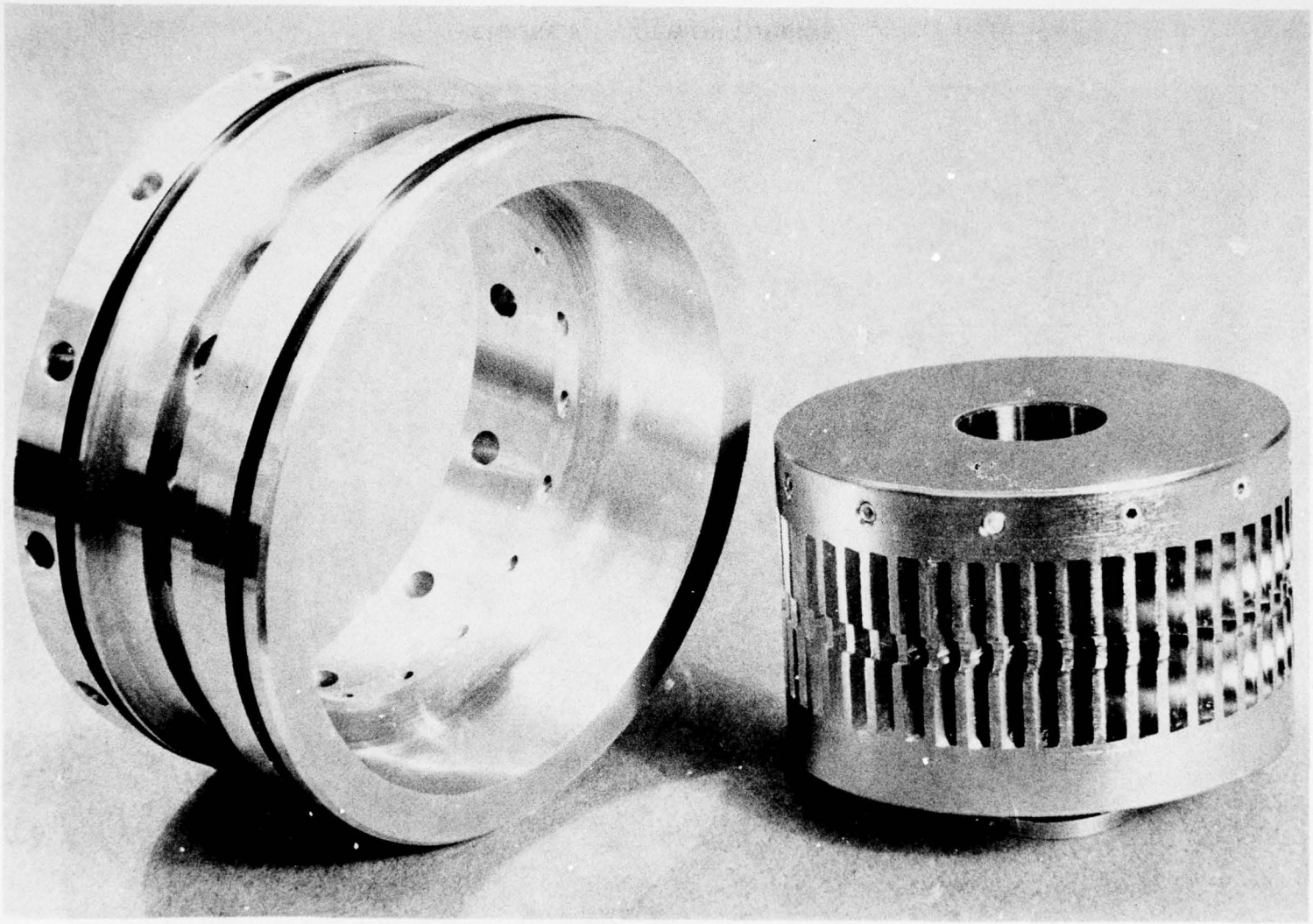

FIGURE 6. VIEW OF NOZZLE RING AND TURBINE

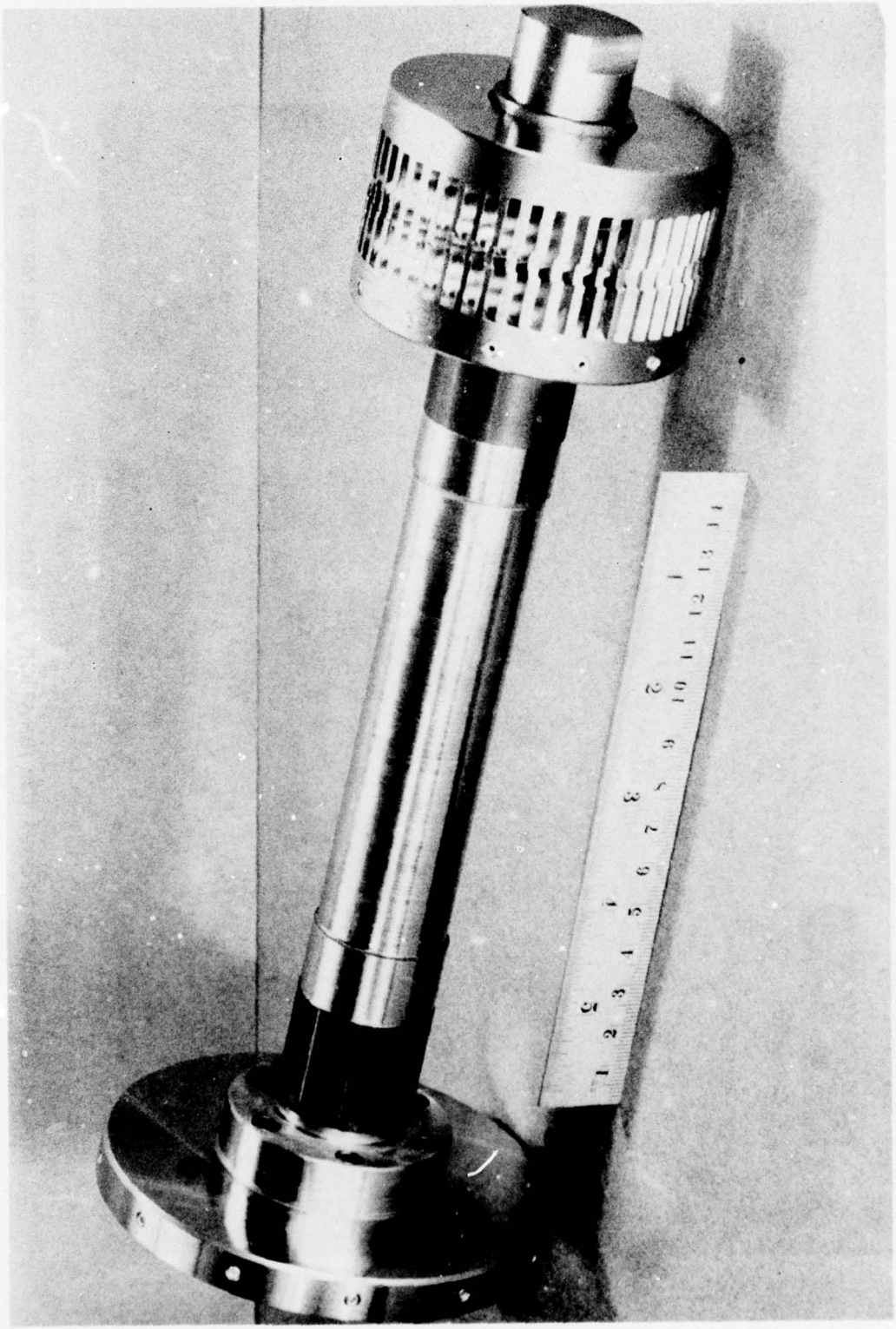

FIGURE 7. VIEW OF ROTOR ASSEMBLY

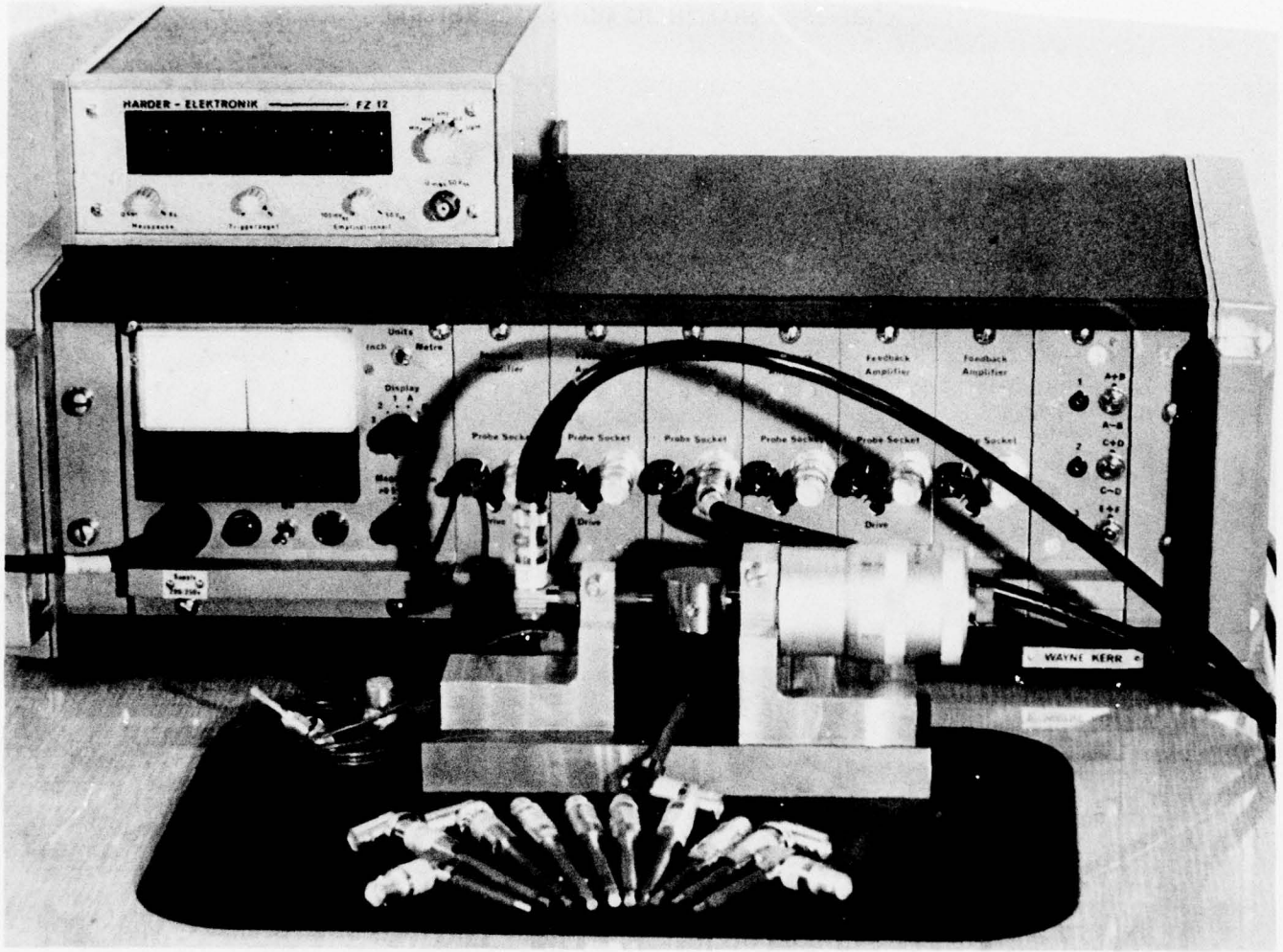

FIGURE 8. VIEW OF PROBES, CALIBRATION FIXTURE AND DISPLACEMENT METER

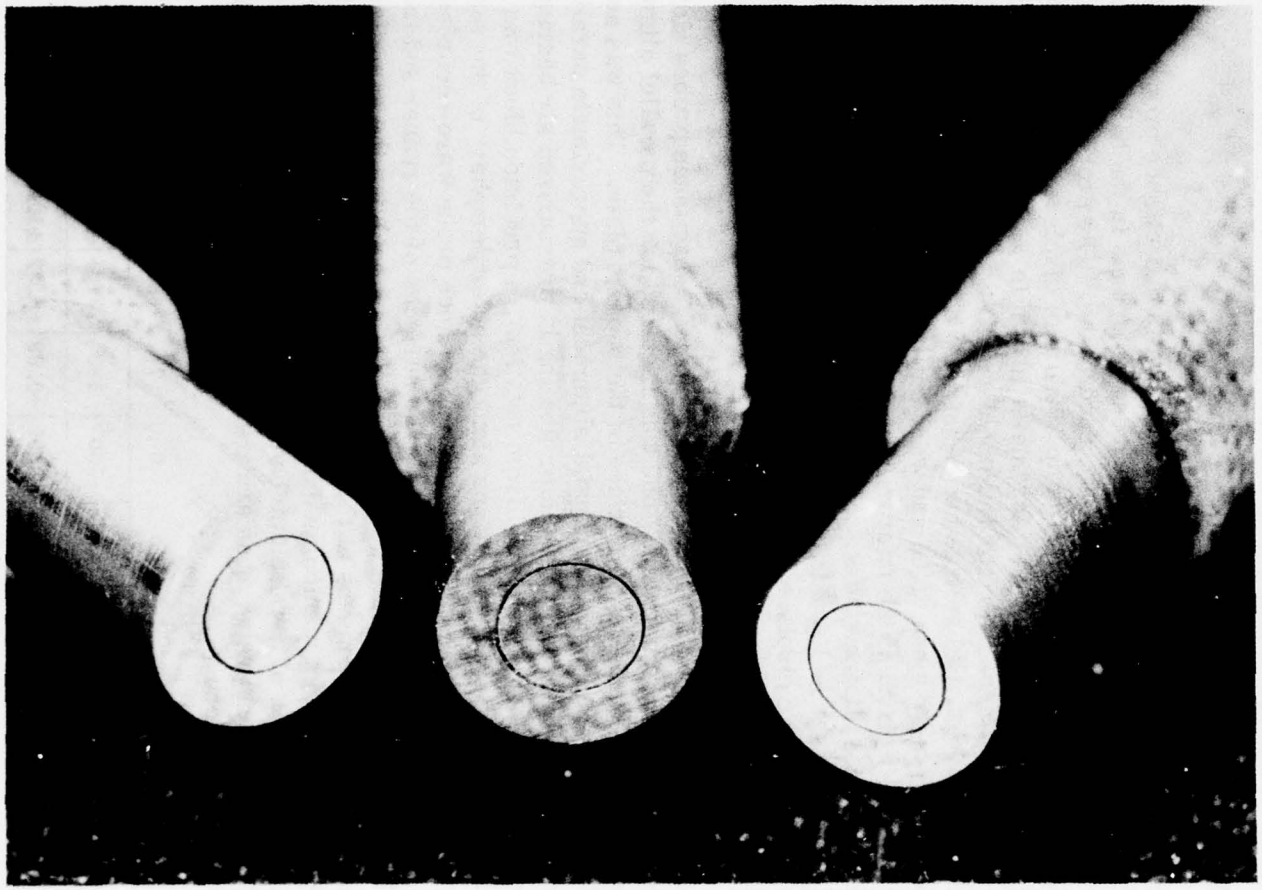

FIGURE 9. CLOSEUP VIEW OF CAPACITANCE PROBES

shows the central, 2.5 mm-diameter, active elements of the probe, surrounded by a concentric guard-ring and separated from it by a 0.03 mm-thick layer of insulation.

The assembled test rig, the pneumatic panel and part of the instrumentation are illustrated in two views contained in Figure 10, in the lower of which a spirally grooved membrane is clearly discernible between the runner and the support plate.

2.2 Instrumentation and Accuracy

Dynamic and static displacements were measured with capacitance probes and a six-channel Wayne Kerr meter having a flat frequency response in the bandwidth exceeding by a considerable margin the experimental speed range. The probes, Figure 9, were carefully calibrated in steps of 10 μm, up to 250 μm of displacement, by means of the calibration fixture and precision micrometer shown in Figure 8. The probes used for monitoring the motion of the rotor in the planes $(XY)_1$ and $(XY)_2$, at the runner and turbine-end bearings, had voltage and sensitivity characteristics congruent within approximately 3% of their mean value and were calibrated with 30 mm diameter dummy journals attached to the end of the micrometer spindle. Other capacitance probes were calibrated against flat surfaces. Each calibration was repeated five times and average values of voltage and sensitivity were then plotted. Measurements of amplitudes of motion and static displacements are estimated to be accurate within 5% of recorded values.

Provision was made for mounting three equally-spaced capacitance probes along the outer rim of the support plate, but only one was required for the parallel alignment of the runner and the lapped reference-surface of the support plate. This was accomplished in the following manner. After axial alignment and approximate parallelism had been achieved with both rotor and stator floating in pressurized air bearings (in a fixed angular position, i.e. constrained from rotation), a precision block was lightly clamped in twelve equally spaced positions along the outer periphery of the runner and the support plate, and the readings of the capacitance probe were recorded. The light clamping of the precision block between the surfaces of the runner and the reference plane of the support plate was accomplished by applying the same force of approximately one newton by means of the loading cylinder, Figure 1. The adjusting screws, Figure 1, were then manipulated and the housing bolts tightened to the base, until a satisfactory degree of parallelism had been achieved. A typical tabulation of deviations ϵ from the mean value of an arbitrarily selected spacing is given below for twelve angular positions θ.

		1	2	3	4	5	6	7	8	9	10	11	12
θ	DEG	0°	30°	60°	90°	120°	150°	180°	210°	240°	270°	300°	330°
ϵ	μm	+0.09	-0.35	-1.02	-0.13	+0.54	+0.09	+0.09	+0.32	+1.20	-0.13	-0.57	-0.13

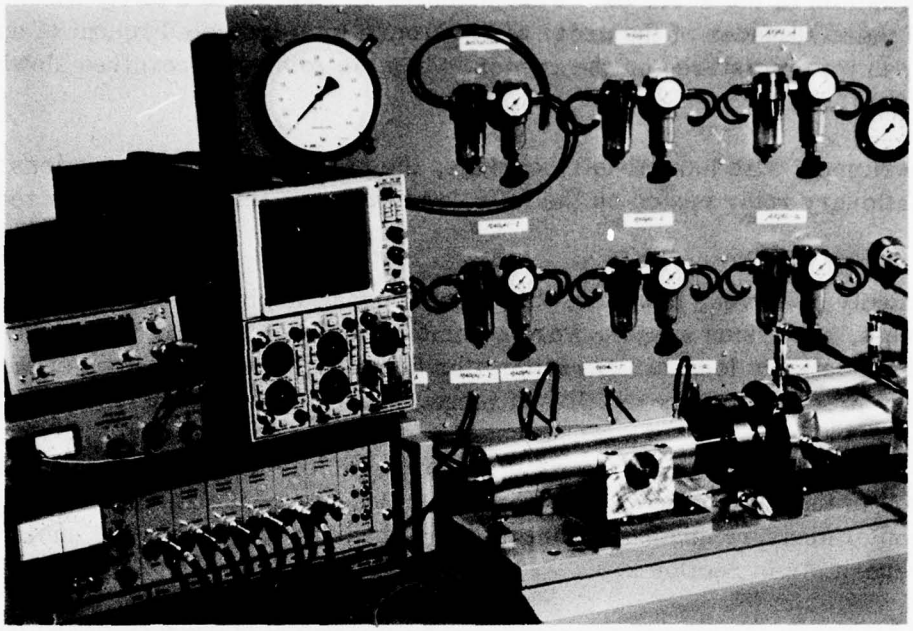

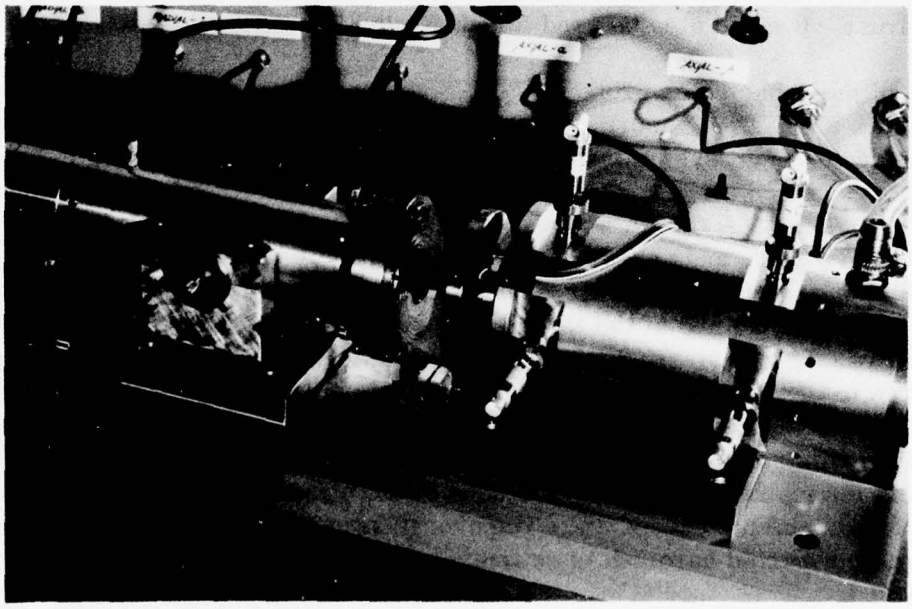

FIGURE 10. VIEW OF ASSEMBLED TEST RIG AND INSTRUMENTATION

These deviations include necessarily both departure from flatness as well as from overall parallelism of the surfaces. Furthermore, in addition to a fairly symmetric convexity of these surfaces of the order of 1.0 μm, a total indicated runout of approximately 3.0 μm was registered on the runner, when the rotor was revolved slowly in the air bearings.

In later experiments with journal foil-bearings, the parallel alignment was less perfect, since the stationary rotor rested on the foils, rather than floating in pressurized air bearings.

It was repeatedly observed, however, that mean journal displacements from the position of rest, at various speeds, were commensurate in magnitude and attitude. This, and the relatively long, 18 cm separation between the outboard ends of the journal foil-bearings, precluded the possibility of large increase in deviation from parallelism.

The capacitance probe located in the rigid support plate of the flexible thrust bearing was also used in the determination of clearance. Because of the significance and interpretation of measurements relevant to thrust-bearing clearance, the subject is discussed separately in Section 2.3.

The capacitance probe located in the center of the thrust pad (item 9 in Figure 1) served the purpose of calibrating the clearance versus the applied load on the loaded side of pressurized thrust bearing, in order to insure that a safe minimum was available at maximum thrust. It could also be used for observing the axial vibrations of the rotor.

The reading of the capacitance probe of the torque sensor was calibrated directly, in conjunction with a 1.0 x 6.5 x 30.0 mm, cantilevered Cu-Be spring and an essentially friction-free dead-weight system. With the stator assembly floated in air bearings, the static unbalance and air-bearing torque were first compensated and reduced to negligible proportions. A fine thread was taped to the cylindrical surface of the support plate, Figure 2, and passed over a circular groove of a small cylinder, supported on a 5 mm diameter, pressurized air-bearing. Weights were then placed on a small platform, attached to the end of the thread, to calibrate the torque sensor. The largest error of this torque-sensing system was due to variation of the point of application of force to the cantilever (by means of a steel ball, or disc, mounted on an extension arm attached to the support plate). These variations were well within $\pm$0.2 mm of the nominal cantilever length of 30 mm. Since the deflection, and also approximately the moment, vary with the cube of the effective length of the cantilever, the error incurred did not exceed 2%. The overall accuracy of measurement of the friction moment reported herewith is estimated to be within 5%, inclusive of the lowest values recorded.

The applied load, practically equal to the product of pressure in the loading cylinder and the cross-section area of the 25 mm-diameter stator-shaft extension, was determined by means of a precision pressure gauge, accurate to within 0.2% of full

scale deflection of 6.0 Kgf/cm^2 (58.86 N/cm^2) and graduated in steps of 0.05 Kgf/cm^2 (0.49 N/cm^2). It is estimated that the loads recorded were accurate well within 2% of the maximum values applied (~150N).

The rotational speed was measured by means of a miniature photoelectric element, comprising an infra-red emitter and a photocell, used in conjunction with an electronic counter. Measurement of speed at any specific value depended primarily on the accuracy of manually controlling the setting by means of a pressure regulator. With foil-bearing supported rotors, the speed could be maintained generally within 1% at 100 rps, and more accurately at higher speeds.

In many scans of the variation of amplitudes of motion with speed, oscilloscope records were obtained, in which the horizontal deflection of the CRO display was proportional to the speed of rotation. This involved the use of a digital-to-analog (frequency to voltage) converter, stable for inputs corresponding to speed values greater than 30 to 40 rps, and linear within 1% in the stable bandwidth of the experimental speed range. Since most scans were obtained during coastdown of the rotor, with deceleration uncontrolled (i.e. turbine inoperative), an unavoidable error was introduced by the counter and converter, particularly at high speeds, when deceleration was large. For example, if during the counter gating-period of 1 second the rotor decelerated from 750 rps to 700 rps, the horizontal deflection of the CRT display at a true speed of 700 rps may have corresponded approximately to an indicated speed of 725 rps, an error the order of 3%. An additional error of equal magnitude may have been introduced in photographing CRO displays of trajectories, due to a reaction-delay between the visual perception of counter readout and manual triggering of the camera shutter.

2.3 Definition and Measurement of Clearance $\tilde{h}$ of Flexible Thrust Bearings

Considerations relevant to the designs of flexible thrust bearings are amplified in Appendix A, to which the reader is referred for further details. Here it will suffice to state that the thrust bearings considered herein were of the inward-pumping, spiral-groove type, and that the grooved membranes were flexibly supported in a manner designed to remain sensibly parallel to the runner, when subjected to a radially nonuniform pressure load. The objective was to approximate the parallel clearance of an ideal, rigid-surface thrust bearing of the spiral-groove type.

Consider a rigid but flexibly mounted plate, with a spirally-grooved bearing surface in contact with a stationary runner. Let an axial load be applied and the corresponding deflection H_{STA} of the plate be measured by means of a capacitance probe, with reference to an arbitrary datum. The same arbitrarily selected datum is then used to determine the displacement H_{ROT}, at an identical load and with a rotating runner. Assuming that parallelism is maintained and thermal warpage is absent in this ideal and undistorted bearing, the uniform clearance is given by the difference $h_o = H_{ROT} - H_{STA}$. Moreover, if an elastic and continuous support could be devised

for a spirally-grooved membrane, to match the pressure loading of a rigid and geometrically identical thrust bearing, then the clearance of the flexible bearing would also be equal to $h_o = H_{ROT} - H_{STA}$.

Needless to say, the determination of the entire clearance topography h of a flexible-surface thrust bearing, with any degree of reliability and accuracy, would be very difficult and costly. In the results of this investigation, the measured quantity $\tilde{h} = H_{ROT} - H_{STA}$ is certainly commensurate with h_o, particularly at higher loads, but no estimate can readily be given of the difference between the relative displacement of the runner and stator, $\tilde{h}$, and the mean value of clearance, $\bar{h}$. Also, assuming that $\bar{h} \approx \tilde{h}$, the magnitudes of deviations $\epsilon = |h-\bar{h}| \approx |h-\tilde{h}|$ cannot be determined with certainty. On the other hand, since the flexible support is designed to produce a sensibly uniform clearance, it is reasonable to assume that $\tilde{h}$ may be a good approximation to h_o, and thus to the mean clearance $\bar{h}$, and that deviations ϵ may not be very large in the region of interest and at the design point.

In the determination of $\tilde{h}$, both H_{STA} and H_{ROT} are average values obtained in the following manner. The runner and membrane are brought into contact under load equal to approximately half of maximum. With the stator assembly and capacitance probe in a fixed angular position, the runner is rotated in increments of 30° and H_{STA} is determined as an average of 12 readings. The runner is then turned to one of the two angular positions corresponding to this average value and H_{STA} is determined for the entire load range. Average values H_{ROT} are then obtained in the same load range, at constant speed, from the voltage outputs of the monitoring probe.

The measurement of $\tilde{h} = H_{ROT} - H_{STA}$ represents a difference of two commensurate quantities (particularly at higher loads), each involving various inaccuracies, both mechanical and inherent in the instrumentation. It is estimated that the maximum overall error in the determination of $\tilde{h}$ may be of the order of 15%, as compared with approximately 5% in oscilloscope records of various trajectories and amplitudes of motion of the rotor axis in the monitoring planes $(XY)_1$ and $(XY)_2$.

3.0 DESIGN AND CONSTRUCTION OF FLEXIBLE THRUST BEARINGS

The objective was to combine the load-generating efficiency of a parallel-surface, spiral-groove thrust bearing with various advantages due to resilience of the bearing surface and of the support. Many of these advantages are enumerated in several references quoted in this report and their relative importance may depend on specific applications, but those universally important are the ability to follow and accommodate relatively large excursions of the runner and to tolerate contact. Resilience of surface and support, and small inertia of components excited by the motion of the rotor, furnish the necessary means for realizing these objectives, provided the flexible thrust bearing can be made to retain the high load-capacity associated with a geometrically identical, rigid bearing.

The pressure generated in the fluid film depends on the clearance topography. In the specific case of the grooved, parallel-surface thrust bearing, the problem requires the maintenance of a uniform gap between a flexible, foil-like membrane and the runner. Ideally, this could be achieved with an elastic support having a distributed stiffness to permit the membrane to displace locally in proportion to the pressure generated in a rigid, parallel-surface, spiral-groove bearing. The membrane would then displace parallel to itself and to the runner.

A continuous stiffness distribution can be approximated by arrays of discrete spring-elements, incorporated in the flexible support of a compliant bearing-surface. The design of two thrust bearings and of their discrete-element support systems is given in Sections 3.1 and 3.2, while the method of design and related calculations are included in Appendix A.

3.1 Spirally Grooved Membrane Supported on Plate-Spring Arrays (Flexible Thrust Bearing LLF-1T)

An assembly drawing and isometric view of the flexible thrust bearing LLF-1T is presented in Fig. 11. Referring to the legend of Fig. 11, the support plate (1) contains six sets of holes, with three equal holes per set. The holes of each set are equally spaced on circles bisecting six concentric annuli, subdivisions of the bearing area bounded by circles of radii R_i and R_o. Each set of holes is angularly displaced from the adjacent set to allow for proper utilization of available space. The edges of the holes provide simple supports for plate springs (4), and since deflections vary inversely with the square of effective diameters, hole dimensions are chosen to produce equal deflections of each set of plate springs for a radially-varying pressure distribution. (Refer to Appendix A and Fig. A-1 for further details).

The load is transmitted to the centers of the plate springs by means of steel balls (2) and relatively slender but rigid support rings (7). There are six such rings, each supported on three balls and plate springs of the same set, and supporting in turn the grooved membrane (8).

The function of the ball cage (2) is to position the balls and the plate springs centrally over the holes in the support plate, and symmetrically with respect to the bearing axis. The cage also serves as a retainer for both balls and plate springs and is doweled and bolted to the support plate. The top side of the cage contains a row of locating pins (6), two for each ring. Their function is to position the rings concentrically and to prevent lateral sliding and bunching of rings. The pins and the corresponding holes in the rings have sufficient clearance, so that the rings are free to rotate within adequate limits about any diameter and to translate axially. Another set of pins (9) prevents rotation of the membrane, and locates the latter concentrically with the bearing axis, within limits of clearance of the slots engaging the anti-rotation pins.

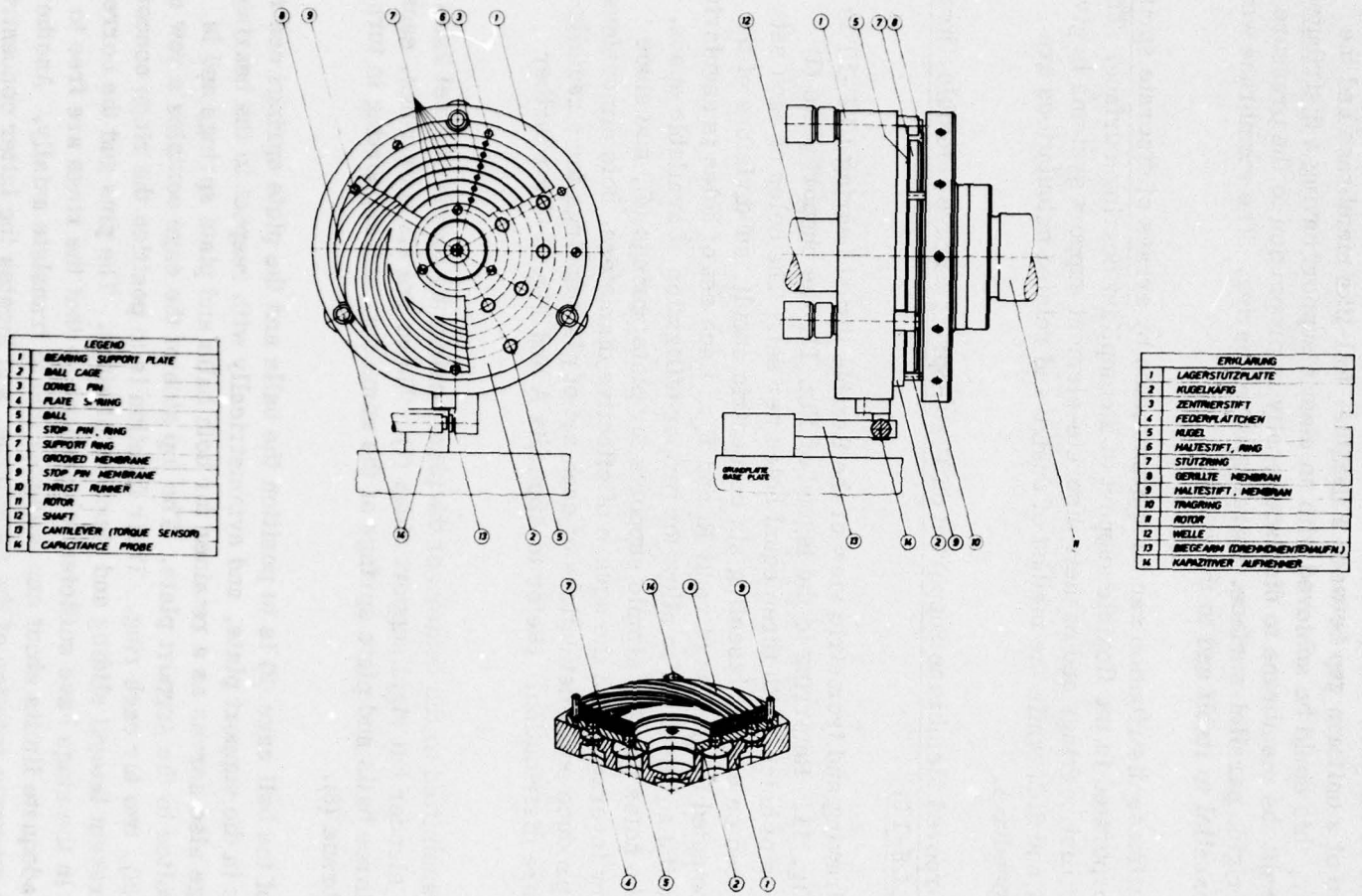

FIGURE 11. ASSEMBLY DRAWING AND ISOMETRIC VIEW OF FLEXIBLE THRUST BEARING LLF-1T

The support rings were ground and lapped flat and parallel within 2.5 μm, and the reference surface of the bearing support-plate was lapped flat to within 1.0 μm. The thickness of the contour-etched plate springs and the diameters of balls were highly uniform, and the components were readily available. This insured parallel stacking of bearing elements to the reference surface of the support plate prior to alignment with the runner, as described in Section 2.2. Although the overall thickness of the membrane was highly uniform, surface flatness could not be controlled to a commensurate degree. Waviness, however, was greatly reduced at moderate pressure loads, except at the outer periphery of the runner.

The drawing of the bearing in Figure 11 shows also the location of capacitance probes (14) and of the torque-sensor cantilever. The probes are, of course, extraneous to bearing design, and the reader will readily recognize that thrust-bearing surfaces would generally be provided on both sides of the runner (10), and that a suitably proportioned support plate would be secured to the machine housing, rather than mounted on the end of the loading shaft (12).

In order to acquaint the reader with the components of this bearing and to provide a better insight into its functioning, a sort of "pictorial disassembly" is provided by a sequence of views contained in Figures 12 through 23.

The fully assembled bearing is shown in Figure 12, and Figure 13 is a similar view, with a sector of the grooved membrane cut away and thus uncovering the support rings in a region containing a row of locating pins. Three anti-rotation pins and corresponding slots along the outer periphery of the membrane are clearly visible. Figure 14 illustrates the assembled components with the membrane removed. In the views of Figure 15 and Figure 16, first one, and then all support rings have been lifted from the locating pins, exposing the topside of the cage and showing the ball-retaining holes.

The topside of the cage is shown again in Figure 17, and the underside is illustrated in Figure 18, in which one can clearly discern: (a) a number of plate springs in locating recesses of the cage, (b) a few steel balls retained in the locating holes, and (c) a series of openings comprising both holes and recesses for the retention of balls and plate springs. Note that the recess and plate-spring dimensions do not determine the active plate-spring diameter of each array. The active diameters are determined by the holes in the bearing support-plate, a view of which is contained in Figure 19. Note that triads of largest holes are located close to the outer and inner bearing peripheries, where the pressure is lowest, while sets of smallest holes are adjacent to the boundary between the grooved and plane regions of the inward-pumping membrane, Figure 20, where pressure is highest. A composite view of parts of the flexible thrust bearing LLF-1T is presented in Figure 21. The hard-faced runner and a membrane are shown together with the rotor in Figure 22, while Figure 23 illustrates the thrust bearing in a close-up photograph of the test rig.

The outer radius of the membrane was 45 mm. The active bearing area was bounded by circles of radii R_o = 40 mm and R_i = 16 mm, and separated into plain and grooved

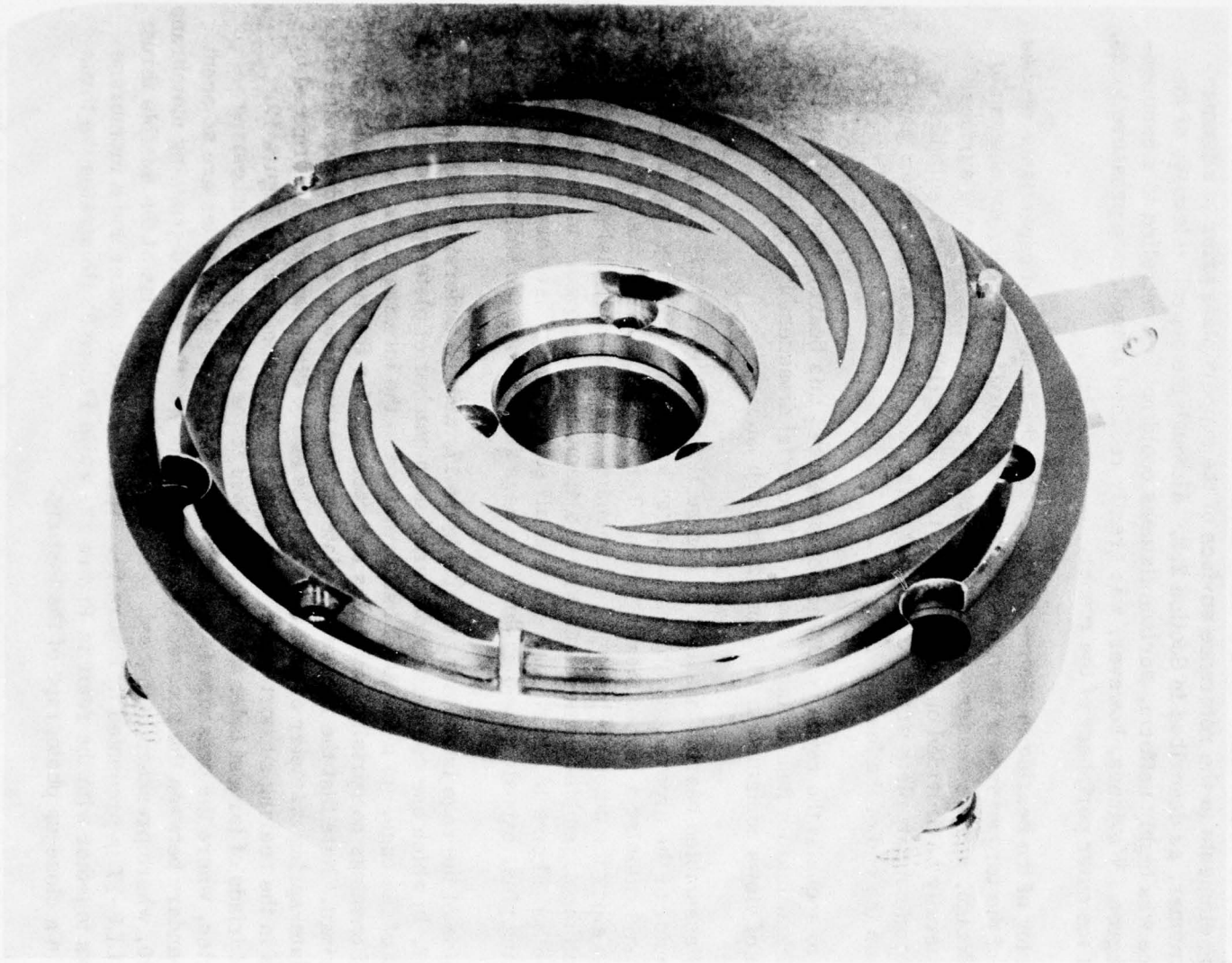

FIGURE 12. VIEW OF ASSEMBLED FLEXIBLE THRUST BEARING LLF-1T

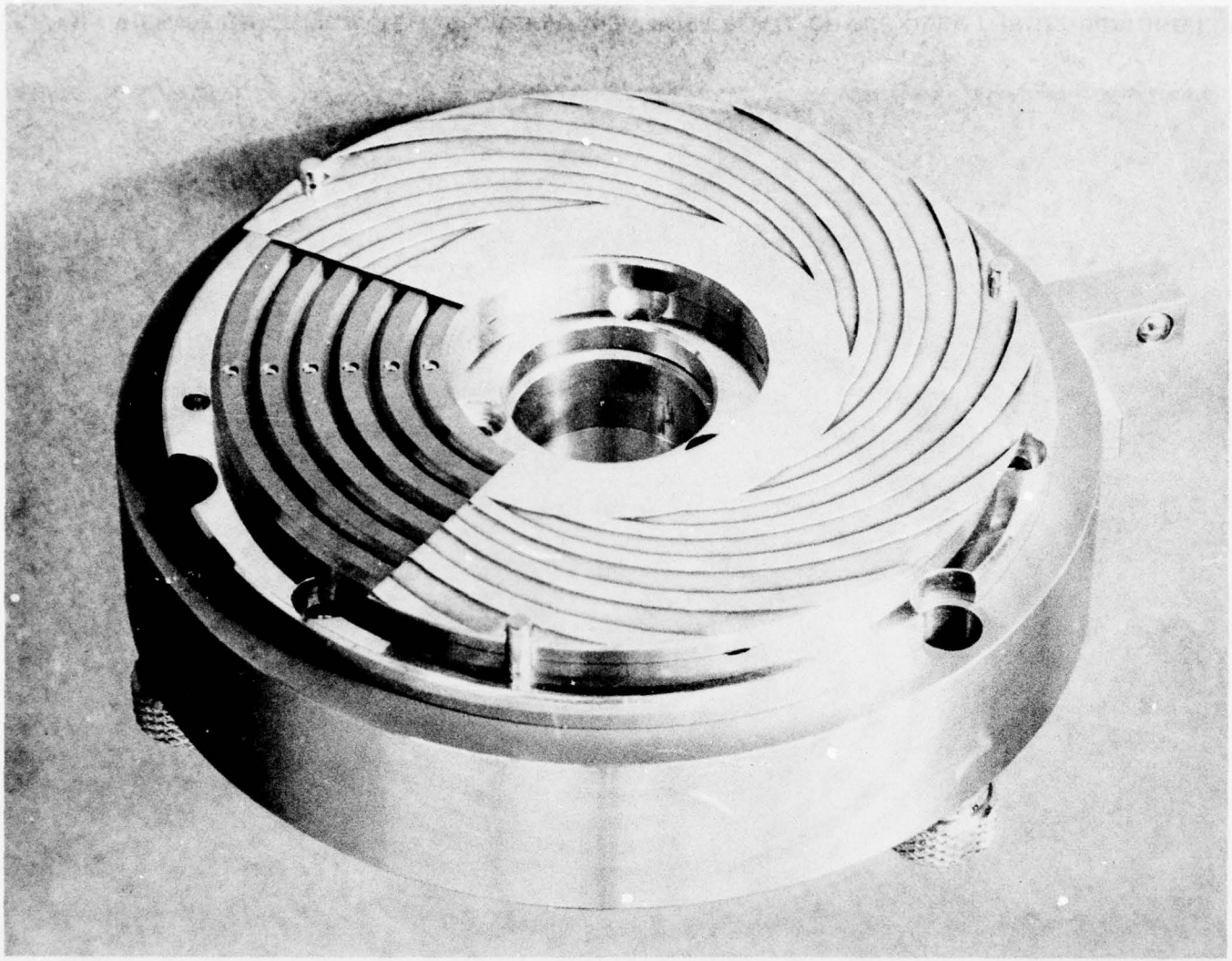

FIGURE 13. VIEW OF FLEXIBLE THRUST BEARING LLF-1T WITH SECTOR OF SPIRALLY GROOVED MEMBRANE REMOVED

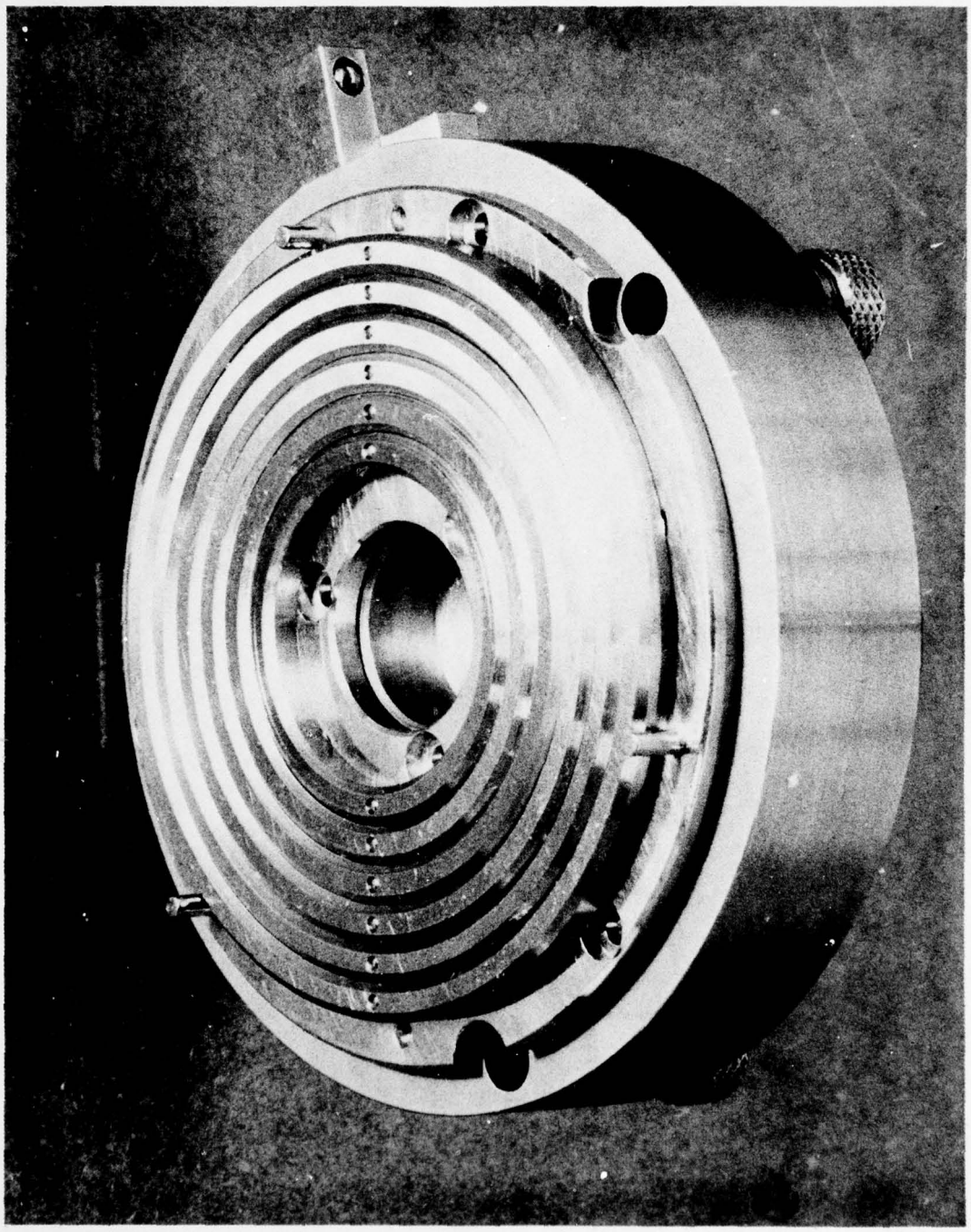

FIGURE 14. VIEW OF RINGS MOUNTED ON CAGE AND SUPPORT PLATE OF FLEXIBLE THRUST BEARING LLF-1T

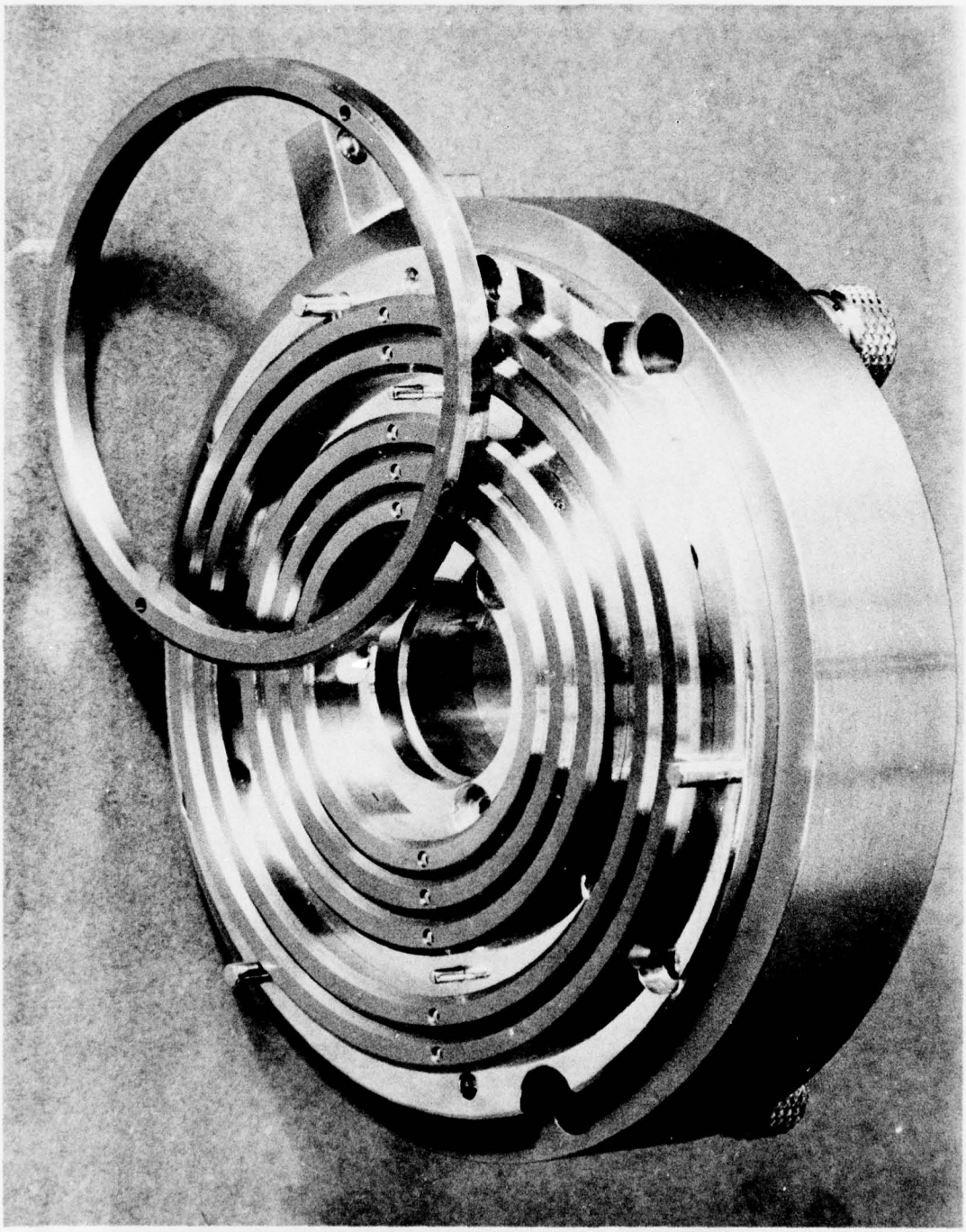

FIGURE 15. VIEW OF FIGURE 14 WITH THIRD (MIDDLE) RING REMOVED

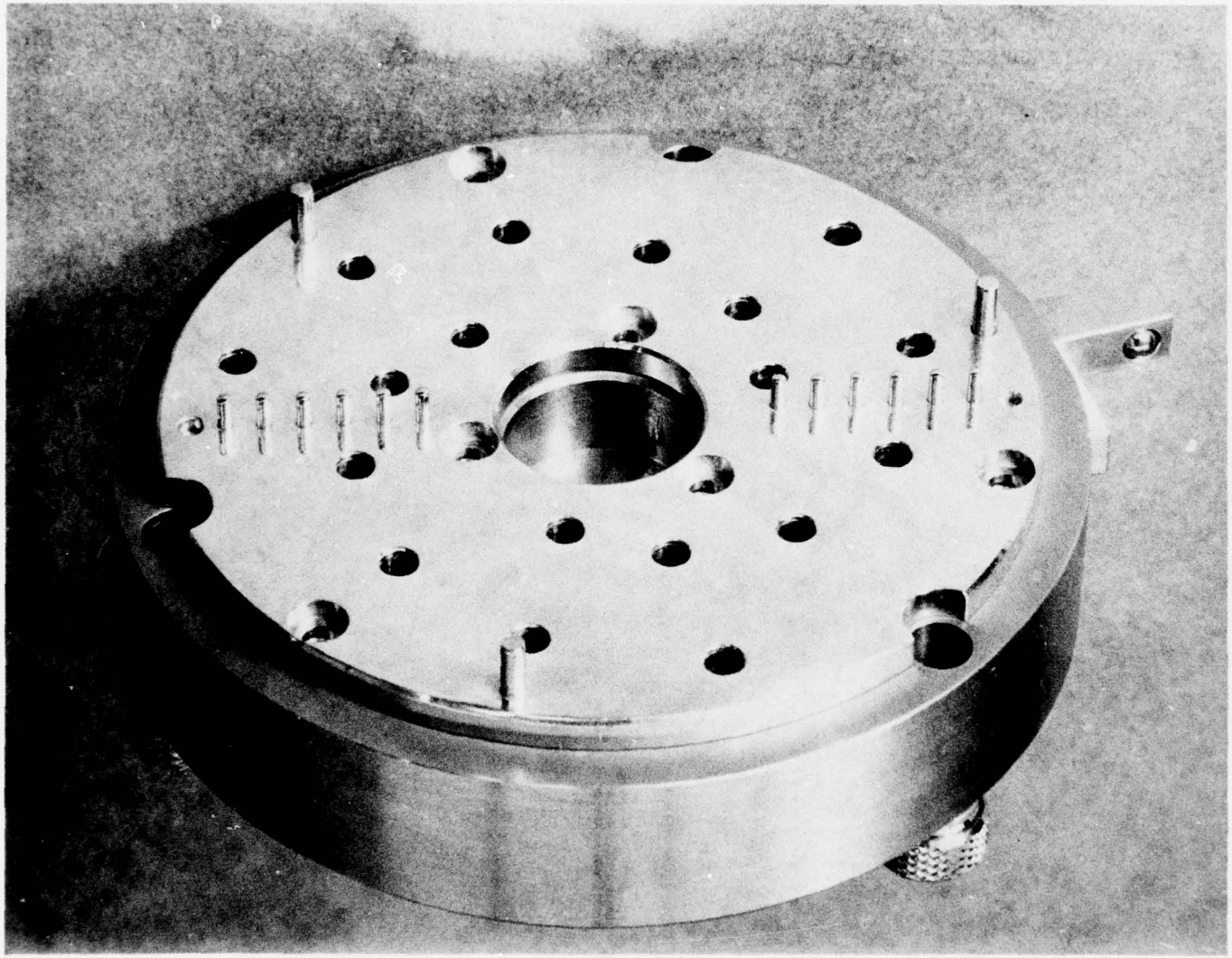

FIGURE 16. VIEW OF CAGE AND SUPPORT PLATE OF FLEXIBLE THRUST BEARING LLF-1T, SHOWING LOCATING PINS OF RINGS AND ANTI-ROTATION PINS OF SPIRALLY GROOVED MEMBRANE

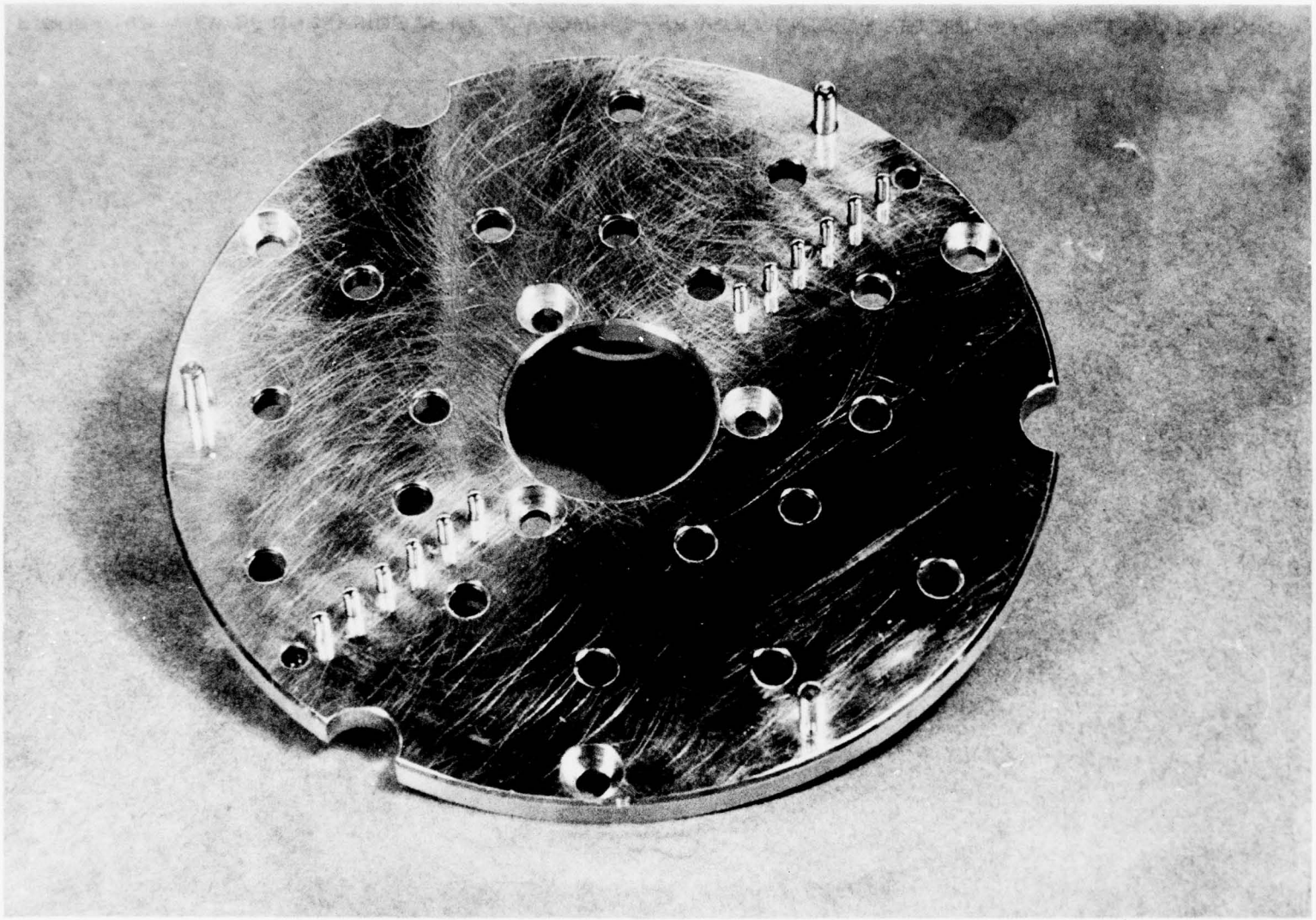

FIGURE 17. TOP VIEW OF CAGE, SHOWING RING-LOCATING AND ANTI-ROTATION PINS AND BALL-RETAINING HOLES (FLEXIBLE THRUST BEARING LLF-1T)

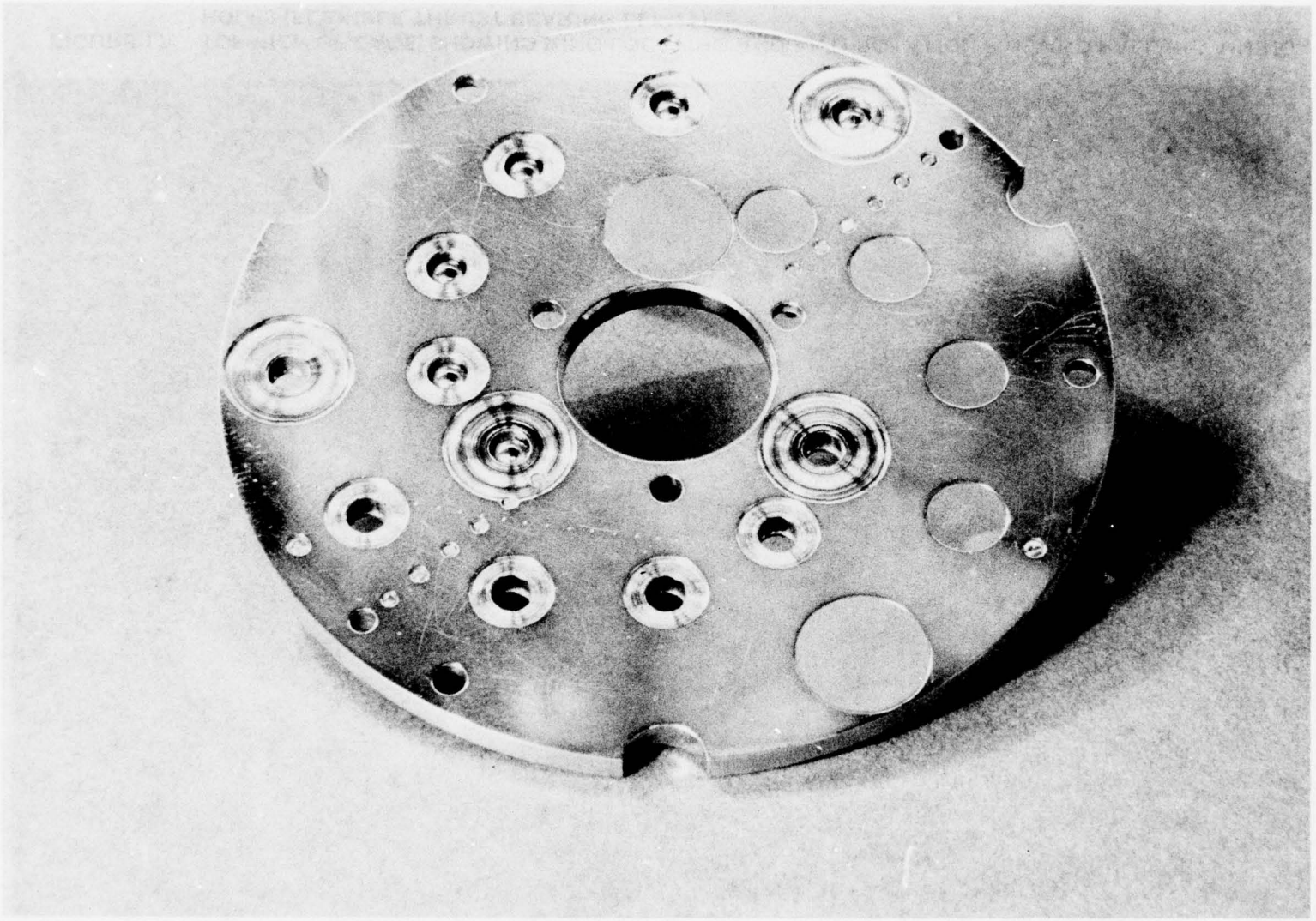

FIGURE 18. VIEW OF UNDERSIDE OF CAGE, SHOWING ARRANGEMENT FOR RETENTION OF BALLS AND SPRING PLATES (FLEXIBLE THRUST BEARING LLF-1T)

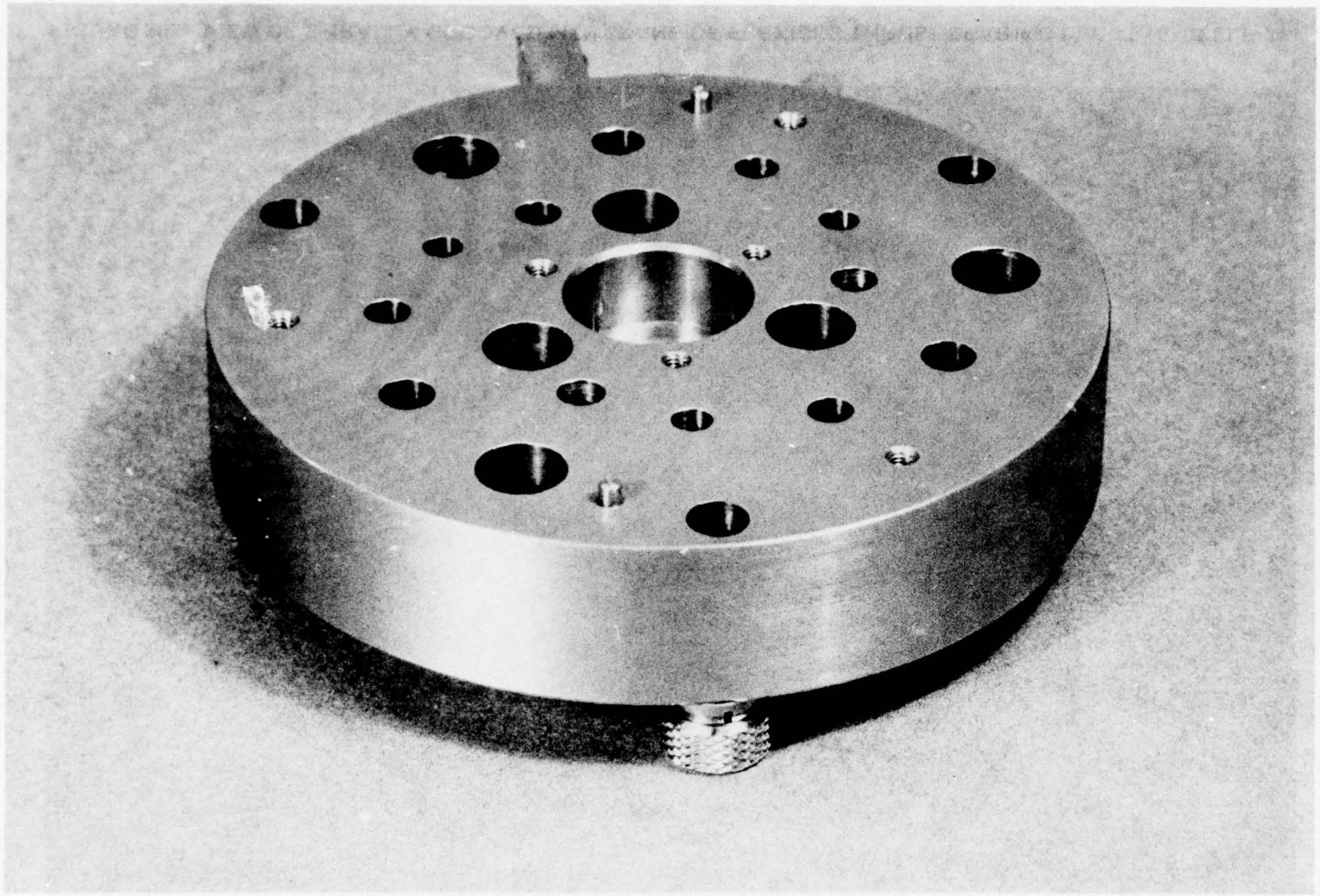

FIGURE 19. VIEW OF SUPPORT PLATE OF FLEXIBLE THRUST BEARING LLF-1T.-HOLE PERIMETERS SUPPORT THE SPRING PLATES AND DETERMINE THE LOCAL STIFFNESS

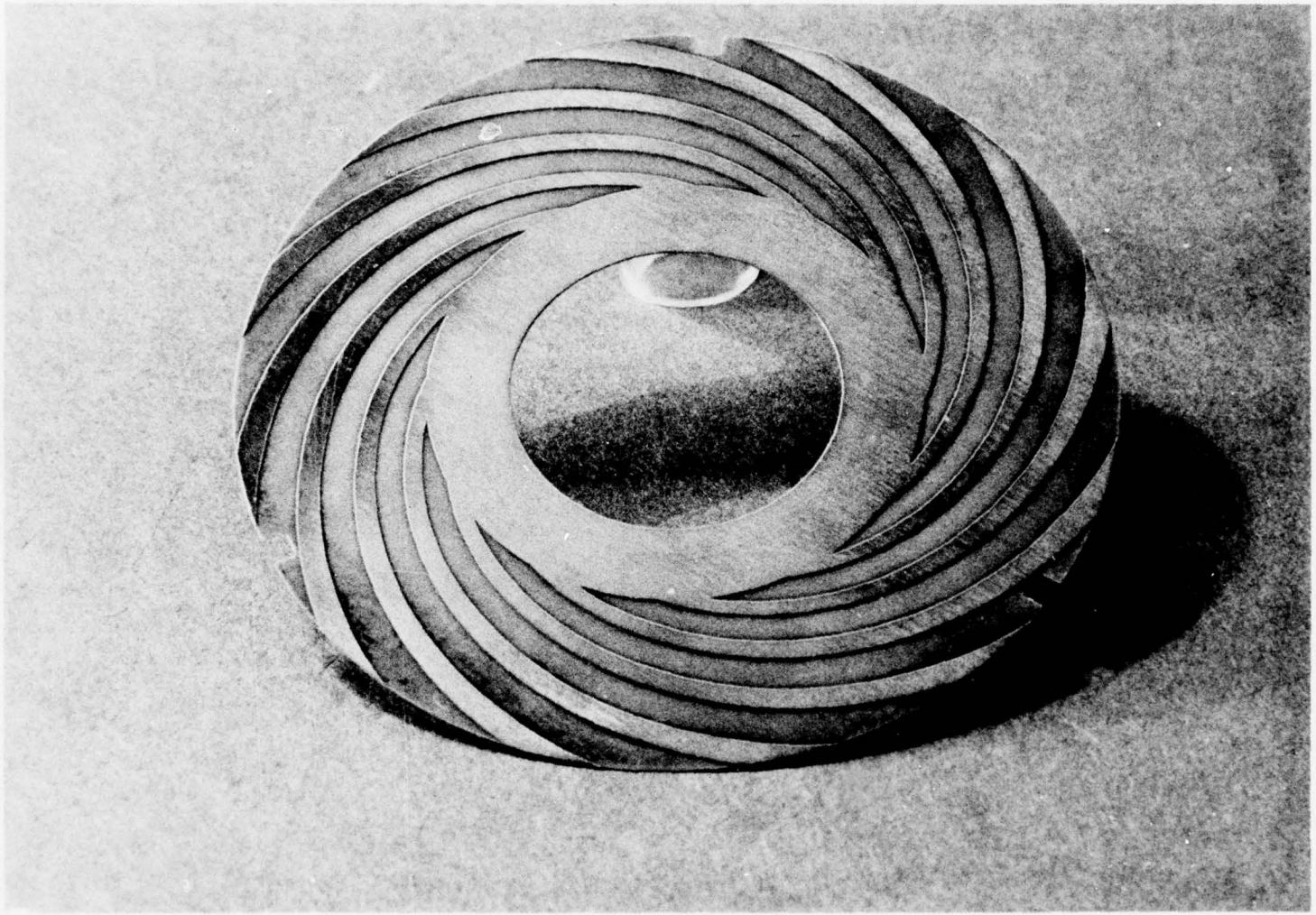

FIGURE 20. VIEW OF SPIRALLY GROOVED MEMBRANE OF FLEXIBLE THRUST BEARING LLF-1T (AND LLF-2T)

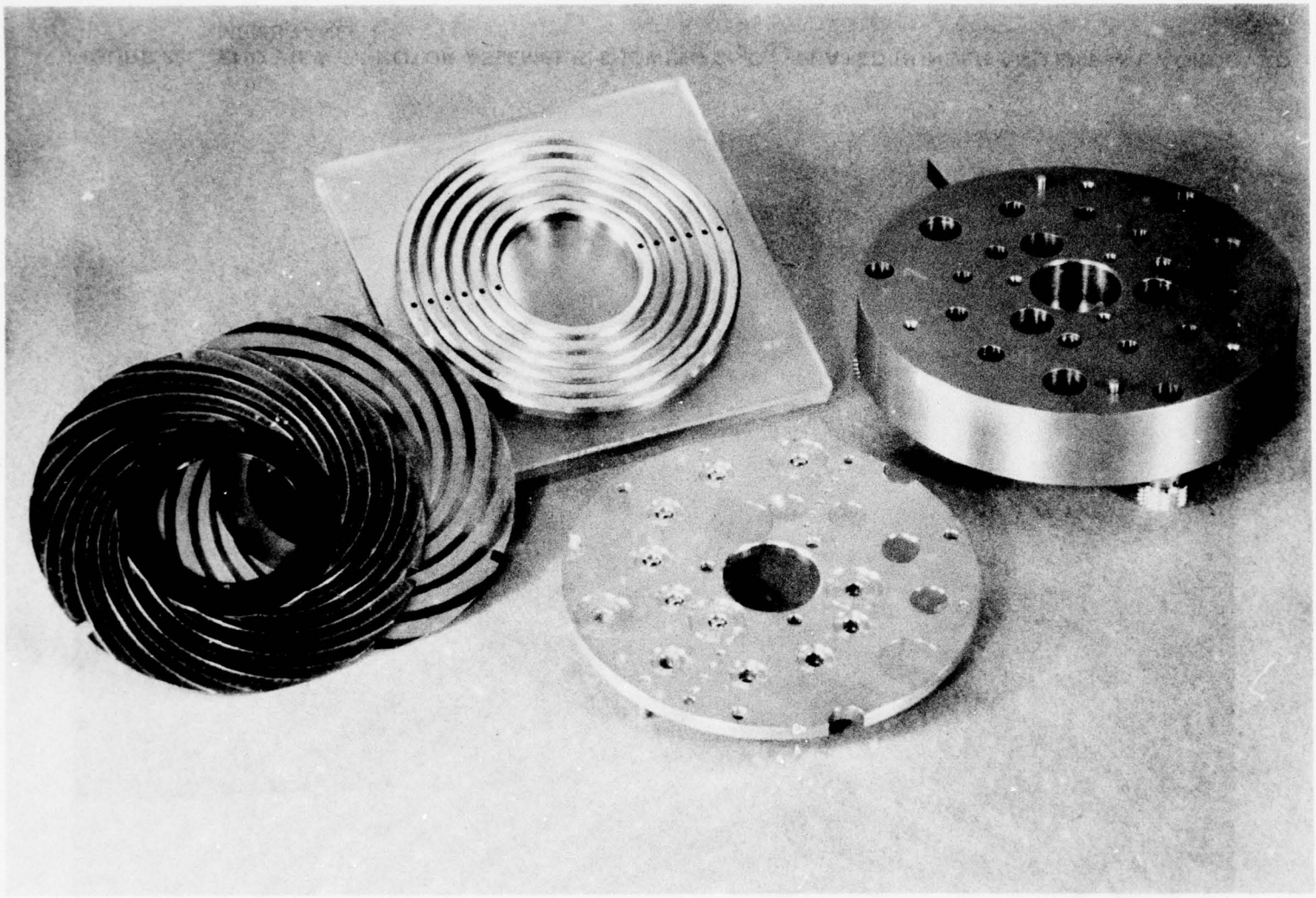

FIGURE 21. VIEW OF COMPONENTS OF FLEXIBLE THRUST BEARING LLF-1T. - SUPPORT PLATE (RIGHT), CAGE WITH BALLS AND SPRING PLATES (BOTTOM), RINGS (TOP) AND MEMBRANES (LEFT)

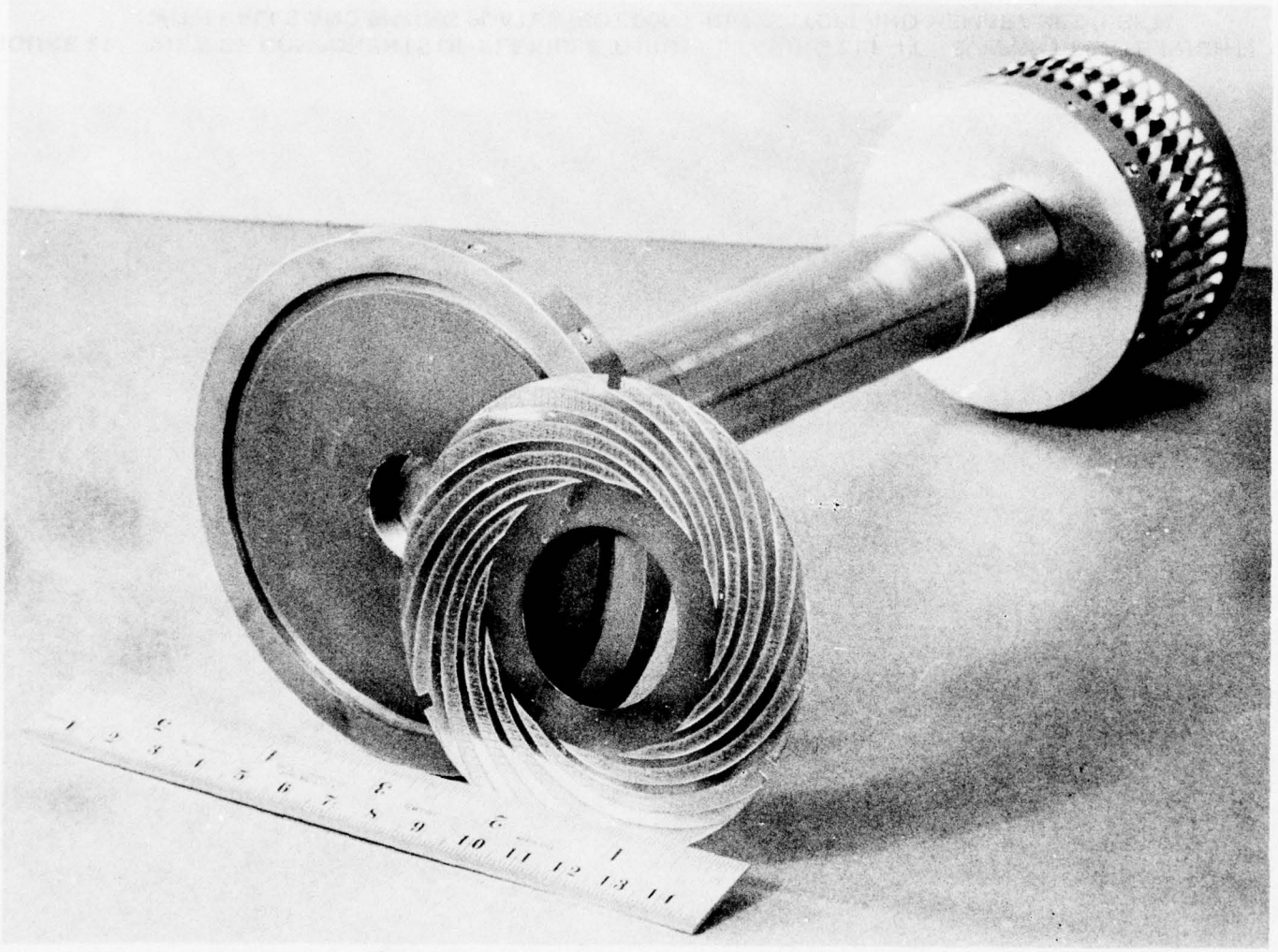

FIGURE 22. END VIEW OF ROTOR ASSEMBLY, SHOWING Cr_2O_3 - PLATED RUNNER AND SPIRALLY GROOVED MEMBRANE

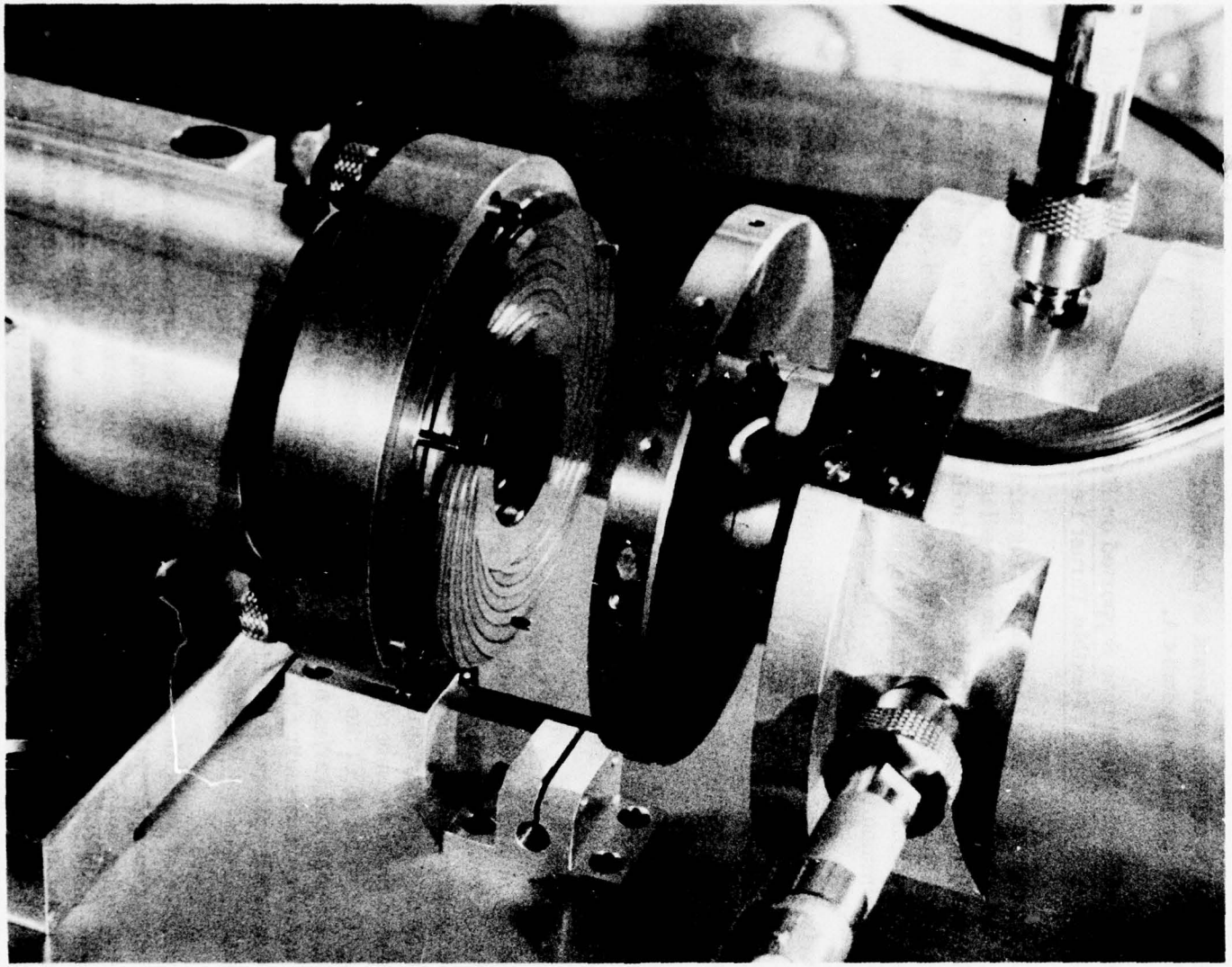

FIGURE 23. CLOSEUP VIEW OF FLEXIBLE THRUST BEARING LLF-1T ON TEST RIG

regions at a radius R_g = 24 mm. Twelve spiral grooves and ridges subtended angles of 18° and 12° respectively, and the groove depth was etched to $\Delta = 45 \pm 5$ μm in copper-beryllium ($t_m \approx 230$ μm) and Inconel X-750 ($t_m \approx 215$ mm) membranes.

Additional details and data relevant to the design of thrust bearings LLF-1T and LLF-2T are contained in Appendix A.

3.2 Spirally Grooved Membrane Supported on Multiple Flexure Arrays Integral with a Single Spider-Spring (Flexible Thrust Bearing LLF-2T)

Although the design outlined in the following paragraphs bears a superficial resemblance to that of the bearing described in the preceding section, the methods of support of grooved membranes differ radically. The similarity is limited to the membrane, and only the objective of attaining a sensibly parallel displacement and clearance, and thus a pressure field and load-capacity approximating that of a rigid, spiral-groove bearing, is common to both configurations.

This bearing consists of three components only; a spirally grooved membrane, a reticulated spider-spring incorporating both support rings and spring elements, and a support plate with narrow, concentric ridges to engage the quasi-rectangular spring elements at their midpoints.

Since the membrane is identical with that described in Section 3.1 and is illustrated in Figures 12, 13 and 20, the description starts with the reticulated spider spring, shown in the drawing of Figure 24 (See also Appendix A for additional design data).

Referring to Figure 24, it will be noted that the spider spring, which may have a thickness (t_p) commensurate with that of the membrane (t_m), consists of a series of relatively narrow, 1.0 mm-wide rings, connected radially by staggered arrays of spring elements of nominally equal thickness (t_s) and of variable width (b). Note that one surface of the spider spring is plane, and that the staggered spring-connectors are recessed from the second surface, leaving narrow, concentric lands for membrane support. The width (b) of the nearly rectangular spring-elements of each array governs the local stiffness and varies in proportion to the pressure-load carried by the annular bearing areas corresponding to each array. The objective here, as before, is to ensure a sensibly uniform deflection of the membrane and an approximately parallel clearance.

The fabrication of the spider spring shown in Figure 24 was accomplished by a two-stage etching process. In the first stage, the entire reticulated contour is etched from foil stock. In the second stage, the radial connections between the rings are recessed by selective etching on one side, thus reducing the thickness of the spring elements from the initial ($150 \lesssim t_p \lesssim 200$ μm) to the required ($50 \lesssim t_s \lesssim 70$ μm) value. In the first etching operation, allowance must be made for the reduction of width of the spring elements (b) during the second etching operation. The effect of errors and inaccuracies of manufacture is discussed in parallel with design calculations in Appendix A.

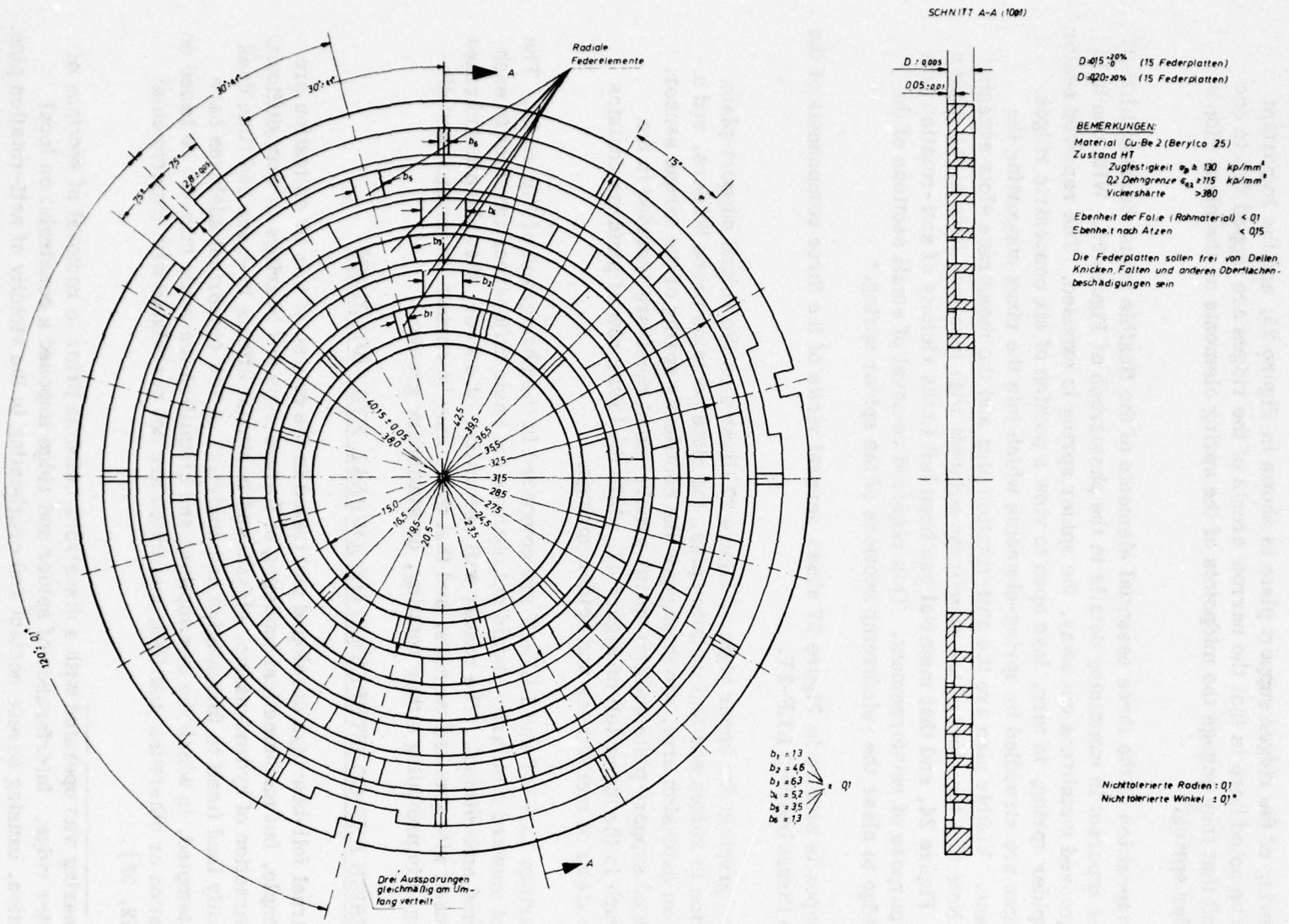

FIGURE 24. SPIDER SPRING OF FLEXIBLE THRUST BEARING LLF-2T

The drawing of the ridged support plate is shown in Figure 25, and the important point to be noted here is that the narrow crests of the ridges are lapped flat in one plane and that they engage the midpoints of the spring elements on the plane side of the spider spring.

The juxtaposition of the three essential elements of the flexible thrust bearing LLF-2T becomes apparent in examining details in the photograph of Figure 26. With one half of the grooved membrane cut away, the spider spring is exposed. The removed sector of the spider spring, in turn, lays open to view a portion of six concentric ridges. The ridges are straddled by spring-elements which join the rings supporting the membrane. Visible also are the anti-rotation pins and the membrane slots engaging them. Note that the slots of the membrane coincide with identical slots in the spider spring, Figure 24, and that material has been left in the vicinity of anti-rotation pins for the purpose of reinforcement. This required removal of small sections of the outer ridge to clear the reinforcing sections of the spider spring. *

The composite picture in Figure 27 shows several views of the three components of the flexible thrust bearing LLF-2T.

The photograph in the upper right of Figure 27 illustrates the ridged support-plate. In addition to ridges and anti-rotation pins, the plate contains probe holders, and a disc on an extension arm, which engages the cantilever spring of the torque sensor. The ridged support-plate and two spiral-groove membranes are included in the photograph in the upper left of Figure 27, while the lower row of pictures contains various views of membranes and spider springs.

The bearings LLF-1T and LLF-2T are compared in the photograph of Figure 28. The apparent outward similarity should not obscure the basic differences inherent in each design and embodiment. The reader will recognize, of course, that plane membranes can be used with grooved runners, and that there may be certain advantages and disadvantages in providing either rotating, or stationary grooves.

4.0 DESIGN AND CONSTRUCTION OF JOURNAL FOIL-BEARINGS

The journal foil-bearings developed and tested in the course of this investigation are very simple, but mathematical modeling of flexure-type foil bearings is very difficult. The interaction of hydrodynamic, elastic and frictional effects in space and time does not readily lend itself to formulation and analysis. A few numerical analyses have been attempted, in which the assumptions and simplification made may not be based on observation or otherwise justified, and which are not correlated with experimental data [52, 53].

*The bearing was operated with a disastrous outcome prior to removal of sections of the outer ridge. Interference of spider and ridge imposed a constraint on local deflection, causing severe contact and overheating in the vicinity of anti-rotation pins. Two membranes buckled locally and failed before the source of trouble was eliminated.

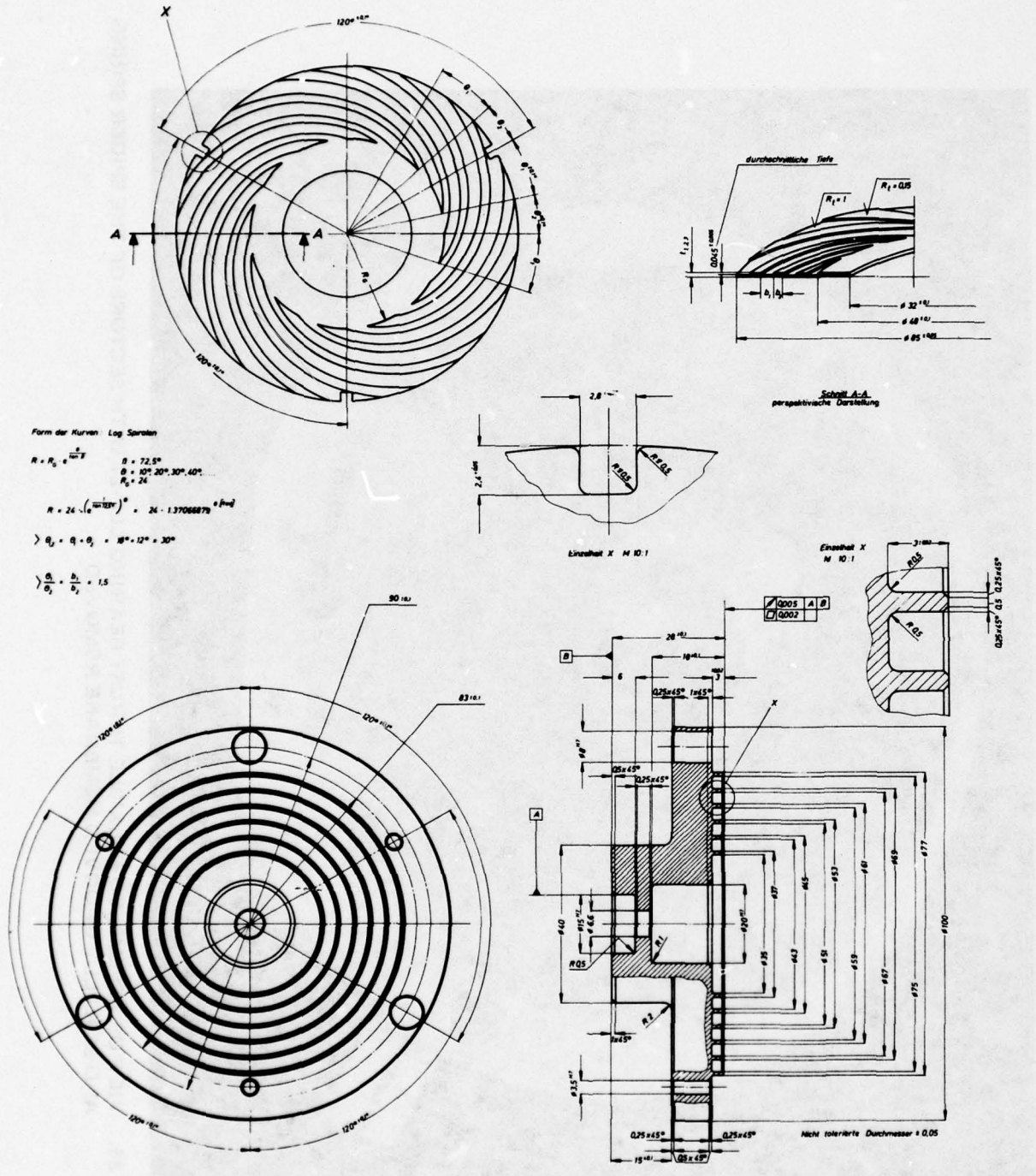

FIGURE 25. SUPPORT PLATE AND GROOVED MEMBRANE OF FLEXIBLE THRUST BEARING LLF-2T

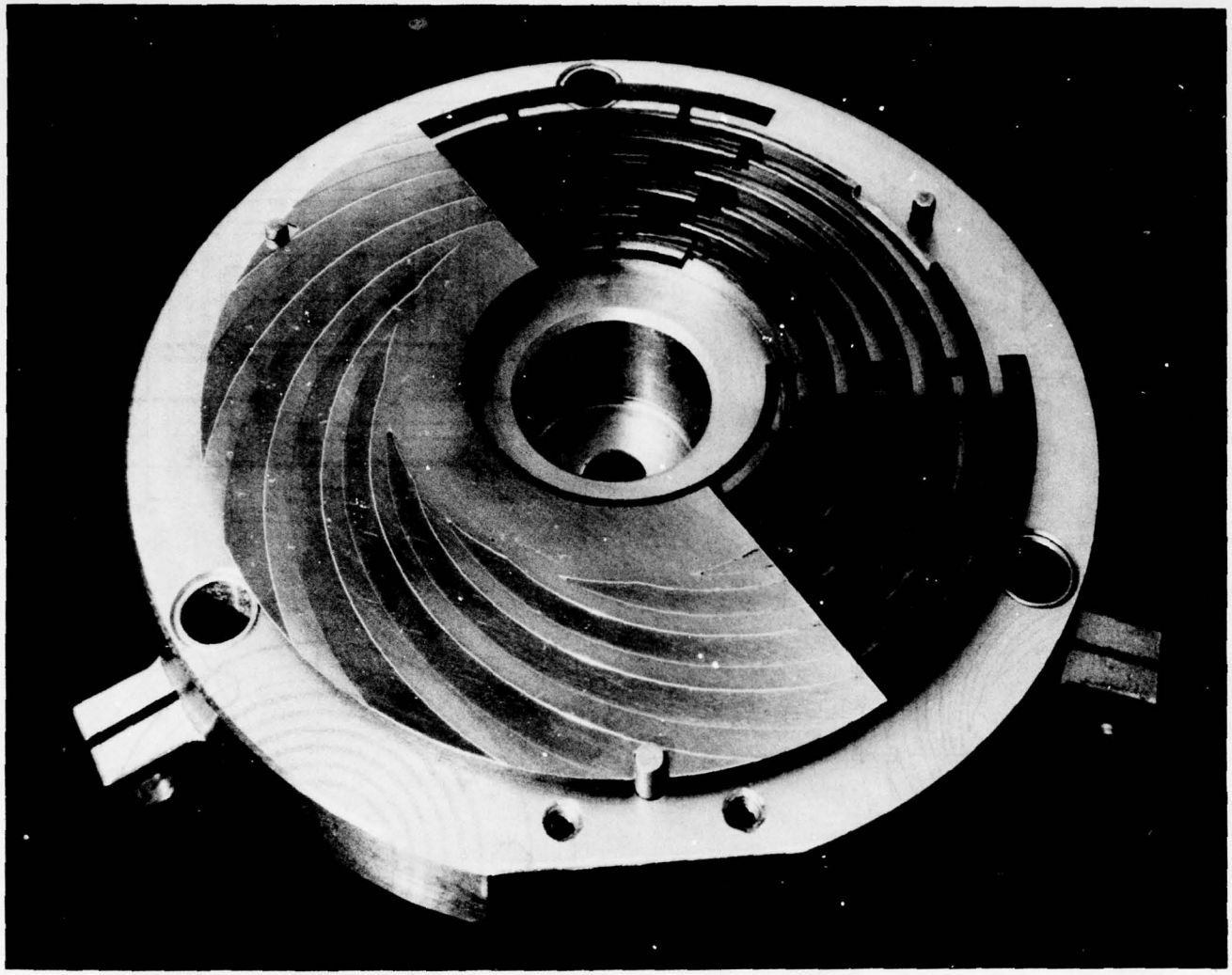

FIGURE 26. VIEW OF ASSEMBLED FLEXIBLE THRUST BEARING LLF-2T WITH SECTORS OF THE SPIDER SPRING AND SPIRALLY GROOVED MEMBRANE REMOVED

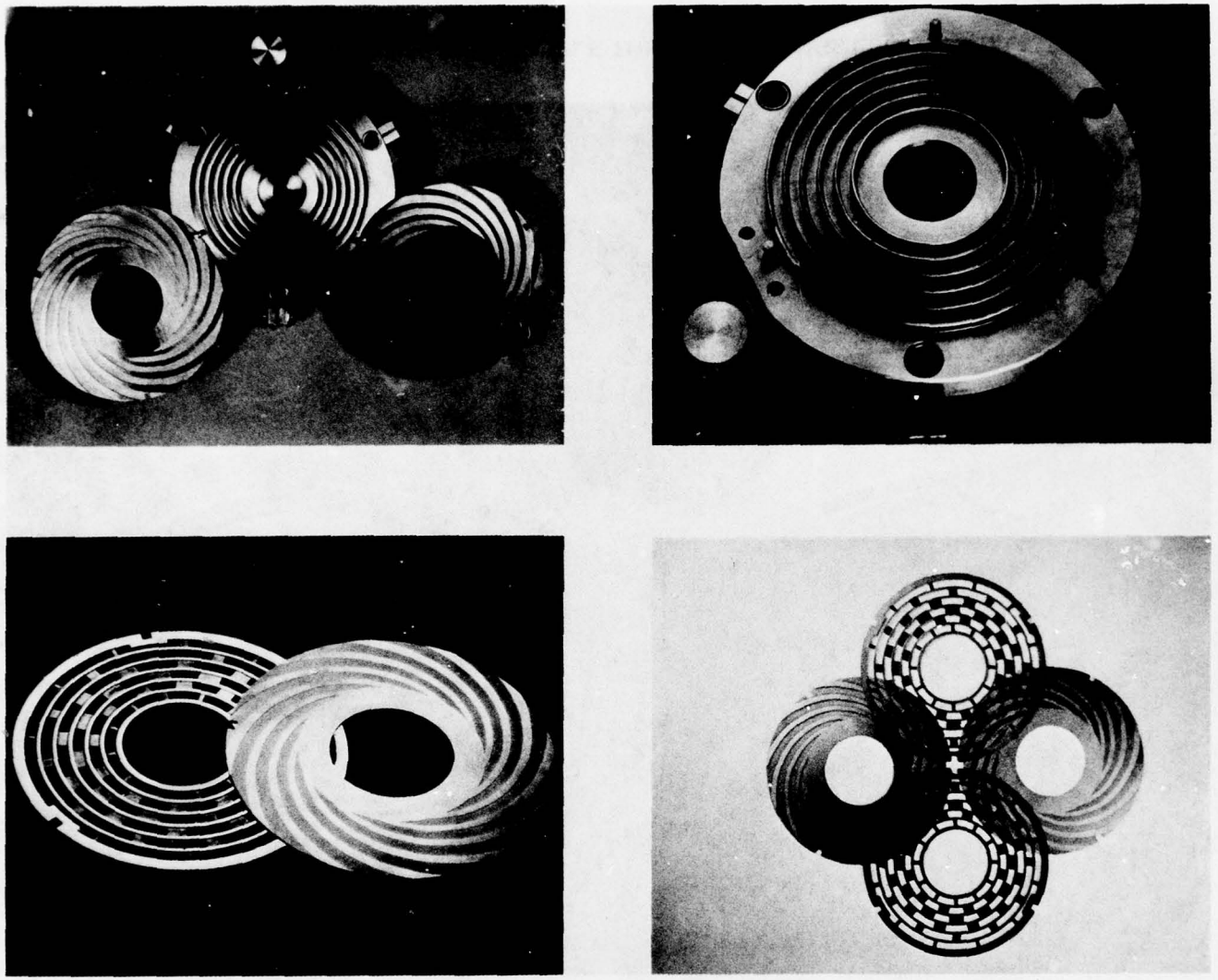

FIGURE 27. VIEW OF COMPONENTS OF FLEXIBLE THRUST BEARING LLF-2T. - SPIRALLY GROOVED MEMBRANES, SPIDER SPRINGS, AND SUPPORT PLATE WITH CONCENTRIC RIDGES

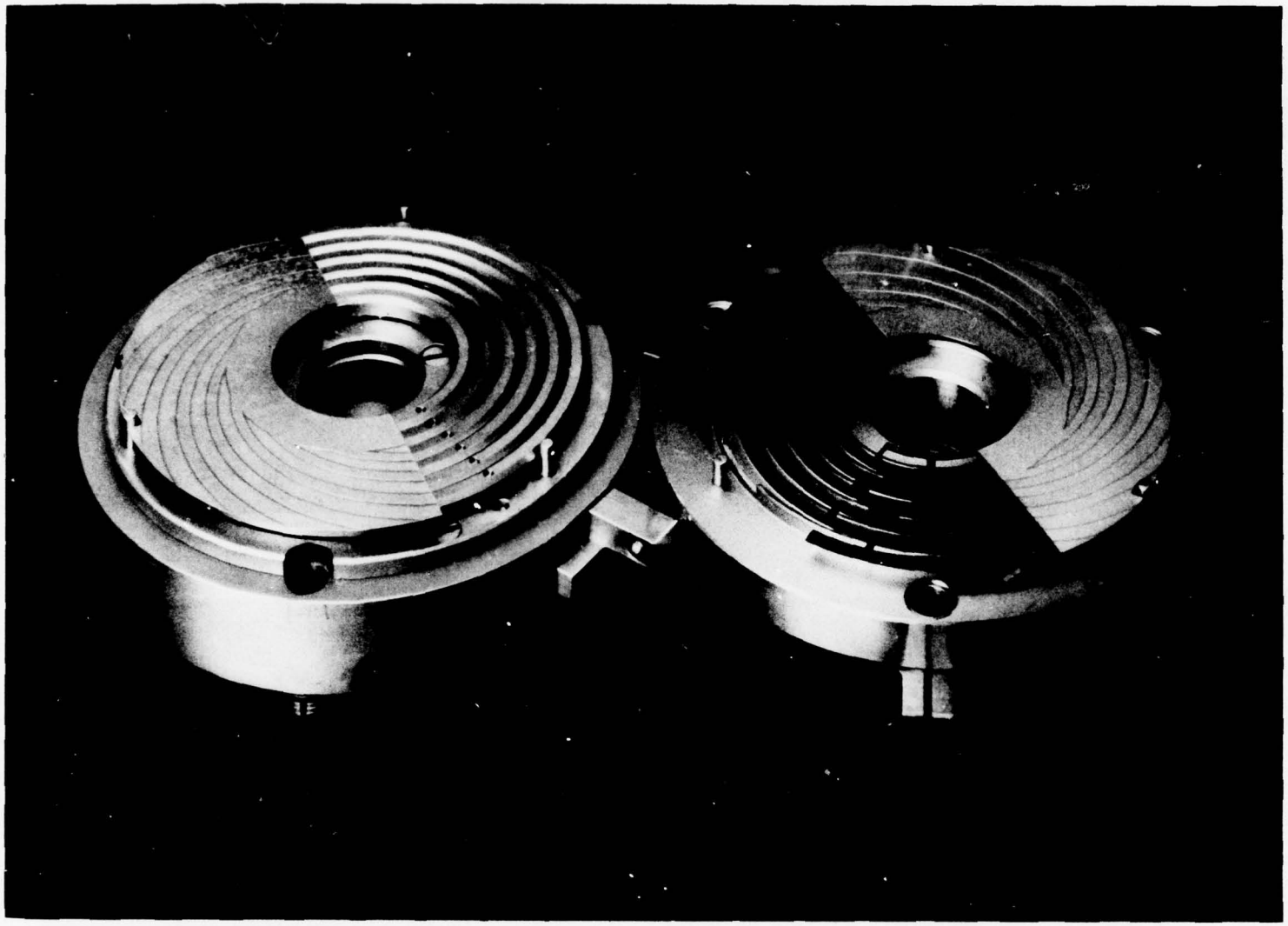

FIGURE 28. VIEW OF FLEXIBLE THRUST BEARINGS LLF-1T AND LLF-2T

The unavailability of design charts is certainly not a valid reason for discarding new and promising bearing concepts, especially if "mechanical breadboarding" and testing are relatively simple, and if reduction to practice, and not merely comparison of one numerical result with another, is the objective. No apology, therefore, is made for simplicity of approach, especially since highly satisfactory performance was demonstrated.

Two types of journal bearings were designed and tested. The first type, designated as LLF-1J, was described in reference [56], together with preliminary experiments with a very small, high-speed rotor (Rotor Weight W $\approx$ 1.48N; Bearings L x D $\approx$ 12.7 x 12.7 mm; Speed N $\approx$ 250,000 rpm).

The LLF-1J bearing consists basically of a plane foil, coiled and retained within a cartridge. The foil conforms only grossly to the cylindrical bore of the cartridge and to the journal within the annulus separating these rigid components. In addition to the clearance of the actual lubricating film between the journal and the inner surface of the coil, interstitial clearances exist between adjacent foil-layers and between the outer layer and the cartridge bore. The orbital motion of the journal causes both rubbing at contact points and squeezing of the fluid between adjacent layers of foil (and between the coil and the retainer bore). The solid and fluid friction have a damping and whirl-suppressing effect, which is absent in rigid-surface journal bearings.

The second bearing type, designated as LLF-2J, has a polygonally-bent, compliant support-section which is integral with the plane length of the foil. The corners of the quasi-polygonal part are bent to a prescribed radius over an arc which includes an angle $\alpha_v \gtrsim 2\pi/j$, where j is the number of sides or vertices of a regular polygon. This bearing, therefore, includes additional radial compliance which, although integral with the coiled section of plane foil, need not be of the same thickness.

The radial stiffness, which increases nonlinearly with displacement, allows for a light preload of the journal. The compliance is influenced by the thickness of the backing, the magnitude of the bending radius, the angle of bend at the vertices, and by the number of vertices. The whirl-suppressing characteristics of the bearing LLF-2J are probably superior to that of the LLF-1J type, and this may be attributed to greater capacity to dissipate the energy of vibration by friction and fluid damping.

The construction of both bearings is extremely uncomplicated, requiring no fixtures whatsoever for the LLF-1J type, and only a very simple bending tool for the quasi-polygonal support-backing of the LLF-2J bearing.

As stated in Section 2.0, the test rig was designed to allow for replacement of externally-pressurized journal bearings with foil bearings. The cartridges, in turn, were designed to accept either single, or dual foil-elements, each 20 mm wide. Furthermore, the same cartridges could be used for both types of journal foil-bearings.

4.1 Journal Bearing with Coiled, Plane Foils (Journal Foil-Bearing LLF-1J)

The retaining cartridges, which accepted foil elements of both journal-bearing types, are illustrated in the drawings of Figure 29. Both cartridges are separated by a land into two, recessed sections, each section accepting nominally 20 mm-wide foils. A dual purpose was served by this arrangement; the 30 mm-diameter journals could be supported on bearings respectively 20 and 40 mm long, and convenient access was provided to the journal for two pairs of capacitance probes $(X, Y)_{1, 2}$ through 6 mm holes in the separating land between foil recesses. The measured bores of these recesses had a mean diameter of 30.610 mm and the mean journal diameter was 29.870 mm, leaving a radial journal-to-cartridge clearance of approximately 0.37 mm. Note that the foils were retained on the inside by the separating land, and on the outside by 1.0 mm-wide shoulders. The mean bore-diameter at the inner land and at the shoulders was 30.160 mm, providing a journal clearance of approximately 0.22 mm. The foil-retaining cartridges were aligned within the rotor housing with the aid of a ground, 30.130 mm diameter arbor and six shims. The cartridges were then securely bolted to the housing, and doweled after removal of the arbor.

While the lateral retention of foils was ensured by the shoulders and the separating land, the outer terminal of each foil engaged the side of a longitudinal 2 x 5 mm groove closest to the vertical centerplane, Figure 29. The inner terminals of foils in each cartridge always pointed in a sense opposite to rotation, while the outer terminals pointed in a like sense. There was a tendency, therefore, for the foil to increase the clearance and to expand and tighten the coil against the cartridge bore, rather than to be dragged along with the journal, particularly when in contact with the latter. The groove prevented gross rotation of the coil and friction attenuated the reaction at the arrested end.

In the present experiments, copper-beryllium foils; $t_f = 51$ μm, and steel foils, $t_f = 54$ μm, were used, the choice of materials, although of importance, being subordinated to the fact that the difference of 3 μm in mean thickness provided convenient means of varying the clearance in bearings having coils with equal number of turns. Both coils had six turns, the innermost coil surfaces being coated to a thickness of approximately 5 μm with a commercially available (Dow-Corning Molykote 88), organically-bonded MoS_2 lubricant.

The reader will readily recognize, that even though a coil may be wound tightly against the bore of a retainer, the inner bearing-surface is not that of a regular, circular cylinder. In the present design, six foil-layers limited the extent of journal displacement almost everywhere, except in the vicinity of the longitudinal groove. The maximum radial clearance thus defined was approximately 60 μm for the copper-beryllium foil-bearing, and approximately 40 μm for the steel-foil journal-bearing. This maximum "clearance" is denoted as $\bar{c}$ throughout the text.

A view of a foil telescoped out of a retainer, with a black stripe painted along one edge for illustrative purposes, is shown in Figure 30. The second view in Figure 30 shows

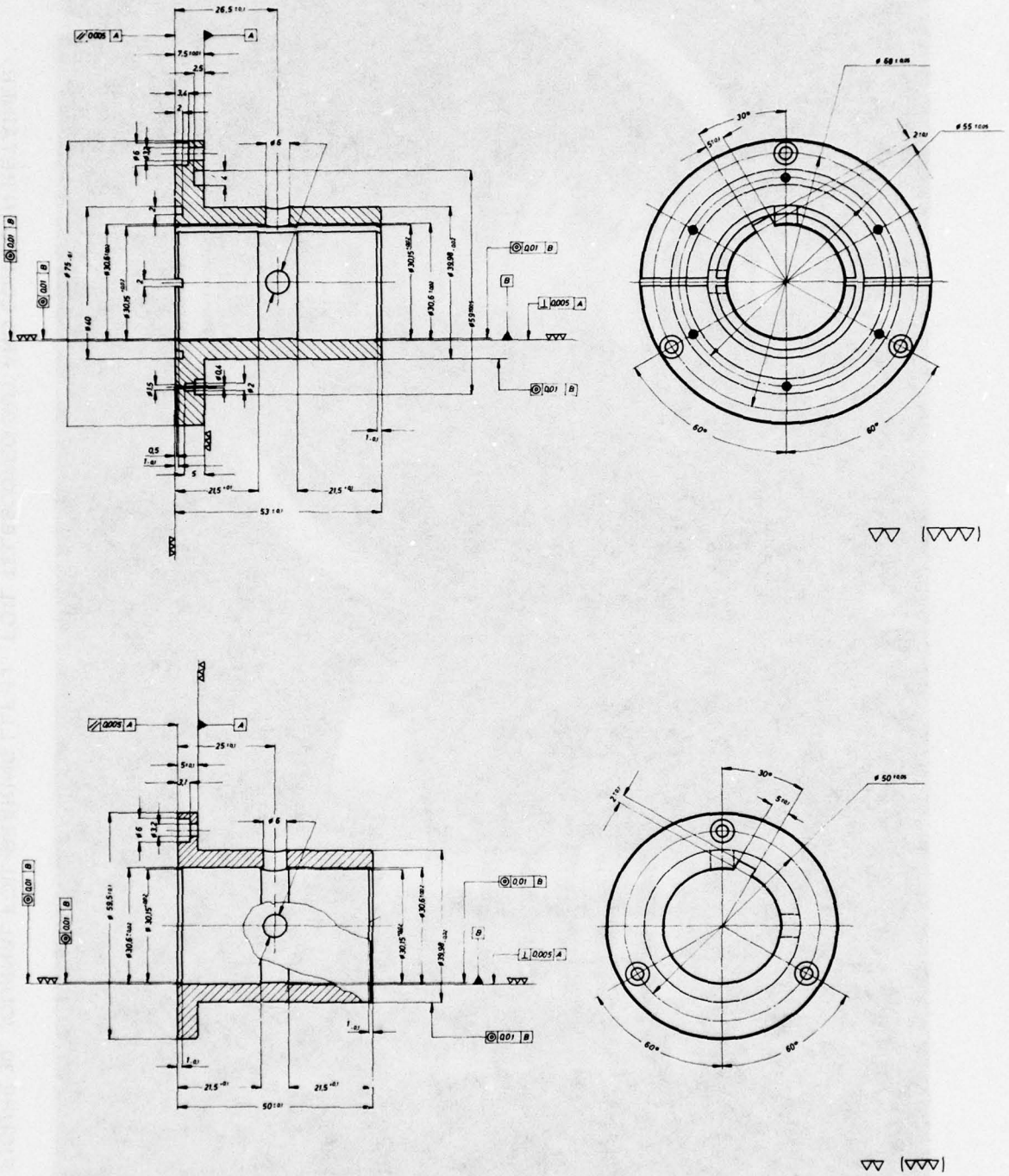

FIGURE 29. CARTRIDGES OF JOURNAL FOIL-BEARINGS

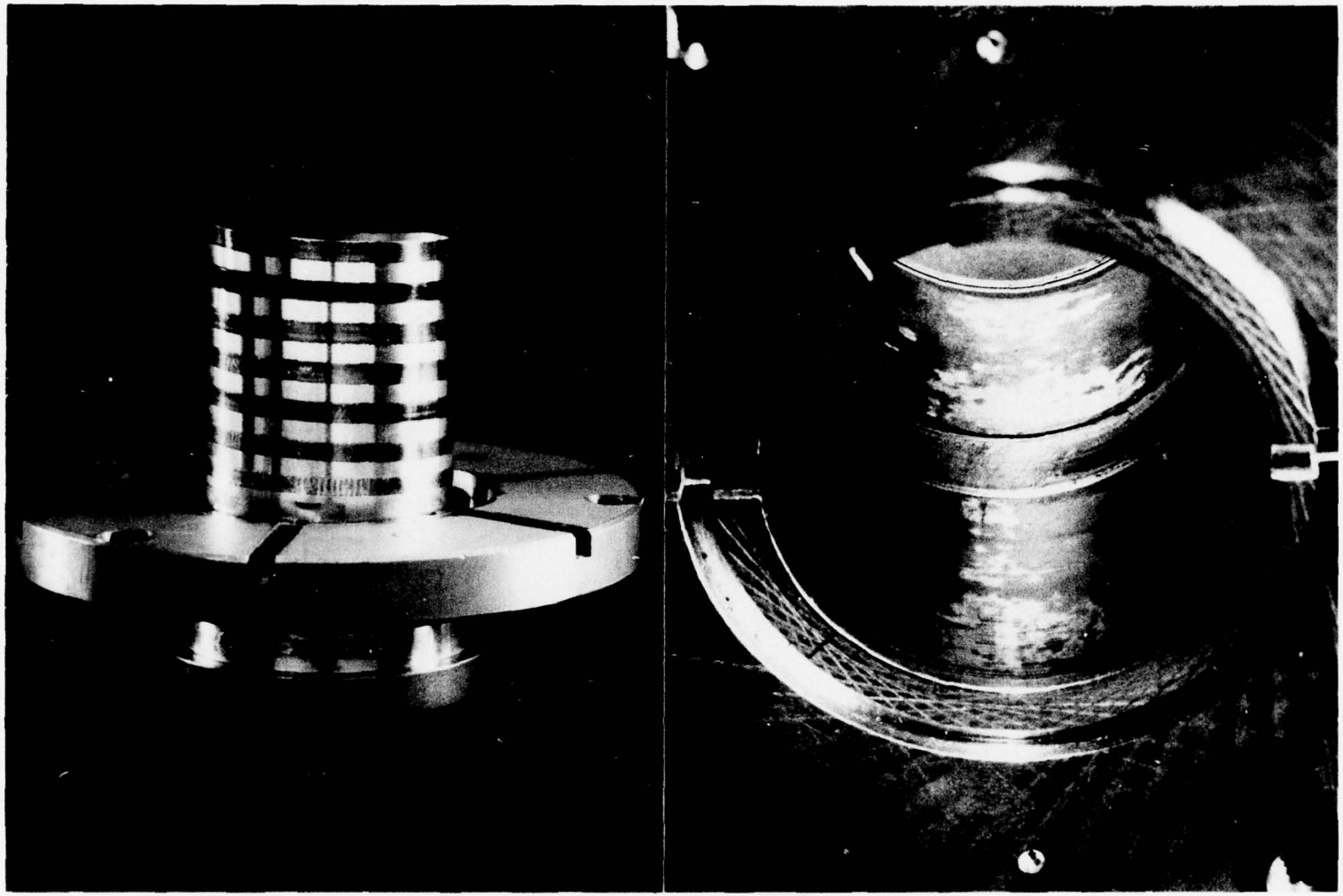

FIGURE 30. JOURNAL FOIL-BEARING LLF-1J. - FOIL TELESCOPED OUT AND COILED IN RETAINER

two foils within the recessed bores of a retaining cartridge. The retainer corresponds to the turbine-end journal bearing (Figure 29) and is integral with the pressurized, inboard pad adjacent to the turbine, Figure 1. The end of the longitudinal slot is discernible in the upper part of the bore, and the foil-retaining shoulders and inner land can be clearly distinguished. The coated foils in this photograph have been used for extended periods of time under highly adverse conditions, when setting up for and photographing oscilloscope displays. This involved operation with excessively large unbalance, and dwelling at speeds corresponding to the largest trajectories, as well as multiple starts and stops. The coating is seen to be partly worn, but the burnished foil showed no sign of distress and continued to be used after the photograph was taken.

4.2 Journal Bearings with Polygonally-Bent Section, Integral with Foil Element (Journal Foil-Bearing LLF-2J)

As stated in the preceding section, identical retaining cartridges were used for both types of journal bearings, but the LLF-2J bearing had fewer coils, in order to accommodate the polygonally bent backing within the same annular space between the journal and the cartridge bore.

The tests described in this report relate to bearings with octagonally bent supports, but coils integral with pentagonally-bent sections were also successfully operated. The method of retention of the foil element by means of a longitudinal groove was identical. The fabrication of the quasi-polygonal backing was very simple and is described below in considerable detail.

A fixture is made, which consists of a simple block and clamping device. The bending block has a cross-section of an equilateral triangle, and the initially sharp edges are rounded to radii of 0.50, 0.75 and 1.00 mm. Two dowel pins on each face of the block locate one foil edge perpendicularly to the bending edge. A relatively thin clamping plate, with a long taper along the bending edge of the block, fits over the dowels and holds the foil strip. The foil is bent over the radiused edge with a flat bar to a desired angle, indicated by the setting of a pointer on the side of the bending block. Accurate indexing is accomplished by equally simple means. Before releasing the foil strip to advance it to the next bending position, a spacer, equal in width to the length of the side of the polygon, is placed against the rear edge of the clamping plate. A small cylindrical stop, actuated by a suction plunger, is placed in contact with the spacer and made to adhere to the foil surface. The measuring spacer is then removed, the clamping plate released, and the foil advanced and clamped again prior to the next bending operation. The time required to make a foil element by this simple and purely manual method is of the order of ten minutes. Details of the LLF-2J bearing and bending tool are illustrated in Figure 31.

There are several advantages associated with this design, in addition to good operational characteristics. The plane and polygonal sections are made from a single ribbon and the polygonally-bent section can be both preceded and succeeded by a plane strip, to provide an outer, as well as an inner coil. Furthermore, the thickness of the foil

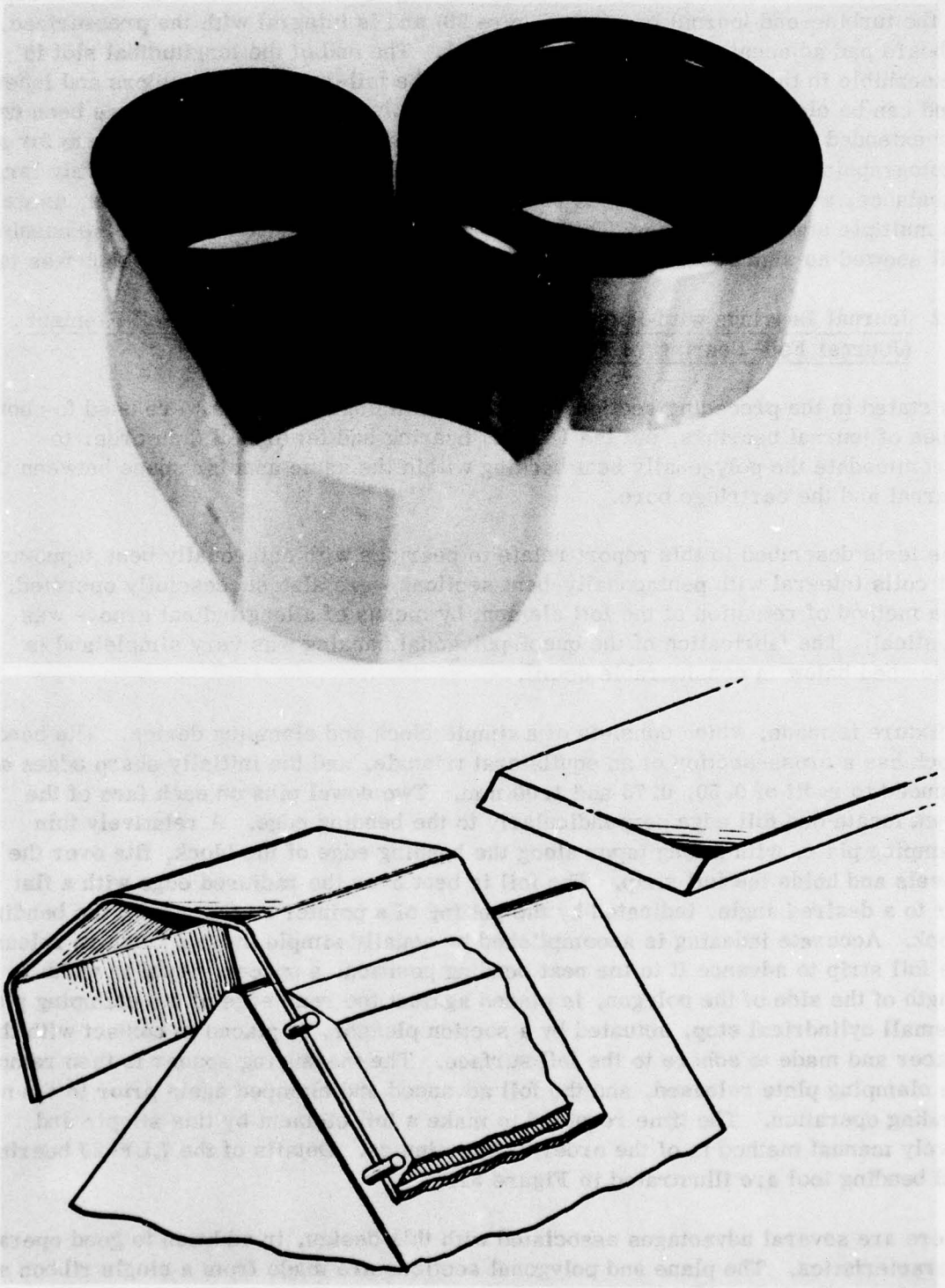

FIGURE 31. JOURNAL FOIL-BEARING LLF-2J.-FOIL ELEMENT WITH QUASI-OCTAGONAL SECTION AND SCHEMATIC DIAGRAM OF BENDING TOOL

can be increased by plating (or coating), or reduced by etching, thus providing another degree of freedom in the variation of stiffness and the determination of clearance. Lastly, there is a rather important and subtle advantage associated with this type of resilient support. When the foil element is assembled with the cartridge and the journal, the sides joining the radiused vertices conform grossly to the journal diameter, while the radiused vertices spread open. The crests of the vertices engage the retainer bore and the relatively sharp curvature makes a slow, S-like transition to that of the journal. These vertices of the polygon-like backing provide spring elements with progressively "hardening" characteristics. If and when plastic deformation occurs, it is gradual and does not result in a buckling failure associated with corrugated backings of foil bearings described in reference [53]. Nor is the radiused vertex prone to develop cracks, a mode of failure associated with the sharply creased backing referred to briefly in reference [56].

When the foil is bent to a more acute angle than would be included between sides of a corresponding regular polygon, and a dummy journal is inserted with the aid of a tapered nosepiece, the preload can be reduced by simultaneously rotating the cartridge and pressing it against the journal. A certain amount of plastic deformation can thus be effected in the vertex regions and the preload reduced in this manner. The same result can be attained by forcing an oversize dummy-journal into the bearing.

The "mechanical breadboarding" of the LLF-2J bearing was accomplished by simple means. Several dummy journals were machined to dimensions in a narrow range, estimated to include the diameter of the journal when ground to size. The fitting was complemented by progressively reducing the length of the foil by small amounts, thereby increasing the effective clearance. The only other guiding criteria, short of actual test runs, were the order of magnitude of the breakaway friction torque and the approximate value of deflection for an arbitrarily small radial force.

With fixed cartridge bores of 30.61 mm and ground journal diameters of 29.87 mm, the octagonally bent support (0.5 mm radius at vertex, 54 μm steel foil, and 5 μm MoS_2 coating on innermost surface of foil) was integral with approximately 2 1/4 turns of plane foil, the inner foil-end terminating within $+2^\circ$ of the horizontal (X_1X_2)-plane.

The journal foil-bearing with the octagonal backing performed faultlessly, with both double and single foil-elements in each cartridge.

5.0 TESTING OF FLEXIBLE THRUST BEARINGS

The rotor of the experimental test-rig, Figure 1, was supported initially by externally pressurized bearings. Several types of pressurized journal-bearings were designed and fabricated, with the objective of attaining as high a speed as possible before the onset of rotor instability. A range of supply-pressure was explored with each type, with equal and unequal settings for each bearing. The diameters of supply orifices were also varied. The results of these systematic and careful trials and variations of parameters were frequently inconsistent with theoretically predicted effects on stability [61].

The externally pressurized bearings were intended merely as auxiliaries in the testing of flexible thrust bearings, and the objective was to establish conditions conducive to good experimentation and data acquisition (alignment, balancing, well defined axis of rotation and so forth). The onset of instability varied within relatively narrow speed-limits for all bearings and pressure settings, and the maximum speed that could be attained was approximately $N_c \approx 33,000$ rpm.

When preliminary runs were first attempted with a flexible thrust bearing, it was hoped that a ten percent safety margin would suffice and that data could be recorded up to N = 30,000 rpm. It was soon discovered, however, that the thrust bearing had an unstabilizing effect and lowered the stability threshold with increasing axial load. It was decided, therefore, to limit the initial tests to speeds not exceeding 27,000 rpm. *

Pressurized journal bearings were not, of course, the subject of this investigation, but those readers concerned with dynamics of rotors supported by pressurized gas bearings may find the relevant data useful. Thus the L x D = 20 x 30 mm bearings had a 150 mm span, and the weight of the rotor (aluminum runner and turbine; steel shaft) was W = 18.5 N, with transverse and polar radii of gyration r_t = 89.8 mm and r_p = 13.1 mm, and the center of mass located at l = 91 mm from the center plane of the bearing adjacent to the 100 mm-diameter runner, Figure 1.

Various aspects of experimental apparatus, instrumentation and measurement were described and discussed in Sections 2.1 through 2.3, and the reader may find it useful to refer to their content in regard to data presented in the remainder of this report. The preamble which follows is directed at engineers concerned with development and applications, and to analysts who lack familiarity with the physical prototype they may wish to model mathematically.

*The influence of thrust bearings on the motion of rotors is frequently, and often unjustifiably neglected.

It is quite easy to obtain foil stock of very uniform thickness, but very difficult to secure flat sheets. Rolled stock generally has residual curvature, and a 0.20 mm-gauge sheet may deviate from flatness by as much as two or three thicknesses within an area bounded by a circle of 50 mm radius, even if carefully selected. In addition to overall cylindricity, a sheet of foil is characterized by major and minor undulations. Moreover, it has residual stresses and directional properties. Distortions increase when residual stresses are relieved in etching the annular contour of a membrane, and this distortion is magnified further when the spiral grooves are etched on one side. Finally, it is difficult to obtain commercially available foils completely free of local indentations and creases.

Both copper-beryllium and Inconel membranes were used. These metals are precipitation hardening alloys, and the writer has attempted to flatten membranes, clamped between lapped surfaces of massive, circular plates and subjected to various heat cycles in a furnace. Results were not particularly encouraging, but a few very flat Inconel X-750 specimen were obtained. Relatively flat and undistorted sheets and finished membranes can undoubtedly be produced by suitable rolling and flattening operations, in conjunction with appropriate heat treatment, but neither time nor funds allowed for complementary research of material processing.

It is surprising, therefore, that more than satisfactory results were obtained with relatively imperfect, off-the-shelf foils, and that reduction from concept to practice was achieved without elaborate means. While initial flatness of membranes improves performance, it is quite apparent that pressure need not be high to reduce waviness to manageable proportions. In general, therefore, the membranes tend to conform to the runner, except at low load and in the low-pressure zone adjacent to the inner and outer bearing perimeters. *

In the case of the spider spring, the initial state of the foil and the distortion after etching are far less problematic, because this reticulated member (see Figures 24, 26 and 27) is very pliable and conformable.

The writer has reason to believe, that with increasing load both membrane supports produce a sensibly parallel clearance, except at the outer and (to a lesser extent) the inner perimeter. In these regions, an asymptotic wear-in process occurs, to an extent governed by initial membrane uneveness.

*Simple design modifications performed after completion of this investigation provide additional control of initial distortion in these zones.

5.1 Test Results of Flexible Thrust Bearing LLF-1T to Speeds of 27,000 rpm

The tests involved determinations of the variation of the friction moment M with the load F, and of F with the clearance $\tilde{h}$, both at constant speed N. (The reader is referred at this point to Section 2.3 for a review of the definition of $\tilde{h}$ and the method of measurement.) Results of two additional tests are also included in this section, namely the determinations of the variation of load with speed at constant clearance, and at constant friction-moment.

The results of the first two runs attempted in the course of this investigation are presented in Figure 32. At this point of time, the writer did not know if this thrust bearing would operate at any load, much less what thrust it would be capable of supporting. The friction moment, of course, would be a good "barometer of impending danger". During the first run, at 400 rps, the load was very gradually increased to a relatively modest value of 67.4 newtons, after the rotor had been brought up to speed. At this point, the observed rate of increase of the friction moment was considered sufficiently high to interrupt the test to examine the coating of the copper-beryllium membrane (Dow-Corning Molykote 88, an organically bonded MoS_2 lubricant, applied very evenly to a thickness $\approx 5\ \mu$m by spraying the membrane mounted on a revolving disc).

The membrane showed no sign of wear, except at the perimeter corresponding to the edge of the runner. Here the sharp edge of the Cr_2O_3-coated runner ground in twelve narrow V-notches, approximately equally spaced on the twelve membrane ridges. This wear pattern was characteristic, but was much less pronounced with initially-flat membranes.

A second run, at 350 rps, produced a similar curve, shown in Figure 32. The load was raised to 72.2 newtons, and then in another step to 77.0 newtons, whereupon failure occurred suddenly. The cause of failure appeared to be due to buckling, but the exact mechanism was not clear. Metal transfer to the runner occurred, and this required resurfacing and rebalancing. A new copper-beryllium membrane was coated and installed, and testing was resumed.

The unusual results obtained in the course of the next two runs, at 450 and 400 rps, are illustrated in Figure 33. The curves are characterized by distinct inflections, indicating that the friction moment actually decreased with increasing load. In the relatively broad range of $25 \lesssim F \lesssim 55$ N, the friction moment would increase suddenly, unless the load was applied very gradually. This indicated a bistable condition, a behavior akin to that observed with an oil can, or a toggle switch. It was possible, however, to traverse the doldrums of the inflection region and to increase the load to 81.9 newtons at N = 450 rps, the highest load realized thus far. Examination of the membrane showed no signs of wear, except notches near the runner edge and a slight burnish at the inner periphery. Testing was resumed at a lower speed of 400 rps and, as can be seen from Figure 33, the trend was identical. The two curves in Figure 33 are very similar,

TABLE 1

LOAD	FRICTION MOMENT						CLEARANCE				
F(N)	M (cm.N)						$\bar{h}$ (μm)				
FIGURE →	32		33		36		35			37	
CURVE →	▽	○	▽	○	○	▽	○	▽	-¦-	○	▽
4.82	0.572	0.540	0.458	0.523	0.556	0.572	31.0	40.0	35.5	37.0	32.5
9.63	0.678	0.629	0.654	0.695	0.670	0.687	57.5	58.0	57.0	54.0	57.5
14.4	0.768	0.711	0.899	0.858	0.744	0.752	60.0	60.5	62.5	56.5	56.5
19.3	0.818	0.777	0.989	0.940	0.760	0.768	52.5	49.0	53.5	51.0	51.5
24.1	0.883	0.834	1.02	0.972	0.777	0.785	46.5	45.5	48.0	45.5	46.5
28.9	0.924	0.883	0.989	0.948	0.793	0.793	41.0	40.5	42.0	40.0	39.5
33.7	0.981	0.924	0.981	0.924	0.818	0.826	37.0	37.0	39.0	35.5	36.5
38.5	1.03	0.973	0.948	0.899	0.842	0.850	34.0	34.5	34.0	33.5	34.0
43.3	1.11	1.03	0.973	0.907	0.875	0.883	31.0	32.0	31.5	30.5	31.0
48.2	1.17	1.09	0.981	0.924	0.899	0.916	28.5	30.0	30.0	28.5	28.0
53.0	1.25	1.17	1.02	0.989	0.948	0.956	27.0	28.0	28.0	26.5	26.5
57.8	1.35	1.23	1.13	1.10	0.981	0.989	25.0	26.5	27.0	25.0	25.5
62.6	1.45	1.29	1.21	1.18	1.01	1.01	24.0	25.5	25.5	23.5	24.0
67.4	1.60	1.39	1.32	1.28	1.05	1.05	23.0	23.5	24.5	22.0	23.0
72.2	—	1.55	1.47	1.43	1.09	1.09	21.5	23.0	23.5	21.5	22.0
77.0	—	*	1.68	1.64	1.13	1.12	21.0	22.0	22.5	21.0	21.5
81.9	—	—	1.99	1.94	1.16	1.16	20.5	21.0	22.0	20.0	20.5
86.7	—	—	—	*	1.23	1.21	—	20.5	21.0	19.5	19.5
89.1	—	—	—	—	—	—	—	—	—	—	—
91.5	—	—	—	—	1.28	1.25	—	20.0	20.5	19.0	18.5
96.3	—	—	—	—	1.31	1.30	—	—	19.5	18.0	18.0
101.0	—	—	—	—	1.36	1.32	—	—	18.5	17.5	17.5
N (rps) →	400	350	450	400	450	450	450	450	450	450	450

FIG.'S 32 AND 33; ○ MEMBRANE FAILURE (*) CAUSED BY BUCKLING DUE TO CONSTRAINT OF THERMAL EXPANSION BY ANTI-ROTATION PINS

FIG. 35; ○ MEMBRANE SLOT DEPTH INCREASED TO PERMIT EXPANSION UNCONSTRAINED BY PINS
▽ TEST REPEATED WITH FIRST LOAD INCREMENT
-¦- TEST REPEATED WITH SECOND LOAD INCREMENT

FIG.'S 36 AND 37; ○ WITHOUT WARMUP OR DWELL AT ANY LOAD
▽ WITH 30 MINUTES WARMUP AT MAXIMUM LOAD AND 5 MINUTES DWELL AT EACH LOAD DECREMENT

Cu-Be, t_m = 230 μm; STEEL PLATE-SPRINGS, t_s = 130 μm

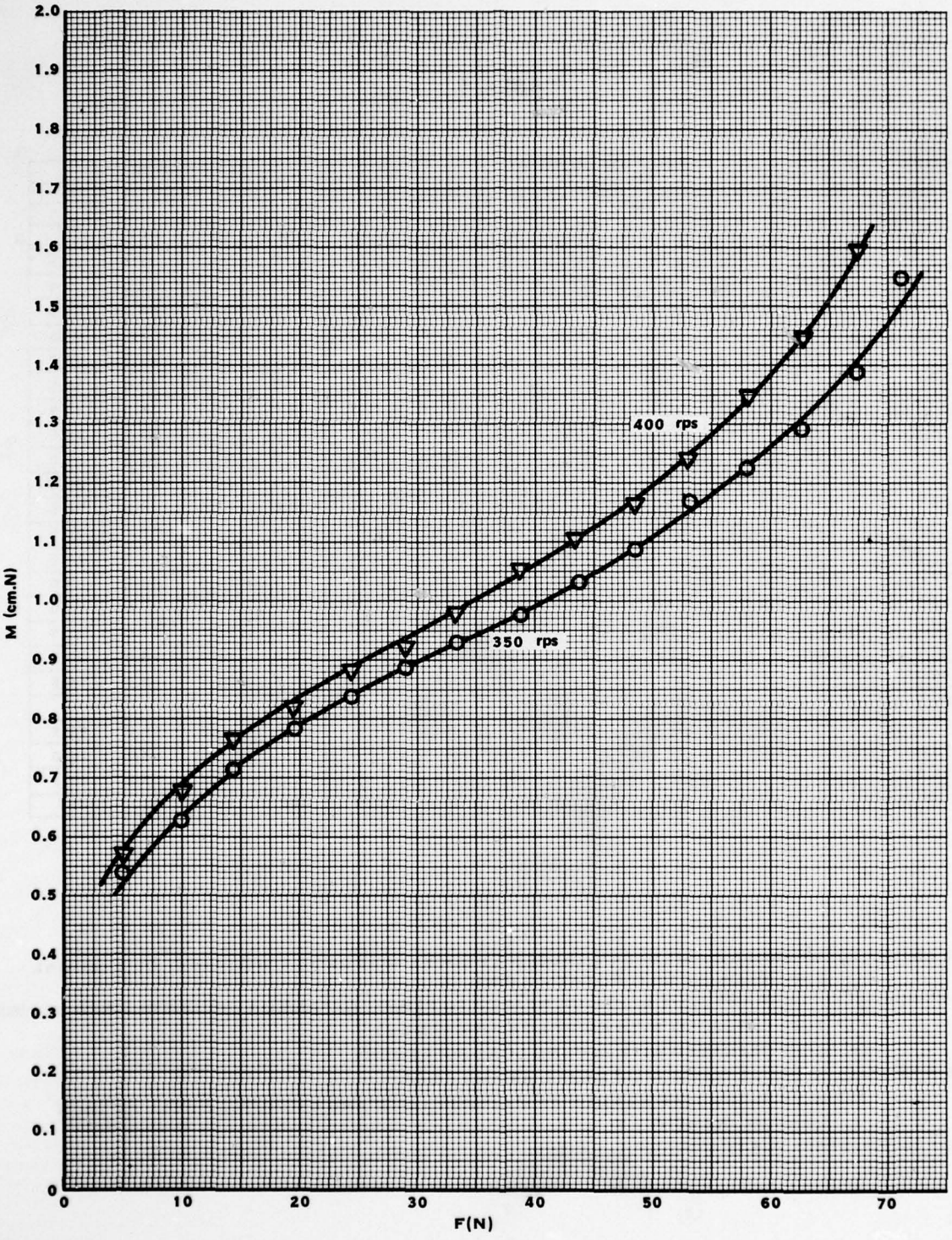

FIGURE 32. FRICTION MOMENT VERSUS LOAD AT N = 350rps AND N = 400rps.- INITIAL RESULTS WITH FLEXIBLE THRUST BEARING LLF-1T (SEE DATA AND REMARKS OF TABLE 1, SECTION 5.1)

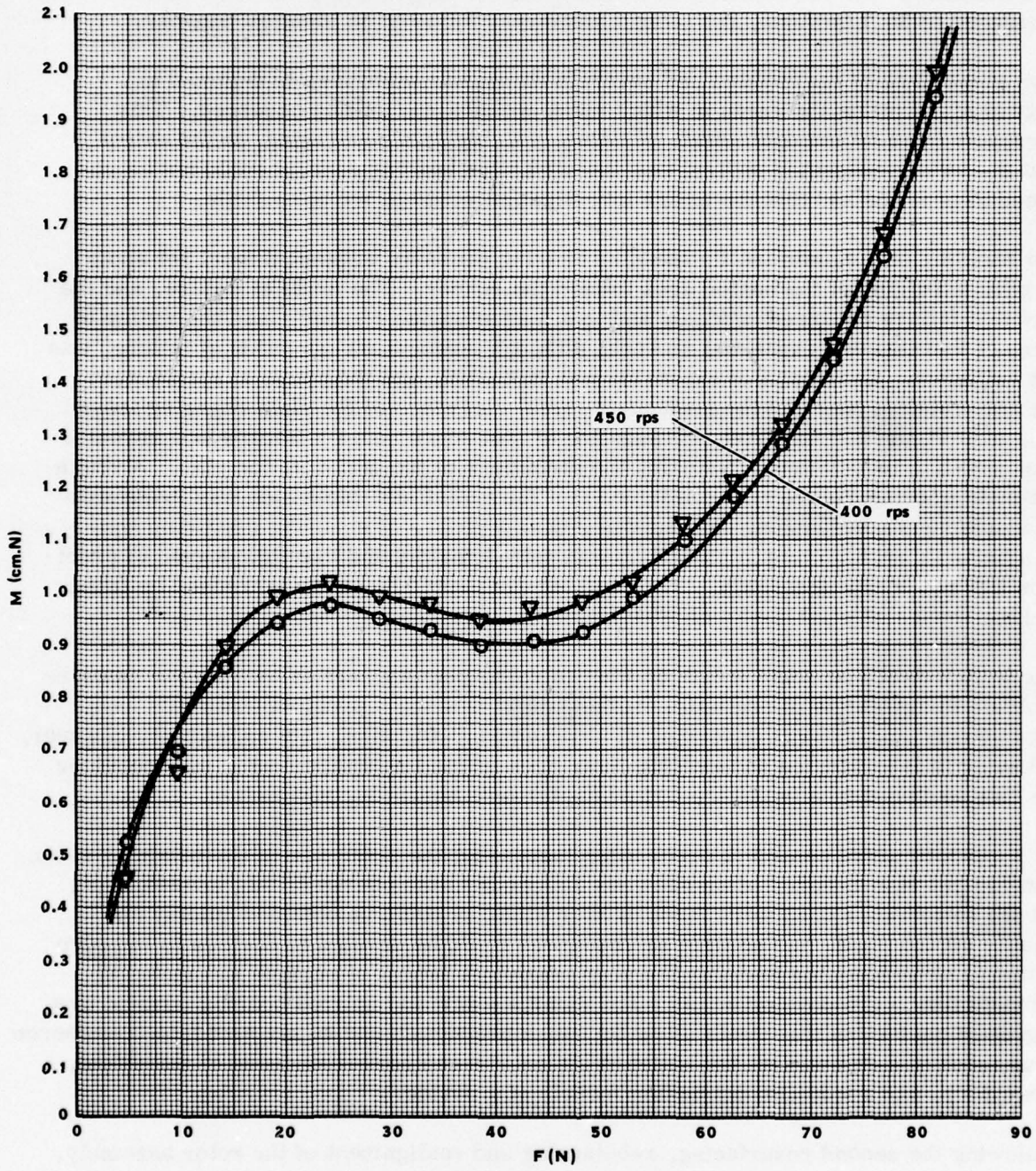

FIGURE 33. FRICTION MOMENT VERSUS LOAD AT N = 400rps AND N = 450rps.- EFFECT OF CONSTRAINT ON EXPANSION OF MEMBRANE. INITIAL RESULTS WITH FLEXIBLE THRUST BEARING LLF-1T (SEE DATA AND REMARKS OF TABLE 1, SECTION 5.1)

except for slightly lower values of friction at equal load and lower speed. The testing was resumed, with the objective of attaining higher load-values, but when the load was increased to 86.7 newtons, the second membrane failed in an identical manner.

The appearance of the buckled and severely damaged membranes is depicted in Figure 34, showing the areas in which metal welding and galling occurred. This unexpected and catastrophic mode of failure was highly discouraging, to the extent that the writer suspected at first that the attractive bearing concept could not be reduced to practice and that the entire investigation would prove to be futile.

But buckling of a membrane flattened by bearing pressure suggested local hot spots to initiate bulging of the heated area toward the runner. The mode of failure, and the fact that failure occurred suddenly and in a discontinuous manner, lead the writer to suspect that thermal expansion as such, although a necessary condition of failure, was not sufficient. Constraint of expansion was indicated, and the prime suspects were the anti-rotation pins and the inadequate radial clearance of the slots engaging these pins (see Figure 12). Indeed, examination of slot edges under a microscope revealed crescent-like indentations, matching the diameters of the anti-rotation pins. A rough estimate of temperature rise confirmed that the radial slot-clearance was inadequate to accommodate expansion, and that the initial objective of ensuring maximum concentricity through minimum clearance was self-defeating and that this degree of precision was not really necessary. The depth of slots could be easily increased by filing, and the source of trouble was eliminated.

The writer dwells at some length on what in retrospect appears to be a rather mundane problem to architects of realistic, mathematical models; a problem that could have been avoided and thus not deserving of "holmensian" attention. My colleagues, however, tinkering in laboratories and keeping their eyes trained on instruments, may consider the "watsonian" narrative of the writer useful and, hopefully, instructive.

This type of failure ceased to occur after increasing the clearance of the retaining slots. Random but rare failures of membranes did occur in the course of this investigation, but the membranes used were made of such stock as could be obtained quickly and readily off the shelf, and no time or resources could be devoted to devices to improve flatness, or to examine in detail the very important aspect of surface and material compatibility. (To develop within a few months a new and untried bearing concept to a degree of perfection that would allow for mass production and highly profitable commerce is as much of a delusion as the belief of the one-to-one correspondence of analytical, laboratory, and ready-for-marketing models of a device.)

Following the second resurfacing, rebalancing and realignment of the rotor assembly, testing was resumed again with a third copper-beryllium membrane, and measurements of variation of friction moment with load, and of load with clearance, were recorded at $N = 450$ rps. With greater confidence gained in operation at loads to approximately 82 newtons, the load was progressively increased to a value of $F = 101$ newtons (22.7 lb).

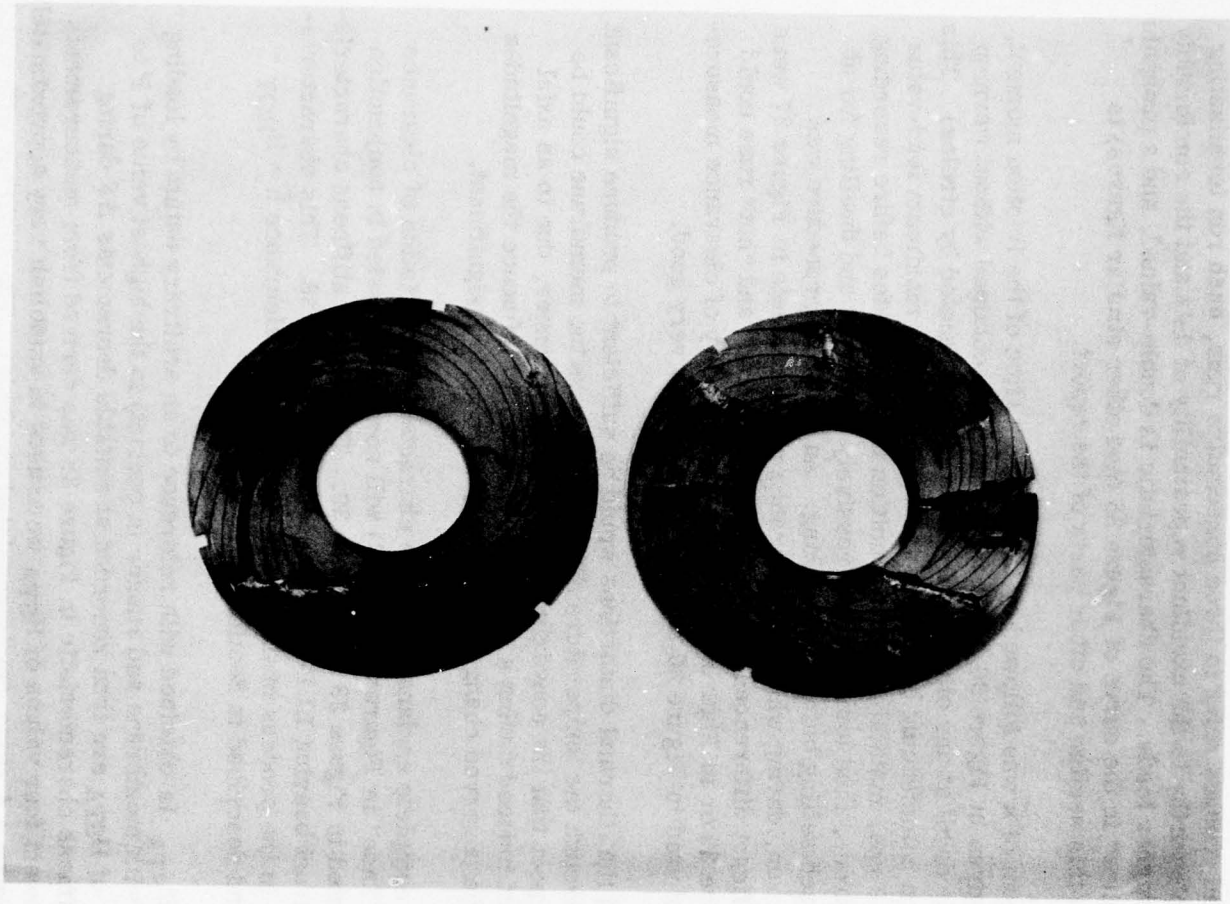

FIGURE 34. VIEW OF SPIRALLY GROOVED MEMBRANES FAILED THROUGH CONSTRAINT OF THERMAL EXPANSION BY ANTI-ROTATION PINS

This corresponded to a unit-load $F/\pi\,(R_o^2 - R_i^2) = 2.39\ N/cm^2$ (3.47 lb/in^2), at N = 27,000 rpm, for a bearing of 80 mm (3.15 in) outside and of 32 mm (1.26 in) inside-diameter.

The variation of load with clearance is shown in Figure 35, and the points denoted by circles, triangles and crosses refer to three consecutive runs, each run terminating at a higher load. Noteworthy is the excellent repeatability of data and the comfortably large values of $\tilde{h}$ at higher loads. The characteristic is double-valued, and a probable explanation of the "knee" in the curve of Figure 35 (and other similar figures) is offered elsewhere in this section and other parts of the report.

The first measurement of $\tilde{h}$ was followed by the determination of the friction moment, and the results are given in Figure 36. The first data were obtained without warmup at maximum load, or dwell at any other load-setting (points denoted by circles). This was followed by a run commencing by loading the bearing to the maximum load-value of 101 newtons at 450 rps, maintaining this condition for 30 minutes before recording the corresponding torque, then lowering progressively the thrust and dwelling for at least 5 minutes at each setting before data-taking. An identical procedure was followed in a repeat run, during which the clearance measurements in Figure 37 were recorded. No significant differences between results of "cold" and "hot" runs could be observed in Figure 36 or in Figure 37, and the repeatability of clearance measurements of five runs plotted in Figure 35 and in Figure 37 was very good.

The writer expected that thermal distortions would be sufficient to produce significant differences. Even though the temperature difference across the membrane could be small, one might expect that the convexity of the aluminum runner, due to an axial temperature gradient induced during a 30 minute run, would influence the magnitudes of both $\tilde{h}$ and M. The observed changes, however, were quite insignificant.

The cause, if not a complete explanation of the characteristic variation of clearance $\tilde{h}$ at low loads (the "knee" in Figures 35 and 37) will now be suggested in conjunction with the data presented in Figure 38 and Figure 39. The overall stiffness characteristic of the flexible thrust bearing LLF-1T is presented in Figure 38. This characteristic may be obtained in the process of the determination of the clearance $\tilde{h} = H_{ROT} - H_{STA}$, as defined and described in Section 2.3.

The displacement H_{STA} is obtained with reference to an arbitrary datum by loading the thrust bearing (with membrane and runner in contact) to the highest value of F to be applied. Values of H_{STA} are then recorded at suitable decrements ΔF during unloading. The stiffness characteristic in Figure 38 was derived from measurements of H_{STA}, and the lowest four values of H_{STA} were used to establish very approximately the origin of the F versus δ curve (an extrapolated parabola). The accuracy with which the origin is established and the precise value of δ are not particularly important in themselves, but to be noted is the nonlinearity of the stiffness characteristic ($dF/d\delta \neq$ constant) for values of $F \lesssim 50$ N.

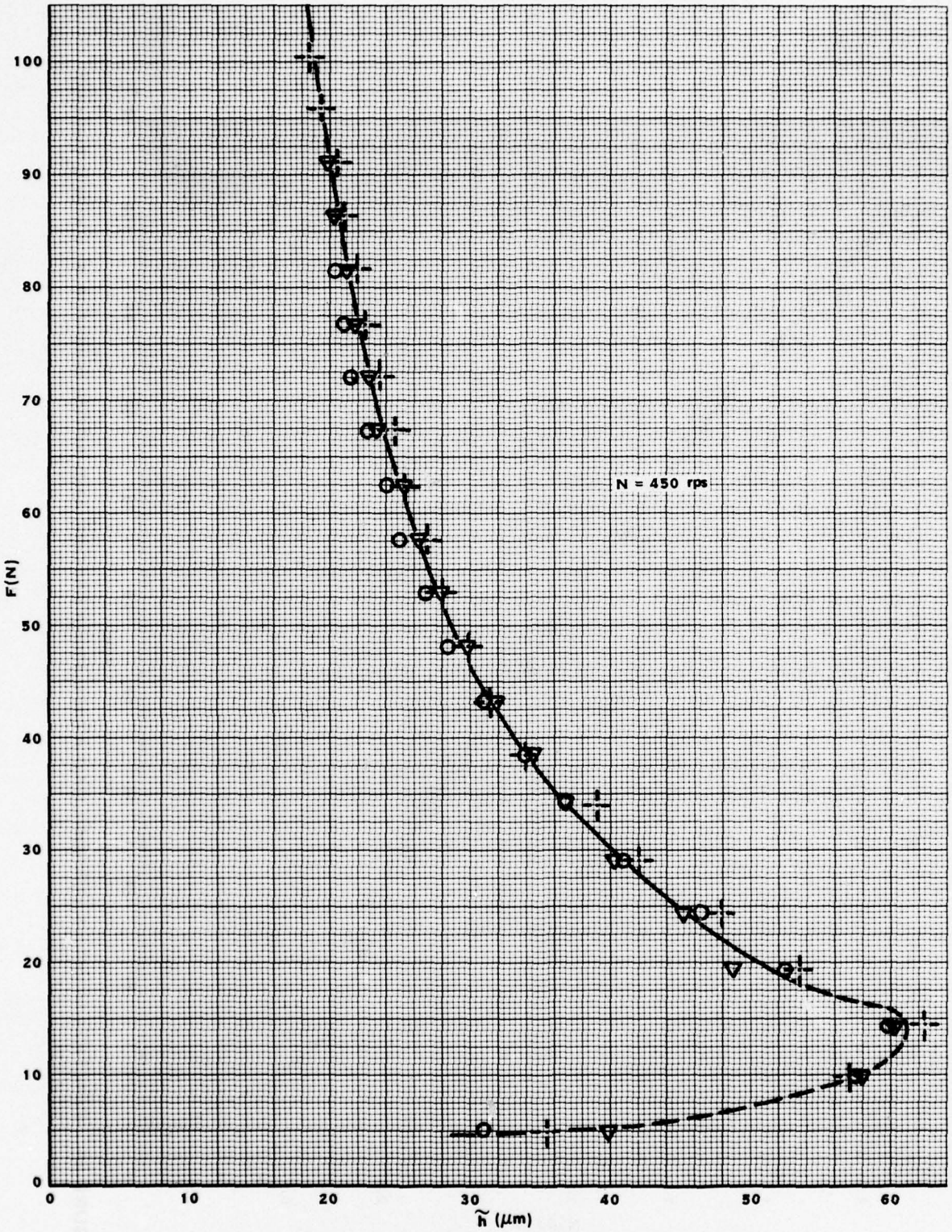

FIGURE 35. LOAD VERSUS CLEARANCE AT N = 450rps.-FLEXIBLE THRUST BEARING LLF-1T. POINTS DENOTED BY CIRCLES, TRIANGLES AND CROSSES REFER TO RUNS REPEATED UNDER NEARLY IDENTICAL CONDITIONS AND WITH PROGRESSIVE INCREASE OF LOAD (SEE DATA AND REMARKS OF TABLE 1, SECTION 5.1)

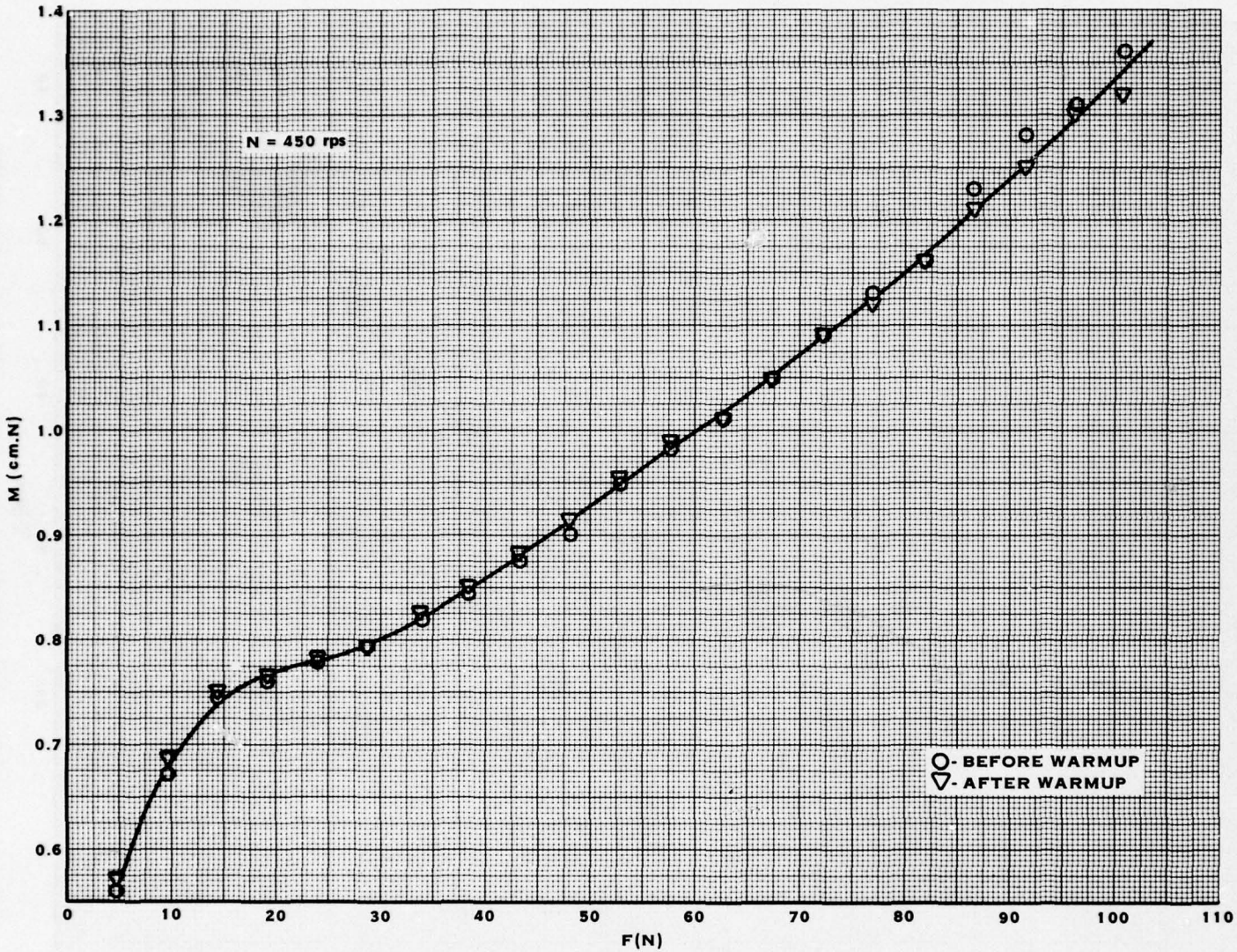

FIGURE 36. FRICTION MOMENT VERSUS LOAD AT N = 450rps BEFORE AND AFTER WARMUP.-FLEXIBLE THRUST BEARING LLF-1T

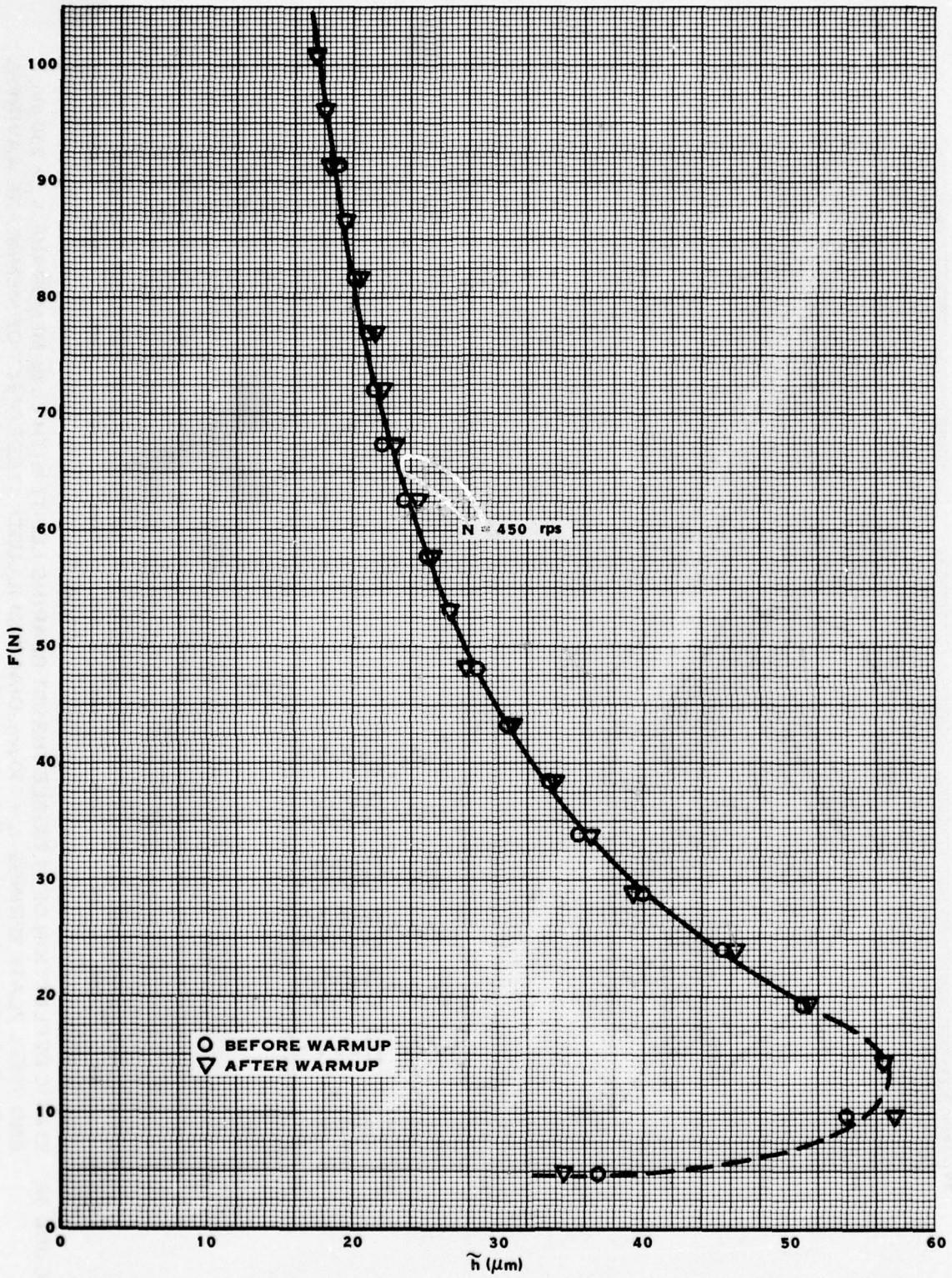

FIGURE 37. LOAD VERSUS CLEARANCE AT 450rps BEFORE AND AFTER WARMUP.-FLEXIBLE THRUST BEARING LLF-1T

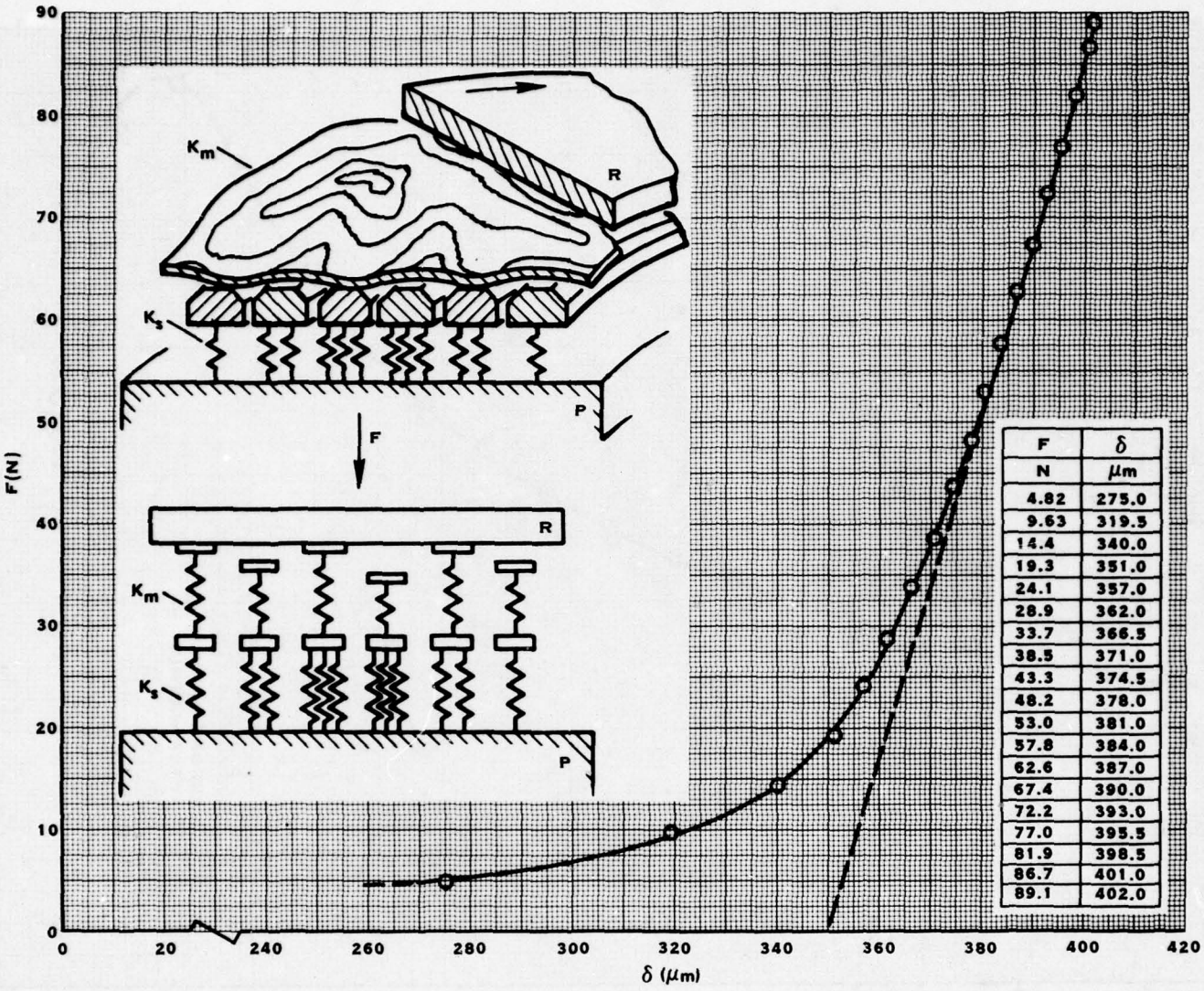

F	δ
N	μm
4.82	275.0
9.63	319.5
14.4	340.0
19.3	351.0
24.1	357.0
28.9	362.0
33.7	366.5
38.5	371.0
43.3	374.5
48.2	378.0
53.0	381.0
57.8	384.0
62.6	387.0
67.4	390.0
72.2	393.0
77.0	395.5
81.9	398.5
86.7	401.0
89.1	402.0

FIGURE 38. STATIC DEFLECTION OF FLEXIBLE THRUST BEARING LLF-1T WITH Cu-Be MEMBRANE, t_m = 230 μm, AND STEEL PLATE SPRINGS, t_s = 130 μm.-DIAGRAM ILLUSTRATES EFFECT OF MEMBRANE WAVINESS AND DEVIATIONS FROM FLATNESS ON NONLINEARITY OF STIFFNESS

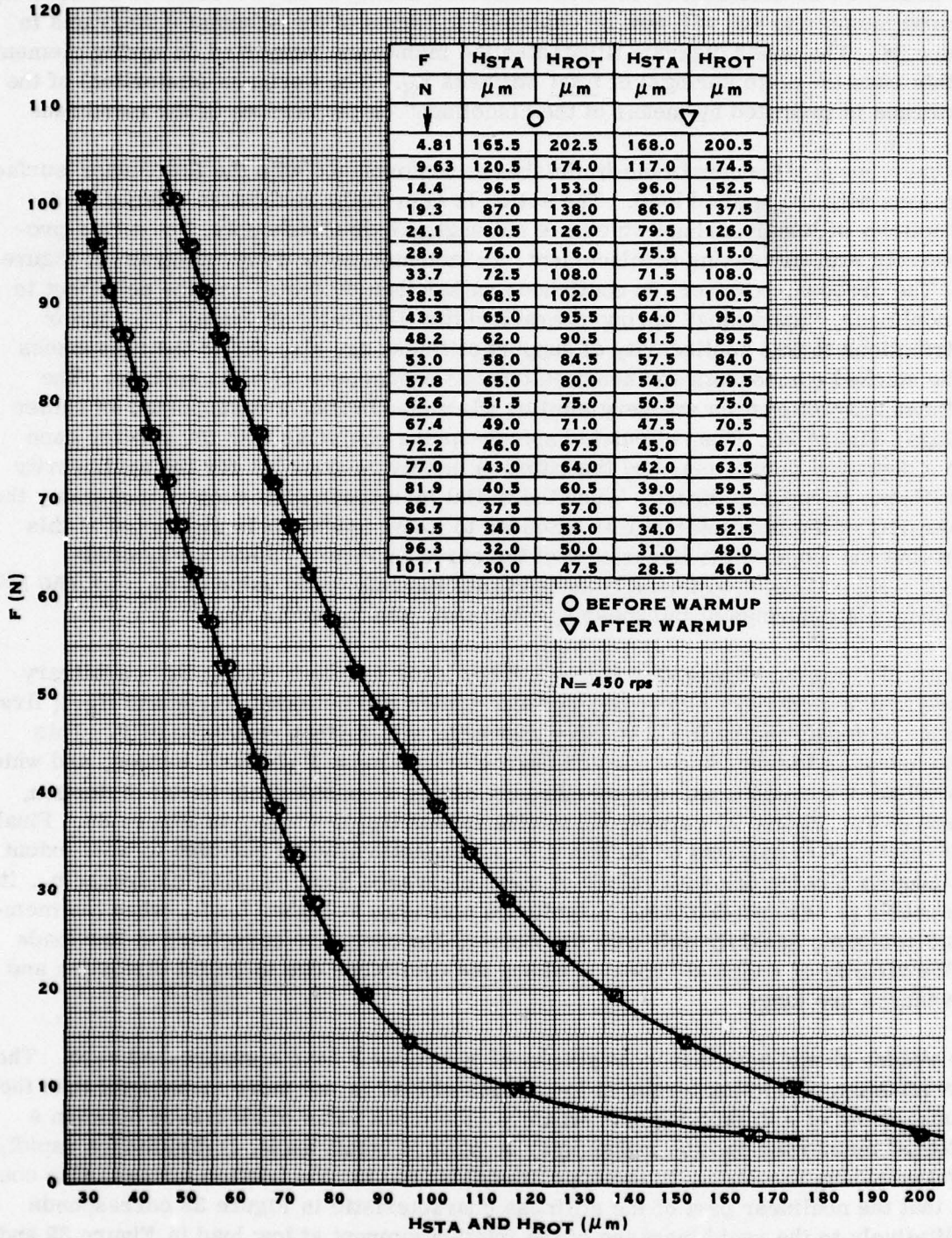

F	H_{STA}	H_{ROT}	H_{STA}	H_{ROT}
N	μm	μm	μm	μm
↓	O		▽	
4.81	165.5	202.5	168.0	200.5
9.63	120.5	174.0	117.0	174.5
14.4	96.5	153.0	96.0	152.5
19.3	87.0	138.0	86.0	137.5
24.1	80.5	126.0	79.5	126.0
28.9	76.0	116.0	75.5	115.0
33.7	72.5	108.0	71.5	108.0
38.5	68.5	102.0	67.5	100.5
43.3	65.0	95.5	64.0	95.0
48.2	62.0	90.5	61.5	89.5
53.0	58.0	84.5	57.5	84.0
57.8	65.0	80.0	54.0	79.5
62.6	51.5	75.0	50.5	75.0
67.4	49.0	71.0	47.5	70.5
72.2	46.0	67.5	45.0	67.0
77.0	43.0	64.0	42.0	63.5
81.9	40.5	60.5	39.0	59.5
86.7	37.5	57.0	36.0	55.5
91.5	34.0	53.0	34.0	52.5
96.3	32.0	50.0	31.0	49.0
101.1	30.0	47.5	28.5	46.0

FIGURE 39. DISPLACEMENT OF RUNNER RELATIVE TO SUPPORT PLATE WITH AND WITHOUT ROTATION (DETERMINATION OF CLEARANCE $\tilde{h} = H_{ROT} - H_{STA}$, FIGURE 37). - FLEXIBLE THRUST BEARING LLF-1T

The cause of this nonlinearity is to be attributed mainly to the waviness of the spirally-grooved membrane and will now be explained in terms of the schematic diagrams in Figure 38. The upper diagram illustrates the membrane supported on spring elements (in this case the plate springs) of total stiffness K_S. The waviness (distortion) of the membrane is indicated by means of the "isoclines" on the surface of the membrane.

The unevenness of the membrane diminishes as conformance with the flat runner-surface increases with the applied load. The action is akin to the resistance offered by a multiplicity of linear springs which are not engaged simultaneously, but rather progressively with increasing displacement, as indicated in the lower diagram of Figure 38. The process, however, is continuous rather than discrete, and the net effect is the nonlinear, "hardening" spring-characteristic illustrated in Figure 38. Minor contributions to this nonlinearity of support stiffness are also due to the unevenness of the stacked components and nonsimultaneous engagement of plate springs. The stiffness characteristics are very similar when membranes are supported on spider springs, Figure 26. The reticulated spider-spring conforms with far greater ease than a distorted membrane, and the latter is mainly responsible for the nonlinearity of stiffness at reduced thrust. When the initial membrane distortion is moderate, the linear part of the characteristic is extended to lower loads. It is also noted at this point that the slope of the linear part of the curve in Figure 38 has a magnitude $dF/d\delta = K_S = 17,200$ N/cm, as compared with the calculated value of $K_S = 17,050$ N/cm (eighteen plate springs of thickness $t_s = 130\ \mu$m, see Appendix A).

Graphs of H_{STA} and H_{ROT} ($\tilde{h} = H_{ROT} - H_{STA}$, and $\delta = H_C - H_{STA}$; H_C = arbitrary offset) are presented in Figure 39, and the reader will note that H_{ROT} and H_{STA} first diverge with decreasing load, but then converge with further reduction of F. This trend accounts for the "knee", which characterizes most F versus $\tilde{h}$ curves, and which is particularly pronounced with membranes having a considerable initial distortion. The values of $\tilde{h}$ in Figure 37 correspond to differences $H_{ROT} - H_{STA}$ in Figure 39. Finally, with reference to contents of Section 2.3, and specifically the question to what extent the quantity $\tilde{h}$ coincides with values of mean clearance $\bar{h}$ and parallel clearance h_o, it is reasonable to assume that these magnitudes converge at higher loads, when the membrane conforms sensibly well with the runner, but cannot be correlated at low loads (in the vicinity of a typical "knee"), where the deviations due to initial distortion and unevenness are large.

The reader should note that most graphs of M versus F have a suppressed zero. The determination of friction torque at low values of load is not more meaningful than the measurement of $\tilde{h}$ in this region. Whatever the mean value of clearance between a distorted membrane and the runner may be at very small loads, it diminishes rapidly with increasing thrust, while the opposite holds true for the friction torque. One could say that the nonlinear part of the stiffness characteristic in Figure 38 corresponds qualitatively to the rapid increase of the friction moment at low load in Figure 32 and in Figure 36 (zero suppressed), and in similar curves presented elsewhere in this report.

Two additional results in the relatively low speed-range to 450 rps were obtained. In Figure 40, the variation of load with speed at a constant value of $\tilde{h}$ is fairly linear, except at low speed-and load values, where the constancy of $\tilde{h}$ is not very meaningful. The nearly discontinuous change at 400 rps may have been caused by a slight shift of the membrane, possibly by contact of a small, local indentation, or by some other peculiarity of this specific membrane. In Figure 41, the variation of load with speed takes place at a constant value of the friction moment.

5.2 Test Results of Flexible Thrust Bearing LLF-2T to Speeds of 27,000 rpm

The design and construction of this bearing were discussed in Section 3.2 and additional information is contained in Appendix A. The outward appearance of both thrust bearings is very similar and this is well illustrated in Figure 28. Furthermore, were one to view the spiral-groove pattern facing the membrane, Figure 12, no distinction could be made between these bearings, nor could they be distinguished from a rigid bearing of identical surface topography.

The heart of the flexible thrust bearing LLF-2T is the reticulated spider-spring, Figures 24, 26 and 27, which at first sight gives the appearance of a fragile filigree ornament, rather than of a sturdy bearing component. The pleasing appearance of this element delighted the writer, as did its simplicity and practicality. The membranes supported on spider springs performed as well as those mounted on the support described in Section 3.1.

The material contained in this report should be read sequentially. The type of data presented in the preceding section recurs in this and other parts of the report, and it will be assumed that the reader has at this point acquired sufficient familiarity with the manner of presentation of various characteristics to warrant description and comment which are more condensed.

The graph of F versus $\tilde{h}$ in Figure 42 relates to data obtained with an Inconel X-750 membrane and a copper beryllium spider-spring. The mean thickness of the 72 spring elements, Figure 24, was $\bar{t}_S = 72\ \mu m$. Note that there is no "knee" in the curve of Figure 42. If a comparison is made with the data of Figure 37, it will be noted that at higher loads, at F = 81.9 N for example, the magnitudes of $\tilde{h}$ differ only by approximately 15%, but that with decreasing load the values diverge. The data in Figure 43 correspond to Figure 42, and the stiffness characteristics in Figure 44 was derived from H_{STA} in Figure 43. The slope of the linear part of the characteristic is approximately $K_S = dF/d\delta \approx 55,385$ N/cm, as compared with the calculated value $K_S = 56,975$, based on $\bar{t}_s = 72\ \mu m$. This integrated result lends credence to the assumptions made in regard to estimates of stiffness for design purposes. In this case also, although to a lesser extent than in Figure 38, the nonlinearity of the system at low loads is a consequence of membrane unevenness, and to other deviations from ideal flatness and parallelism.

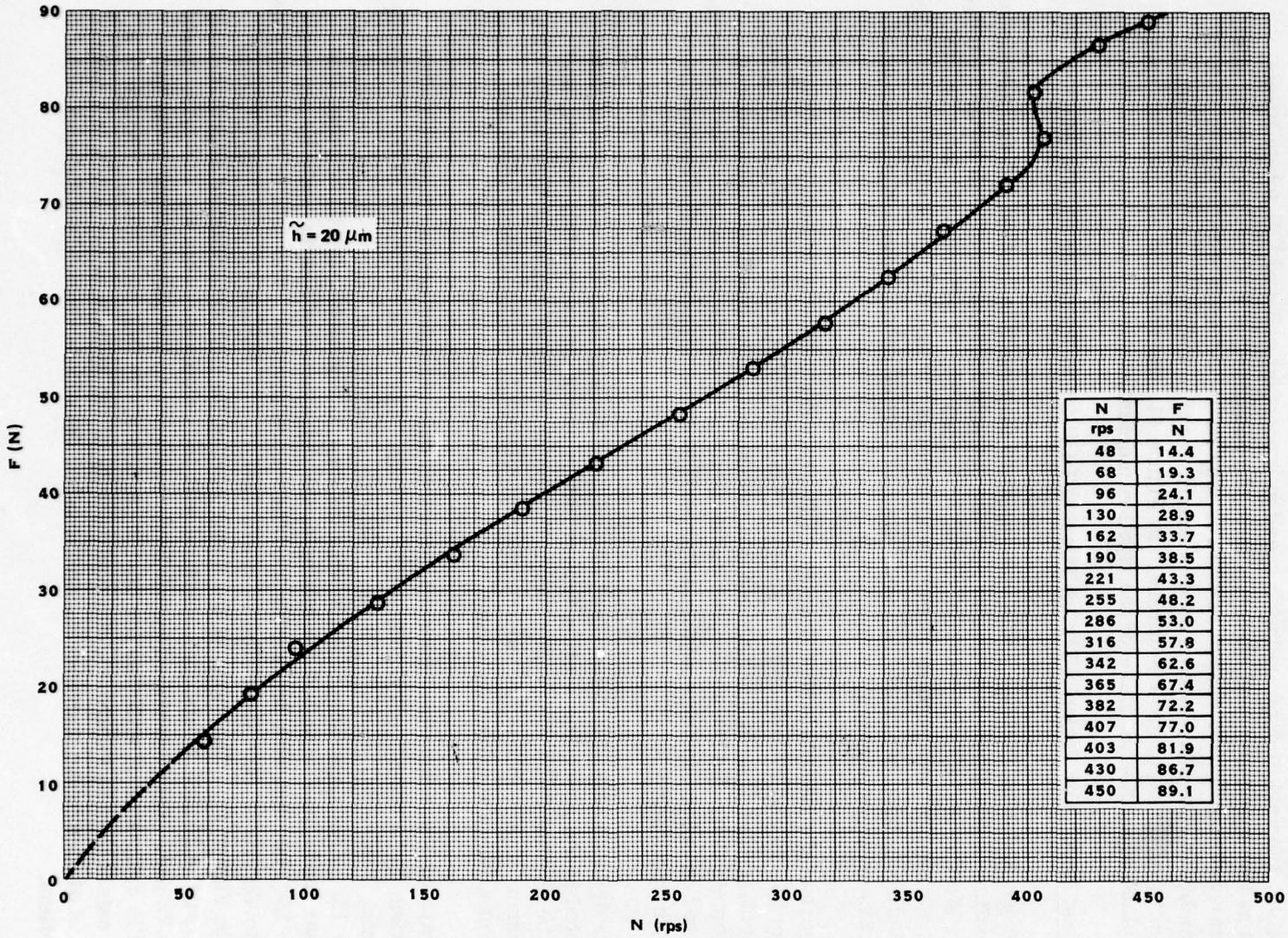

N rps	F N
48	14.4
68	19.3
96	24.1
130	28.9
162	33.7
190	38.5
221	43.3
255	48.2
286	53.0
316	57.8
342	62.6
365	67.4
382	72.2
407	77.0
403	81.9
430	86.7
450	89.1

FIGURE 40. LOAD VERSUS SPEED AT CONSTANT CLEARANCE.-FLEXIBLE THRUST BEARING LLF-1T

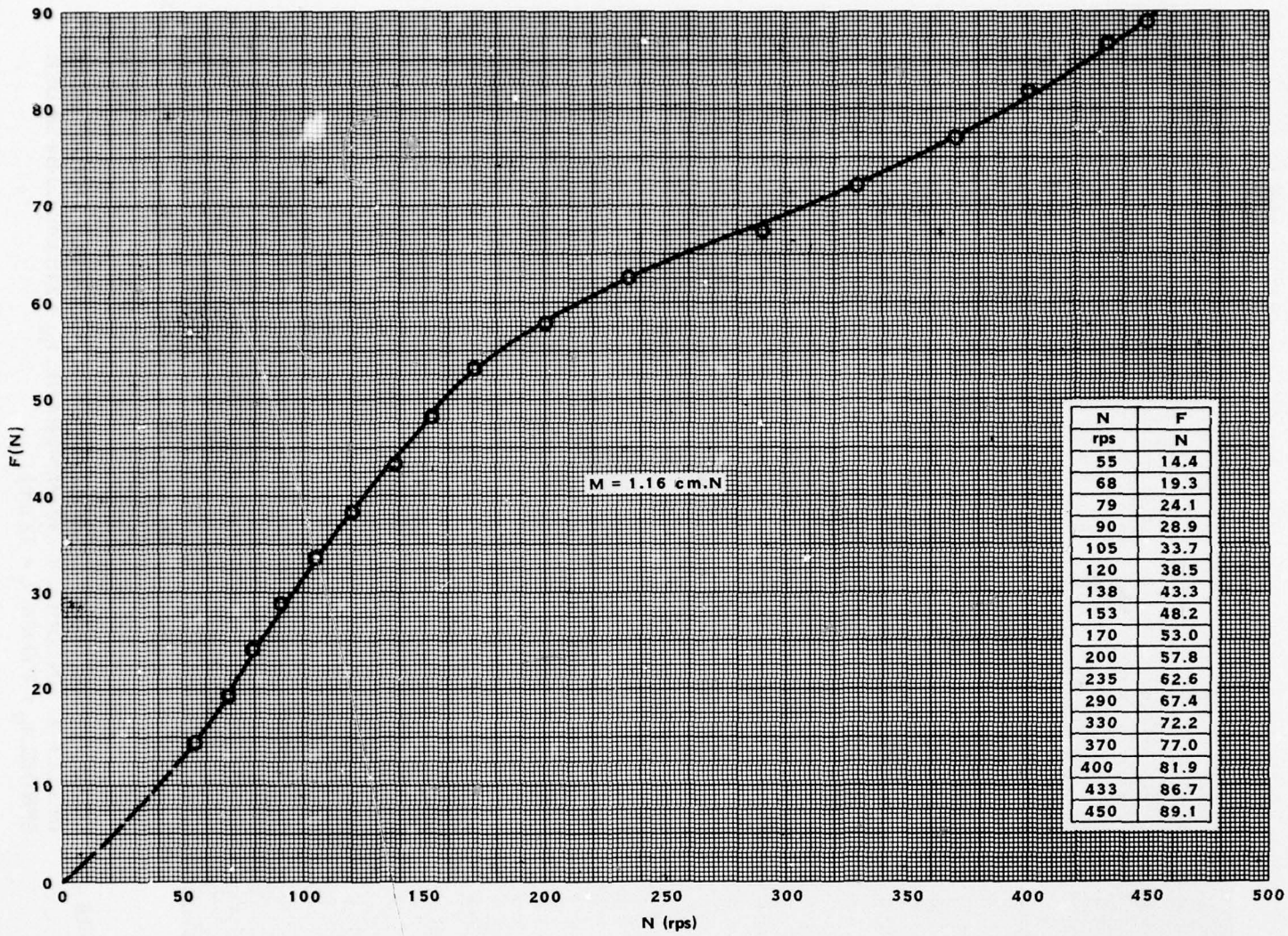

N	F
rps	N
55	14.4
68	19.3
79	24.1
90	28.9
105	33.7
120	38.5
138	43.3
153	48.2
170	53.0
200	57.8
235	62.6
290	67.4
330	72.2
370	77.0
400	81.9
433	86.7
450	89.1

FIGURE 41. LOAD VERSUS SPEED AT CONSTANT FRICTION MOMENT.-FLEXIBLE THRUST BEARING LLF-1T

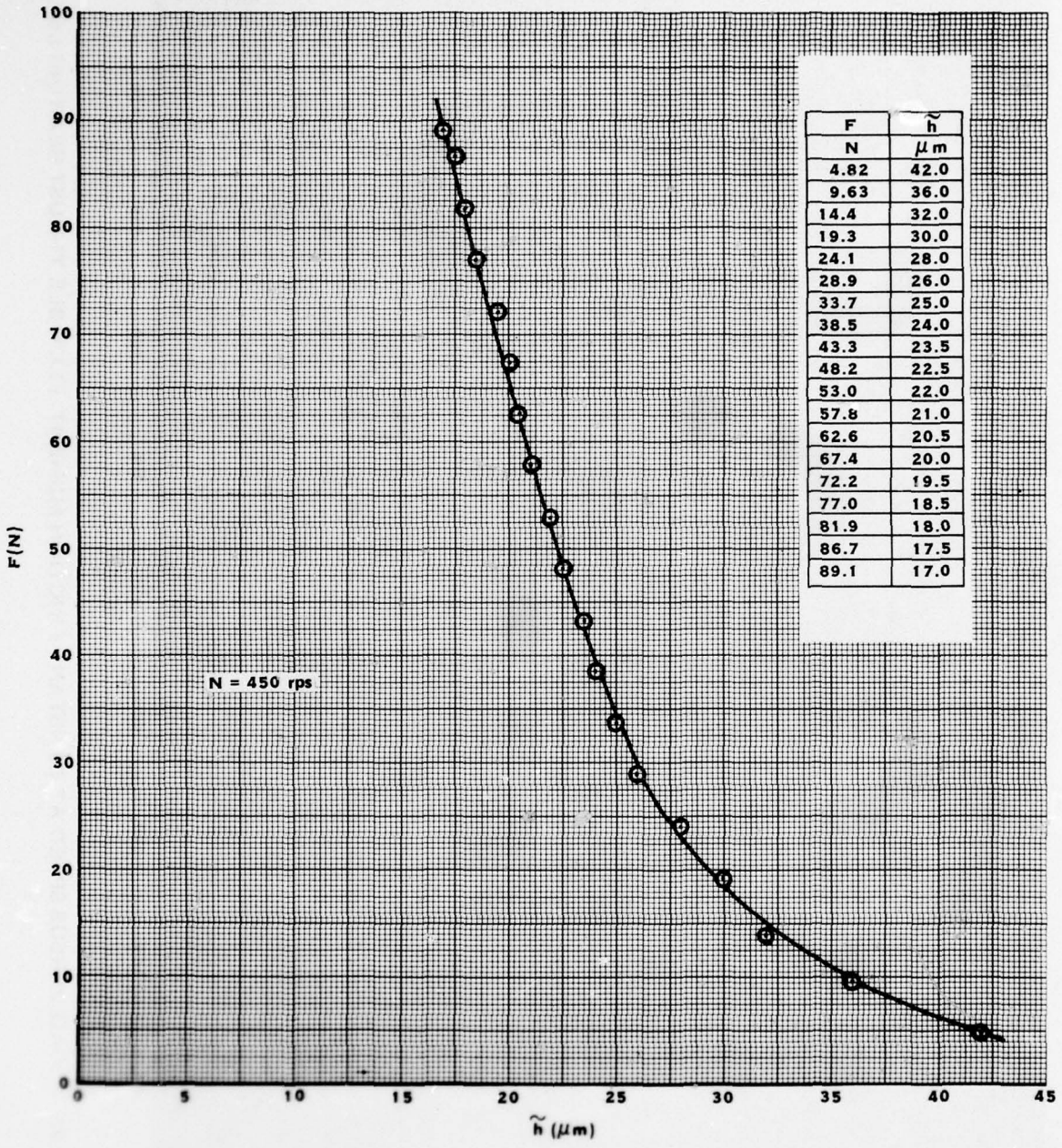

FIGURE 42 LOAD VERSUS CLEARANCE AT N = 450rps.-FLEXIBLE THRUST BEARING LLF-2T (INCONEL X-750 MEMBRANE, t_m = 215 μm, Cu-Be SPIDER SPRING, t_p = 200 μm; $\bar{T}_s$ = 72 μm)

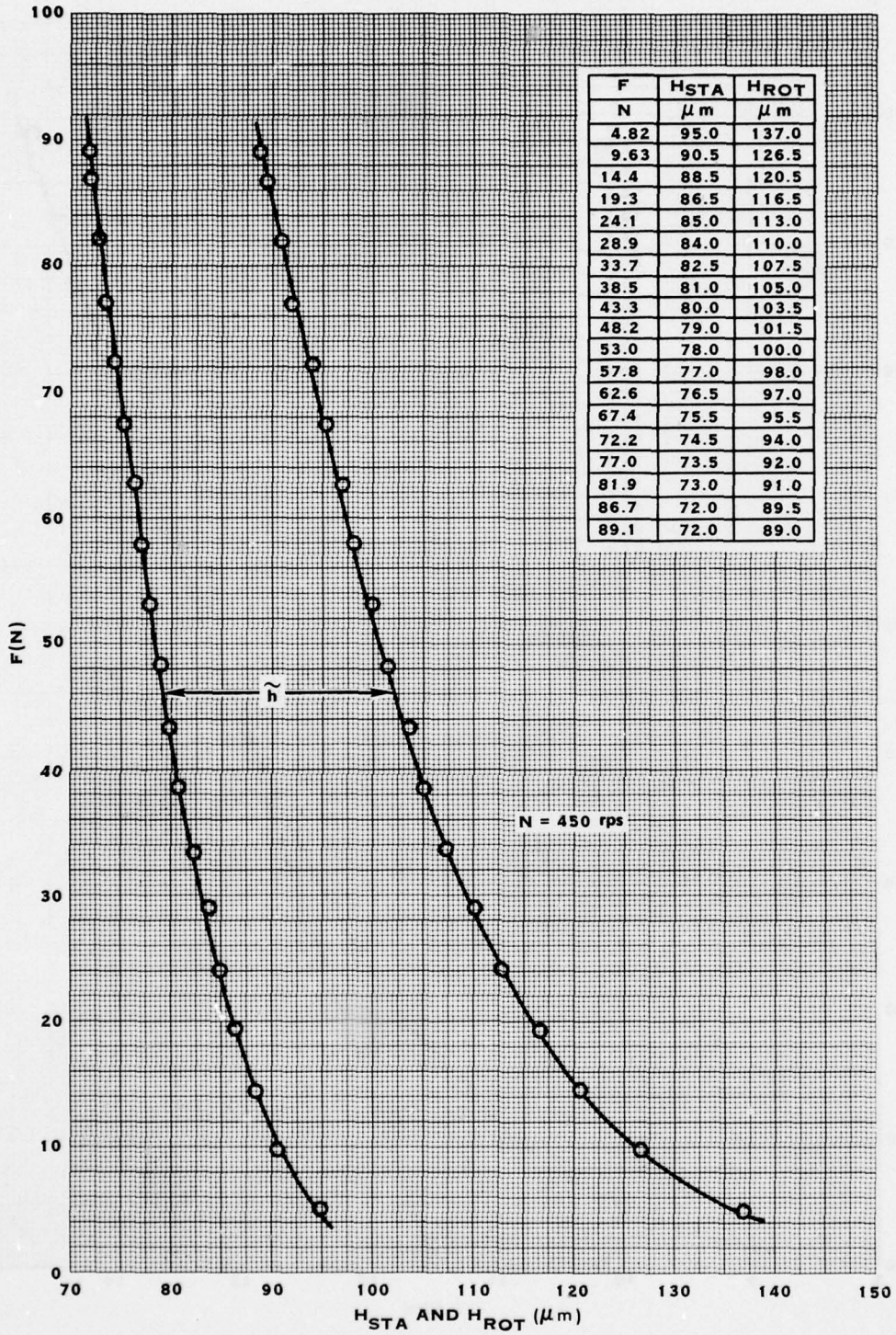

F	H_{STA}	H_{ROT}
N	μm	μm
4.82	95.0	137.0
9.63	90.5	126.5
14.4	88.5	120.5
19.3	86.5	116.5
24.1	85.0	113.0
28.9	84.0	110.0
33.7	82.5	107.5
38.5	81.0	105.0
43.3	80.0	103.5
48.2	79.0	101.5
53.0	78.0	100.0
57.8	77.0	98.0
62.6	76.5	97.0
67.4	75.5	95.5
72.2	74.5	94.0
77.0	73.5	92.0
81.9	73.0	91.0
86.7	72.0	89.5
89.1	72.0	89.0

FIGURE 43. DISPLACEMENT OF RUNNER RELATIVE TO SUPPORT PLATE (DETERMINATION OF CLEARANCE $\tilde{h} = H_{ROT} - H_{STA}$ AT N = 450rps, FIGURE 42).-FLEXIBLE THRUST BEARING LLF-2T (INCONEL X-750 MEMBRANE, t_m = 215μm, Cu-Be SPIDER SPRING, t_p = 200 μm; $\bar{t}_s$ = 72 μm)

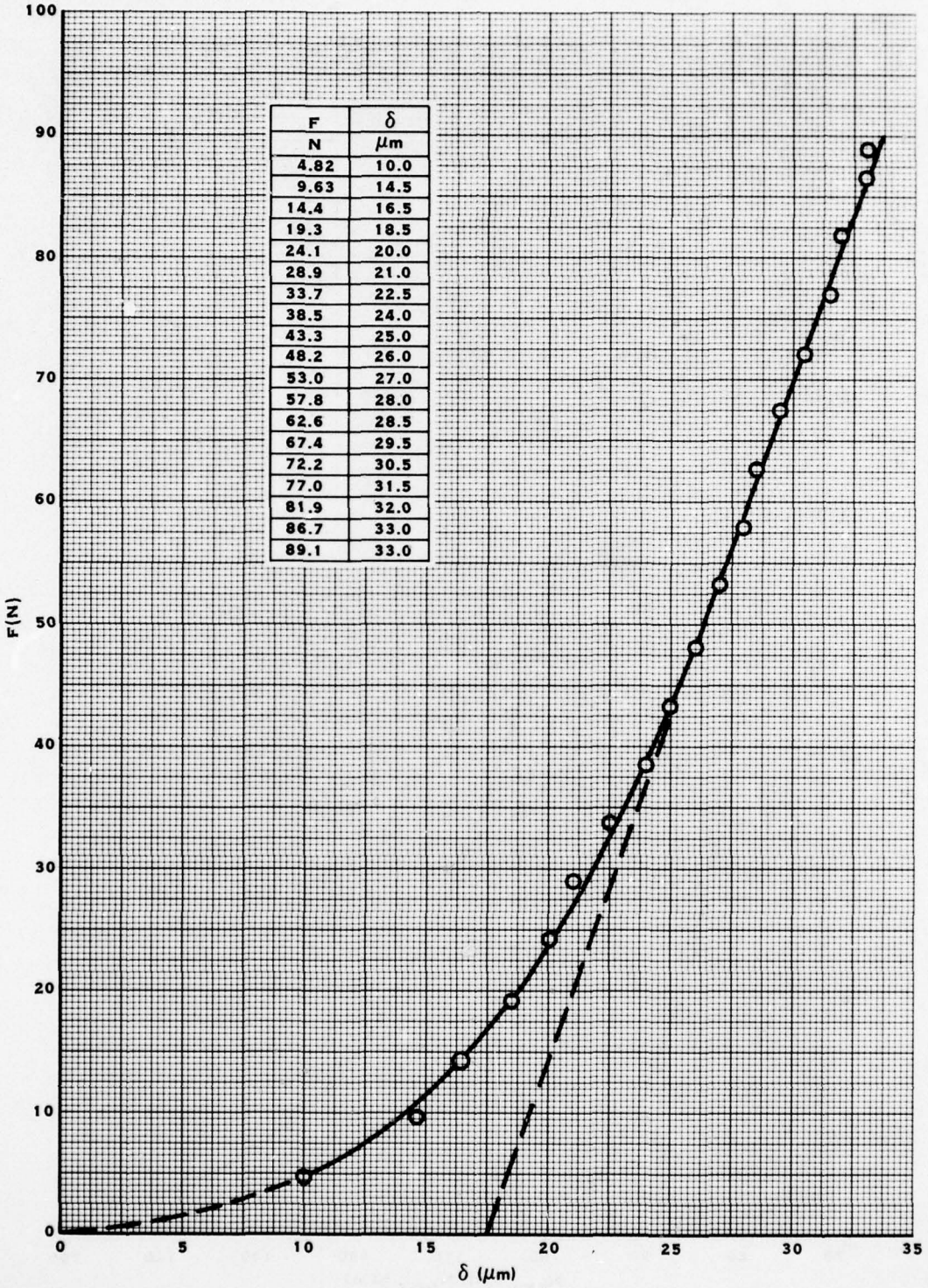

F N	δ μm
4.82	10.0
9.63	14.5
14.4	16.5
19.3	18.5
24.1	20.0
28.9	21.0
33.7	22.5
38.5	24.0
43.3	25.0
48.2	26.0
53.0	27.0
57.8	28.0
62.6	28.5
67.4	29.5
72.2	30.5
77.0	31.5
81.9	32.0
86.7	33.0
89.1	33.0

FIGURE 44. STATIC DEFLECTION OF FLEXIBLE THRUST BEARING LLF-2T (INCONEL X-750 MEMBRANE, t_m = 215 μm, Cu-Be SPIDER SPRING, t_p = 200 μm; $\bar{t}_s$ = 72 μm)

Turning now to the variation of the friction moment with load at constant speed, presented in Figure 45, it will be noted that following the characteristically rapid increase of torque at low loads, a region strongly affected by the initial distortion, the friction moment increases approximately linearly and in a manner comparable with that in Figure 36.

Replacement of the relatively flat, Inconel X-750 membrane with a more wavy, copper-beryllium specimen, while retaining the same spider-spring, leads to results presented in Figure 46. Both curves are characterized by the "knee" at low thrust. The speeds of 450 rps in Figure 42 and of 425 rps in Figure 46 are commensurate, which allows for a comparison of results obtained with two membranes differing in degree of initial flatness. In the upper load-range the values of $\tilde{h}$ differ by a small amount only, but with decreasing load the curves diverge.

The determination of $\tilde{h}$ in Figure 46 (at N = 400 rps) is related to the results given in Figure 47, and the stiffness characteristic in Figure 48 is derived from the H_{STA} curve of Figure 47. As expected, this characteristic is similar to that contained in Figure 44 (same spider spring, but not identical membranes). The slope of the linear part in Figure 47 is approximately $K_S = dF/d\delta = 52,286$ N/cm and differs by 5.6% from the corresponding value in Figure 44.

A qualitative comparison of M versus F curves in Figure 45 and Figure 49 (same spider spring, but not identical membranes and speeds) reveals a similar trend up approximately $F \approx 70$ N, but a noticeable increase of torque is observed at higher loads in Figure 49.

In the next series of experiments and measurements of variations of M with F, and of F with $\tilde{h}$, results were obtained for two speeds, N = 400 rps and N = 450 rps, for several combinations of two membranes and two spider springs. The results are tabulated and plotted in Figures 50 through 57, and the curves display similar trends to those previously reviewed.

As confidence was gained in the capability of the bearing to support thrusts of the order of $F \approx 90$ N, data was recorded at progressively higher loads, up to approximately $F \approx 106$ N is this series of tests. The load limitation was not actually dictated by the capacity of the bearing, but the fact that an increase in thrust would destabilize the rotor supported in pressurized journal-bearings. On several occassions, the rotor and bearings were nearly destroyed by the sudden onset of half-frequency whirl and were saved only by the watchfulness of the experimenters and a fast cutoff of the turbine air-supply. The rotor would run stably up to $N \approx 550$ rpm without the spiral-groove thrust bearing, and be free of self-excited vibration at N = 450 rpm up to a certain level of thrust. A critical thrust-level would then be reached, at which a small increment in load would precipitate a sudden onset of whirl. Data acquisition close to the limit of stability was an uncomfortable undertaking, especially since the

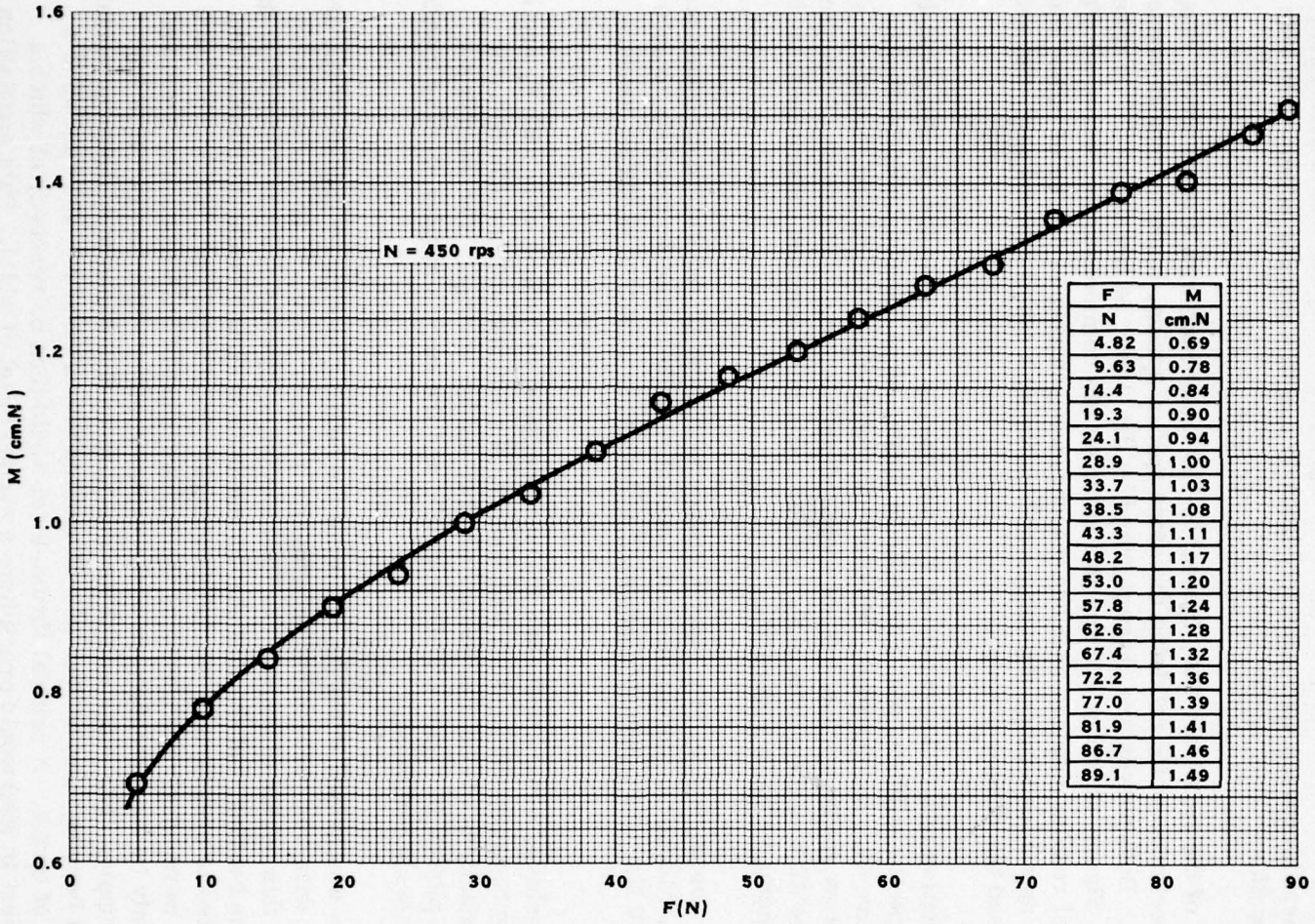

F N	M cm.N
4.82	0.69
9.63	0.78
14.4	0.84
19.3	0.90
24.1	0.94
28.9	1.00
33.7	1.03
38.5	1.08
43.3	1.11
48.2	1.17
53.0	1.20
57.8	1.24
62.6	1.28
67.4	1.32
72.2	1.36
77.0	1.39
81.9	1.41
86.7	1.46
89.1	1.49

FIGURE 45. FRICTION MOMENT VERSUS LOAD AT N = 450rps.-FLEXIBLE THRUST BEARING LLF-2T (INCONEL X-750 MEMBRANE, t_m = 215 μm, Cu-Be SPIDER SPRING, t_p = 200 μm; $\overline{t}_s$ = 72 μm)

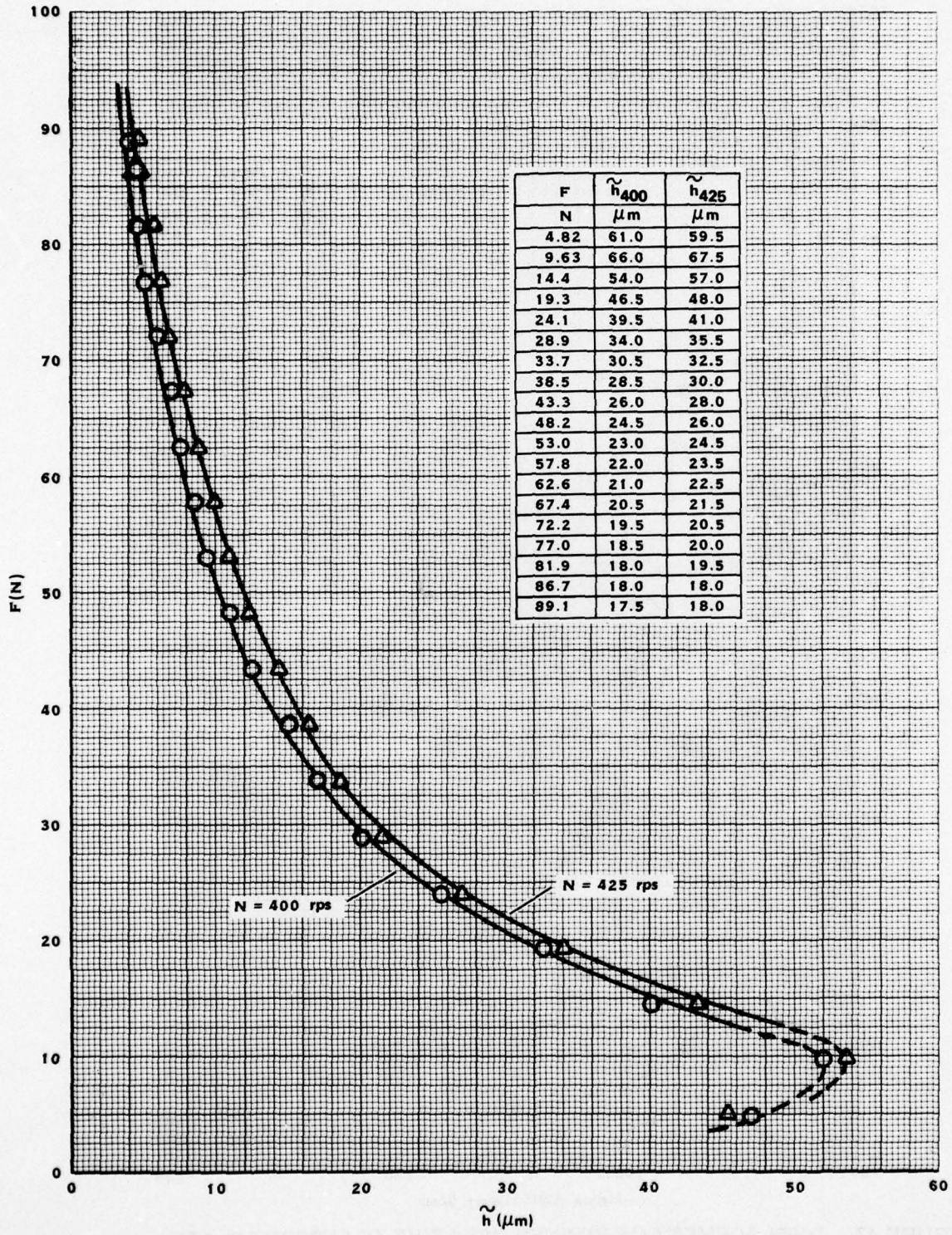

F	$\tilde{h}_{400}$	$\tilde{h}_{425}$
N	μm	μm
4.82	61.0	59.5
9.63	66.0	67.5
14.4	54.0	57.0
19.3	46.5	48.0
24.1	39.5	41.0
28.9	34.0	35.5
33.7	30.5	32.5
38.5	28.5	30.0
43.3	26.0	28.0
48.2	24.5	26.0
53.0	23.0	24.5
57.8	22.0	23.5
62.6	21.0	22.5
67.4	20.5	21.5
72.2	19.5	20.5
77.0	18.5	20.0
81.9	18.0	19.5
86.7	18.0	18.0
89.1	17.5	18.0

FIGURE 46. LOAD VERSUS CLEARANCE AT N = 400rps AND N = 425rps.-FLEXIBLE THRUST BEARING LLF-2T (Cu-Be MEMBRANE, t_m = 230 μm, Cu-Be SPIDER SPRING, t_p = 200 μm; $\bar{t}_s$ = 72 μm)

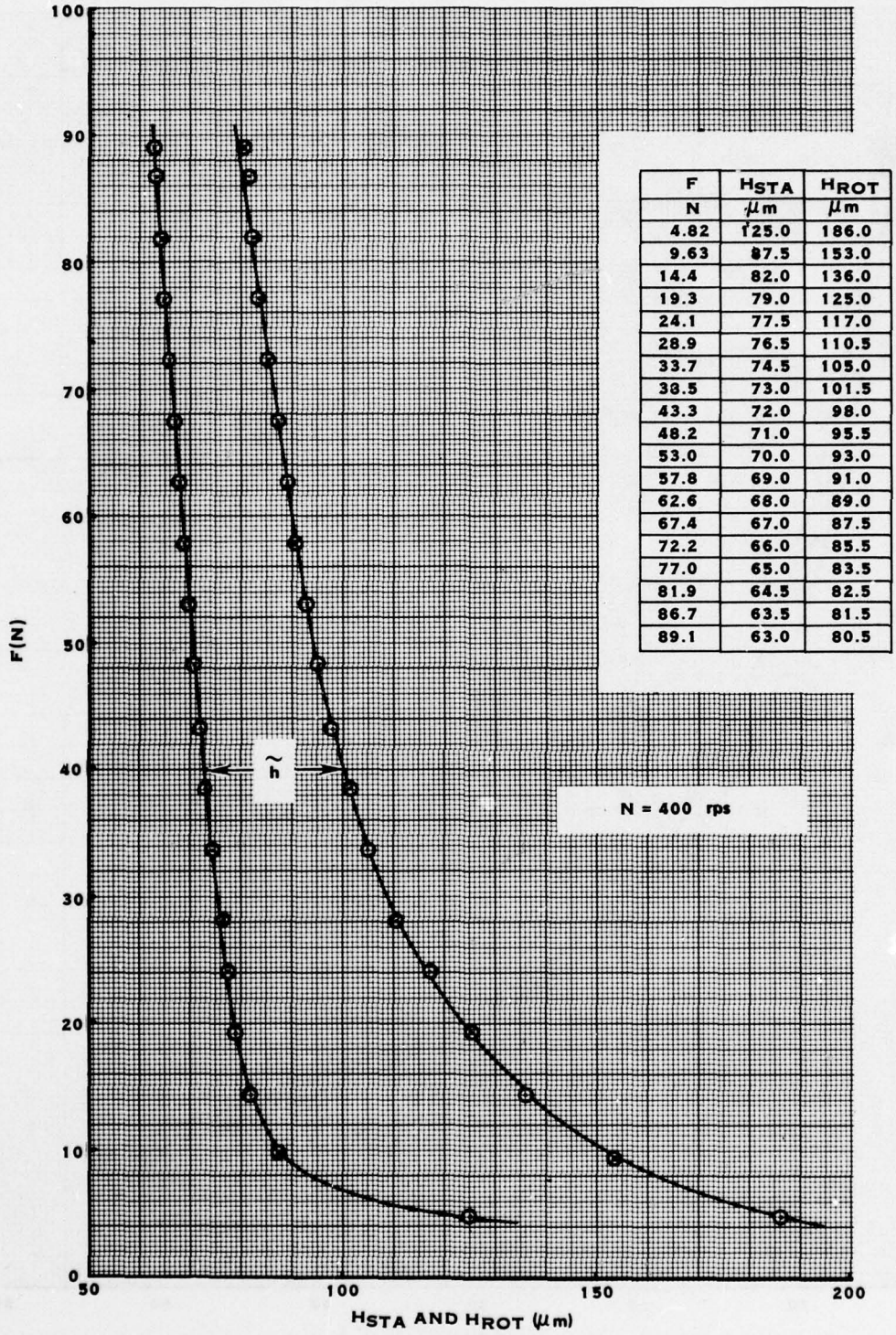

F	H_{STA}	H_{ROT}
N	μm	μm
4.82	125.0	186.0
9.63	87.5	153.0
14.4	82.0	136.0
19.3	79.0	125.0
24.1	77.5	117.0
28.9	76.5	110.5
33.7	74.5	105.0
38.5	73.0	101.5
43.3	72.0	98.0
48.2	71.0	95.5
53.0	70.0	93.0
57.8	69.0	91.0
62.6	68.0	89.0
67.4	67.0	87.5
72.2	66.0	85.5
77.0	65.0	83.5
81.9	64.5	82.5
86.7	63.5	81.5
89.1	63.0	80.5

FIGURE 47. DISPLACEMENT OF RUNNER RELATIVE TO SUPPORT PLATE (DETERMINATION OF CLEARANCE $\tilde{h} = H_{ROT} - H_{STA}$ AT 400rps, FIGURE 46).-FLEXIBLE THRUST BEARING LLF-2T (Cu-Be MEMBRANE, t_m = 230 μm, Cu-Be SPIDER SPRING, t_p = 200 μm; $\bar{t}_s$ = 72 μm)

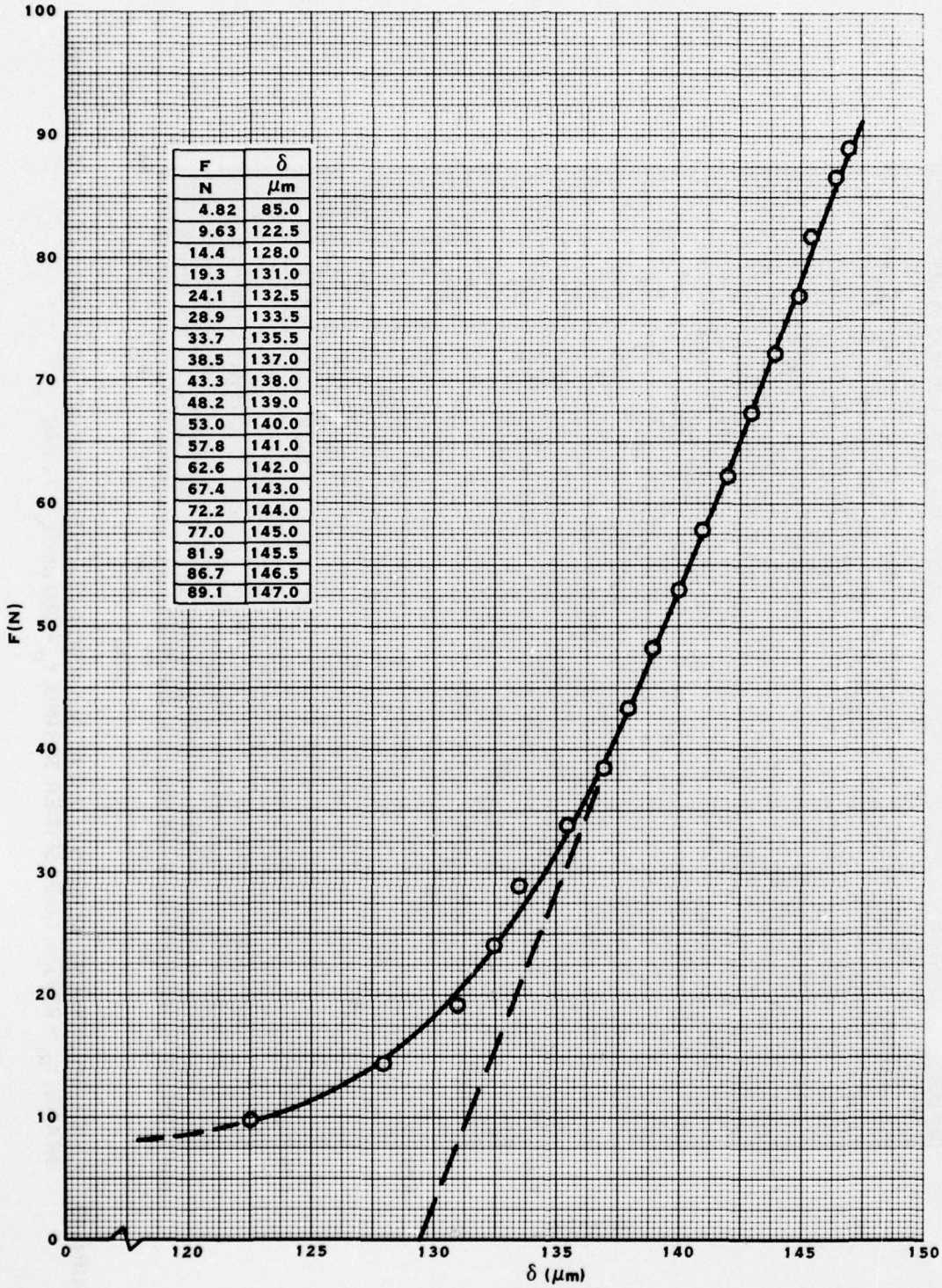

F N	δ μm
4.82	85.0
9.63	122.5
14.4	128.0
19.3	131.0
24.1	132.5
28.9	133.5
33.7	135.5
38.5	137.0
43.3	138.0
48.2	139.0
53.0	140.0
57.8	141.0
62.6	142.0
67.4	143.0
72.2	144.0
77.0	145.0
81.9	145.5
86.7	146.5
89.1	147.0

FIGURE 48. STATIC DEFLECTION OF FLEXIBLE THRUST BEARING LLF-2T (Cu-Be MEMBRANE, t_m = 230 μm, Cu-Be SPIDER SPRING, t_p = 200 μm; $\bar{t}_s$ = 72 μm)

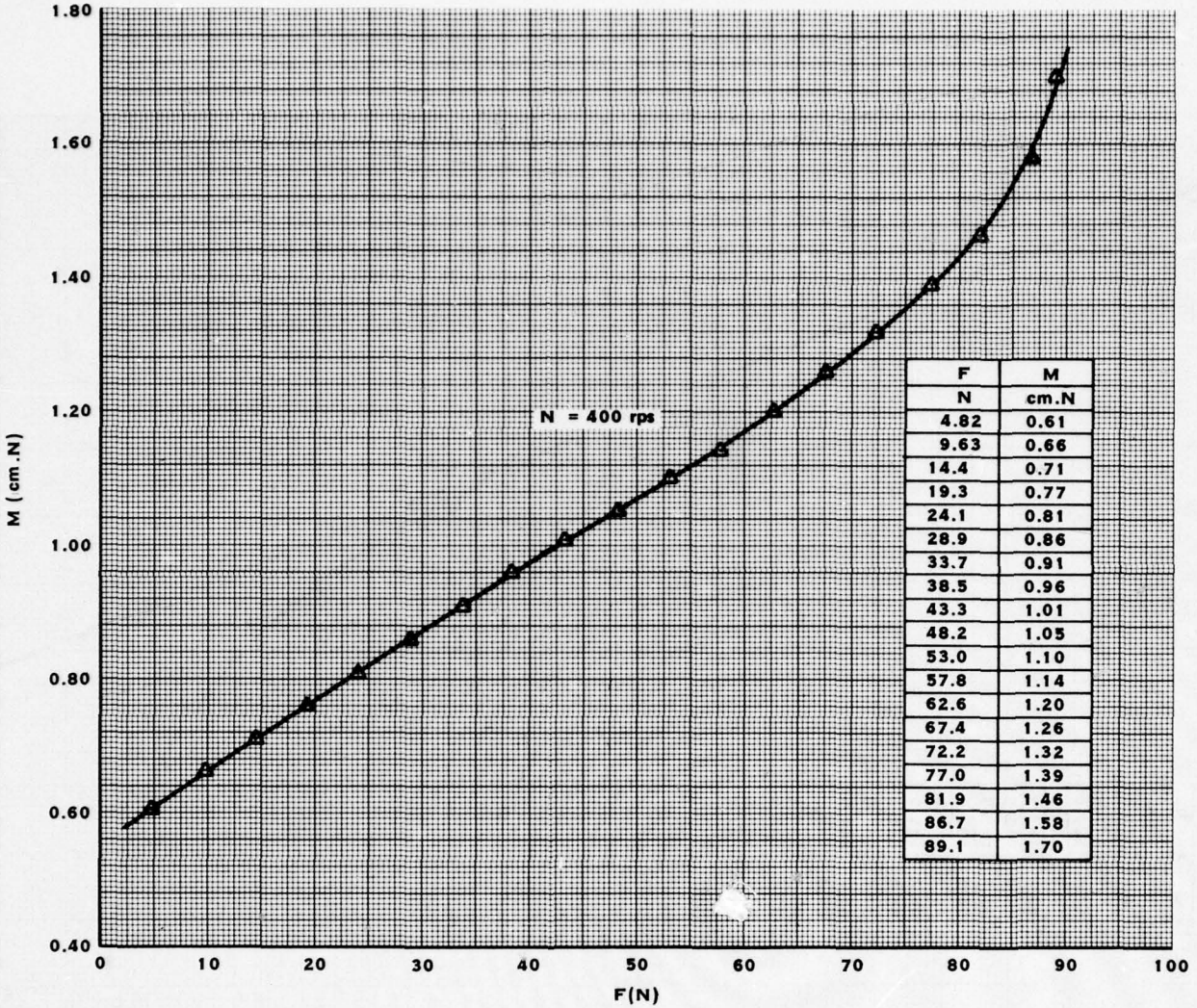

F N	M cm.N
4.82	0.61
9.63	0.66
14.4	0.71
19.3	0.77
24.1	0.81
28.9	0.86
33.7	0.91
38.5	0.96
43.3	1.01
48.2	1.05
53.0	1.10
57.8	1.14
62.6	1.20
67.4	1.26
72.2	1.32
77.0	1.39
81.9	1.46
86.7	1.58
89.1	1.70

FIGURE 49. FRICTION MOMENT VERSUS LOAD AT N = 400rps.-FLEXIBLE THRUST BEARING LLF-2T (Cu-Be MEMBRANE, t_m = 230 μm, Cu-Be SPIDER SPRING, t_p = 200 μm; $\overline{t}_s$ = 72 μm)

growth of trajectory from a negligibly small to an intolerably large orbit could occur in a fraction of a second. It was, nevertheless, possible to increase the load to $F \approx 106$ N at the lower speed of $N = 400$ rps.

The two membranes were sensibly flat Inconel X-750 specimen, $t_m = 215$ μm, and a relatively more undulated copper-beryllium element, $t_m = 230$ μm. The spider-springs had flexure elements which were thinner than in previously used supports. One spider-spring was etched from steel foil of thickness $t_p = 150$ μm and had a mean thickness of spring elements $\bar{t}_s = 53$ μm. The second spider-spring was etched from copper-beryllium foil of thickness $t_p = 200$ μm and had a mean thickness of flexure elements $\bar{t}_s = 40$ μm.

The previously observed differences in the variation of F versus $\tilde{h}$, when using a relatively flat Inconel X-750 and a more wavy copper-beryllium membrane, are pointedly illustrated in Figures 50, 51, 52 and 53. These results were recorded at two speeds, N = 400 and N = 450 rpm, and each of the two membranes was supported successively by one of the two spider springs. The curves always converge at higher load-values and diverge with decreasing load. The main influence appears to be due to membrane flatness, rather than to the spider spring, and the curves of the initially more distorted membrane are characterized by a "knee" in the region of low load. There is, of course, sufficient variability in "like" membranes when mounted on different supports, as well as in test conditions, to account for some divergence of data. The quantitative agreement between the "A"-curves and the "B"-curves in Figure 50 and Figure 52 (at 400 rps) and in Figure 51 and 53 (at 450 rps) is suprisingly good, however.

The data of the friction movement versus load, at speeds N = 400 and N = 450 rps, which correspond to the same membrane and spider-spring combinations relevant to Figures 50 through 53, are presented in graphs and tabulations contained in Figures 54 through 57. The results in each figure correspond to one of the four membrane and spider-spring combinations. In this case, the agreement between all curves is fairly good and no substantial differences exist between results obtained with either membrane and spider-spring combination. Except at low and high extremeties of the load range, the torque characteristics have nearly constant slopes.

A rather interesting set of results is presented in Figure 58 and Figure 59. The same spider-spring (copper-beryllium, $t_p = 200$ μm; $\bar{t}_s = 40$ μm) was first used with a more wavy copper-beryllium membrane of thickness $t_m = 230$ μm, Figure 58, and then with a flatter Inconel X750 membrane of thickness $t_m = 215$ μm, Figure 59. These figures pertain to the variation of the friction moment with speed at constant load.

All curves in Figure 58 are characterized by a minimum, qualitatively similar to curves obtained with rigid bearings. Obviously, a transition from hydrodynamic to boundary lubrication occurs, but the nature of this transition differs from that which characterizes rigid-surface bearings [66]. In rigid, air-lubricated bearings, the transition at constant

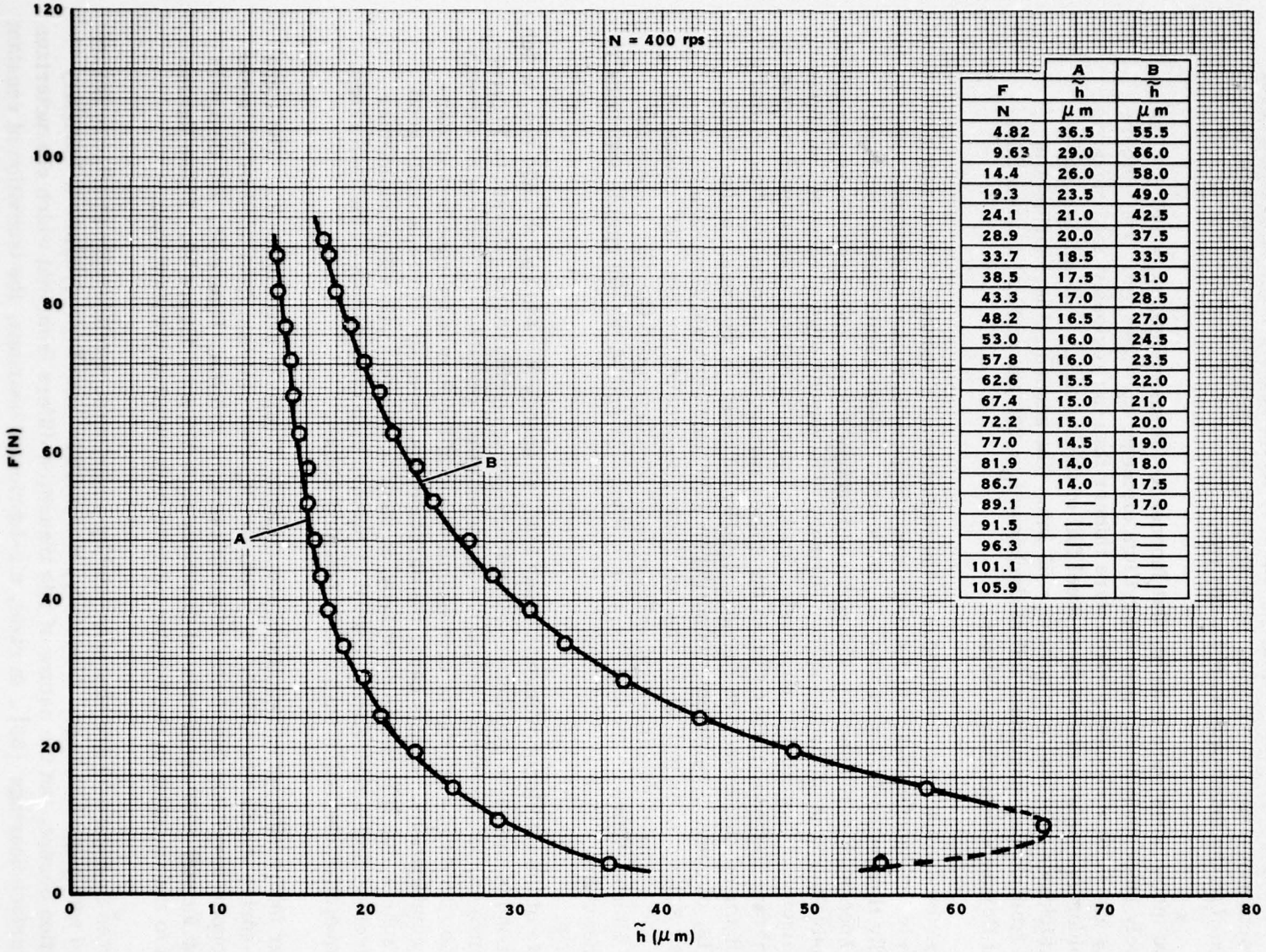

F	A $\tilde{h}$	B $\tilde{h}$
N	μm	μm
4.82	36.5	55.5
9.63	29.0	66.0
14.4	26.0	58.0
19.3	23.5	49.0
24.1	21.0	42.5
28.9	20.0	37.5
33.7	18.5	33.5
38.5	17.5	31.0
43.3	17.0	28.5
48.2	16.5	27.0
53.0	16.0	24.5
57.8	16.0	23.5
62.6	15.5	22.0
67.4	15.0	21.0
72.2	15.0	20.0
77.0	14.5	19.0
81.9	14.0	18.0
86.7	14.0	17.5
89.1	—	17.0
91.5	—	—
96.3	—	—
101.1	—	—
105.9	—	—

FIGURE 50. LOAD VERSUS CLEARANCE AT N = 400rps.-FLEXIBLE THRUST BEARING LLF-2T (A: INCONEL X-750 MEMBRANE, t_m = 215 μm, STEEL SPIDER SPRING, t_p = 150 μm; t_s = 53 μm. B: CuBe MEMBRANE, t_m = 230 μm. STEEL SPIDER SPRING, t_p = 150 μm; t_s = 53 μm)

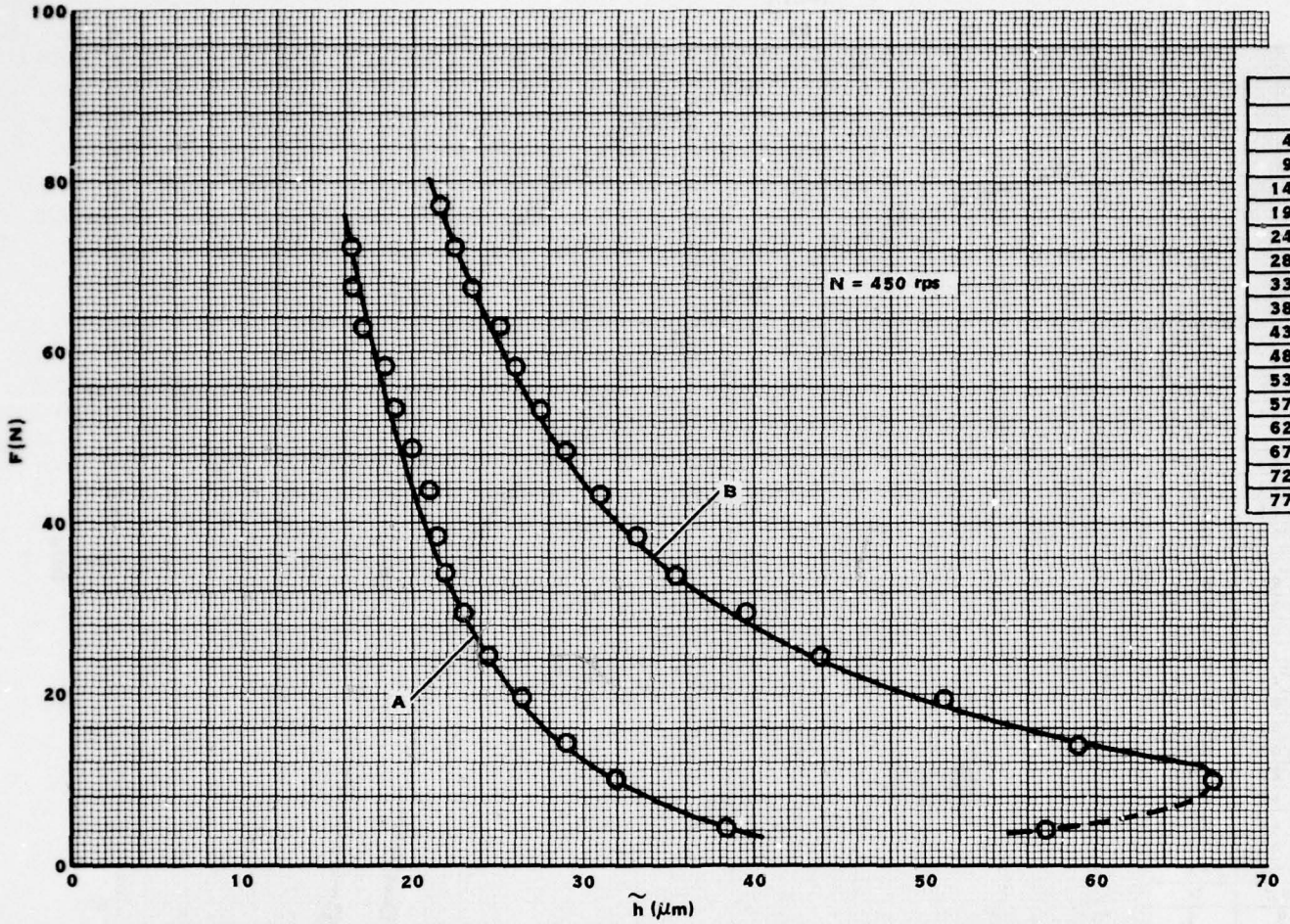

F	A $\tilde{h}$	B $\tilde{h}$
N	μm	μm
4.82	38.5	57.0
9.63	32.0	67.0
14.4	29.0	59.0
19.3	26.5	51.0
24.1	24.5	44.0
28.9	23.0	39.5
33.7	22.0	35.5
38.5	21.5	33.0
43.3	21.0	31.0
48.2	20.0	29.0
53.0	19.0	27.5
57.8	18.5	26.0
62.6	17.0	25.0
67.4	16.5	23.5
72.2	16.5	22.5
77.0	—	21.5

FIGURE 51. LOAD VERSUS CLEARANCE AT N = 450rps.-FLEXIBLE THRUST BEARING LLF-2T (A: INCONEL X-750 MEMBRANE, t_m = 215 μm, STEEL SPIDER SPRING, t_p = 150 μm; $\bar{t}_s$ = 53 μm. B: Cu-Be MEMBRANE, t_m = 230 μm, STEEL SPIDER SPRING, t_p = 150 μm; $\bar{t}_s$ = 53 μm)

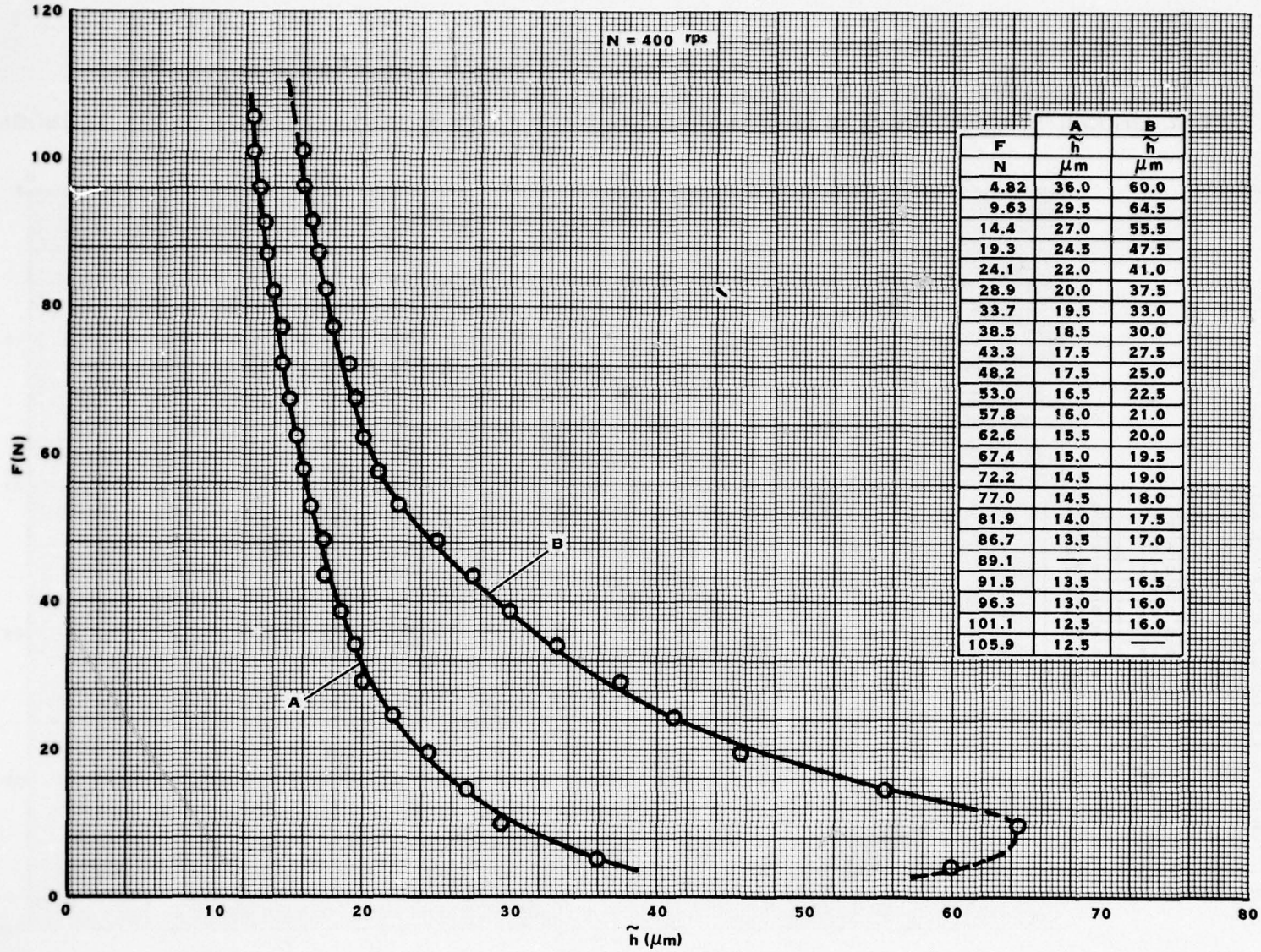

F	A $\tilde{h}$	B $\tilde{h}$
N	μm	μm
4.82	36.0	60.0
9.63	29.5	64.5
14.4	27.0	55.5
19.3	24.5	47.5
24.1	22.0	41.0
28.9	20.0	37.5
33.7	19.5	33.0
38.5	18.5	30.0
43.3	17.5	27.5
48.2	17.5	25.0
53.0	16.5	22.5
57.8	16.0	21.0
62.6	15.5	20.0
67.4	15.0	19.5
72.2	14.5	19.0
77.0	14.5	18.0
81.9	14.0	17.5
86.7	13.5	17.0
89.1	—	—
91.5	13.5	16.5
96.3	13.0	16.0
101.1	12.5	16.0
105.9	12.5	—

FIGURE 52. LOAD VERSUS CLEARANCE AT N = 400rps.-FLEXIBLE THRUST BEARING LLF-2T (A: INCONEL X-750 MEMBRANE, t_m = 215 μm. Cu-Be SPIDER SPRING, t_p = 200 μm; $\bar{t}_s$ = 40 μm. B: Cu-Be MEMBRANE, t_m = 230 μm. Cu-Be SPIDER SPRING, t_p = 200 μm; $\bar{t}_s$ = 40 μm)

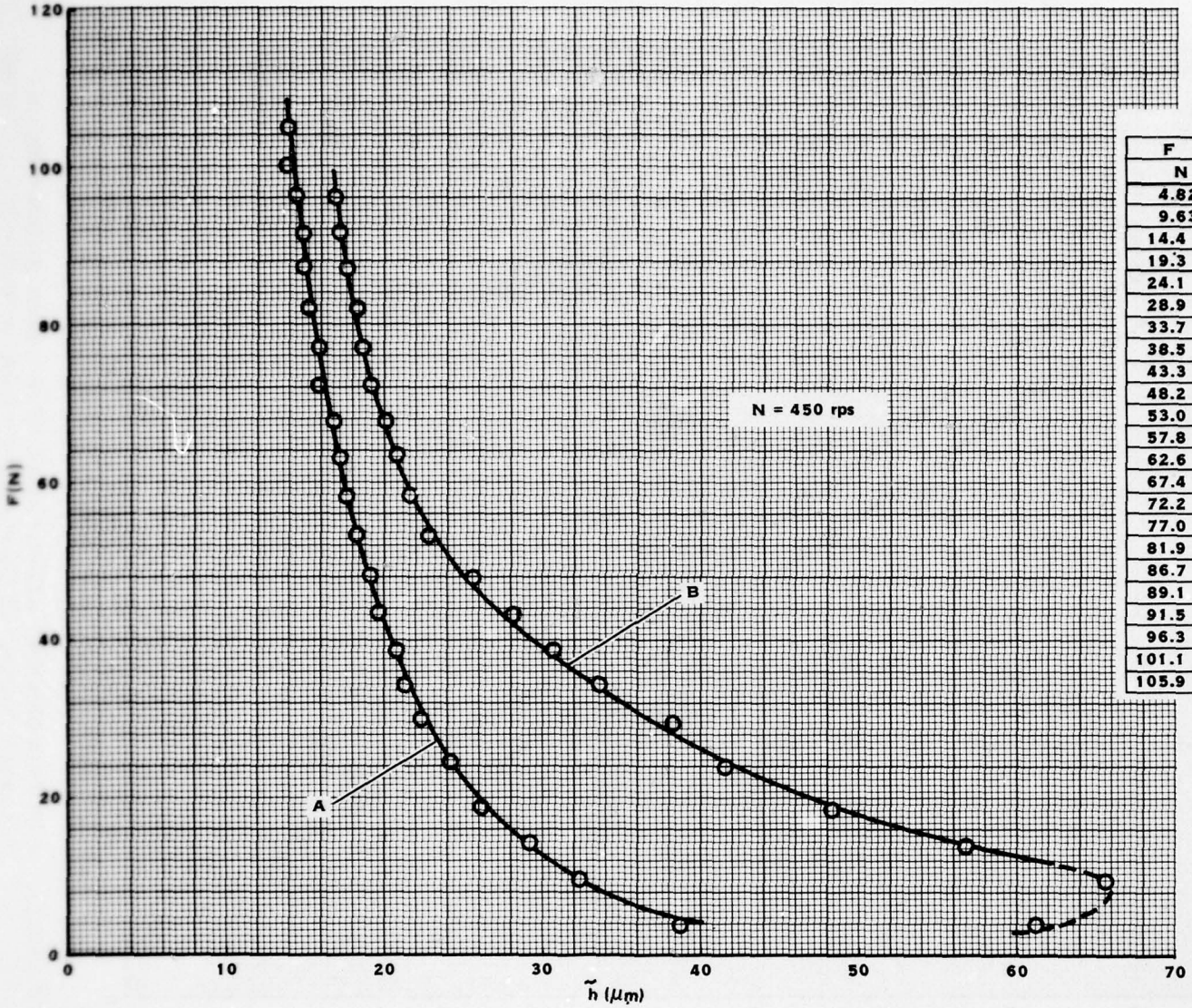

F	A $\tilde{h}$	B $\tilde{h}$
N	μm	μm
4.82	39.0	61.0
9.63	32.5	66.0
14.4	29.5	57.0
19.3	26.5	48.5
24.1	24.5	42.0
28.9	22.5	38.5
33.7	21.5	34.0
38.5	21.0	31.0
43.3	20.0	28.5
48.2	19.5	26.0
53.0	18.5	23.0
57.8	18.0	22.0
62.6	17.5	21.0
67.4	16.5	20.5
72.2	16.0	19.5
77.0	16.0	19.0
81.9	15.5	18.5
86.7	15.0	18.0
89.1	—	—
91.5	15.0	17.5
96.3	14.5	17.0
101.1	14.0	—
105.9	14.0	—

FIGURE 53. LOAD VERSUS CLEARANCE AT N = 450rps. - FLEXIBLE THRUST BEARING LLF-2T (A: INCONEL X-750 MEMBRANE, t_m = 215 μm, Cu-Be SPIDER SPRING, t_p = 200 μm; $\bar{t}_s$ = 40 μm. B: Cu-Be MEMBRANE, t_m = 230 μm. Cu-Be SPIDER SPRING, t_p = 200 μm; $\bar{t}_s$ = 40 μm)

AD-A053 735 LICHT (L) SAN MATEO CA F/G 13/9
FOIL BEARINGS FOR AXIAL AND RADIAL SUPPORT OF HIGH SPEED ROTORS--ETC(U)
JAN 78 L LICHT N00014-76-C-0191
UNCLASSIFIED NASA-CR-2940 NL

2 OF 2
AD A053735

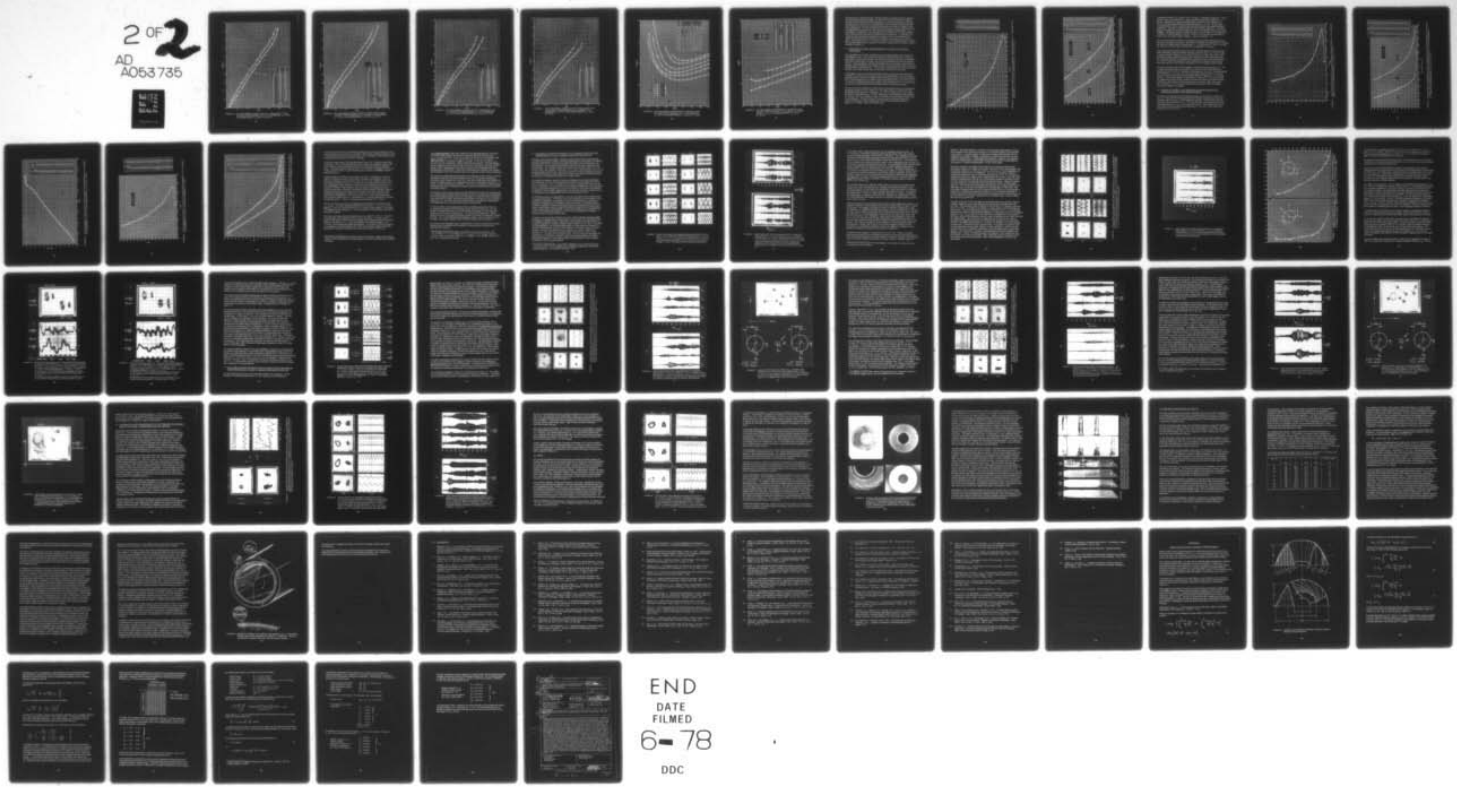

END
DATE FILMED
6-78
DDC

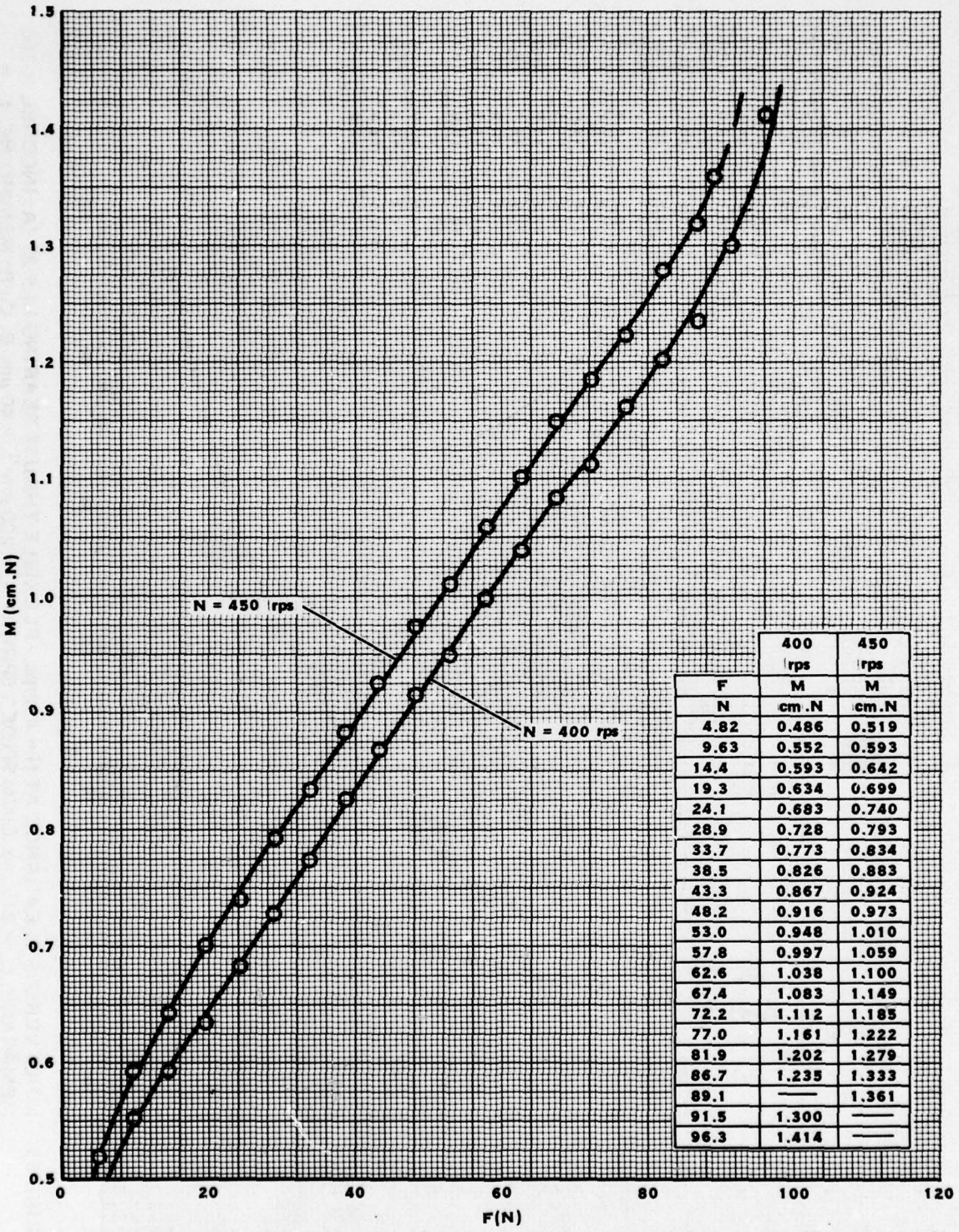

F	400 rps M	450 rps M
N	cm.N	cm.N
4.82	0.486	0.519
9.63	0.552	0.593
14.4	0.593	0.642
19.3	0.634	0.699
24.1	0.683	0.740
28.9	0.728	0.793
33.7	0.773	0.834
38.5	0.826	0.883
43.3	0.867	0.924
48.2	0.916	0.973
53.0	0.948	1.010
57.8	0.997	1.059
62.6	1.038	1.100
67.4	1.083	1.149
72.2	1.112	1.185
77.0	1.161	1.222
81.9	1.202	1.279
86.7	1.235	1.333
89.1	——	1.361
91.5	1.300	——
96.3	1.414	——

FIGURE 54. FRICTION MOMENT VERSUS LOAD AT N = 400rps AND N = 450 rps.- FLEXIBLE THRUST BEARING LLF-2T (Cu-Be MEMBRANE, t_m = 230 μm Cu-Be SPIDER SPRING, t_p = 200 μm; $\bar{t}_s$ = 40 μm)

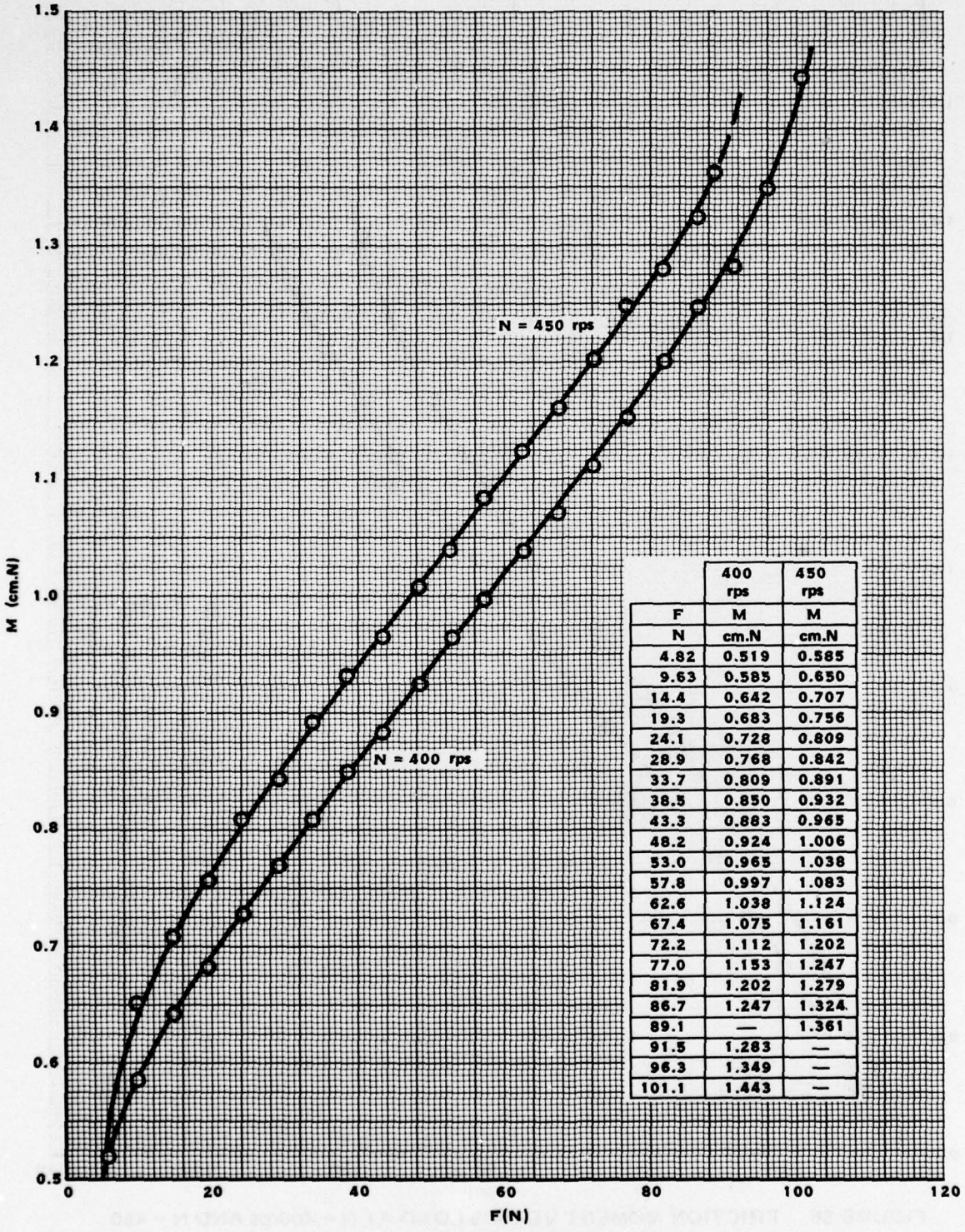

	400 rps	450 rps
F	M	M
N	cm.N	cm.N
4.82	0.519	0.585
9.63	0.585	0.650
14.4	0.642	0.707
19.3	0.683	0.756
24.1	0.728	0.809
28.9	0.768	0.842
33.7	0.809	0.891
38.5	0.850	0.932
43.3	0.883	0.965
48.2	0.924	1.006
53.0	0.965	1.038
57.8	0.997	1.083
62.6	1.038	1.124
67.4	1.075	1.161
72.2	1.112	1.202
77.0	1.153	1.247
81.9	1.202	1.279
86.7	1.247	1.324
89.1	—	1.361
91.5	1.283	—
96.3	1.349	—
101.1	1.443	—

FIGURE 55. FRICTION MOMENT VERSUS LOAD AT N = 400rps AND N = 450rps.- FLEXIBLE THRUST BEARING LLF-2T (INCONEL X-750 MEMBRANE, t_m = 215 μm. Cu-Be SPIDER SPRING, t_p = 200 μm; $\bar{t}_s$ = 40 μm)

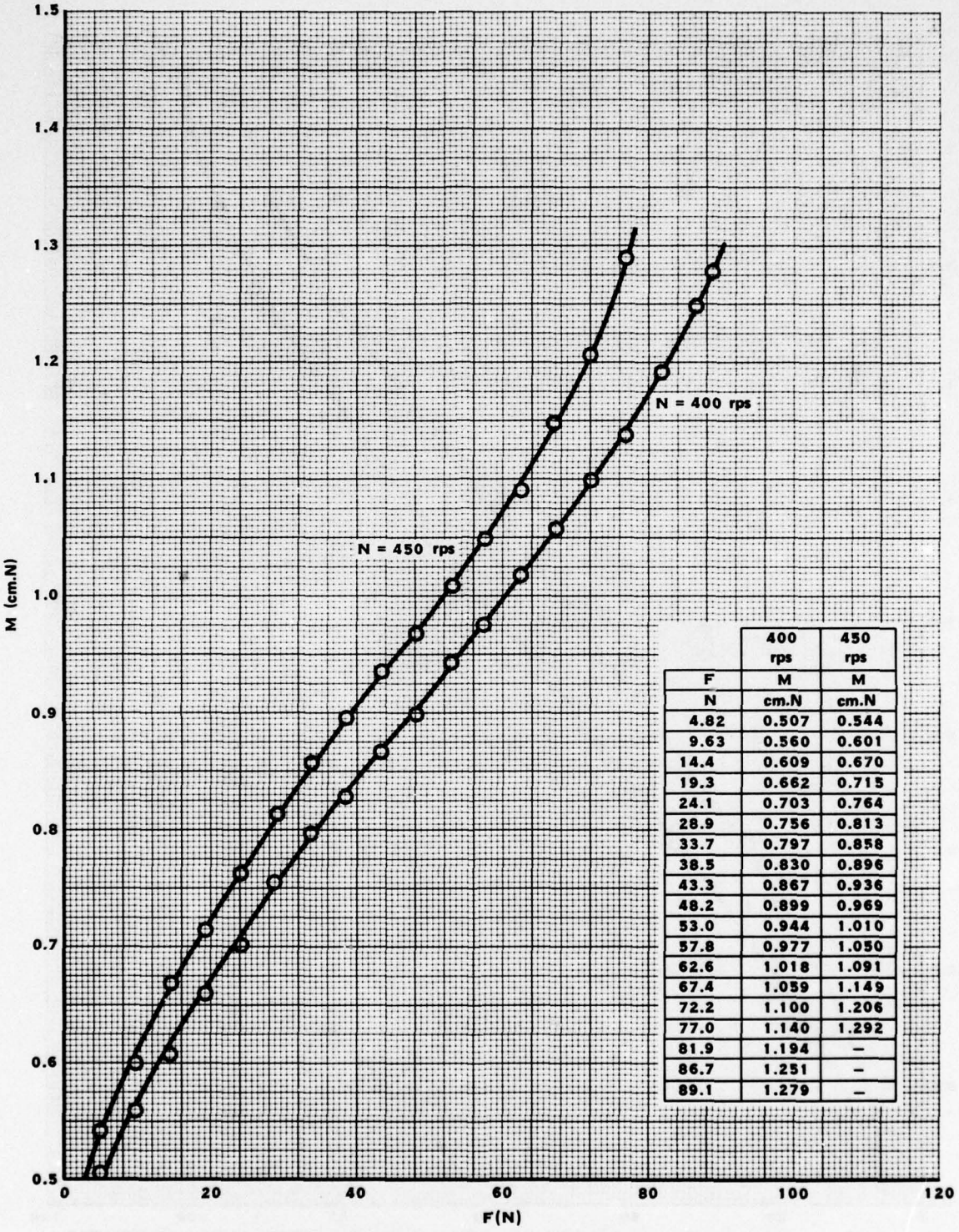

F	400 rps M	450 rps M
N	cm.N	cm.N
4.82	0.507	0.544
9.63	0.560	0.601
14.4	0.609	0.670
19.3	0.662	0.715
24.1	0.703	0.764
28.9	0.756	0.813
33.7	0.797	0.858
38.5	0.830	0.896
43.3	0.867	0.936
48.2	0.899	0.969
53.0	0.944	1.010
57.8	0.977	1.050
62.6	1.018	1.091
67.4	1.059	1.149
72.2	1.100	1.206
77.0	1.140	1.292
81.9	1.194	–
86.7	1.251	–
89.1	1.279	–

FIGURE 56. FRICTION MOMENT VERSUS LOAD AT N = 400rps AND N = 450 rps.- FLEXIBLE THRUST BEARING LLF-2T (Cu-Be MEMBRANE, t_m = 230 μm. STEEL SPIDER SPRING, t_p = 150 μm; $\bar{t}_s$ = 53 μm)

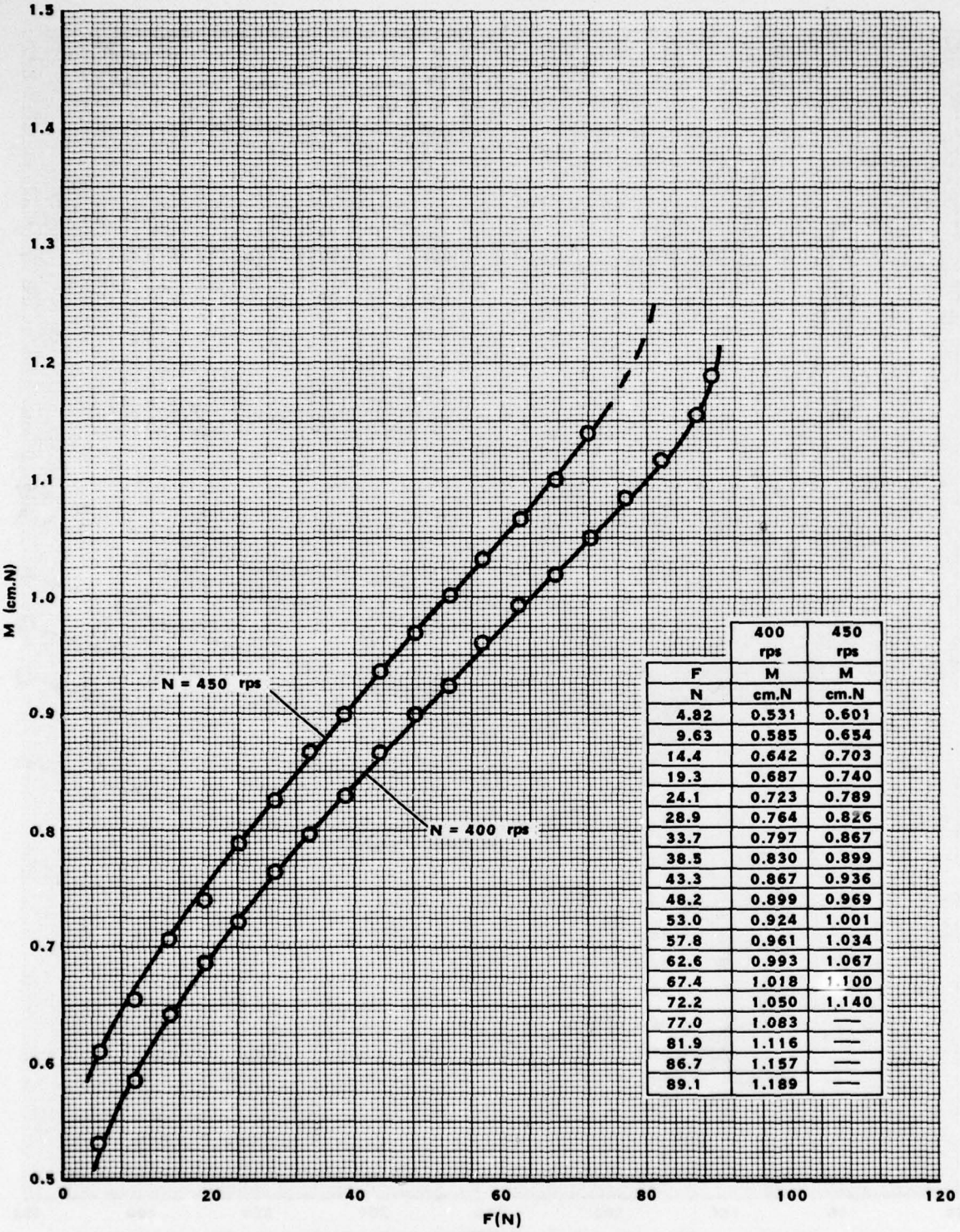

F	400 rps M	450 rps M
N	cm.N	cm.N
4.82	0.531	0.601
9.63	0.585	0.654
14.4	0.642	0.703
19.3	0.687	0.740
24.1	0.723	0.789
28.9	0.764	0.826
33.7	0.797	0.867
38.5	0.830	0.899
43.3	0.867	0.936
48.2	0.899	0.969
53.0	0.924	1.001
57.8	0.961	1.034
62.6	0.993	1.067
67.4	1.018	1.100
72.2	1.050	1.140
77.0	1.083	—
81.9	1.116	—
86.7	1.157	—
89.1	1.189	—

FIGURE 57. FRICTION MOMENT VERSUS LOAD AT N = 400rps AND N = 450 rps.-FLEXIBLE THRUST BEARING LLF-2T (INCONEL X-750 MEMBRANE, t_m = 215 μm, STEEL SPIDER SPRING, t_p = 150 μm; $\bar{t}_s$ = 53 μm)

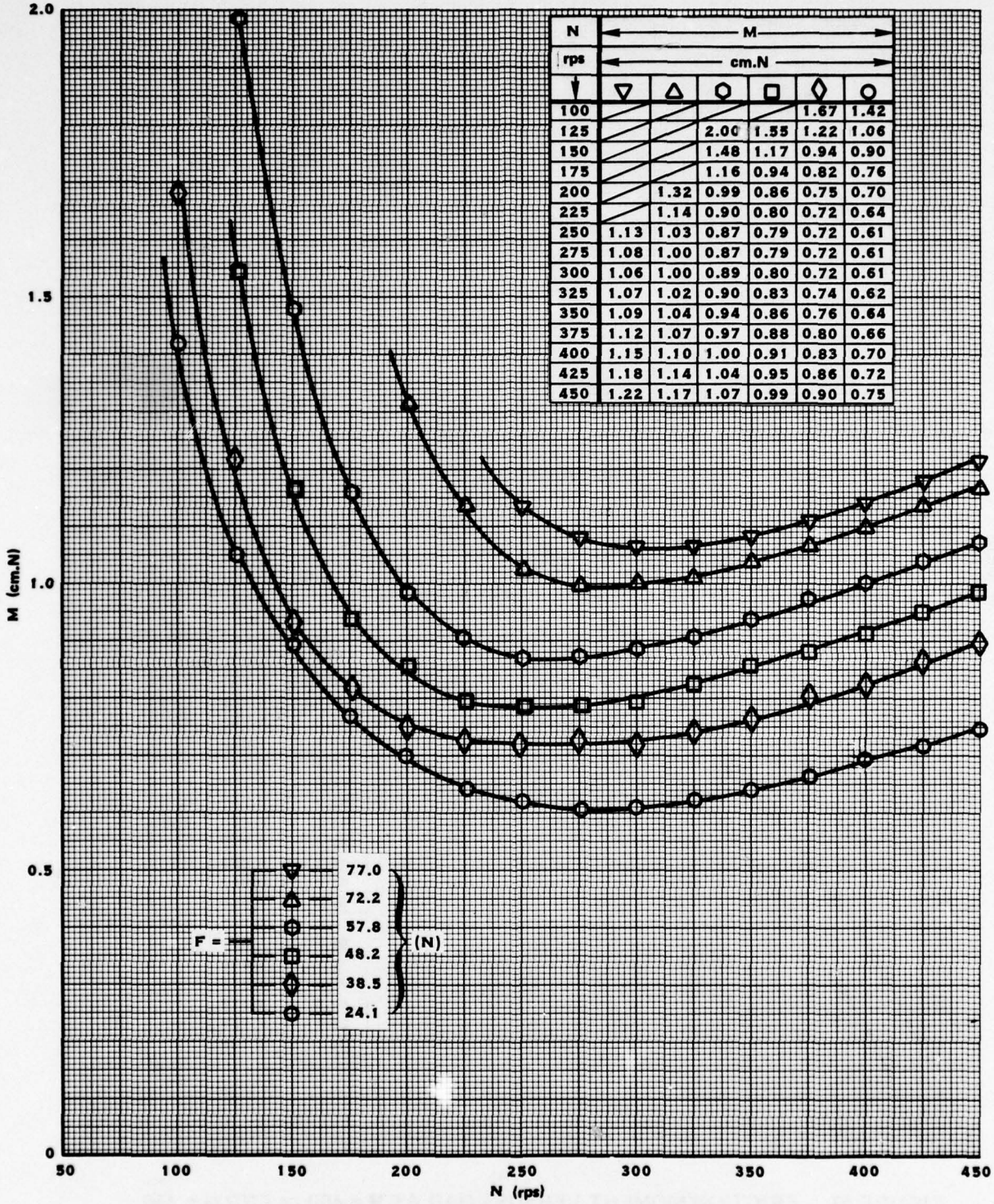

N	M					
rps	cm.N					
	▽	△	○	□	◇	○
100					1.67	1.42
125			2.00	1.55	1.22	1.06
150			1.48	1.17	0.94	0.90
175			1.16	0.94	0.82	0.76
200		1.32	0.99	0.86	0.75	0.70
225		1.14	0.90	0.80	0.72	0.64
250	1.13	1.03	0.87	0.79	0.72	0.61
275	1.08	1.00	0.87	0.79	0.72	0.61
300	1.06	1.00	0.89	0.80	0.72	0.61
325	1.07	1.02	0.90	0.83	0.74	0.62
350	1.09	1.04	0.94	0.86	0.76	0.64
375	1.12	1.07	0.97	0.88	0.80	0.66
400	1.15	1.10	1.00	0.91	0.83	0.70
425	1.18	1.14	1.04	0.95	0.86	0.72
450	1.22	1.17	1.07	0.99	0.90	0.75

FIGURE 58. FRICTION MOMENT VERSUS SPEED AT CONSTANT LOAD. FLEXIBLE THRUST BEARING LLF-2T (Cu-Be MEMBRANE, t_m = 230 μm Cu-Be SPIDER SPRING, t_p = 200 μm; $\bar{t}_s$ = 40 μm)

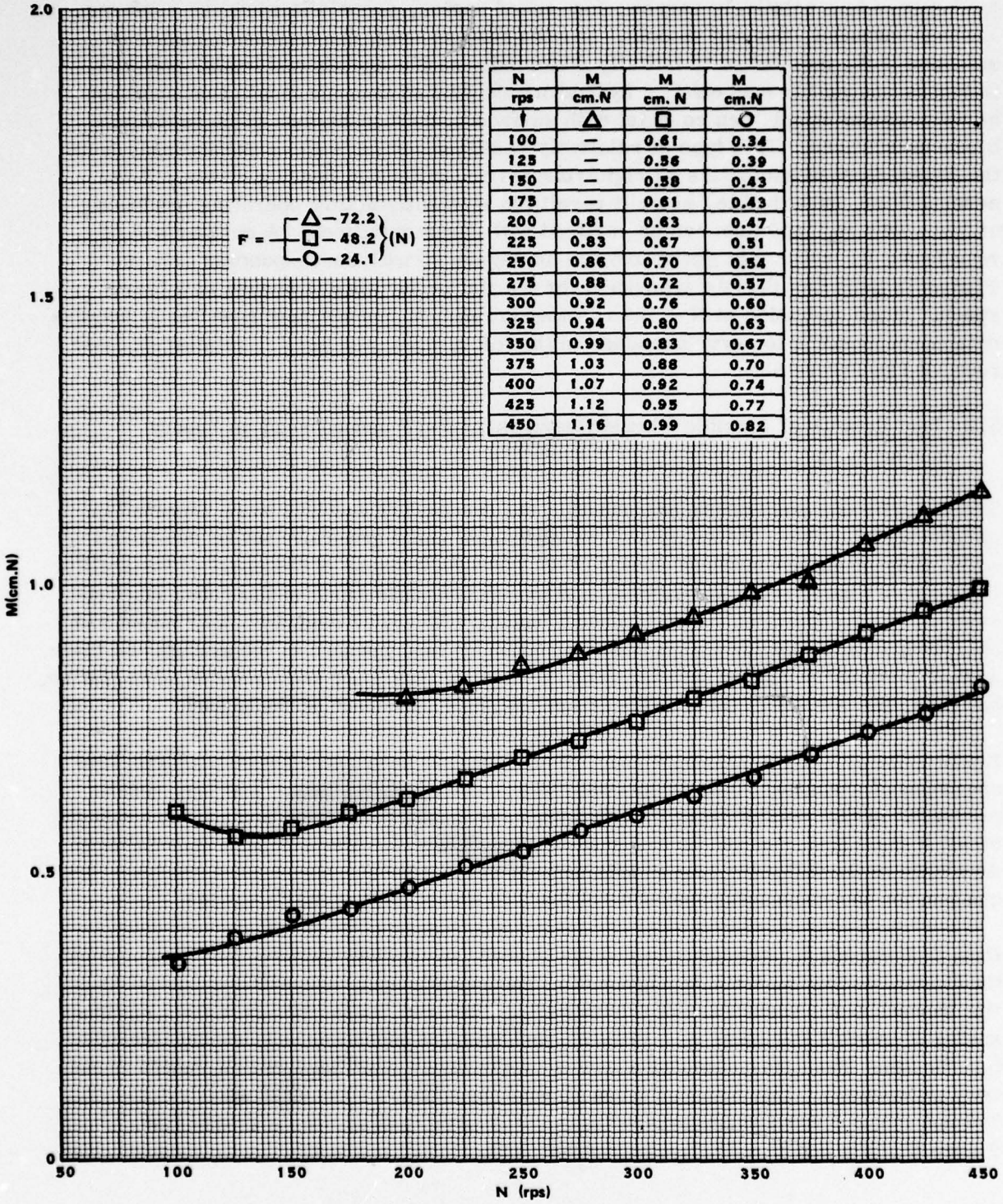

N rps	M cm.N △	M cm. N □	M cm.N ○
100	—	0.61	0.34
125	—	0.56	0.39
150	—	0.58	0.43
175	—	0.61	0.43
200	0.81	0.63	0.47
225	0.83	0.67	0.51
250	0.86	0.70	0.54
275	0.88	0.72	0.57
300	0.92	0.76	0.60
325	0.94	0.80	0.63
350	0.99	0.83	0.67
375	1.03	0.88	0.70
400	1.07	0.92	0.74
425	1.12	0.95	0.77
450	1.16	0.99	0.82

FIGURE 59. FRICTION MOMENT VERSUS SPEED AT CONSTANT LOAD.- FLEXIBLE THRUST BEARING LLF-2T (INCONEL X-750 MEMBRANE, t_m =215 μm. Cu-Be SPIDER SPRING, t_p = 200 μm; $\bar{t}_s$ = 40 μm)

load occurs in a relatively narrow, low-speed region, especially when the surfaces are very parallel, flat and smooth. For the case at hand, the transition region is extended if the membrane is initially distorted. At low speeds and loads, and with waviness not yet "ironed out", a hydrodynamic film of average height that need not be necessarily small can co-exist with surface contact in regions of highest membrane undulations. This type of relatively resilient contact differs qualitatively from the engagement of asperities on rigid runners and inflexible bearing plates. It is, nevertheless, undesirable, since it results in less satisfactory operating conditions at low speed and load than can be realized with flat membranes. A comparison of results for the relatively flat membrane in Figure 59 with corresponding data in Figure 58 indicates that the transition for the flatter membrane occurs at a lower speed. Since operation at N < 100 rps was erratic, it has not been possible to acquire data corresponding to curve branches to the left of minimum points, similar to those recorded in Figure 58.

5.3 Test Results of Flexible Thrust Bearings LLF-1T and LLF-2T to Speeds of 45,000 rpm

The experiments and results described in the preceeding sections were reported in chronological order. It was pointed out that tests could generally not be conducted with safety at speeds much in excess of 27,000 rpm because of the onset of instability. High-speed experiments, therefore, had to await modifications of the rotor support-system. More specifically, foil journal-bearings had to be designed, fabricated and operated, before flexible thrust bearings could be incorporated in the system and their testing resumed at higher speeds. For the sake of continuity and cohesion of narrative, however, the results of these tests are presented in this part of the report.

It will suffice to say at this point that the foil journal-bearings allowed problem-free operation of a similar rotor to speeds of the order of 50,000 rpm. The test results presented in this section were obtained with a well balanced rotor and correspondingly small journal trajectories, in order to acquire data with reference to a known datum. As shown in the following part of this report, small unbalance was not a condition sine qua non for the successful operation of flexible thrust and journal bearings.

Data of F versus $\tilde{h}$, analogous to results given in preceding sections, is presented for the thrust bearing LLF-2T in Figure 60. The results apply to a similar and fairly flat Inconel X-750 membrane of thickness t_m = 215 μm, supported on a steel spider-spring of overall thickness t_p = 170 μm, and having a mean spring-element thickness $\bar{t}_s$ = 50 μm. The curve contains a "knee" in the lower most load region, which is not very pronounced. The data in Figure 60 was recorded at a constant speed of N = 720 rps (43,200 rpm) and is related to the measured displacements graphed in Figure 61 ($\tilde{h} = H_{ROT} - H_{STA}$; see Section 2.3).

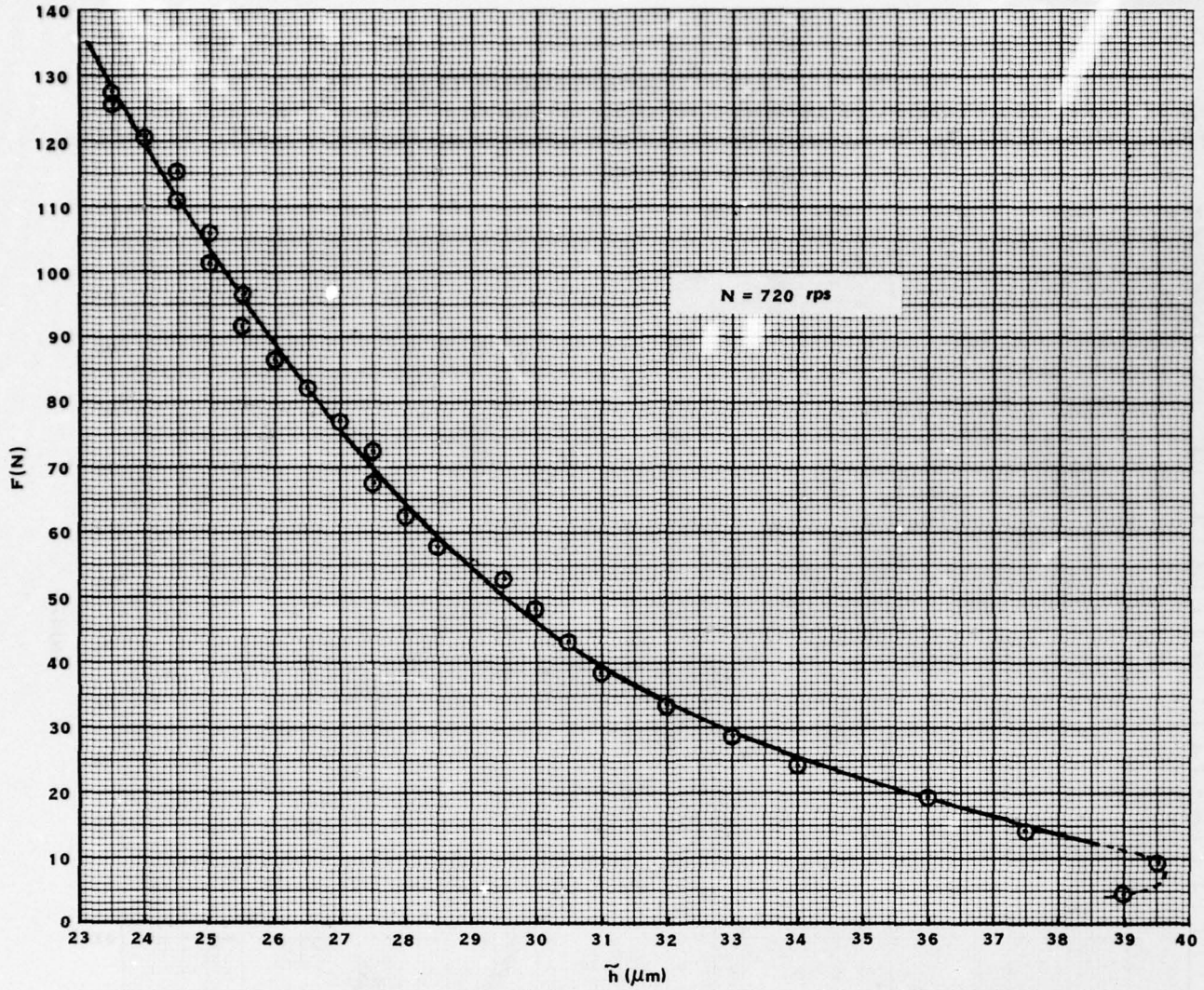

F	$\tilde{h}$
N	μm
4.81	39.0
9.63	39.5
14.4	37.5
19.3	36.0
24.1	34.0
28.9	33.0
33.7	32.0
38.5	31.0
43.3	30.5
48.2	30.0
53.0	29.5
57.8	28.5
62.6	28.0
67.4	27.5
72.2	27.5
77.0	27.0
81.9	26.5
86.7	26.0
91.5	25.5
96.7	25.5
101.1	25.0
105.9	25.0
110.8	24.5
115.6	24.5
120.4	24.0
125.2	23.5
127.6	25.5

FIGURE 60. LOAD VERSUS CLEARANCE AT N = 720rps.-FLEXIBLE THRUST BEARING LLF-2T. (INCONEL X-750 MEMBRANE, t_m = 215 μm. STEEL SPIDER SPRING, t_p = 170 μm; $\bar{t}_s$ = 50 μm)

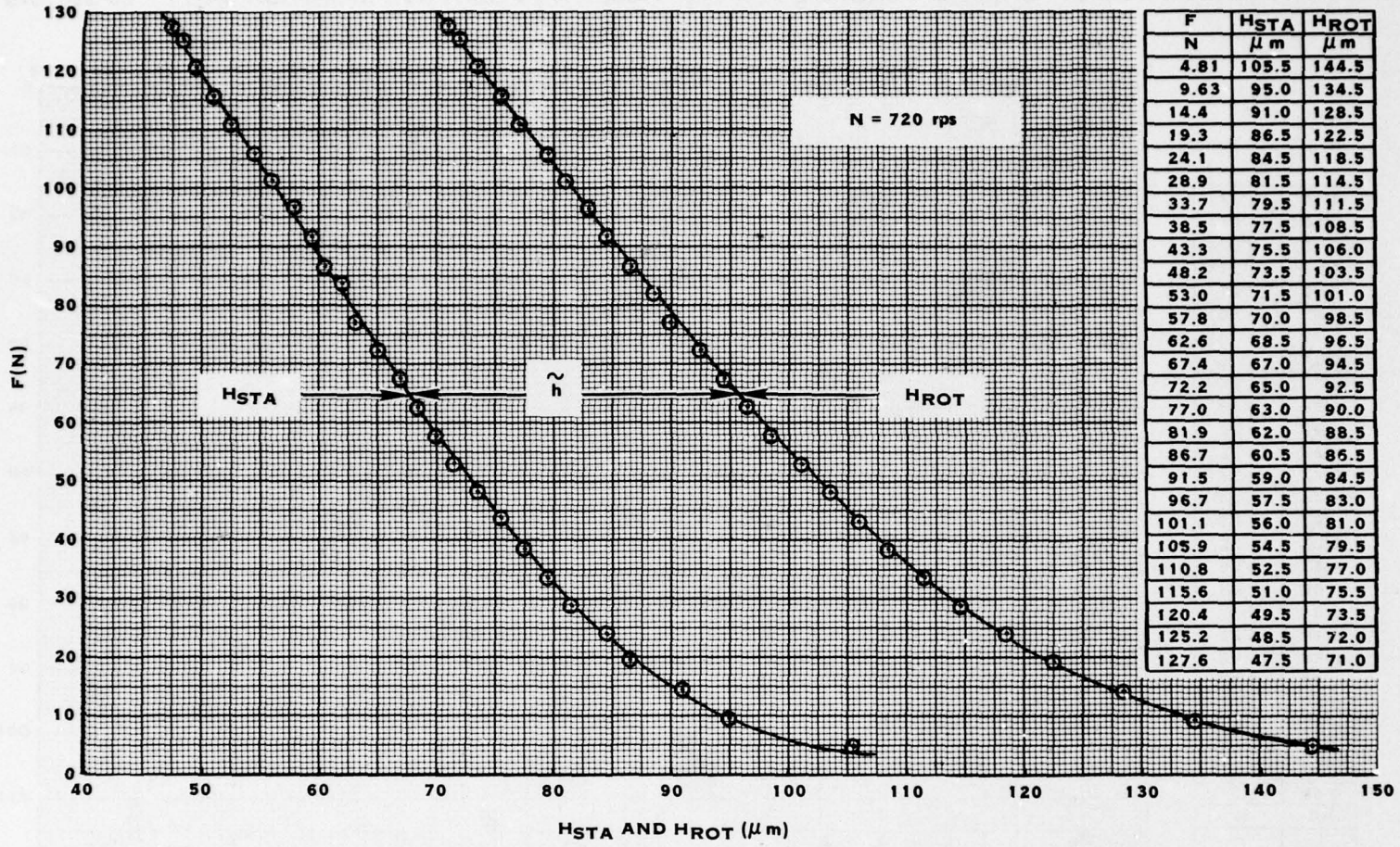

F	H_{STA}	H_{ROT}
N	μm	μm
4.81	105.5	144.5
9.63	95.0	134.5
14.4	91.0	128.5
19.3	86.5	122.5
24.1	84.5	118.5
28.9	81.5	114.5
33.7	79.5	111.5
38.5	77.5	108.5
43.3	75.5	106.0
48.2	73.5	103.5
53.0	71.5	101.0
57.8	70.0	98.5
62.6	68.5	96.5
67.4	67.0	94.5
72.2	65.0	92.5
77.0	63.0	90.0
81.9	62.0	88.5
86.7	60.5	86.5
91.5	59.0	84.5
96.7	57.5	83.0
101.1	56.0	81.0
105.9	54.5	79.5
110.8	52.5	77.0
115.6	51.0	75.5
120.4	49.5	73.5
125.2	48.5	72.0
127.6	47.5	71.0

FIGURE 61. DISPLACEMENT OF RUNNER RELATIVE TO SUPPORT PLATE (DETERMINATION OF CLEARANCE $\tilde{h} = H_{ROT} - H_{STA}$, FIGURE 60).-FLEXIBLE THRUST BEARING LLF-2T (INCONEL X-750 MEMBRANE, t_m = 215 μm, STEEL SPIDER SPRING, t_p = 170 μm; $\bar{t}_s$ = 50 μm)

A similar set of data of F versus $\tilde{h}$, at N = 720 rps, is contained in Figure 62. These results relate to an initially wavy, copper-beryllium membrane of thickness t_m = 230 μm, supported on a copper-beryllium spider spring of overall thickness t_p = 215 μm, and an average thickness of spring elements t_s = 71 μm. The curve has a very pronounced "knee", characteristic of results obtained with initially distorted membranes. The data in Figure 62 was derived from that in Figure 63. The slope of H_{STA} in Figure 63, and also in Figure 61, gives the magnitude of the overall static stiffness. Note that the linear portion of the H_{STA} curve in Figure 63 is steeper than in Figure 61, and that $(K_S/K'_S) = (t_s/t'_s)^3$. $(E/E') \approx 1.72$ checks very well with the slope-ratio of the linear sections of H_{STA} - curves of $(K_S/K'_S) \approx 1.7$.

The F versus $\tilde{h}$ curves in Figure 60 and Figure 62 diverge with decreasing load and converge as the load is increased. Note that at the highest load applied (at N = 720 rpm) the values of $\tilde{h}$ differ only by approximately 4%. The unit load at F = 127.6 N (13 Kgf; 28.7 lb) was $F/\pi\ (R_o^2 - R_i^2) = 3.02$ N/cm^2 (0.31 Kgf/cm^2; 4.38 lb/in^2).

The variation of the friction moment with load at constant speed, for the same membrane and spider-spring combination relevant to Figures 60 and 61, is shown in the M versus F graph in Figure 64, at a speed of 750 rps. Except at low loads, where the friction torque probably decreases very sharply and in which region data could not be reliably recorded, the characteristic is sensibly linear, up to approximately F $\approx$ 107 N. No precise explanation can be offered for the unusual trend observed above this load value and no thrust exceeding 127.6 N was applied to this bearing.

The last set of data in this section relates to the flexible foil bearing LLF-1T. The F versus $\tilde{h}$ characteristic was recorded at N = 750 rps with a relatively flat but slightly convex Inconel X-750 membrane of thickness t_m = 215 μm. The plate springs had a thickness t_s = 130 μm. The data is presented in Figure 65 and was derived from the relative displacement measurements included in Figure 66. A maximum load of F = 149.3 N was applied, at which point a value of $\tilde{h}$ = 15 μm was recorded. No significant indication of gross contact was observed upon the examination of the membrane, other than the usual notch-type wear at the outer edge of the runner and a burnished 1.5 mm-wide band along the inner periphery of the membrane. This was the highest load applied.

6.0 TESTING OF JOURNAL FOIL-BEARINGS AND JOINT OPERATION OF COMPLIANT JOURNAL AND THRUST BEARINGS

The design and construction of journal foil-bearings was described in Sections 3.1 and 3.2. The same foil-retaining cartridges were used with both types of journal bearings; either with twin, or with single foil-elements. When twin foil-elements were used, the bearing span was L = 125 mm and equal to the distance between the monitoring planes $(X, Y)_{1,2}$ of the capacitance probes. When single foil-elements were used, the bearing span was approximately L = 154 mm. The overall rotor length was 270 mm (10.6 in).

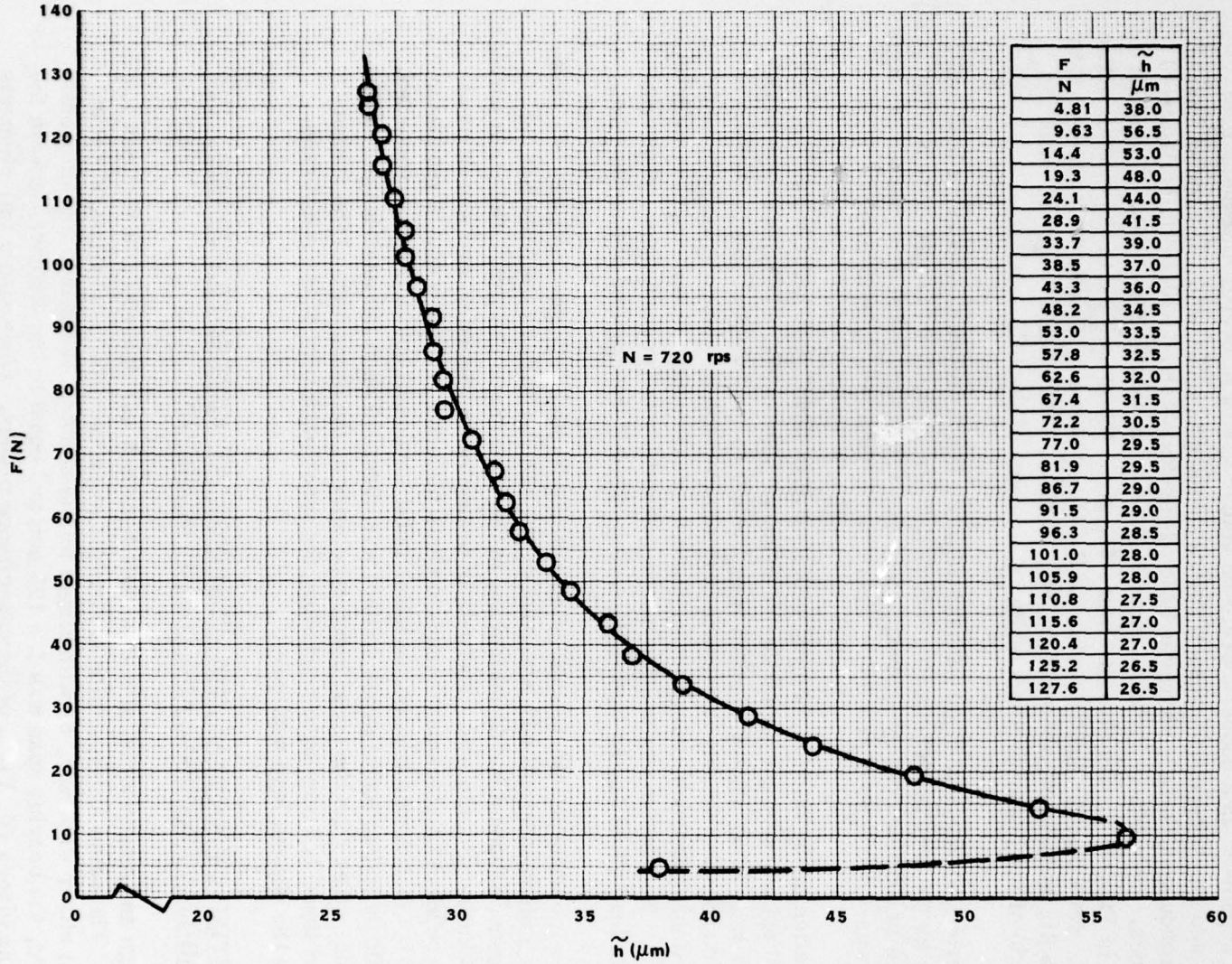

F N	$\tilde{h}$ μm
4.81	38.0
9.63	56.5
14.4	53.0
19.3	48.0
24.1	44.0
28.9	41.5
33.7	39.0
38.5	37.0
43.3	36.0
48.2	34.5
53.0	33.5
57.8	32.5
62.6	32.0
67.4	31.5
72.2	30.5
77.0	29.5
81.9	29.5
86.7	29.0
91.5	29.0
96.3	28.5
101.0	28.0
105.9	28.0
110.8	27.5
115.6	27.0
120.4	27.0
125.2	26.5
127.6	26.5

FIGURE 62. LOAD VERSUS CLEARANCE AT N = 720rps. FLEXIBLE THRUST BEARING LLF-2T (Cu-Be MEMBRANE, t_m = 230. Cu-Be SPIDER SPRING, t_p = 215 μm; $\bar{t}_s$ = 71 μm)

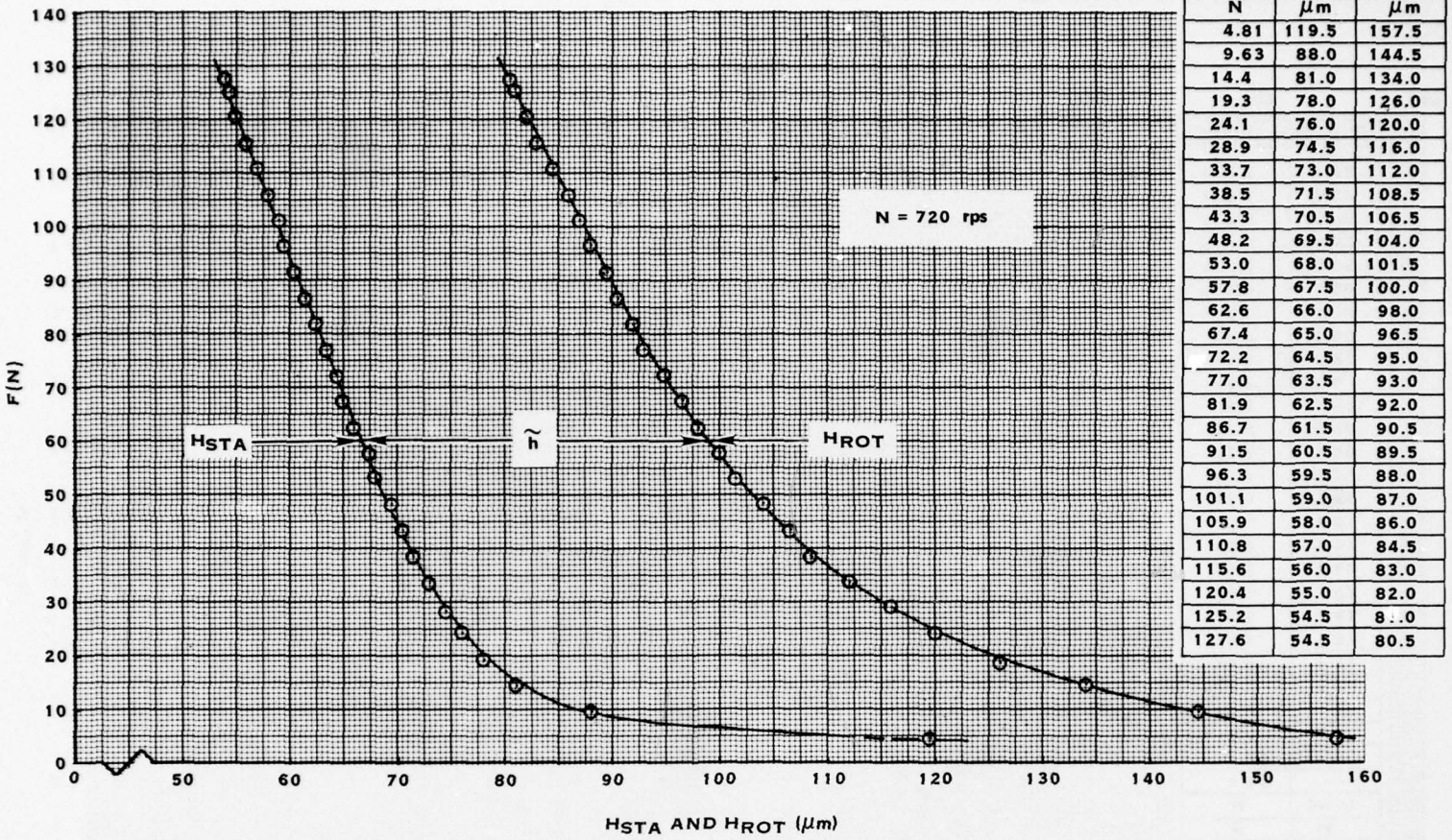

F	H_{STA}	H_{ROT}
N	μm	μm
4.81	119.5	157.5
9.63	88.0	144.5
14.4	81.0	134.0
19.3	78.0	126.0
24.1	76.0	120.0
28.9	74.5	116.0
33.7	73.0	112.0
38.5	71.5	108.5
43.3	70.5	106.5
48.2	69.5	104.0
53.0	68.0	101.5
57.8	67.5	100.0
62.6	66.0	98.0
67.4	65.0	96.5
72.2	64.5	95.0
77.0	63.5	93.0
81.9	62.5	92.0
86.7	61.5	90.5
91.5	60.5	89.5
96.3	59.5	88.0
101.1	59.0	87.0
105.9	58.0	86.0
110.8	57.0	84.5
115.6	56.0	83.0
120.4	55.0	82.0
125.2	54.5	8..0
127.6	54.5	80.5

FIGURE 63. DISPLACEMENT OF RUNNER RELATIVE TO SUPPORT PLATE (DETERMINATION OF CLEARANCE $\tilde{h} = H_{ROT} - H_{STA}$, FIGURE 62).-FLEXIBLE THRUST BEARING LLF-2T (Cu-Be MEMBRANE, t_m = 230 μm; Cu-Be SPIDER SPRING, t_p = 215 μm; $\bar{t}_s$ = 71 μm)

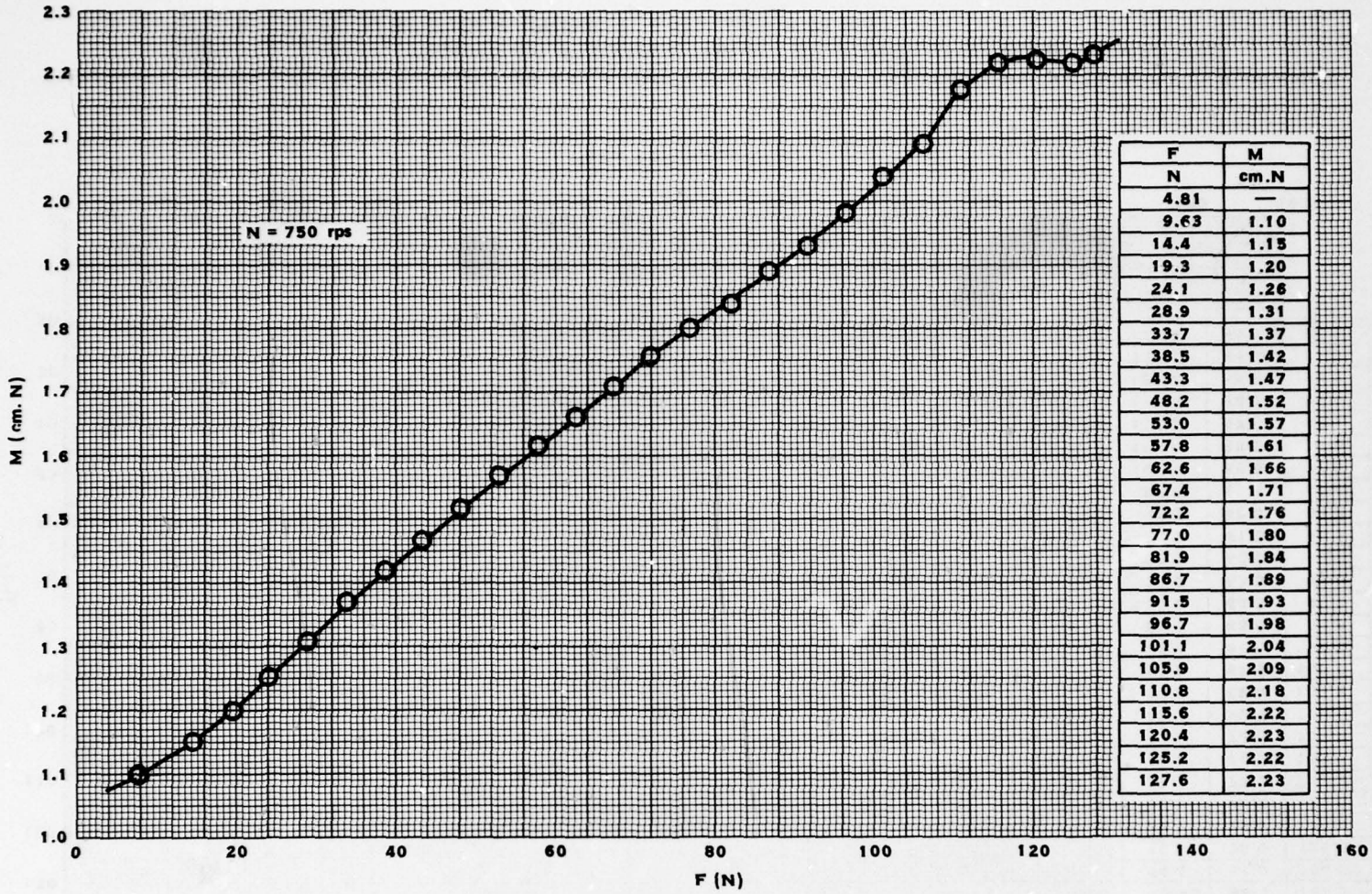

F N	M cm.N
4.81	—
9.63	1.10
14.4	1.15
19.3	1.20
24.1	1.26
28.9	1.31
33.7	1.37
38.5	1.42
43.3	1.47
48.2	1.52
53.0	1.57
57.8	1.61
62.6	1.66
67.4	1.71
72.2	1.76
77.0	1.80
81.9	1.84
86.7	1.89
91.5	1.93
96.7	1.98
101.1	2.04
105.9	2.09
110.8	2.18
115.6	2.22
120.4	2.23
125.2	2.22
127.6	2.23

FIGURE 64. FRICTION MOMENT VERSUS LOAD AT 750rps.-FLEXIBLE THRUST BEARING LLF-2T (INCONEL X-750 MEMBRANE, t_m = 215 μm. STEEL SPIDER SPRING, t_p = 170 μm; $\bar{t}_s$ = 50 μm)

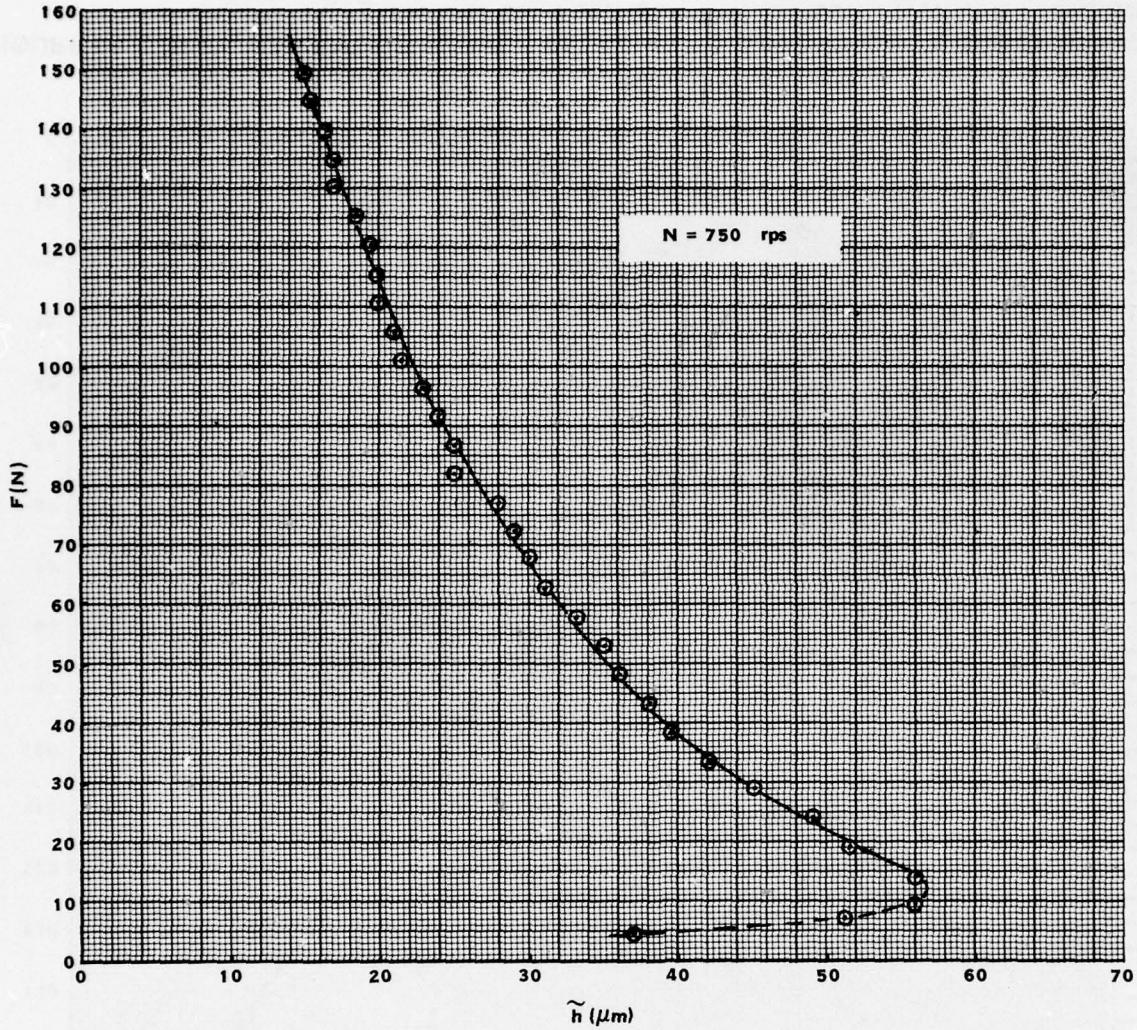

F N	$\tilde{h}$ μm
4.81	36.5
9.63	56.0
14.4	56.0
19.3	51.5
24.1	49.0
28.9	45.0
33.7	42.0
38.5	39.5
43.3	38.0
48.2	36.0
53.0	35.0
57.8	33.0
62.6	31.0
67.4	30.0
72.2	29.0
77.0	28.0
81.9	25.0
86.7	25.0
91.5	24.0
96.3	23.0
101.1	21.5
105.9	21.0
110.8	20.0
115.6	20.0
120.4	19.5
125.2	18.5
130.0	17.0
134.8	17.0
139.6	16.5
144.5	15.5
149.3	15.0

FIGURE 65. LOAD VERSUS CLEARANCE AT N = 750rps.-FLEXIBLE THRUST BEARING LLF-1T (INCONEL X-750 MEMBRANE, t_m = 215 μm. STEEL PLATE SPRINGS, t_s = 130 μm)

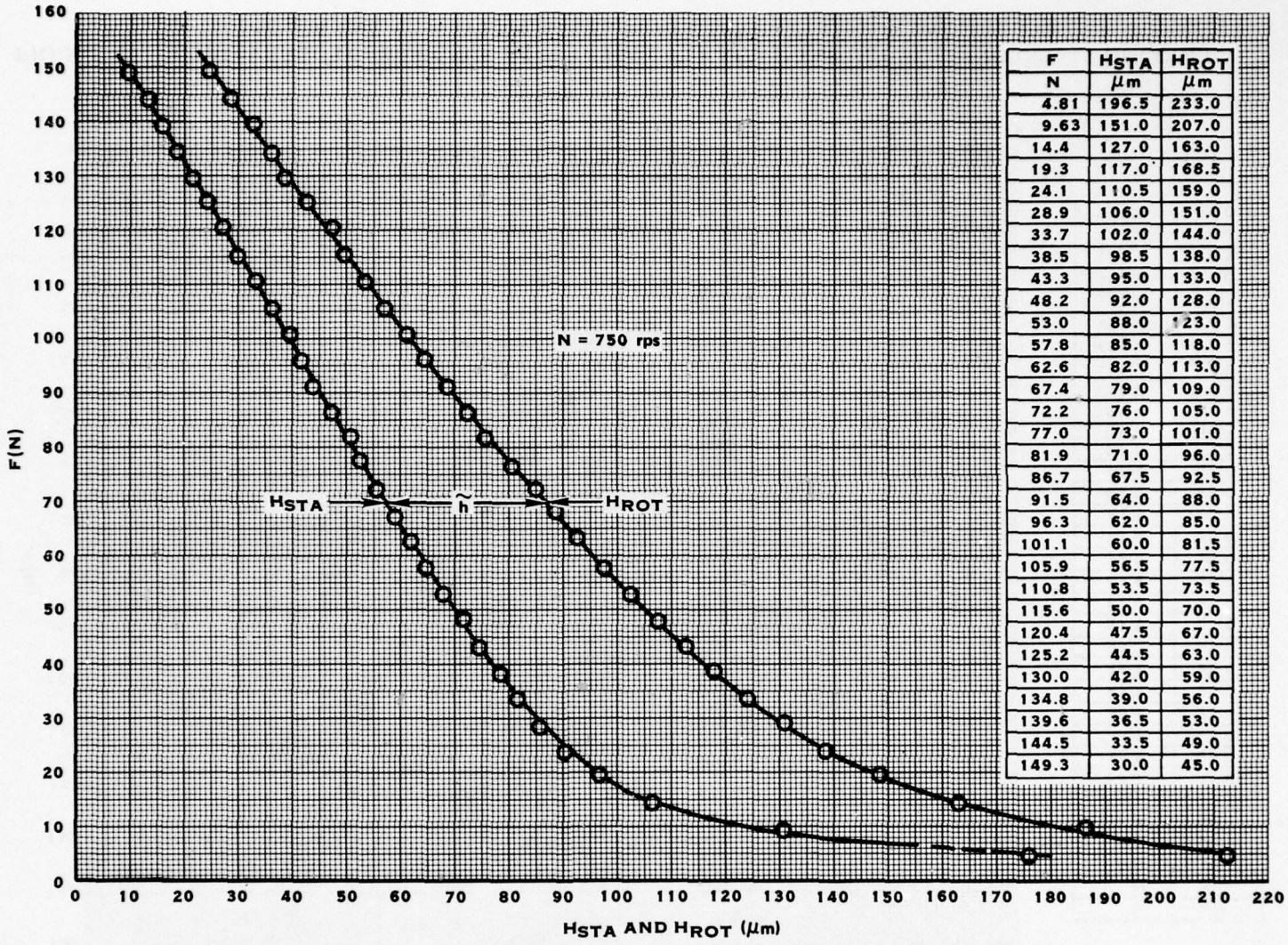

F N	HSTA μm	HROT μm
4.81	196.5	233.0
9.63	151.0	207.0
14.4	127.0	163.0
19.3	117.0	168.5
24.1	110.5	159.0
28.9	106.0	151.0
33.7	102.0	144.0
38.5	98.5	138.0
43.3	95.0	133.0
48.2	92.0	128.0
53.0	88.0	123.0
57.8	85.0	118.0
62.6	82.0	113.0
67.4	79.0	109.0
72.2	76.0	105.0
77.0	73.0	101.0
81.9	71.0	96.0
86.7	67.5	92.5
91.5	64.0	88.0
96.3	62.0	85.0
101.1	60.0	81.5
105.9	56.5	77.5
110.8	53.5	73.5
115.6	50.0	70.0
120.4	47.5	67.0
125.2	44.5	63.0
130.0	42.0	59.0
134.8	39.0	56.0
139.6	36.5	53.0
144.5	33.5	49.0
149.3	30.0	45.0

FIGURE 66. DISPLACEMENT OF RUNNER RELATIVE TO SUPPORT PLATE (DETERMINATION OF CLEARANCE $h = H_{ROT} - H_{STA}$, FIGURE 65).-FLEXIBLE THRUST BEARING LLF-1T (INCONEL X-750 MEMBRANE, $t_m = 215\mu m$. STEEL PLATE SPRINGS, $t_s = 130\ \mu m$).

The recessed bores of the foil-retaining cartridges had 30.610 mm diameters and the journal diameters were 29.870 mm, leaving a radial annulus of approximately 0.37 mm to accommodate the plane foil-elements of the LLF-1J bearings, or the elements with polygonally-bent sections of the LLF-2J bearings.

Preliminary experiments with a bearing similar to the LLF-1J type were described in reference [56], which contained also a brief mention of a hexagonal support with sharp corners, made by deforming the foil over a chisel-like edge of a thin glass plate.* The quasi-polygonal backing of the LLF-2J bearing had rounded vertices, the radius and angle of bend, as well as the spacing of vertices, constituting important design parameters.

Copper-beryllium and steel foils were used in the LFF-1J bearings, the choice of material, although important, representing a secondary consideration. Here the difference in thickness of the two foils, $\Delta t_f \approx 54-51 \approx 3$ μm, afforded simple means for varying the effective clearance. In each coil, the number of turns was six, so that the maximum radial clearance $\bar{c}$ could not exceed respectively 59 and 41 μm, if allowance is made for approximately 5 μm of coating on the innermost surface. Actual measurements, obtained by pressing the journals against the foils in opposite directions along several diameters of the cartridge (except in the direction of the longitudinal retaining groove, Figure 29), showed the "average" clearances thus defined to have magnitudes of $\bar{c} \approx 59.0$ μm and $\bar{c} \approx 39.8$ μm. Experimental data was recorded for both values of $\bar{c}$, with either two, or one foil-element per cartridge (nominal foil width L = 20 mm, and nominal bearing diameter D_j = 30 mm).

The LLF-2J foil bearing with an octagonally-bent backing had a steel foil-element (t_f = 54 μm). The quasi-octagonal section had vertex radii r_v = 0.5 mm and vertex angles $\alpha_v \approx 130°$ (as compared with 135° for a regular closed octagon). The backing was integral with approximately 2 1/4 turns of plane foil, the innermost turn terminating in the X-plane.

The rotor used in this series of experiments was of weight W = 19.08 N. The transverse and polar radii of gyration were r_t = 89.9 mm and r_p = 15.8 mm, and the location of the center of mass from the midplane of the bearing adjacent to the runner, Figure 1, was either (a) l = 73 mm, for bearings with dual foil-elements, or (b) l = 87 mm, for bearings with single foil-elements. An estimate of the critical speed corresponding to the first bending mode of the rotor (aluminum runner and turbine) showed that it would fall well outside the contemplated range of 45,000 rpm.

*The writer experimented with elements made in this manner. Sharp corners caused failure, either in fabrication or during operation, due to the formation and propagation of cracks.

The residual unbalance of the rotor, referred to the balancing planes in the runner and in the turbine, located 125 mm and 82 mm from the center of mass, was $u_1 \approx 0.71$ μm·N (100 μin. oz) and $u_2 \approx 0.28$ μm·N (40 μin. oz), as compared with added unbalance of: (a) $U_1 = 21.0$ μm·N (2974 μin. oz) and $U_2 = 23.2$ μm·N (3285 μin. oz) for "symmetric" unbalance, and (b) $U_1 = 19.3$ μm·N (2733 μin. oz) and $U_2 = 23.2$ μm·N (3285 μin. oz) for "asymmetric" unbalance. The total unbalance per unit weight of rotor was of the order of 2.3 μm·N per newton (1449 μin. oz per pound), which is approximately ten times of what may be an acceptable level for a turbomachine at 45,000 rpm.* Most of the oscilloscope data relevant to the dynamic characteristics of the rotor-bearing system were recorded at these levels of unbalance.

The records of oscilloscope data presented in the following sections consist of journal trajectories (orbits) in the monitoring planes $(XY)_1$ and $(XY)_2$ and corresponding time-base traces of the probes Y_1 and Y_2. These data, which define the character of motion at selected speeds, are complemented by scans of amplitude component X_1, Y_1, and X_2, Y_2 with the frequency of rotation. The scans were generally recorded during coastdown of the rotor, to eliminate excitation caused by the interaction of nozzle jets and turbine buckets.

An attempt was also made to measure the eccentricity loci of the LLF-1J bearing, but these results must be interpreted with caution, because of the following considerations: (a) The normalizing quantity, that is the "clearance" $\bar{c}$, cannot be taken as equivalent to the clearance of a rigid, cylindrical bearing; neither in magnitude, nor in regard to uniformity. (b) The error due to thermal expansion, which cannot be distinguished from displacement by the capacitance probes, is considerable.

To aid the reader in the interpretation of data, the following should be observed: (a) Rotation is clockwise when viewing the runner from the turbine end. (b) The positive Y-direction is downward, and the positive X-direction is to the right when viewing the runner from the turbine end. The vectors thus defined form a right-handed system, and the positive directions coincide with those in which probe voltages increase. (c) On the oscilloscope photographs, positive Y and X are upward and to the right. The angular velocity vector, therefore, points toward the viewer.

The results of the concluding series of experiments, relevant to both the journal foil-bearings and to the flexible thrust bearings, are presented and reviewed in the following three sections.

---

*The following range for upper limits of unbalance is quoted in reference [67]: $6.35 \times 10^3 \frac{W}{N} < U < 15.9 \times 10^3 \frac{W}{N}$, where U is in μm. N, W is the rotor weight in newtons, and N is the speed in rpm (or: $4 \times 10^6 \frac{W}{N} < U < 10 \times 10^6 \frac{W}{N}$, where U is in μin. oz, W in pounds and N in rpm)

6.1 Test Results of Journal Foil-Bearings LLF-1J to Speeds of 45,000 rpm (Dual Foil-Elements; $\bar{c} \approx 59\ \mu m$). - Operation without and with Axial Load

Following "static breadboarding", which consisted mainly of gauging and matching several coils and dummy journals, the flame-plated journals were ground to a finished diameter of 29.870 mm, and a six-turn copper-beryllium coil was selected for the first trial run. The coating (Dow-Corning Molykote 88) was evenly sprayed, cured and burnished. The average thickness of the coating was between 5 and 6 μm. The average value of the maximum "clearance" was $\bar{c} = 59\ \mu m$, approximately 0.004 cm/cm of journal radius (0.004 in/in). This value is large for a rigid air-lubricated bearing, but since the elastic coil always tends to unwind and to produce interstitial clearances between turns, the effective clearance had a smaller value.

The choice was judicious (absence of analytical guidance and numerical predictors notwithstanding), and the rotor-bearing system performed exceedingly well on first trial. The first run, with a well balanced rotor and the experimental thrust-bearing (LLF-2T) unloaded, was so uneventful that recording of oscilloscopic data was omitted. Instead, symmetric unbalance of $U_1 = 21.0\ \mu m.N$ and $U_2 = 23.2\ \mu m.N$ was added in two planes; U_1 in the runner, approximately 125 mm from the center of mass, and U_2 in the turbine wheel, approximately 82 mm from the center of mass. *

The following remarks are appropriate at this point and apply to this and other types of journal foil-bearings. The response of a rotor supported in such bearings is characterized by subharmonic components of motion and nonsynchronous resonances. Regions of instability exist, but unlike in rigid air bearings, in which the onset of instability is generally associated with discontinuous and unbounded growth of trajectories, the unstable motion in journal foil-bearings is bounded and the trajectories of limit cycles remain sensibly small. Regions of instability may be traversed with safety, and the performance appears not to be adversely affected by continuous operation within an unstable speed-range.

Turning now to the results of the first run (with a rather unhealthy amount of added unbalance), the complementary data in Figure 67 and Figure 68 clearly indicate that the amplitude response of rotors supported by foil bearings of this type does not in the least resemble that of linear, or quasi-linear systems [68, 69, 70]. It is useful and complemental to view the paired photographs of trajectories and waveforms in Figure 67 simultaneously with the scans in Figure 68, bearing in mind that correspondence of speeds and amplitudes in these figures may involve a slight error (Section 2.2). The data will be described briefly in the reverse order in which recorded, i.e. starting in the low-speed region. Note that the speed identifying the trajectories and waveforms in Figure 67 are marked approximately in the upper photograph of Figure 68. The scans in Figure 68a and Figure 68b were recorded consecutively and are nearly identical.

---

*The terms "symmetric" and "asymmetric" unbalance are not used in the strict, geometrical sense. What is implied is that unbalance weights were added in like angular positions, or in locations displaced by 180°.

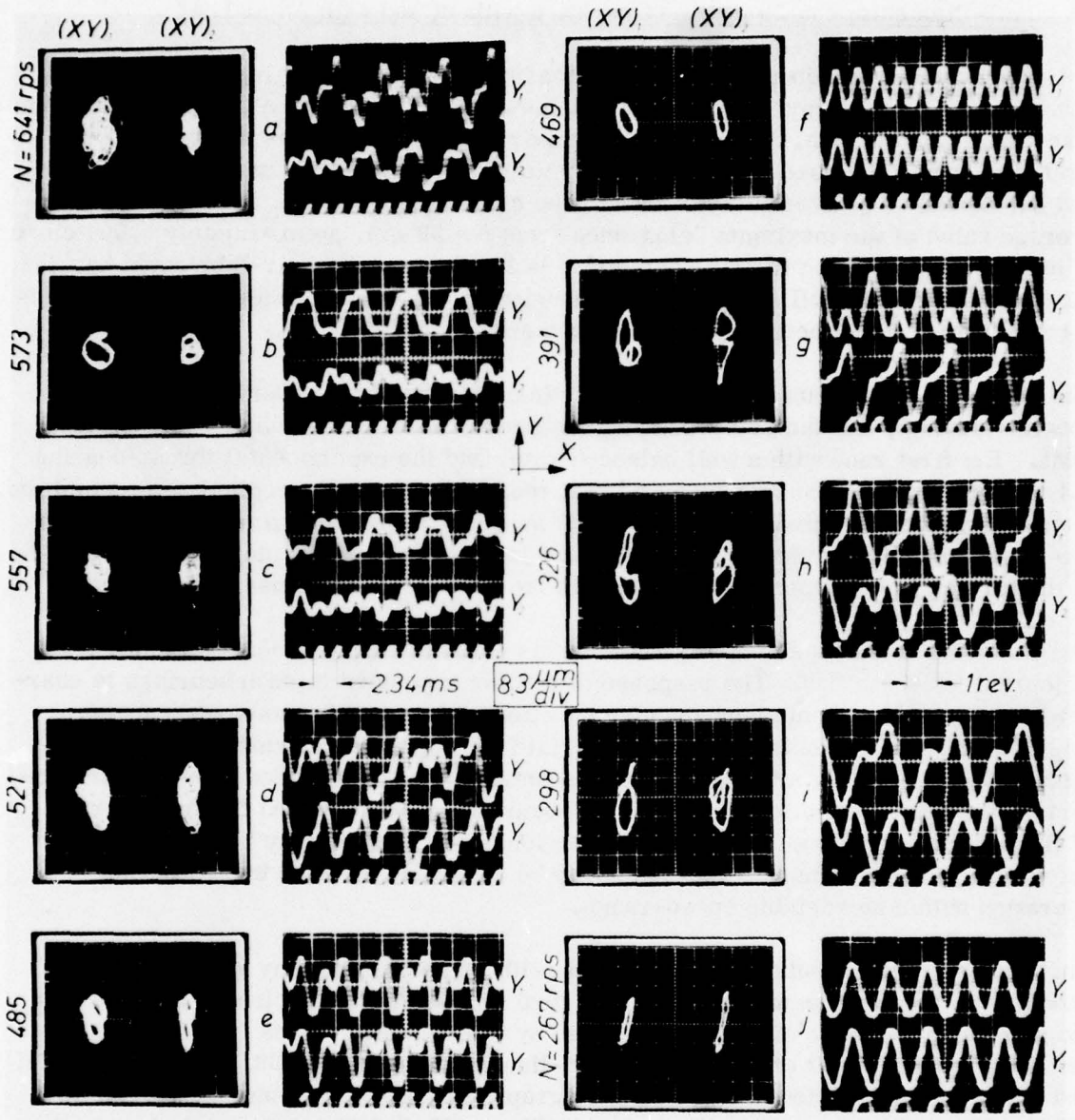

FIGURE 67. TRAJECTORIES AND TIME-BASE RECORDS OF MOTION IN $(XY)_{1,2}$ AND $(Y_1 Y_2)$ PLANES WITH SYMMETRIC UNBALANCE U_1 = 21.0 μm. N AND U_2 = 23.2 μm. N.-JOURNAL FOIL-BEARING LLF-1J (TWO Cu-Be FOILS PER BEARING, EACH L x D x t_f = 20 x 30 x 0.051 mm. SIX TURNS, $\bar{c} \approx 59$ μm. FLEXIBLE THRUST BEARING UNLOADED)

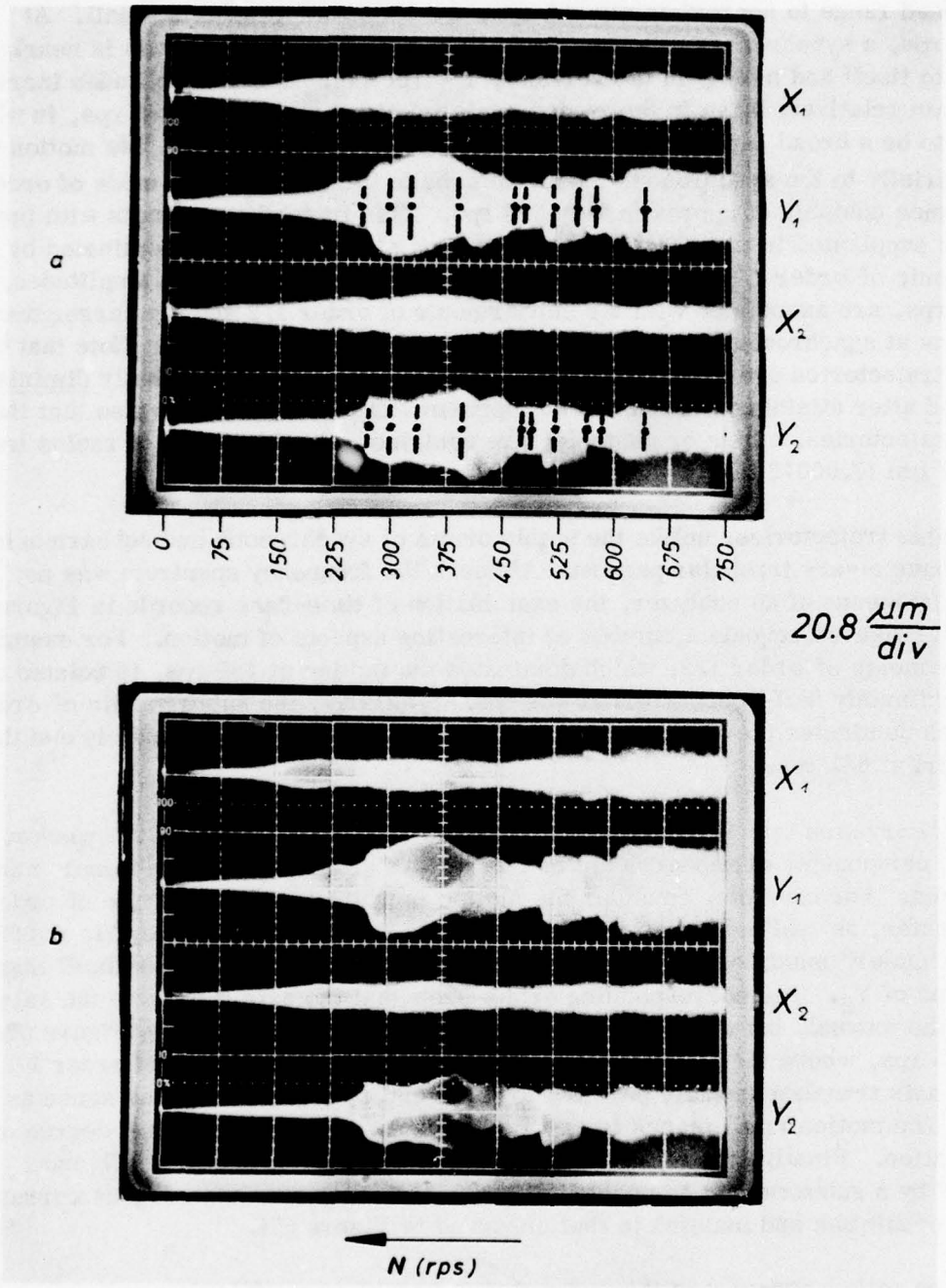

FIGURE 68. AMPLITUDE SCAN DURING COASTDOWN WITH SYMMETRIC UNBALANCE U_1 = 21.0 μm. N AND U_2 = 23.2 μm. N.-JOURNAL FOIL-BEARING LLF-1J (TWO Cu-Be FOILS PER BEARING, EACH L x D x t_f = 20 x 30 x 0.051mm. SIX TURNS, $\bar{c} \approx 59$ μm. FLEXIBLE THRUST BEARING UNLOADED).-SCANS (a) AND (b) ARE IDENTICAL, AND MARKED POINTS IN (a) CORRESPOND APPROXIMATELY TO SPEED VALUES INDICATED IN FIGURE 67.

In the speed range to approximately 200 rps, the amplitude growth is small. At $N \approx 267$ rps, a synchronous resonance occurs and the motion of the axis is nearly parallel to itself and mainly in the vertical, Y-direction. The Y-amplitudes increase and remain relatively large in the region centered at approximately 350 rps, in what appears to be a broad band of subharmonic resonance of order 1/2.* The motion then reverts briefly to the synchronous mode, returns to the subharmonic mode of order 1/2, and becomes unstable at approximately 500 rps. This instability persists with increasing speed, is supplanted in the vicinity of 573 rps by a stable trajectory dominated by a subharmonic of order 1/3, and resumes at $N \approx 620$ rps. The highest amplitudes, at $N \approx 326$ rps, are associated with the subharmonic of order 1/2 and are larger than the excursions at synchronous resonance, or when the motion is unstable. Note that the unstable trajectories are not only bounded, but that their envelope actually diminishes with speed after attaining a maximum at approximately 641 rps. Note also that the largest trajectories, stable or unstable, are contained within a circle of radius less than 18.2 μm (0.00072 in).

The unstable trajectories, unlike the stable orbits of synchronous and subharmonic motion, have a very irregular pattern. Although the frequency spectrum was not resolved by means of an analyzer, the examination of time-base records in Figure 67 and similar figures reveals a number of interesting aspects of motion. For example, the subharmonic of order 1/2, which dominates the motion at 485 rps, is related to the approximately half-speed whirl at 521 rps. Similarly, the subharmonic of order 1/3, which dominates the motion at 573 rps, is related to the approximately one third-speed whirl at 641 rps.

Another observation may be of interest and is drawn to the attention of the reader. The amplitude components of subharmonic motion always display major and minor minima and maxima. For example, consider the motion in which the subharmonic of order 1/2 dominates, as typified by the time-base traces Y_1 and Y_2 in Figure 67i, at 298 rps. Here the "major" maxima and minima of Y_1 coincide in time with the "minor" maxima and minima of Y_2. The corresponding orbits show that the axis rotates in the same sense as the journal, but at half speed. On the other hand, referring to Figure 67e, at $N \approx 485$ rps, where the motion is also dominated by a subharmonic of order 1/2, the rotor axis translates nearly paralled to itself and rotates in the same sense as the journal. The motion in all planes is nearly identical, at least to the first degree of approximation. Finally, the motion at $N \approx 573$ rps, depicted in Figure 67b and dominated by a subharmonic component of order 1/3, displays an analogous correspondence of minima and maxima to that observed in Figure 67i.

It should be rather apparent at this point that it may be very difficult to construct mathematical models which would properly account for the physical characteristics of these and similar foil bearings, and thus difficult to predict by analytical and numerical means the dynamic response and stability of rotors mounted on flexible supports of

*The lowermost trace in most time-base displays is a marker, in which each cycle corresponds to one revolution.

this type. Numerical analysis, regardless of mathematical sophistication, will not aid the engineer if the model does account for the essential physical characteristics of the system. A complex model, in which such essential characteristics are not weighted even-handedly, missing, or excluded, is as naive and useless as an over-simplified representation. "Mechanical breadboarding", therefore, may still have merit, and foil bearings of proven utility and performance will not be discarded in the absense of "analytical respectability", if they can be made).

The data in Figure 69 and Figure 70 are similar to the results presented in the preceding two figures and relate to the motion of the rotor in the same bearings, with asymmetric unbalance $U_1 = 19.3$ μm. N and $U_2 = 23.2$ μm. N. The Y-amplitudes are considerably larger than the X-amplitudes. There are two bandwidths related to synchronous resonances, and the corresponding excursions in the (Y_1 Y_2)-plane are clearly discernible; one distinct peak at approximately 225 rps (Y_1), and a flat region centered at approximately 300 rps (Y_2). Subharmonic resonances of orders 1/2 and 1/3 occur between 375 and 450 rps and between 550 and 600 rps. Figure 69 contains several trajectories and time-base traces recorded in the above and other speed intervals. The motion becomes unstable above 600 rps, and a typical trajectory and time-base trace, at 638 rps, are contained in the photographs of Figure 69a. The whirl speed is approximately 1/3 of the rotational speed and the onset of instability is preceded by a subharmonic resonance of order 1/3. The maximum amplitudes of motion recorded with symmetric and asymmetric unbalance were commensurate, and in the present case the largest trajectories were contained within a circle of radius less than 13 μm (0.0005 in).

The plots in Figure 71 are of the apparent eccentricity loci of the journals, when the bearings support the gravity load only and the rotor speed is decreased from 700 to 80 rps. The decrements were in steps of 50 rps for $200 < N < 700$ rps, and 20 rps for $80 < N < 200$. As pointed out in Section 6.0, these results should be interpreted with caution. Even in a rigid journal bearing, the clearance c in $\epsilon = e/c$ is generally unknown under nonisothermal operating conditions. In the present case, the normalizing quantity $\bar{c} \approx R_c - n.t_f$, where R_c is the radius of the cartridge bore, n the number of foil turns, and t_f the foil thickness, cannot be taken as equivalent to the "cold" clearance of a rigid bearing. The elastic foil has undulations and the coil tends to unwind, increasing the interstitial clearance and decreasing the thickness of the lubricating air-film. The differential expansion is, of course, as significant as in rigid bearings and introduces a substantial error in measurement. The probes are mounted in the massive aluminum housing, which remains at room temperature, while the journal and cartridge, made of different material and varying in temperature, expand differentially. The probe cannot, of course, distinguish between thermal expansion and displacement. Finally, the reference points are obtained at room temperature (with the journals at the bottom of bearings), while data points are taken at higher and not necessarily equal temperature levels. Many of these difficulties and errors are unavoidable.

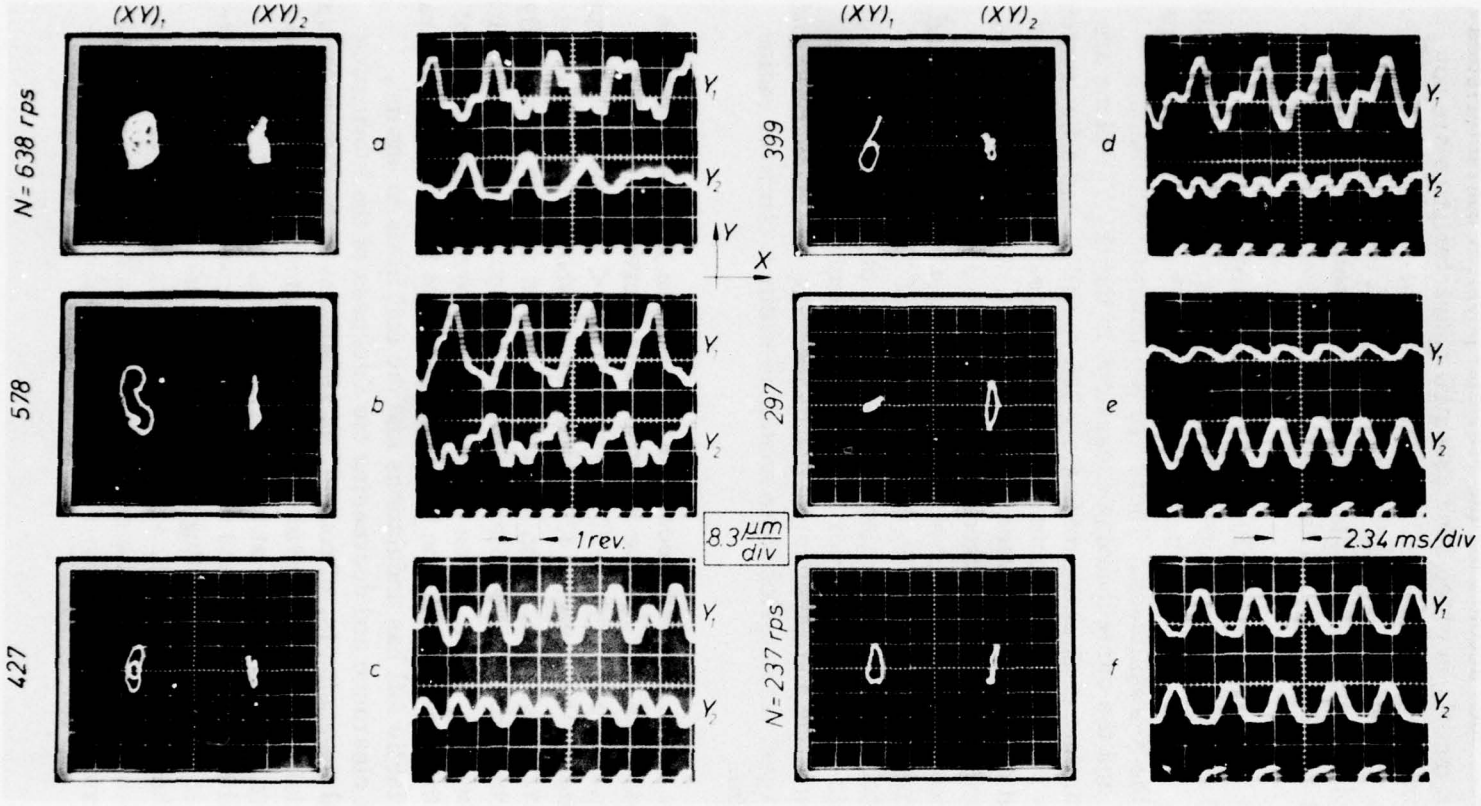

FIGURE 69. TRAJECTORIES AND TIME-BASE RECONDS OF MOTION IN $(XY)_{1,2}$ AND (Y_1Y_2) PLANES WITH ASYMMETRIC UNBALANCE U_1 = 19.3 μm. N AND U_2 = 23.2 μm. N.-JOURNAL FOIL-BEARING LLF-1J (TWO Cu-Be FOILS PER BEARING, EACH L x D x t_f = 20 x 30 x 0.051 mm. SIX TURNS, $\bar{c} \approx 59$ μm. FLEXIBLE THRUST BEARING UNLOADED)

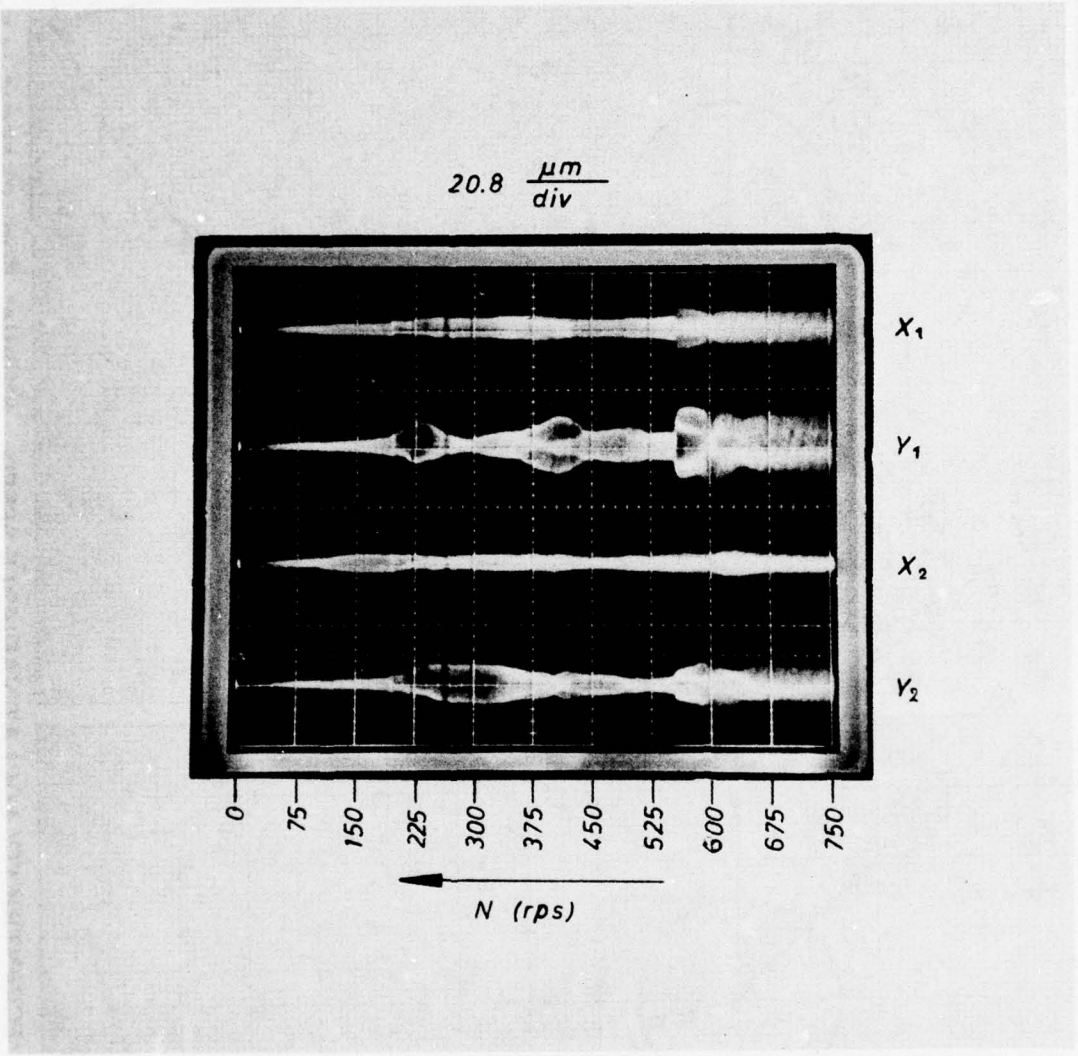

FIGURE 70. AMPLITUDE SCAN DURING COASTDOWN WITH ASYMMETRIC UNBALANCE U_1 = 19.3 μm. N AND U_2 = 23.2 μm. N.-JOURNAL FOIL-BEARING LLF-1J (TWO-Cu-Be FOILS PER BEARING, EACH L x D x t_f = 20 x 30 x 0.051 mm. SIX TURNS, $\bar{c} \approx 59$ μm. FLEXIBLE THRUST BEARING UNLOADED)

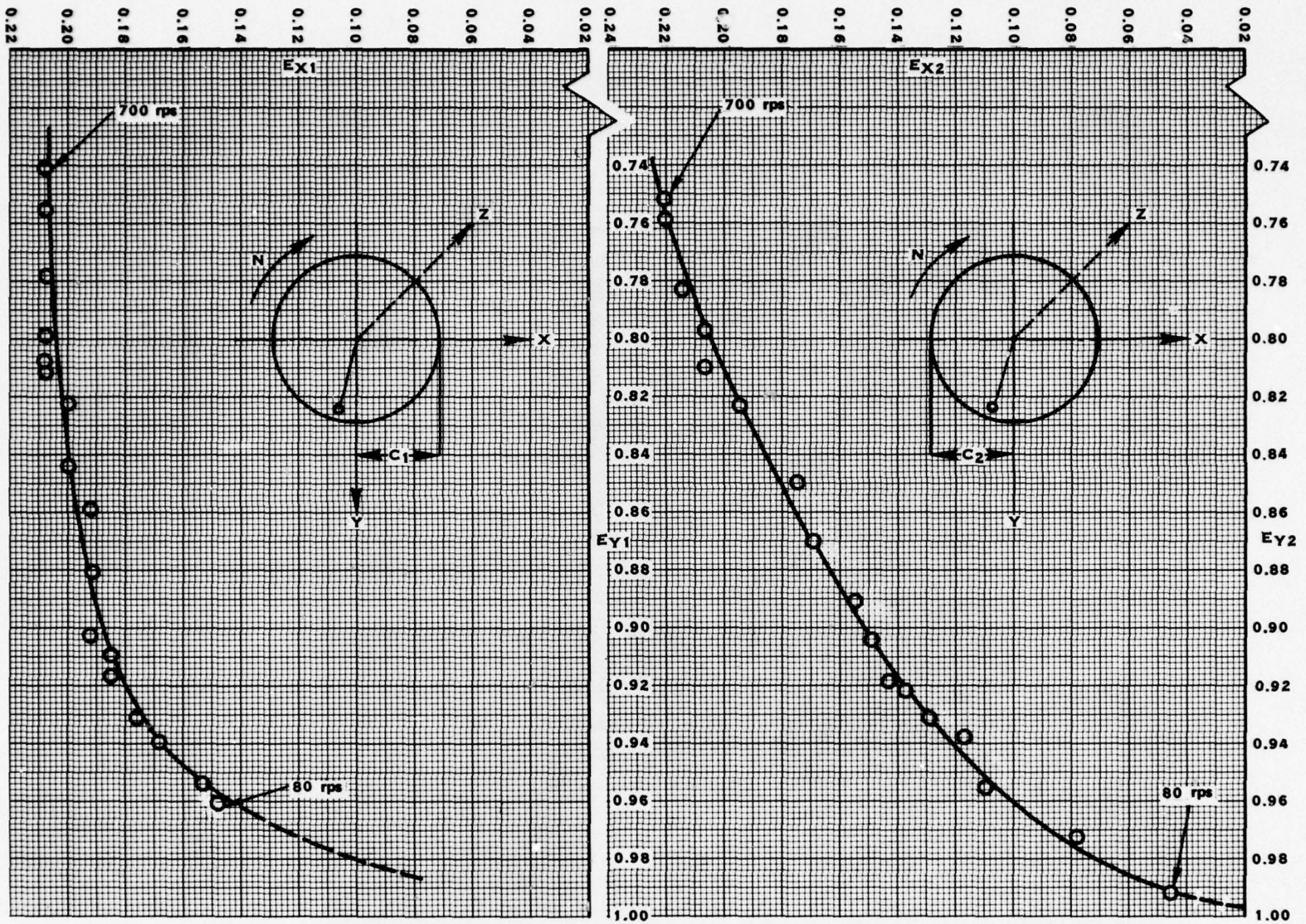

FIGURE 71. APPARENT ECCENTRICITY LOCI AT VARIABLE SPEED. JOURNAL FOIL-BEARING LLF-1J (TWO Cu-Be FOILS PER BEARING, EACH L x D x t_f = 20 x 30 x 0.051 mm. SIX TURNS, $\bar{c}_1 \approx 58$ μm, $\bar{c}_2 \approx 60$ μm). GRAVITY LOAD W = $W_1 + W_2$ = 11.14 + 7.94 = 19.08 N

It is inferred that the effective eccentricity at 700 rps was smaller than $\epsilon \approx 0.78$, where $\epsilon = [(1 - \Delta Y/\bar{c})^2 + (\Delta X/\bar{c})^2]^{1/2}$, ΔX and ΔY are the displacement referred to the lowermost journal position at rest, and $\bar{c} = R_c - n.\ t_f$. Similar considerations apply to the apparent eccentricity at other speeds.

The purpose of presenting the foregoing results is to include data that may be qualitatively correct, and at the same time alert the reader to errors and physical limitations associated with this type of measurement.

Experimental results of flexible thrust bearings at higher speeds (made possible through replacement of pressurized journal bearings with foil bearings) were presented in Section 5.3. This implied that a successful union was established between the axial and radial supports. It soon became apparent that such joint operation was possible not only with a well balanced rotor, but also with asymmetric unbalance, which represents the most dangerous type of excitation in regard to a heavily loaded thrust bearing operating at a small clearance.

The effect of an axial load F = 127.6N, applied via the flexible thrust bearing LLF-2T at N = 720 rps, is illustrated in Figure 72 and Figure 73. The excitation was provided by asymmetric unbalance $U_1 = 19.3\ \mu m.N$ and $U_2 = 23.3\ \mu m.N$, and the speed was in an unstable region. The trajectories in the upper left-hand side of Figure 72a correspond to motion in the absence of axial load, while those in the lower right-hand side depict the motion when the thrust was applied. The thrust-bearing membrane was a relative flat, Inconel X-750 specimen, $t_m = 215\ \mu m$, mounted on a steel spider-spring, $t_p = 170\ \mu m$ and $\bar{t}_s = 53\ \mu m$. The thrust-bearing load appeared to have little effect on the motion, which was unstable, but limited to a peak-to-peak amplitude $\Delta Y_{max} \approx 29\ \mu m$. This is a sensibly small excursion, particularly in view of the very large unbalance and the fact that the motion was unstable. The rotor was operated in this condition for extended periods of time, and the bearings suffered no ill effects.

It is highly unlikely that rigid journal and thrust bearings of comparable dimensions could be operated with this amount of unbalance, and it is also well known that the increase of speed beyond the onset of instability leads to the destruction of bearings.

In the time-base traces of Figure 72b, the upper trace (Z) is difficult to interpret. It comprises the wobble, runout and waviness of the thrust runner, as it rotates past a probe secured to the bearing support-plate, as well as the axial motion of the stator in pressurized air bearings (Figure 1). No attempt is made to elaborate further on the significance of the Z-trace, either here or in relation to other figures. The reader may note, however, that in the determination of $\tilde{h}$ with a well balanced rotor, Z is the time-dependent component of H_{ROT} (see Section 2.3). The Y-trace in Figure 72b indicates quite clearly that the whirl speed is approximately 1/3 the speed of rotation.

The test conditions and bearings relevant to Figure 73 were identical with those of Figure 72, except that a relatively wavy copper-beryllium membrane, $t_m = 230\ \mu m$,

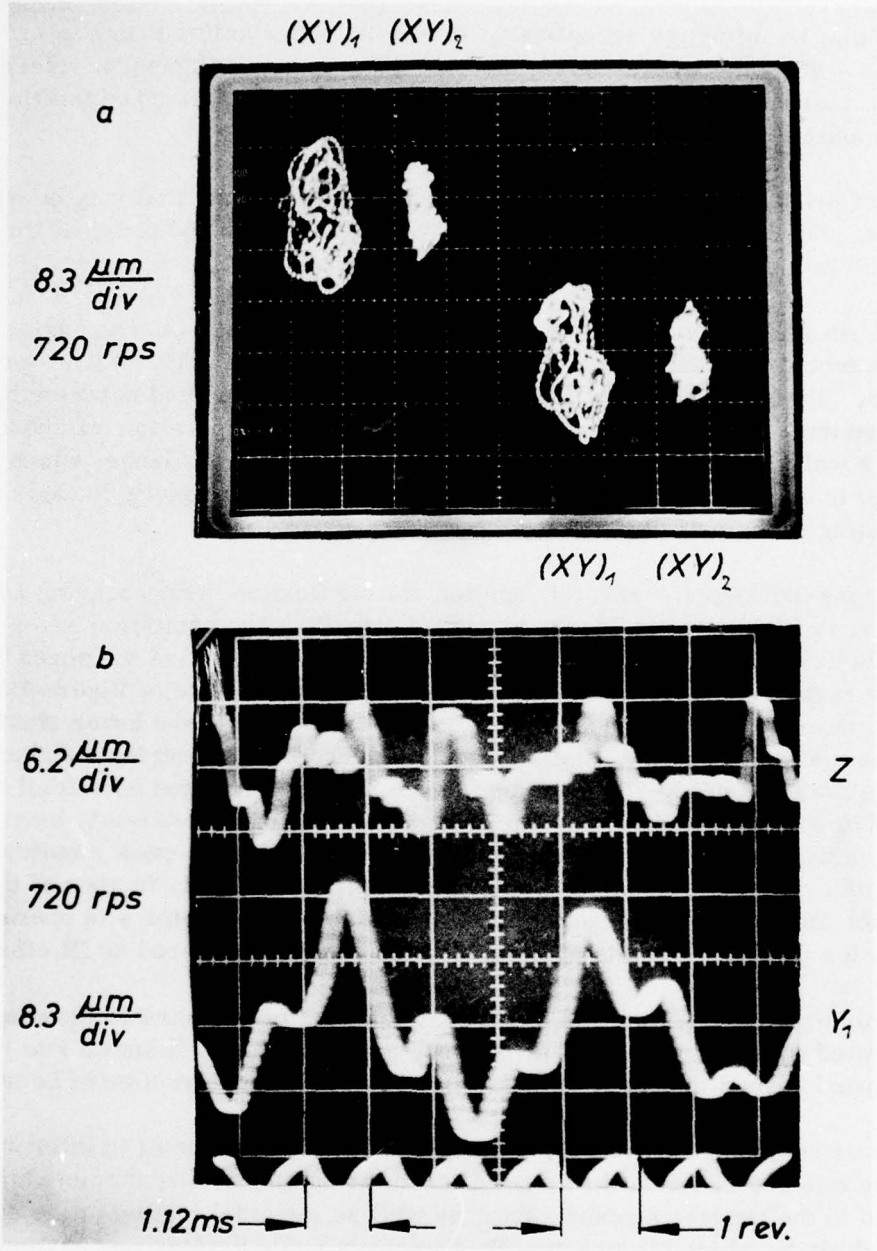

FIGURE 72. EFFECT OF THRUST LOAD AT N = 720rps ON MOTION OF ROTOR IN JOURNAL FOIL-BEARINGS LLF-1J (TWO Cu-Be FOILS PER BEARING, EACH L x D x t_f = 20 x 30 x 0.051 mm. SIX TURNS, $\bar{c} \approx 59$ μm).- FLEXIBLE THRUST BEARING LLF-2T (INCONEL X-750 MEMBRANE, t_m = 215 μm. STEEL SPIDER SPRING, t_p = 170 μm; $\bar{t}_s$ = 53 μm).
(a) UPPER LEFT: TRAJECTORIES IN THE ABSENCE OF THRUST LOAD. LOWER RIGHT: TRAJECTORIES WITH THRUST LOAD F = 127.6 N
(b) AXIAL MOTION OF RUNNER RELATIVE TO SUPPORT PLATE (Z) AND VERTICAL MOTION (Y_1). THRUST LOAD F = 127.6N

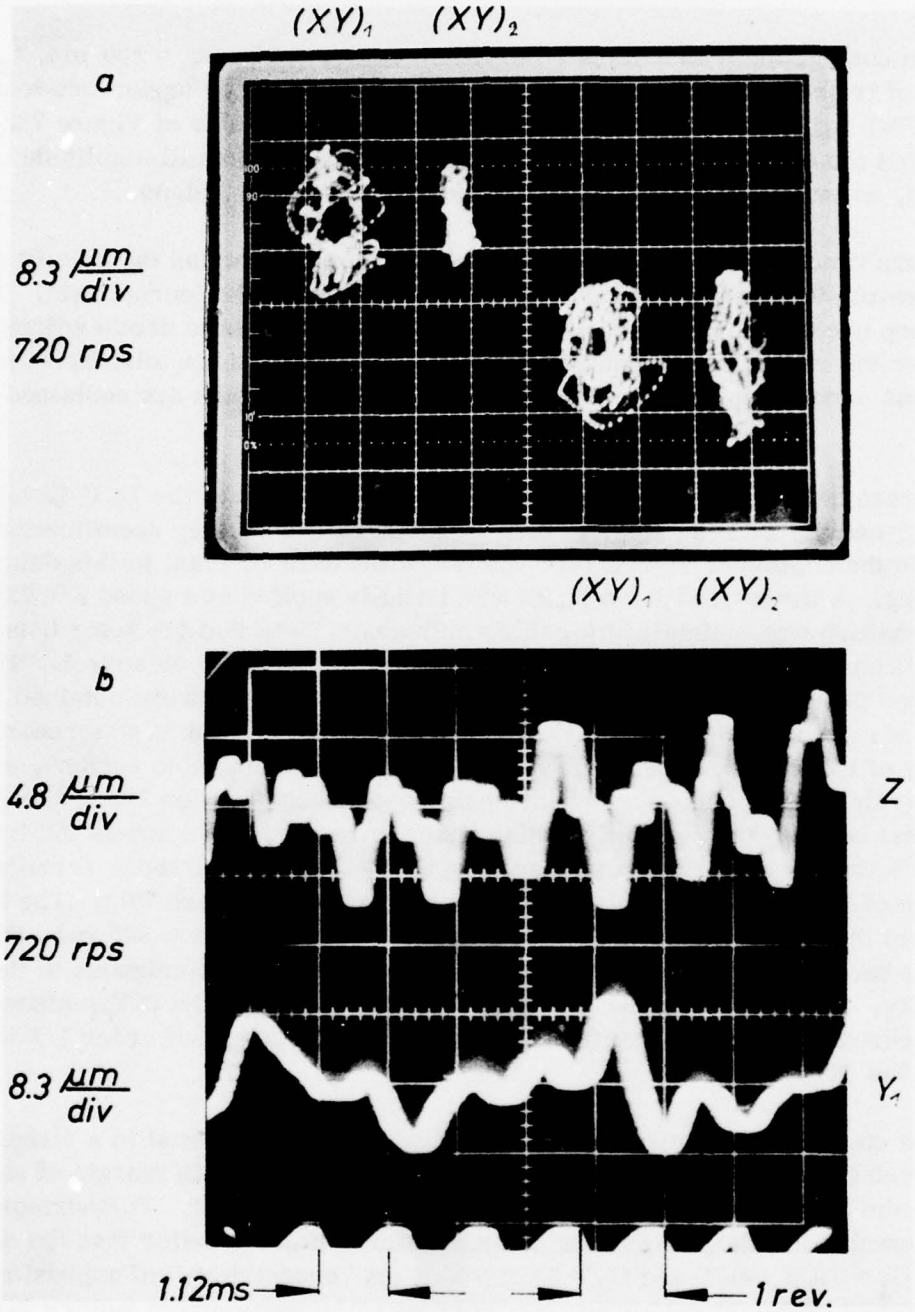

FIGURE 73. EFFECT OF THRUST LOAD AT N = 720rps ON MOTION OF ROTOR IN JOURNAL FOIL-BEARINGS LFF-1J (TWO Cu-Be FOILS PER BEARING, EACH L x D x t_f = 20 x 30 x 0.051 mm, SIX TURNS, $\bar{c} \approx 59\ \mu m$).- FLEXIBLE THRUST BEARING LLF-2T (Cu-Be MEMBRANE, t_m = 230 μm. Cu-Be SPIDER SPRING, t_p = 200 μm; $\bar{t}_s$ = 71 μm).
(a) UPPER LEFT: TRAJECTORIES IN THE ABSENCE OF THRUST LOAD. LOWER RIGHT: TRAJECTORIES WITH THRUST LOAD F = 127.6 N
(b) AXIAL MOTION OF RUNNER RELATIVE TO SUPPORT PLATE (Z) AND VERTICAL MOTION Y_1. THRUST LOAD F = 127.6 N

was used in conjunction with a copper-beryllium spider spring; t_p = 200 μm, $\bar{t}_s$ = 71 μm. Inspection of trajectories relevant to operation with an unloaded (upper left-hand side of Figure 73a) and a loaded thrust bearing (lower right-hand side of Figure 73a), indicates that the effect of axial loading was to increase the overall amplitude at the turbine end, as evidenced by the record of motion in the $(XY)_2$-plane.

The exposure time of trajectory photographs in Figure 72 contains the history of very nearly 30 revolutions of the journal and close to 10 loops of the journal axis. The single-sweep photograph of the Y_1-motion in Figure 72 relates to another time interval and contains the record corresponding to more than 6 revolutions, displaying unequal peak-to-peak excursions of 2 consecutive loops. Analogous data are contained in Figure 73.

The data presented in Figure 74 pertain to the joint operation of the LLF-1J journal foil-bearing and the LLF-2T flexible thrust bearing. The bearing specifications are contained in the caption of Figure 74. The test procedure relevant to this data was the following. A thrust load F = 127.6N was initially applied at a speed N = 720 rps and this condition was maintained for thirty minutes. (Note that the rotor thus supported becomes unstable above 600 rps and whirls at a speed close to 1/3N). The load was then decreased by approximately 15% and records were obtained at specific loads and speeds along a straight line F = 0.15N. The data was recorded in the vicinity of local maxima of the Y-amplitudes, either in unstable regions, or in speed intervals corresponding to subharmonic resonances of order 1/3 and 1/2. The loaded thrust bearing has a slightly destabilizing influence, inasmuch as the trajectories at the turbine end of the rotor have larger Y-extrema than those recorded in the absence of load (approximately 38 μm, at N $\approx$ 700 rps, Figure 74b). The largest trajectory in the stable region ($\Delta Y_1 \approx 34$ μm peak-to-peak, at N $\approx$ 600 rps, Figure 74c) occurs in a bandwidth of subharmonic resonance of order 1/3, contiguous to the region of instability. In the photographs in Figure 74e, the motion in the $(XY)_1$-plane is nearly synchronous, while a significant subharmonic component of order 1/2 is still present in the $(XY)_2$-plane.

The results contained in Figure 74 are very significant. The thrust in a turbomachine may approach the maximum at a rate which leaves an appreciable margin of safety in relation to the linear increase of load with speed during this test. Furthermore, the limit of allowable unbalance would be an order of magnitude smaller than the asymmetric unbalance U_1 = 19.3 μm.N and U_2 = 23.2 μm.N (an "eccentricity" of approximately 2.23 μm, or 88 μin). Also, in anticipation of remarks contained in Section 7.0, the state of the bearing surfaces showed no sign of excessive damage and imminent failure upon completion of these experiments.

6.2 Test Results of Journal Foil-Bearing LLF-1J to Speeds of 45,000 rpm (Dual and Single Foil-Elements; $\bar{c} \approx 40$ μm). - Operation without and with Axial Load

The tests described in this and in the preceding sections were analogous, with the exception of the following differences: (a) The "clearance" was decreased by

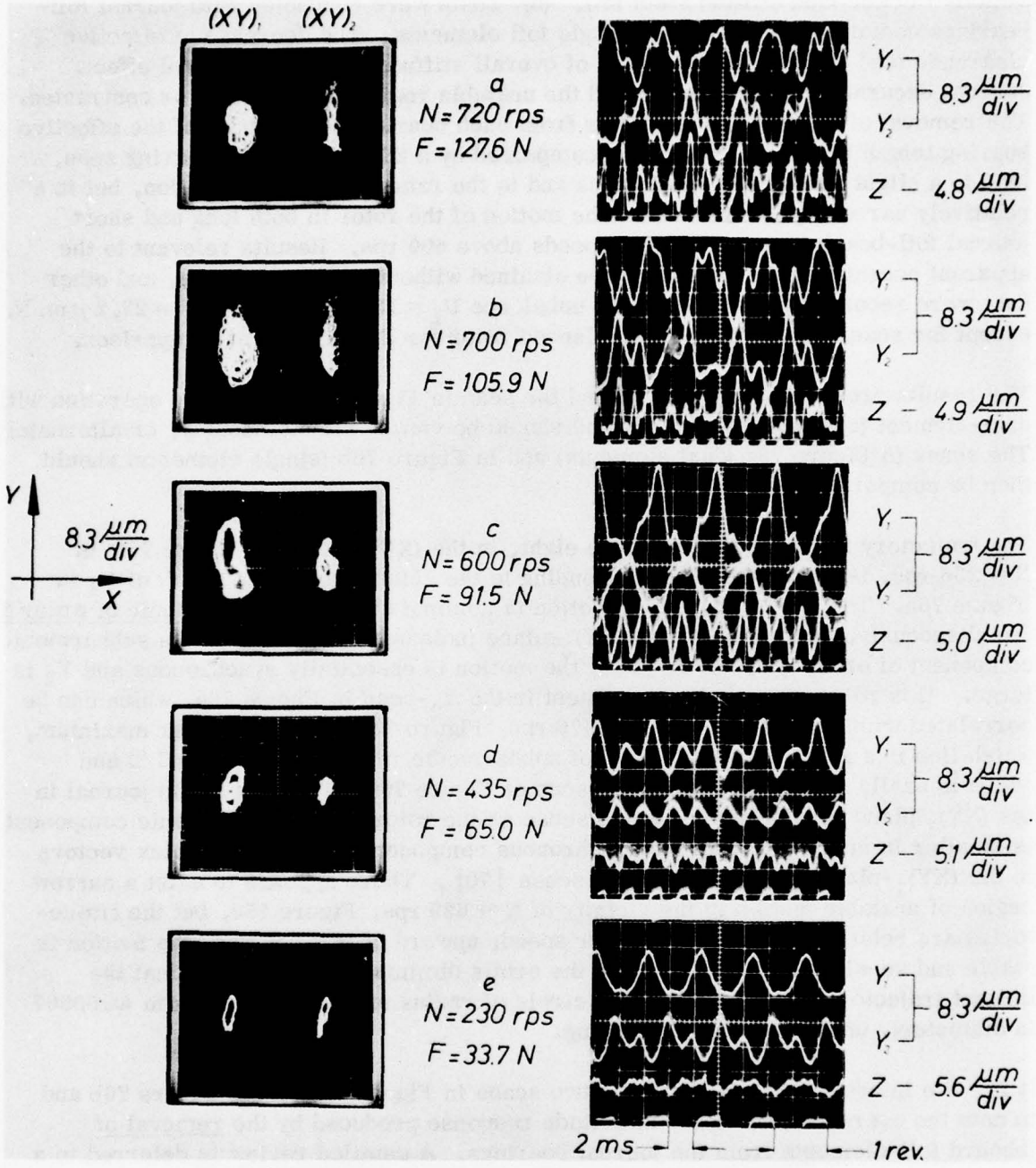

FIGURE 74. TRAJECTORIES AND TIME-BASE RECORDS OF MOTION AT VARIOUS SPEEDS AND THRUST LOADS, WITH ASYMMETRIC UNBALANCE U_1 = 19.3 μm. N AND U_2 = 23.2 μm. N.-JOURNAL FOIL BEARING LLF-1J (TWO Cu-Be FOILS PER BEARING, EACH L x D x t_f = 20 x 30 x 0.051 mm. SIX TURNS, $\bar{c} \approx 59$ μm) AND FLEXIBLE THRUST BEARING LLF-2T (Cu-Be MEMBRANE, t_m = 230 μm. Cu-Be SPIDER SPRING, t_p = 200 μm; $\bar{t}_s$ = 71 μm)

approximately one third, to $\bar{c} \approx 40\ \mu m$, by replacing the copper-beryllium foil with a slightly thicker (and stiffer) steel foil. (b) Tests were conducted with journal foil-bearings containing both dual and single foil elements. The decrease of effective clearance (and possibly the increase of overall stiffness) had a beneficial effect. Journal excursions were reduced and the unstable regions eliminated, or contracted. The removal of inboard foil-elements from each bearing, a reduction of the effective bearing length by a factor of two, accompanied by a 23% increase in bearing span, lead to a slight increase of amplitudes and to the return of unstable motion, but in a relatively narrow speed interval. The motion of the rotor in both long and short journal foil-bearings was stable at speeds above 600 rps. Results relevant to the apparent eccentricity of journals were obtained without added unbalance, and other data were recorded with asymmetric unbalance $U_1 = 19.3\ \mu m.N$ and $U_2 = 23.2\ \mu m.N$, except for scans made with a well balanced rotor for the purpose of comparison.

The results presented in Figure 75 and the scan in Figure 76a pertain to operation with dual-element journal foil-bearings and should be viewed simultaneously, or alternately. The scans in Figure 76a (dual elements) and in Figure 76b (single elements) should then be compared.

The trajectory in the form of a figure eight, in the $(XY)_1$-plane of Figure 75f, at $N \approx 256$ rps, is a resonance corresponding to the "Matterhorn-like" peak of Y_1 in Figure 76a. The X_1-component of motion is dominated by an ultraharmonic of order 2. Simultaneously, the motion in the $(XY)_2$-plane indicates the presence of a subharmonic component of order 1/3. At N = 361, the motion is essentially synchronous and Y_2 is large. This resonance is also prominent in the Y_2-scan in Figure 76a, which can be correlated with Figure 75e. At $N \approx 479$ rps, Figure 75d, Y_1 has another maximum, which lies in a relatively broad band of subharmonic resonance of order 1/2 and which is easily discernible in the Y_1-scan of Figure 76a. The axis of the journal in the $(XY)_1$ plane revolves in the same sense as the rotor. The subharmonic component is smaller in magnitude than the synchronous component, and both complex vectors in the $(XY)_1$-plane rotate in the same sense [70]. There appears to exist a narrow region of unstable motion in the vicinity of $N \approx 629$ rps, Figure 75c, but the trajectories are relatively small. At higher speed, upward of $N \approx 650$ rps, the motion is stable and sensibly synchronous, and the orbits diminish in size. Note that the largest trajectories are bounded by a circle of radius smaller than 8.5 μm (0.00067 in diameter), unbalance notwithstanding.

It is quite interesting to compare the two scans in Figure 76a and in Figure 76b and to note the overall effect on the amplitude response produced by the removal of inboard foil-elements from the journal bearings. A detailed review is deferred to a later part of this section, in which an identical scan is presented in conjunction with corresponding oscilloscope photographs of trajectories and waveforms.

The information contained in Figure 77 is related to that in Figure 71. The oscilloscope photograph pertains to the measurement of apparent eccentricity. The points B_1 and B_2 are reference points corresponding to the dc-levels of probe outputs when

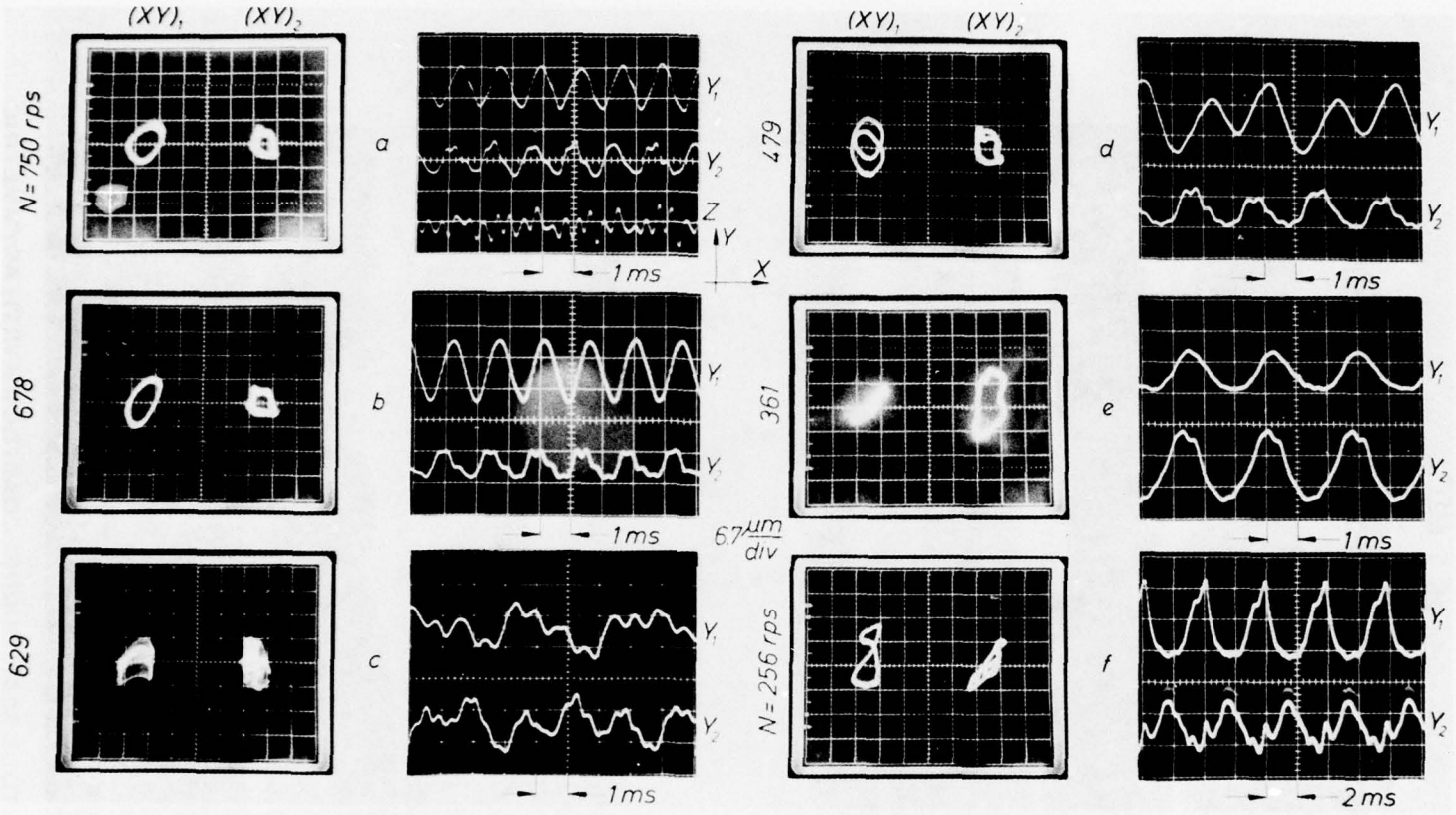

FIGURE 75. TRAJECTORIES AND TIME-BASE RECORDS OF MOTION IN $(XY)_{1,2}$ AND $(Y_1 Y_2)$ PLANES WITH ASYMMETRIC UNBALANCE U_1 = 19.3 μm. N AND U_2 = 23.2 μm. N.-JOURNAL FOIL-BEARING LLF-1J (TWO STEEL FOILS PER BEARING, EACH L x D x t_f = 20 x 30 x 0.054 mm. SIX TURN, $\bar{c} \approx$ 39.8 μm) FLEXIBLE THRUST BEARING UNLOADED, EXCEPT IN (a) WHERE AXIAL LOAD F = 127.6 N.

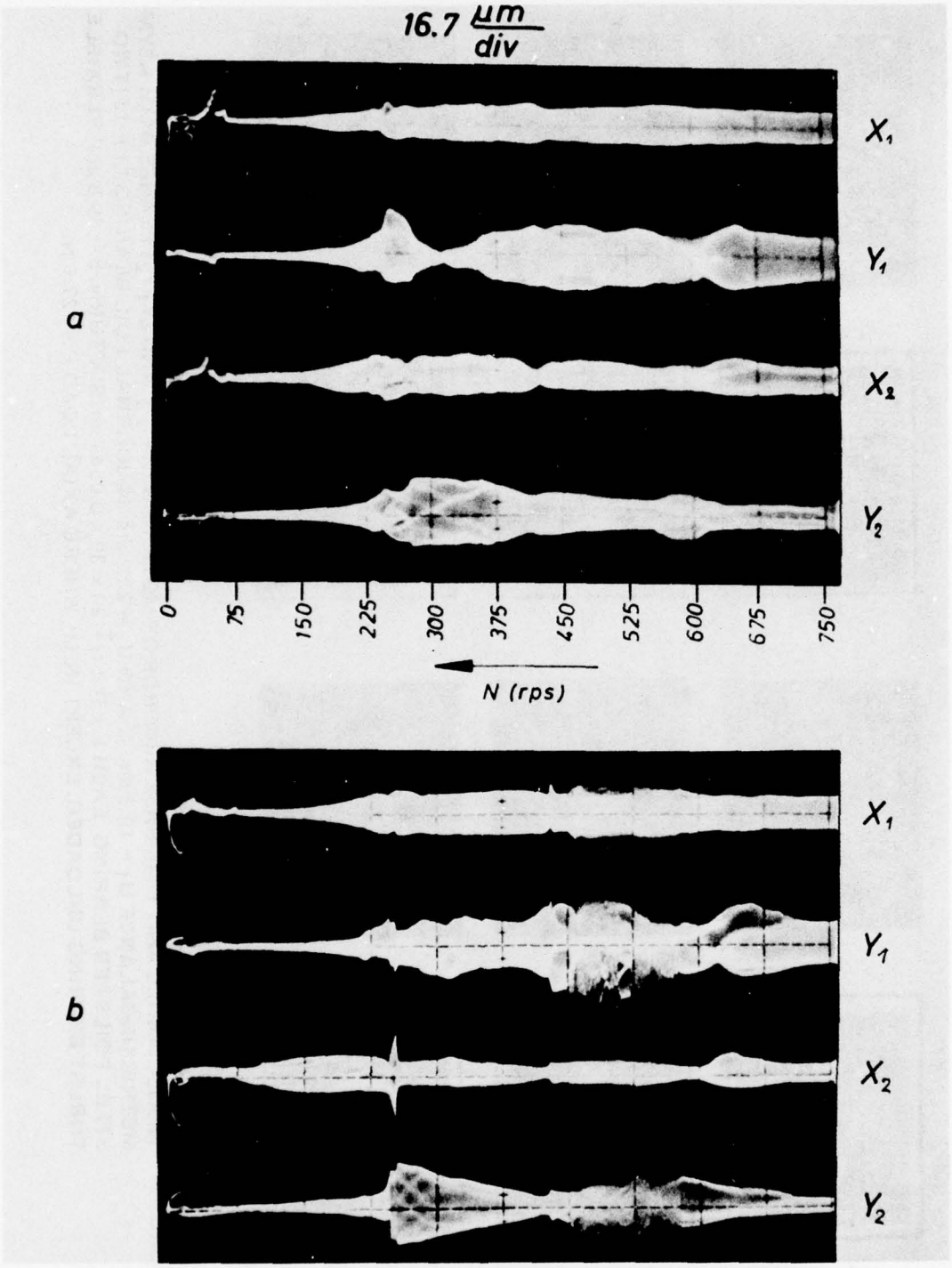

FIGURE 76. AMPLITUDE SCAN DURING COASTDOWN WITH ASYMMETRIC UNBALANCE U_1 = 19.3 μm. N AND U_2 = 23.2 μm. N.-JOURNAL FOIL-BEARING LLF-1J (STEEL FOILS, EACH L x D x t_f = 20 x 30 x 0.054 mm. SIX TURNS, $\bar{c} \approx$ 39.8 μm).-FLEXIBLE THRUST BEARING UNLOADED. (a) TWO FOILS PER BEARING; (b) ONE FOIL PER BEARING

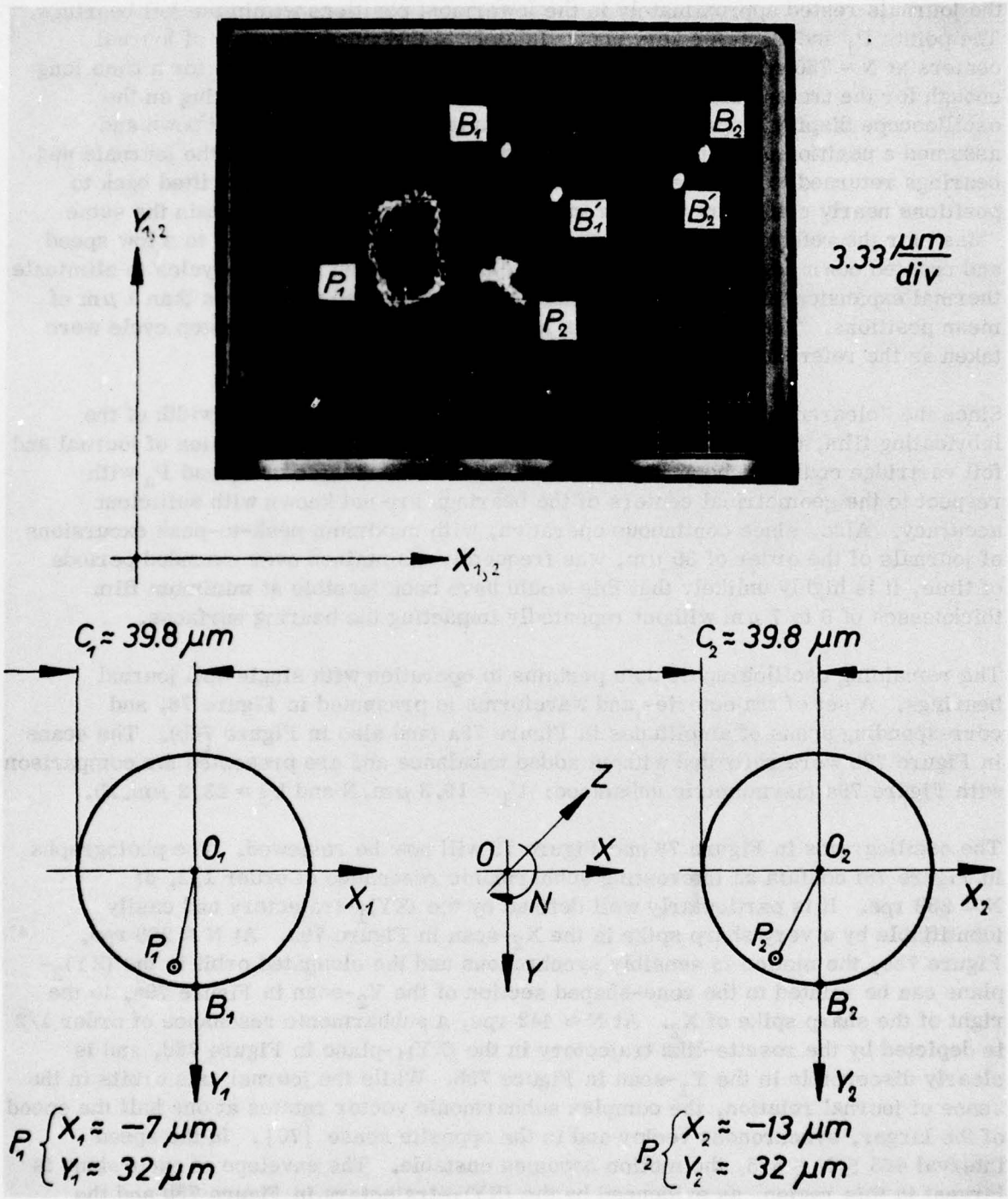

FIGURE 77. LOCI OF ROTOR AXIS IN PLANES $(XY)_{1,2}$.- JOURNAL FOIL-BEARING LLF-1J (TWO STEEL FOILS PER BEARING, EACH L x D x t_f = 20 x 30 x 0.054 mm. SIX TURNS, $\bar{c} \approx 39.8$ μm).-POINTS $B_{1,2}$ AT N = 0, ON STARTING. POINTS $P_{1,2}$ AT N = 750rps. POINTS $B'_{1,2}$ AT N = 0, IMMEDIATELY AFTER COASTDOWN

the journals rested approximately in the lowermost positions within the foil bearings.* The points P_1 and P_2 refer very approximately to the mean positions of journal centers at N = 750 rps. After the rotor has been operated at 750 rps for a time long enough for the trajectories corresponding to P_1 and P_2 to cease drifting on the oscilloscope display (approximately 20 to 30 minutes), it was coasted down and assumed a position of rest represented by points B'_1 and B'_2. When the journals and bearings returned to room temperature, the points B'_1 and B'_2 had drifted back to positions nearly coincident with the initial reference. In order to obtain the same "bias" for the reference points B_1 and B_2, the rotor was accelerated to a low speed and coasted down several times, with sufficient time given between cycles to eliminate thermal expansion-effects. The journals generally settled within less than 1 μm of mean positions. The journal positions assumed after the last start-stop cycle were taken as the reference points B_1 and B_2.

Since the "clearance" $\bar{c} = R_c - n.t_f$ is probably larger than the mean width of the lubricating film, and since the difference between the thermal expansion of journal and foil cartridge could not be accounted for, the true coordinates of P_1 and P_a with respect to the geometrical centers of the bearings are not known with sufficient accuracy. Also, since continuous operation, with maximum peak-to-peak excursions of journals of the order of 30 μm, was frequently maintained over extended periods of time, it is highly unlikely that this would have been feasible at minimum film thicknesses of 5 to 7 μm without repeatedly impacting the bearing surfaces.

The remaining oscillographic data pertains to operation with single-foil journal bearings. A set of trajectories and waveforms is presented in Figure 78, and corresponding scans of amplitudes in Figure 79a (and also in Figure 76b). The scans in Figure 79b were recorded without added unbalance and are presented for comparison with Figure 79a (asymmetric unbalance: $U_1 = 19.3$ μm. N and $U_2 = 23.2$ μm. N).

The oscillograms in Figure 78 and Figure 79 will now be reviewed. The photographs in Figure 78f contain an interesting subharmonic resonance of order 1/2, at $N \approx 253$ rps. It is particularly well defined by the $(XY)_1$-trajectory and easily identifiable by a very sharp spike in the X_2-scan in Figure 79a. At $N \approx 289$ rps, Figure 78e, the motion is sensibly synchronous and the elongated orbit in the $(XY)_2$-plane can be related to the cone-shaped section of the Y_2-scan in Figure 79a, to the right of the sharp spike of X_2. At $N \approx 442$ rps, a subharmonic resonance of order 1/2 is depicted by the rosette-like trajectory in the $(XY)_1$-plane in Figure 78d, and is clearly discernible in the Y_1-scan in Figure 79b. While the journal axis orbits in the sense of journal rotation, the complex subharmonic vector rotates at one half the speed of the larger, synchronous vector and in the opposite sense [70]. In the speed interval $465 \lesssim N \lesssim 575$, the motion becomes unstable. The envelope of excursions is largest in this region, as evidenced by the $(XY)_1$-trajectory in Figure 78b and the Y_1-scan in Figure 79a. With increasing speed, the rotor stabilizes, traverses a

*It is difficult to ensure with accuracy that journals rest on "lowermost" points of well aligned, rigid bearings, and more difficult with foil bearings.

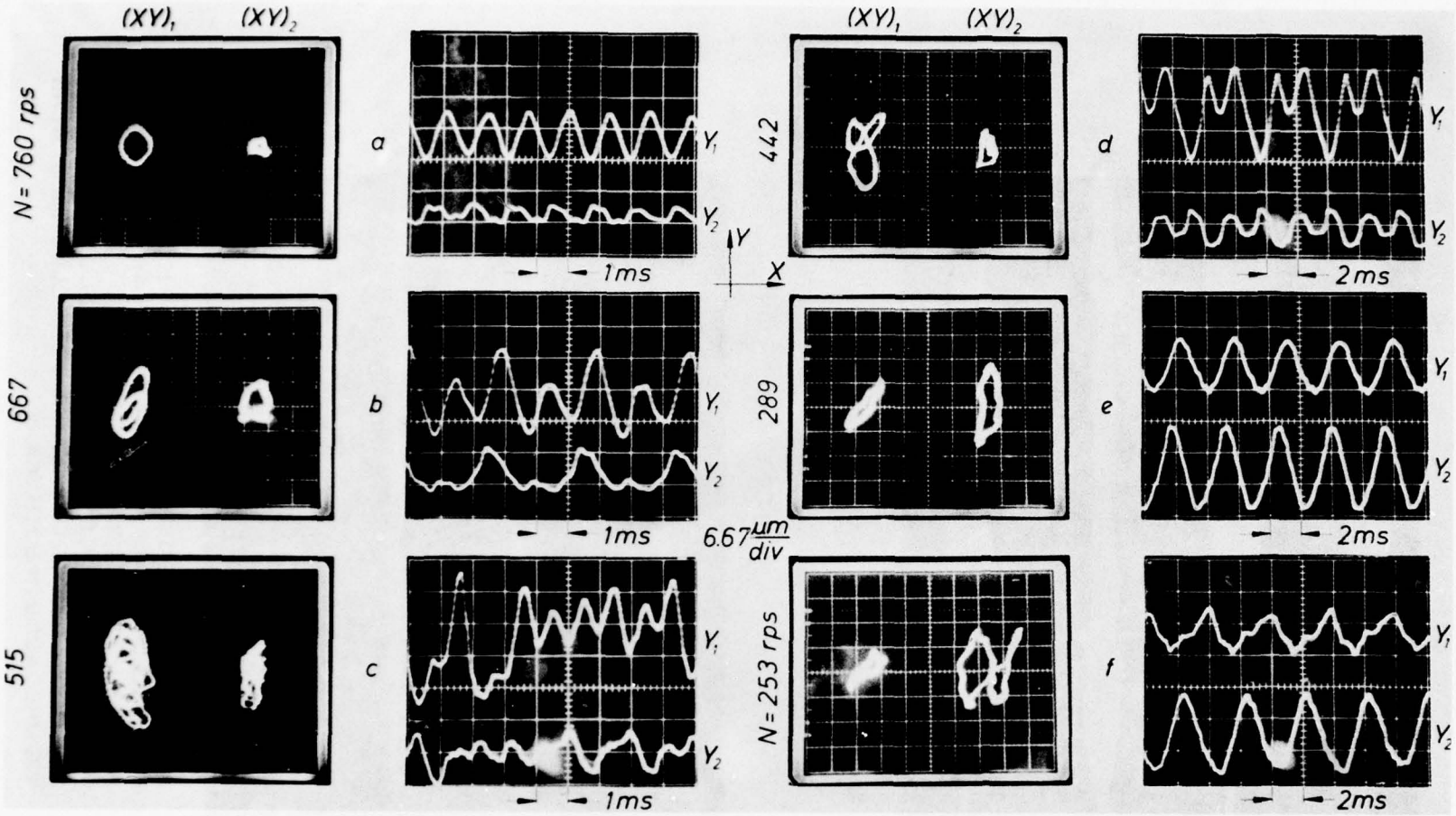

FIGURE 78. TRAJECTORIES AND TIME-BASE RECORDS OF MOTION IN $(XY)_{1,2}$ AND $(Y_1 Y_2)$ PLANES WITH ASYMMETRIC UNBALANCE U_1 = 19.3 μm. N AND U_2 = 23.2 μm. N-JOURNAL FOIL-BEARING LLF-1J (ONE STEEL FOIL PER BEARING, L x D x t_f = 20 x 30 x 0.054 mm. SIX TURNS, $\bar{c} \approx$ 39.8 μm).-FLEXIBLE THRUST BEARING UNLOADED

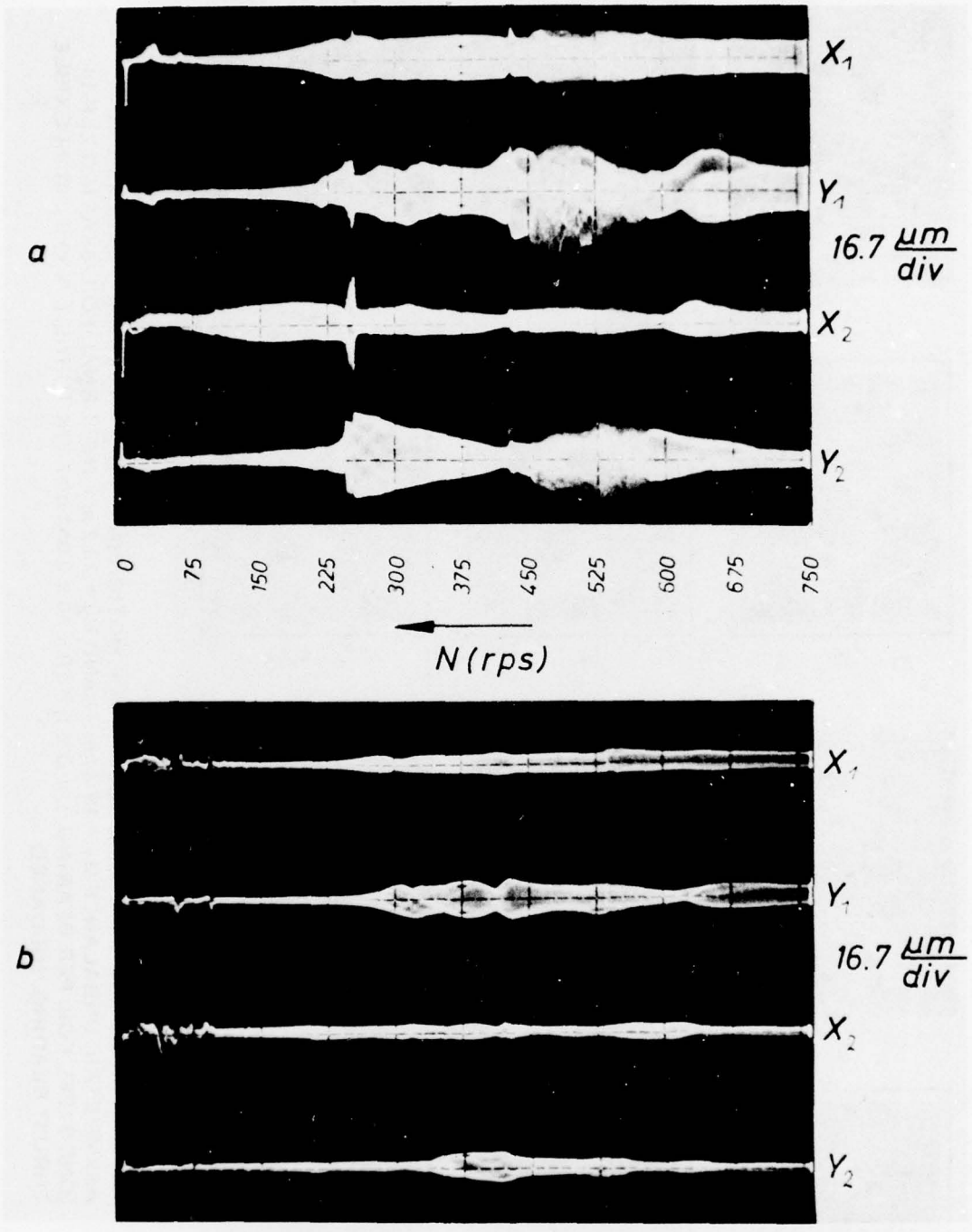

FIGURE 79. AMPLITUDE SCANS DURING COASTDOWN.-JOURNAL FOIL BEARING LLF-1J (ONE STEEL FOIL PER BEARING, L x D x t_f = 20 x 30 x 0.054 mm. SIX TURNS, $\bar{c} \approx 39.8$ μm).- (a) WITH ASYMMETRIC UNBALANCE U_1 = 19.3 μm. N AND U_2 = 23.2 μm. N: (b) WITHOUT ADDED UNBALANCE.-FLEXIBLE THRUST BEARING UNLOADED IN BOTH SCANS

subharmonic resonance at $N \approx 667$ rps, and orbits synchronously above $N \approx 700$ rps, while amplitudes decrease with speed. In the subharmonic trajectory in the Figure 78b (unlike in Figure 78d), the complex subharmonic vector in the $(XY)_1$-plane rotates in a sense opposite to the larger, synchronous component [70]. The difference in motion of the rotor in the presence and absence of unbalance is rather striking, and a comparison of amplitude scans in Figure 79a and Figure 79b reveals that the responses differ not only quantitatively, but also qualitatively.* Since the largest amplitude of motion of a balanced rotor was of the order of 9 μm, peak-to-peak, additional scans of amplitudes were recorded at higher amplification. These scans are included in Figure 80a and Figure 80b and have sensitivities 2.5 and 5.0 times higher than the corresponding scan in Figure 79b.

The content of Figure 81 is analogous to that of Figure 77, except that the data pertain to single, rather than dual foil-element journal bearings. The conditions under which the data in Figure 81 were recorded were identical with those relevant to Figure 77, and all remarks and observations previously made in regard to difficulties in quantitative interpretation of results apply also to this case.

Another oscilloscope record at high amplification is presented in Figure 82 and contains a photograph of an unstable trajectory in the $(XY)_1$-plane, at $N \approx 525$ rps (see also Figure 78c, a complementary record obtained with the same bearing at 515 rps, under identical operating conditions). The picture contains approximately ten loops and reveals the complexity of motion in greater detail. The oscilloscope amplifier-units were operated in the dc mode, in order to establish a reference for the mean displacement of the journal axis. The difficulty in establishing a reference, due to thermal expansion and flexibility, was discussed in a preceding part of this section, and the remarks apply also to Figure 82. Here point B_1' corresponds to the position of the journal, as "seen" by the $(XY)_1$-probes immediately after coastdown, whereas point B_1 is the position after the journal, foil and cartridge have returned to room temperature. If one now considers the limit of the trajectory prescribed by the lowermost sector of the foil-surface in relation to points B_1 or B_1', it would appear that the journal was pounding the foil at a rate in the order of 500 impacts per second, for a total of some 300,000 impacts during a ten minute interval required to adjust the speed, oscilloscope and camera settings and to develop the film. This is impossible, of course, and although the minimum film thickness at the lower extrema of trajectories may have been not larger than several micrometers, no sustained, high-frequency pounding and hammering of the foil did occur, or could have occurred without failure.

The last experiment to be described in this section relates to the joint operation of the LLF-1J journal foil-bearings (single steel-foil element, $t_f = 54$ μm, six turns, $\bar{c} \approx 40$ μm) and the flexible thrust bearing LLF-2T (Cu-Be membrane, $t_m = 230$ μm. Cu-Be spider spring, $t_p = 200$ μm; $\bar{t}_s = 71$ μm). Trajectories and waveforms are

*In a linear system, the amplitudes would increase with unbalance but the response would be qualitatively similar.

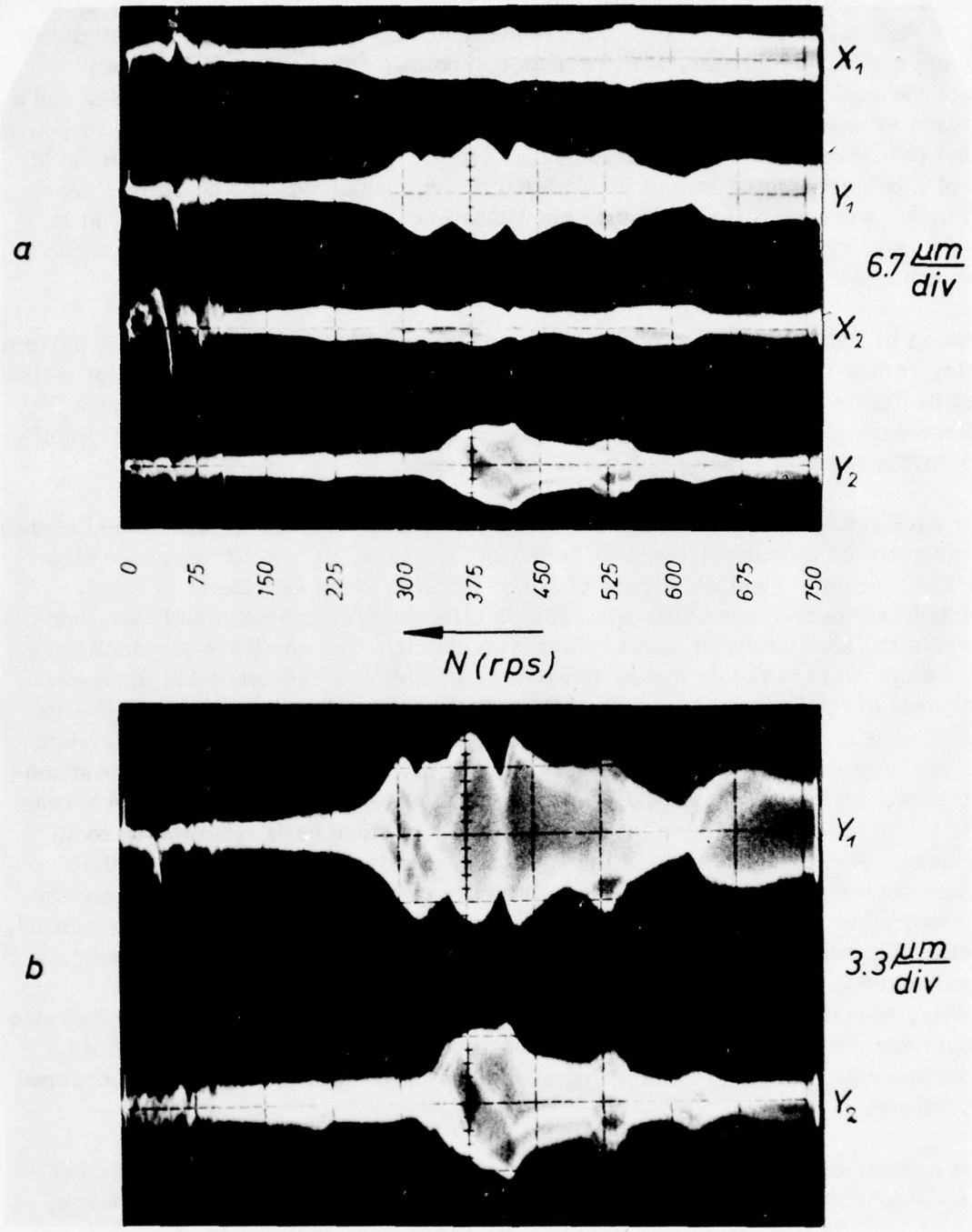

FIGURE 80. AMPLITUDE SCANS DURING COASTDOWN WITHOUT ADDED UNBALANCE SHOWN AT HIGHER AMPLIFICATION.-JOURNAL FOIL BEARING LLF-1J (ONE STEEL FOIL PER BEARING, $L \times D \times t_f = 20 \times 30 \times 0.054$ mm. SIX TURNS, $\bar{c} \approx 39.8$ μm)

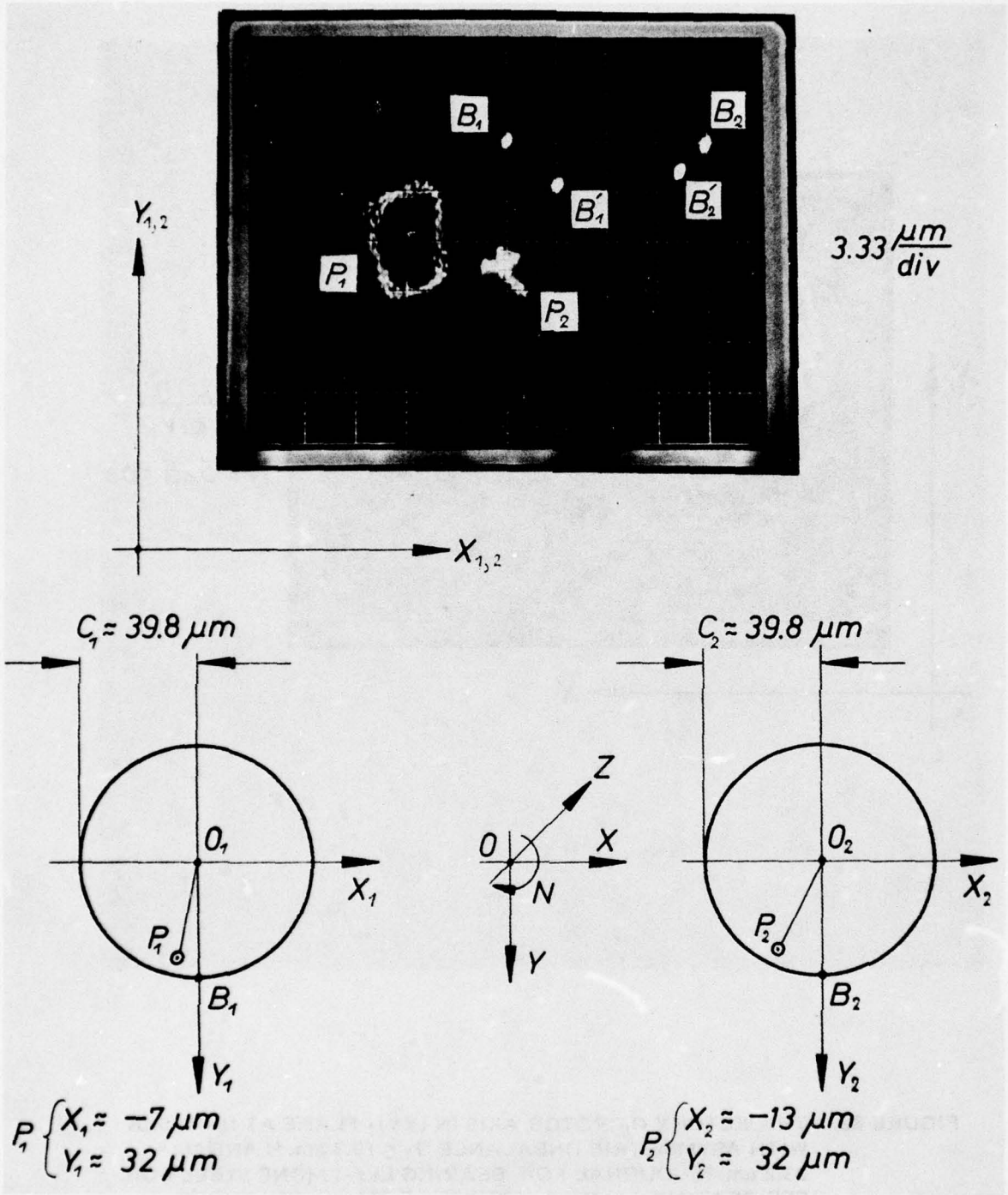

FIGURE 81. LOCI OF ROTOR AXIS IN $(XY)_{1,2}$ PLANES.-JOURNAL FOIL BEARING LLF-1J (ONE STEEL FOIL PER BEARING, L x D x t_f = 20 x 30 x 0.054 mm. SIX TURNS, $\bar{c} \approx 39.8$ mm).-POINTS $B_{1,2}$ AT N = 0 ON STARTING. POINTS $P_{1,2}$ AT N = 750rps. POINTS $B'_{1,2}$ AT N = 0, IMMEDIATELY AFTER COASTDOWN

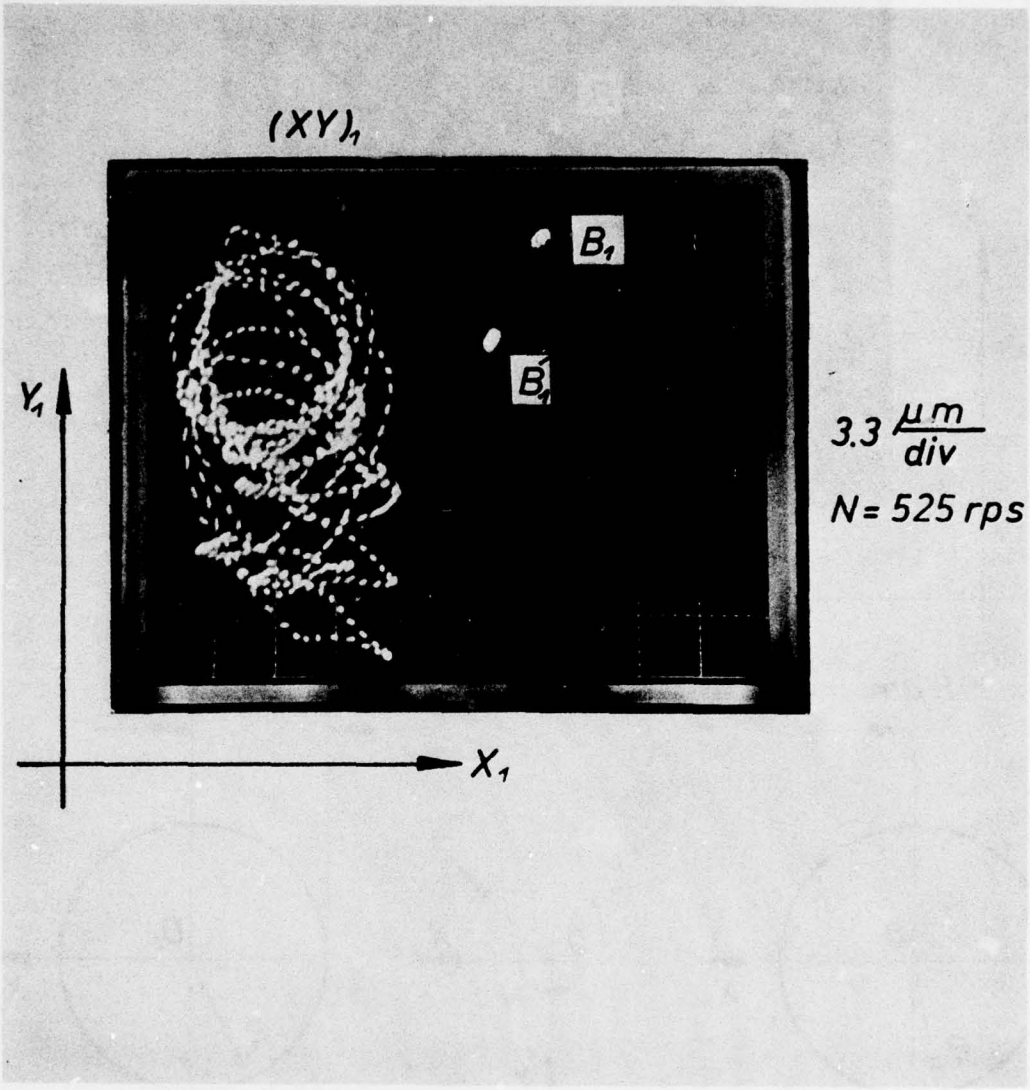

FIGURE 82. TRAJECTORY OF ROTOR AXIS IN $(XY)_1$ PLANE AT N = 525rps WITH ASYMMETRIC UNBALANCE U_1 = 19.3 μm. N AND U_2 = 23.2 μm. N.-JOURNAL FOIL BEARING LLF-1J (ONE STEEL FOIL PER BEARING, L x D x t_f = 20 x 30 x 0.054 mm. SIX TURNS, $\bar{c} \approx$ 39.8 μm).-POINT B_1 IS AFTER COASTDOWN AND COOLING TO ROOM TEMPERATURE AND POINT B'_1 IS AT N = 0, IMMEDIATELY AFTER COASTDOWN

given in Figure 83, for two load-speed settings; F = 127.6N at N = 773 rps and F = 79.5N at N = 532. The bearings performed very well and the effect of thrust load on motion was not significant. The results in Figure 83 can be compared with corresponding data in Figure 72, Figure 73 and Figure 74.

6.3 Test Results of Journal Foil-Bearings LLF-2J with Polygonally-Bent Backing to Speeds of 45,000 rpm. - Operation without and with Axial Load

The design and construction of journal foil-bearings LLF-2J were described in Section 4.2. Tests were first successfully carried out with elements preformed to quasi-pentagonal and hexagonal configurations, but the data presented in this section relates to a journal bearing with a backing in the form of an open octagon. A steel foil 54 μm thick was used, and the vertex radii and angles were 0.5 mm and 130°. The backing was integral with approximately 2 1/4 turns of plane foil. The foil elements were inserted in the recessed cartridge bores (diameter 30.610 mm), starting in the retaining groove and terminating in the X-plane (see Figure 29 and Figure 31). The inner foil-surface was uniformly coated with an organically bonded MoS_2-lubricant (Dow-Corning Molykote 88), to a thickness of 5 to 6 μm. The journals were flame-plated with Ni-Cr bonded Cr_2O_3 and were ground to a 29.870 mm diameter.

The experimental results presented in this section were obtained with journal bearings containing single foil elements, nominally 20 mm wide. Performance data recorded with asymmetric unbalance U_1 = 19.3 μm.N and U_2 = 23.2 μm.N is presented in oscilloscope photographs of trajectories (orbits) and corresponding time-base waveforms in Figure 84, while related scans of amplitudes with the speed of rotation are contained in Figure 85b. Scans of amplitude of response without unbalance are shown in parallel in Figure 85a for the purpose of comparison. The trajectories and waveforms in Figure 84 should be viewed in conjunction with the scans in Figure 85b, and the reader's attention is drawn to the fact that orbits and scans were recorded at higher sensitivities (3.3 and 6.7 μm/div) than was generally the case in the oscilloscope records of the preceding sections.

The description of highly complex, dynamic behavior of rotor-bearing systems is always very interesting to both reader (hopefully) and writer, especially if the presence of dynamically interesting phenomena does not detract from the utility and good performance of bearings. But the user of bearings prefers "uneventful" responses and "prosaic" performance characteristics, where "everything is overdamped and nothing very much occurs", regardless how ill-treated the bearings are. And rightly so. Instabilities and resonances may be exciting, but "lethargic" air bearings are best.

The test history of the journal foil-bearing with a quasi-octagonal backing was certainly "uneventful". No regions of unstable motion were observed, the subharmonic content of motion was greatly diminished, and amplitudes of motion were small in relative and absolute terms. The maximum amplitude occurred at a synchronous resonance at N ≈ 417 rps, in the $(XY)_1$-plane, with a peak-to-peak value of less than

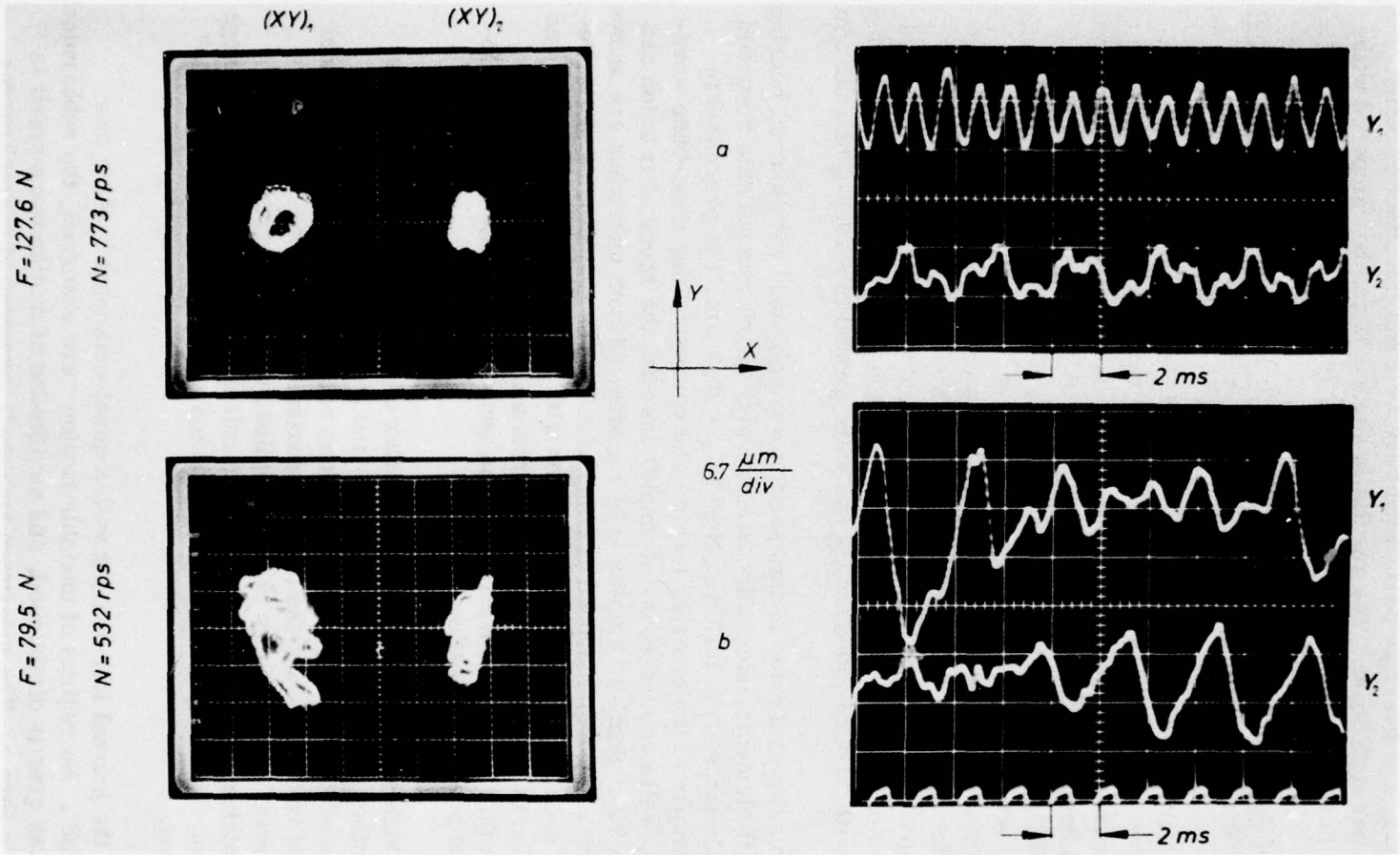

FIGURE 83. TRAJECTORIES AND TIME-BASE RECORDS OF MOTION IN $(XY)_{1,2}$ AND $(Y_1 Y_2)$ PLANES WITH ASYMMETRIC UNBALANCE U_1 = 19.3 μm. N AND U_2 = 23.2 μm. N AT TWO THRUST LOADS AND SPEEDS.-JOURNAL FOIL BEARING LLF-1J (ONE STEEL FOIL PER BEARING, L x D x t_f = 20 x 30 x 0.054 mm. SIX TURNS, $\bar{c} \approx$ 39.8 μm)

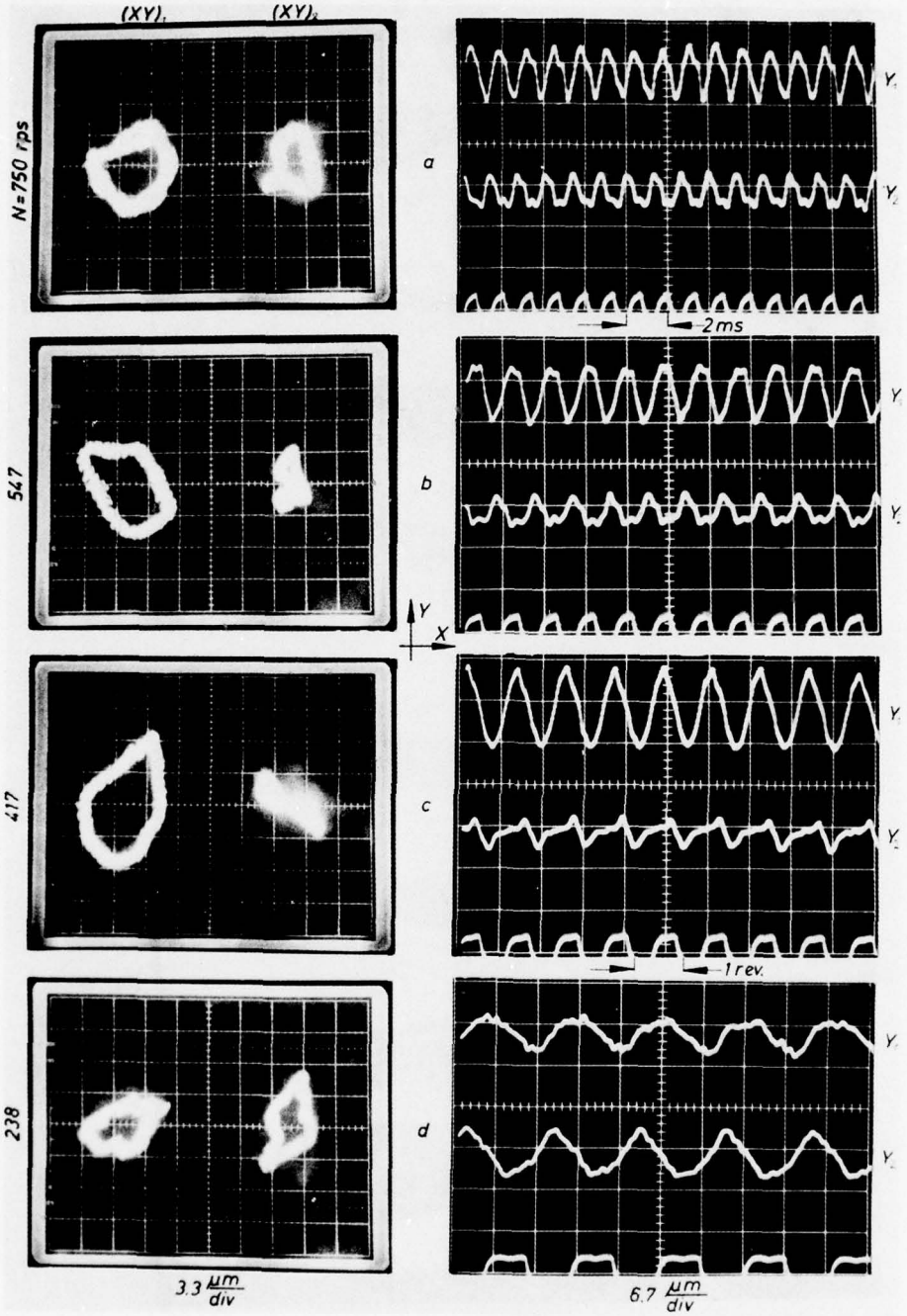

FIGURE 84. TRAJECTORIES AND TIME-BASE RECORDS OF MOTION IN $(XY)_{1,2}$ AND (Y_1Y_2) PLANES WITH ASYMMETRIC UNBALANCE U_1 = 19.3 μm. N AND U_2 = 23.2 μm. N.-JOURNAL FOIL BEARING LLF-2J (OCTAGONALLY BENT BACKING AND 2-1/4 INNER TURNS. ONE STEEL FOIL PER BEARING, L x D x t_f = 20 x 30 x 0.054 mm. JOURNAL DIAMETER = 29.87 mm, FOIL-CARTRIDGE BORE = 30.61 mm).-FLEXIBLE THRUST BEARING UNLOADED.

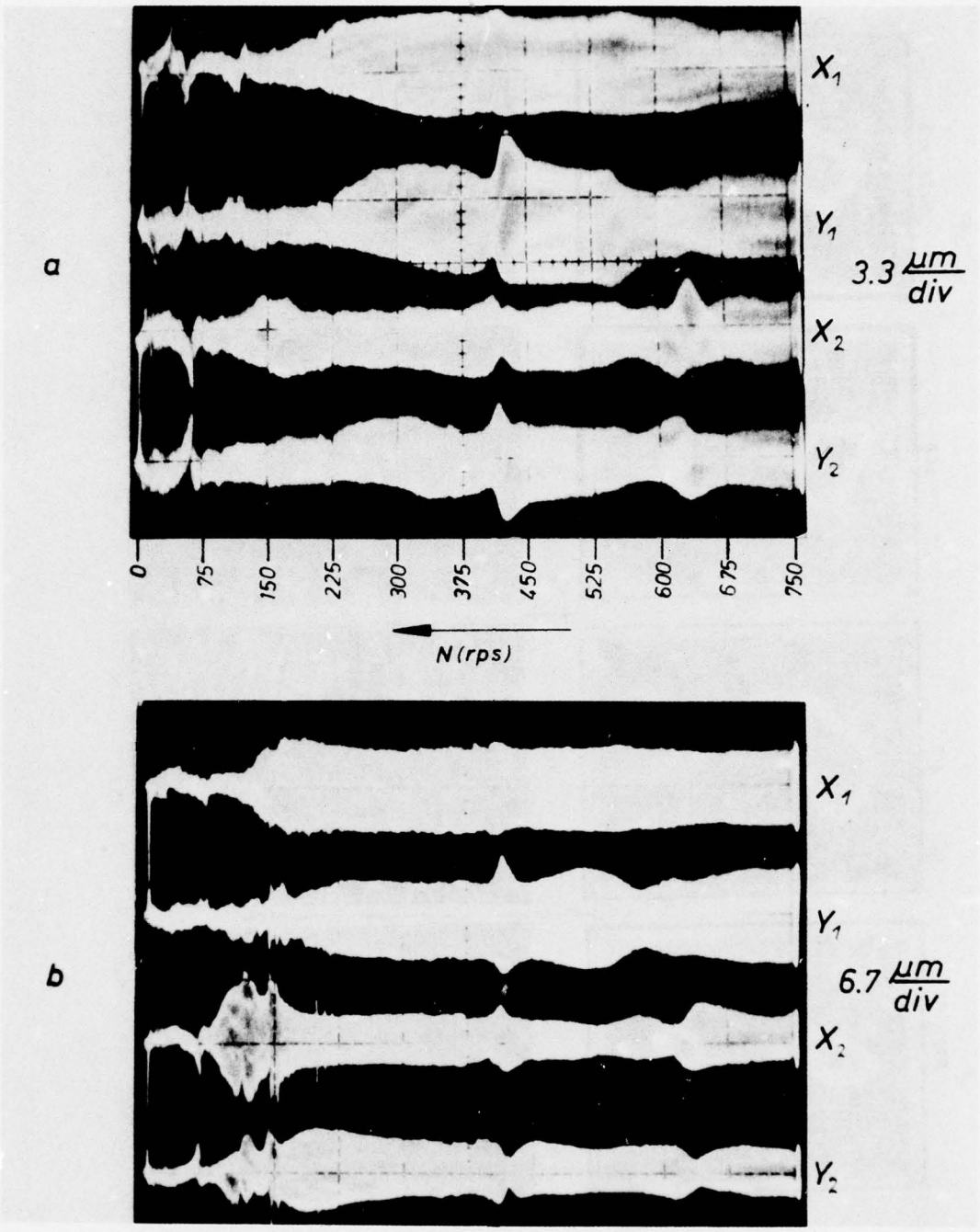

FIGURE 85. AMPLITUDE SCANS DURING COASTDOWN.-JOURNAL FOIL BEARING LLF-2J (OCTAGONALLY BENT BACKING AND 2-1/4 INNER TURNS. ONE STEEL FOIL PER BEARING, L x D x t_f = 20 x 30 x 0.054 mm. JOURNAL DIAMETER = 29.872 mm, FOIL-CARTRIDGE BORE = 30.61 mm).- (a) WITHOUT ADDED UNBALANCE: (b) WITH ASYMMETRIC UNBALANCE U_1 = 19.3 μm. N AND U_2 = 23.2 μm. N

13.5 μm, notwithstanding the rather unhealthy magnitude and mode of unbalance, Figure 84. The distortion of the small orbits in Figure 84 is to be attributed, in part, to surface damage incurred in the journal-strip facing the probes and residual out-of-roundness. (The probes were being adjusted in their holders on one occasion, while the rotor revolved at high-speed. Light contact occurred, resulting in superficial surface-damage).

The scans in Figure 85b display a low-speed resonance in the $(XY)_2$-plane*, peaking in the approximate interval $100 \lesssim N \lesssim 175$ rps, and a more sharply defined maximum at $N \approx 420$ rps. This sharply defined peak (Y_1, at $N \approx 420$ rps) is present in the scans recorded both with and without unbalance, but unbalance increased the peak-to-peak magnitude of the spike by nearly 50%. The scans as a whole are rather "flat" and the motion appears to be very well damped.

Finally, results of joint operation of journal foil-bearings LLF-2J and the flexible thrust bearing LLF-2T are presented in Figure 86. Shown are orbits and waveforms at three loads and speeds, and the effect of the thrust bearing on motion does not appear to be significant, as evidenced by the similarity with orbits at commensurate speeds depicted in Figure 84.

7.0 WEAR

The present investigation did not include extensive testing of surface coatings and boundary lubricants, and was not focused primarily on studies of surface compatibility and wear. This is not to say that such studies are less important. On the contrary, the utilization of gas-lubricated foil bearings, particularly at elevated temperatures, depends strongly on the extent bearing surfaces can be protected by tenaciously adhering, wear resisting and lubricating coatings. Complementary studies, therefore, would be highly useful, if conducted against a realistic background, that is with actual foil bearing. The latter stipulation is important, because the geometrical configuration of the bearing, the compliance of the surface and the nature of contact are as important as chemistry and surface-physics.

Commercially available, off-the-shelf lubricants were used. Specifically, the Dow-Corning, organically-bonded Molykote 88 and the inorganically-bonded Molykote 321R were experimented with. Needless to say, these MoS_2 lubricants were not developed specifically for application to air-lubricated foil bearings, but it is very likely that the protection they offered was not vastly inferior to similar MoS_2 and other coatings "made to prescription". The cleaning and surface-treatment prior to coating, and curing procedures prescribed by the manufacturer, were strictly adhered to. The journal bearing foil-surfaces were finely sandblasted and the thrust-bearing membranes

*Here and elsewhere, the phraseology is imprecise, but convenient. Resonances do not occur "in monitoring planes", but correspond to degrees of freedom and modes of motion of the entire rotor.

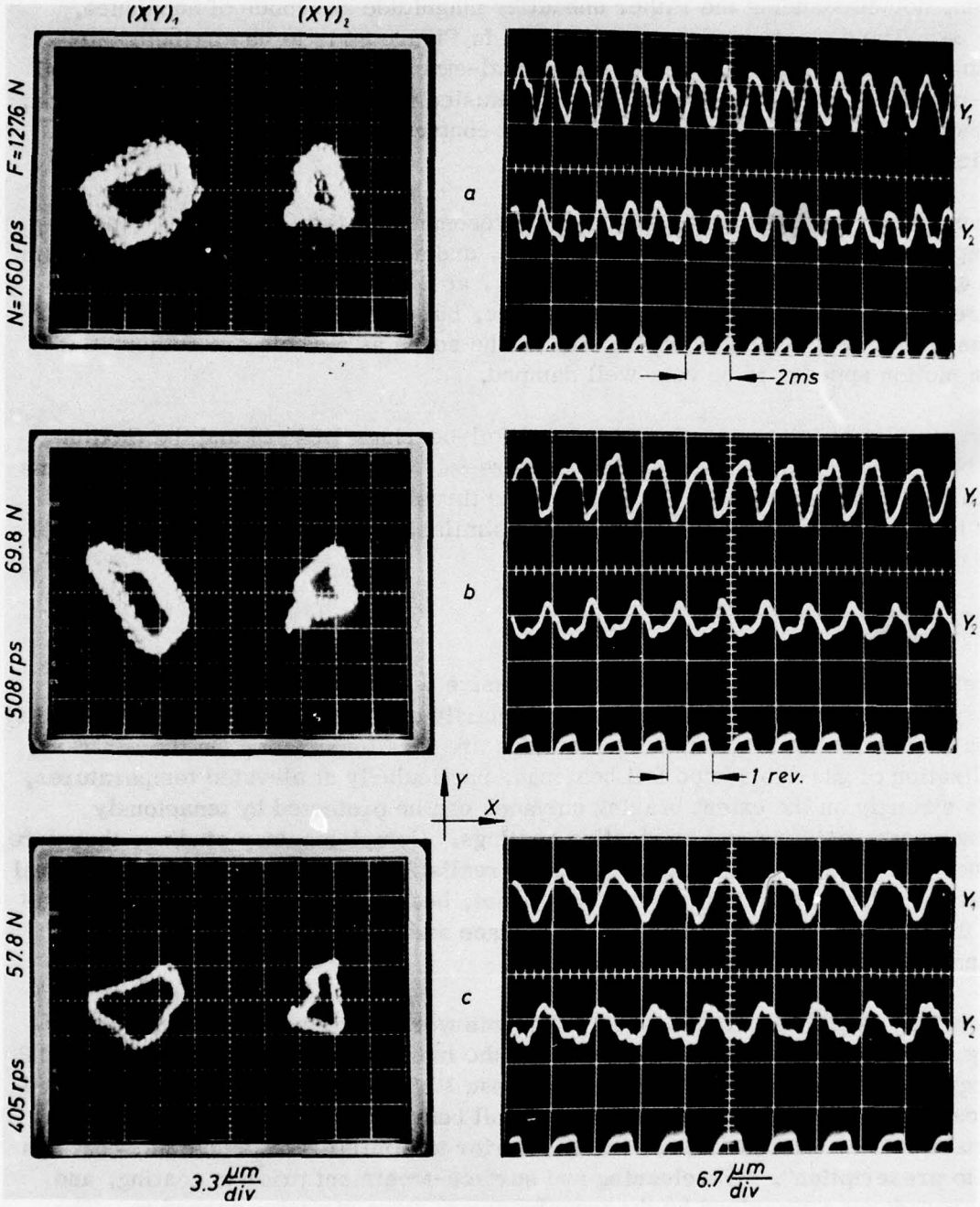

FIGURE 86. TRAJECTORIES AND TIME-BASE RECORDS OF MOTION IN $(XY)_{1,2}$ AND (Y_1Y_2) PLANES WITH ASYMMETRIC UNBALANCE U_1 = 19.3 μm. N AND U_2 = 23.2 μm. N.-JOURNAL FOIL BEARING LLF-2J (OCTAGONALLY BENT BACKING AND 2-1/4 INNER TURNS, ONE STEEL FOIL PER BEARING, L x D x t_f = 20 x 30 x 0.054 mm. JOURNAL DIAMETER = 29.87 mm, FOIL-CARTRIDGE BORE = 30.61 mm).-THRUST LOADS AND SPEEDS AS INDICATED)

were either solvent-cleaned, or solvent-cleaned and lightly roughened by superficial etching.* The lubricant was applied very uniformly by means of a fine, variable-nozzle spray gun. With a little practice, it was very easy to deposit repeatedly a uniform layer 5 to 6 μm thick (and equally simple to strip the layer, if not uniform or uneven, and then spray again). In the case of membranes, the process was aided by placing the specimen on a revolving disc, attached to the spindle of a small dc-motor.

The general experience with Molykote 321R was that the lubricating film adhered rather well at the interface, but that the coating was coarse, and that much of it would either shear off and accumulate as black dust within the bearing clearance, or be removed in burnishing of the film. The organically bonded Molykote 88 was used predominantly. It produced a fine-texture film and provided a reasonably good compromise between adhesion and wear, within the limits of test requirements. The wear debris resembled qualitatively, but on a diminished scale, the abraded strands from a rubber eraser, and was also similar to that which obtains frequently with fluorocarbon (Teflon) coatings.

The flame-plated Cr_2O_3 layers on the runner and on the journals were approximately 0.25 mm thick and moderately porous. They became impregnated with the dry lubricant, both through initial doping and by transfer from the membrane or foil. Such hard-faced bearing members have excellent wear characteristics, which was confirmed once again in the course of the present investigation.

Although no start-stop cycling was included in the program, the bearings had to withstand the effects of unduly large amplitudes due to asymmetric unbalance, were operated with this unbalance for extended periods of time at several resonant and critical points, and were also started and stopped 100 to 250 times, depending on the extent of experimental data to be acquired.

The four photographs of coated copper-beryllium membranes in Figure 87 display typical wear traces. These membranes were loaded up to F = 127.6N, while the rotor was subjected to a very substantial pitching unbalance (U_1 = 19.3 μm.N and U_2 = 23.2 μm.N). The copper-beryllium membranes were characterized by various initial distortions. In particular, the radial profiles displayed an appreciable concavity between the inner and outer perimeters. This accounts for the wear-in notches on twelve ridges along the edge of the runner and for the very smoothly burnished annulus around the inner hole. The membrane in the top left-hand corner of Figure 87 displays also a few shiny spots corresponding to indentation contacts. The coated area between the outer and inner wear tracks shows no sign of wear, except where the coating was purposely burnished and polished, as in the photograph on the lower right-hand side of Figure 87. Most of these wear problems can be largely eliminated by insuring good initial flatness of membranes.

*Sandblasting causes transverse curling of the foil, which vanishes for all practical purposes in coiling. The thrust-bearing membranes, however, were not sandblasted to avoid additional distortion.

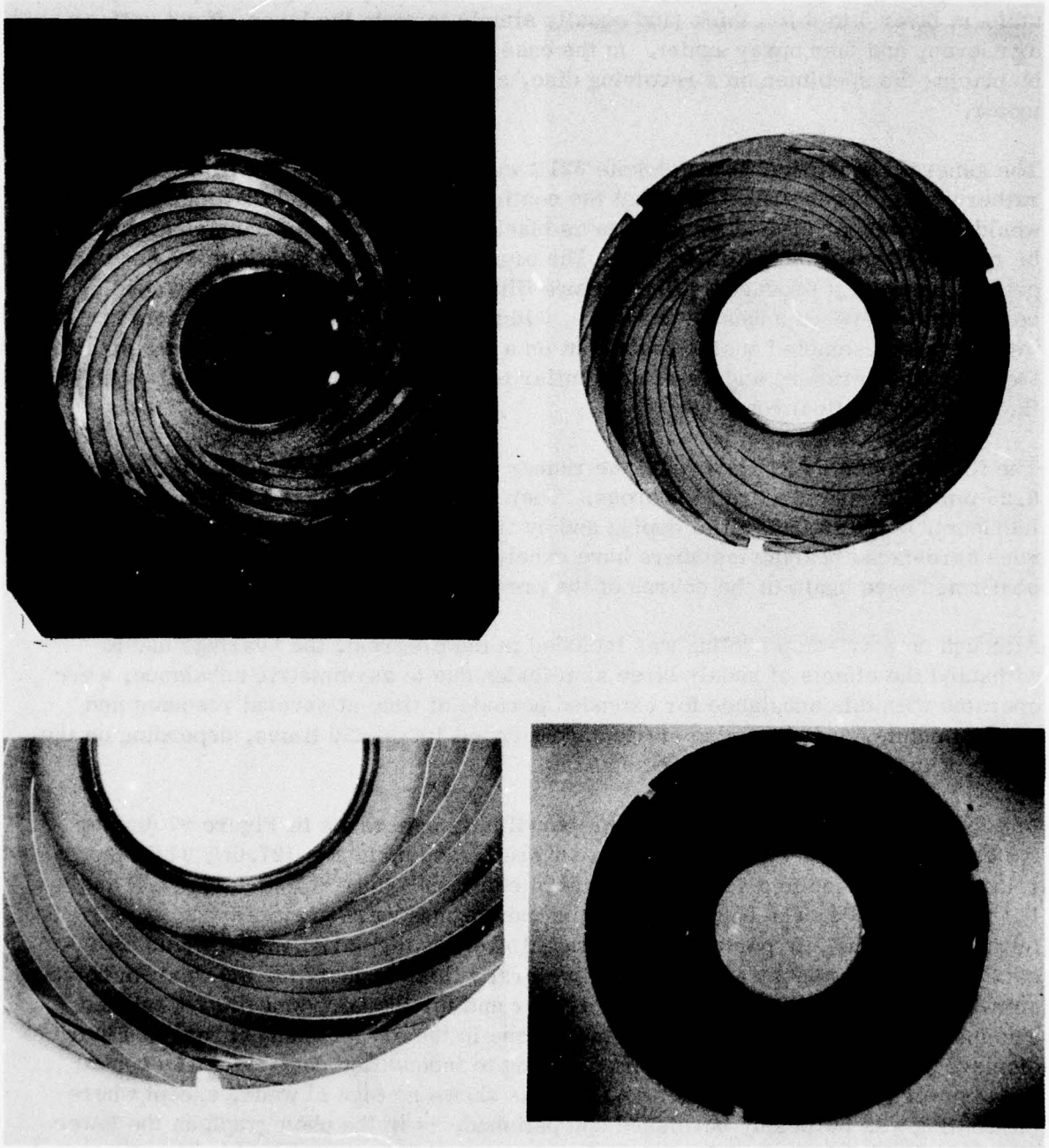

FIGURE 87. TYPICAL SURFACE-WEAR AT OUTER AND INNER PERIMETERS OF SPIRAL-GROOVE MEMBRANE (THRUST BEARINGS LLF-1T AND LLF-2T. COPPER-BERYLLIUM AND ORGANICALLY BONDED MoS_2 COATING).-COMBINED EFFECT ON WEAR OF INITIAL DISTORTION AND OPERATION AT HIGH UNBALANCE. THRUST AND RUNOUT

The photograph on the left-hand side of Figure 88 contains the inner portions of coated steel-foils of the LLF-1J bearings. These foils were used throughout the entire series of tests described in Section 6.2. Initially, all four foils were used; (1) and (2) as the outboard and inboard elements of the bearing adjacent to the runner, and (3) and (4) as the inboard and outboard elements of the bearing adjacent to the turbine. The inboard foils (2) and (3) were simply removed to convert to single-element journal bearings. The following observations apply. The most significant wear occurred, as may have been expected with so large an amount of asymmetric unbalance, at the outer edges of foils (1) and (4), in regions corresponding to minimum film thickness. Since photograph reproductions of wear patterns are generally misleading, the appearance of this region is described as being a very bright and polished foil sector. The lighter portions of foil (4) correspond to a zone containing islands, where the coating was partly worn away. The contrasting-stripe appearance of foil (3) is highly misleading, since the right-hand side represents a very lightly polished strip, while the left-hand side contains well distributed, burnished islands. The coating of foil (3) was hardly worn, and foil (2) was in equally good condition. None of the foils suffered damage to an extent indicating imminent failure.

The photograph on the right-hand side of Figure 88 contains lower halves of bearing surfaces of foil-elements of the LLF-2J bearing. The wear pattern is typical of bearings with polygonally-bent support sections. The transverse stripes, where the coating is partly but not completely worn, lie opposite the vertices of the polygonal support. Note that wear is more pronounced along two strips straddling a central land, where the initial coating is still largely intact. Wear is distributed mainly along areas of support, which lie just beyond the curvature transitions from the radiused vertices to sections conforming to the journal. Unlike in journal foil-bearings described in references [53] and [55], the support reactions on the inner foil are far less concentrated. Further improvement will undoubtedly ensue if the number of turns of the inner coil is increased, and if the foil thickness and geometry of the polygonal backing is modified. The outboard edges of the foil elements of the LLF-2J bearings (the left-side edges of foils in the photograph) do not appear to have suffered any damage due to the large asymmetric unbalance, and this may be attributed to both greater damping and resilience of this bearing, in comparison with the LLF-1J type. The foil elements shown in the right-hand photograph of Figure 88 were subjected to at least 200 start-stop cycles, accumulated during initial testing, data recording with heavy asymmetric unbalance, and numerous demonstration runs. Inspections between runs showed that the local wear approached rapidly an asymptotic state.

In summary, there is much to indicate that the wear characteristics of the journal foil-bearings and of the flexible thrust bearing permit operation under more adverse conditions than could be tolerated with rigid air bearings. There is undoubtedly much room for improvement and innovation in surface coating and boundary lubrication of such bearings to further enhance their performance characteristics.

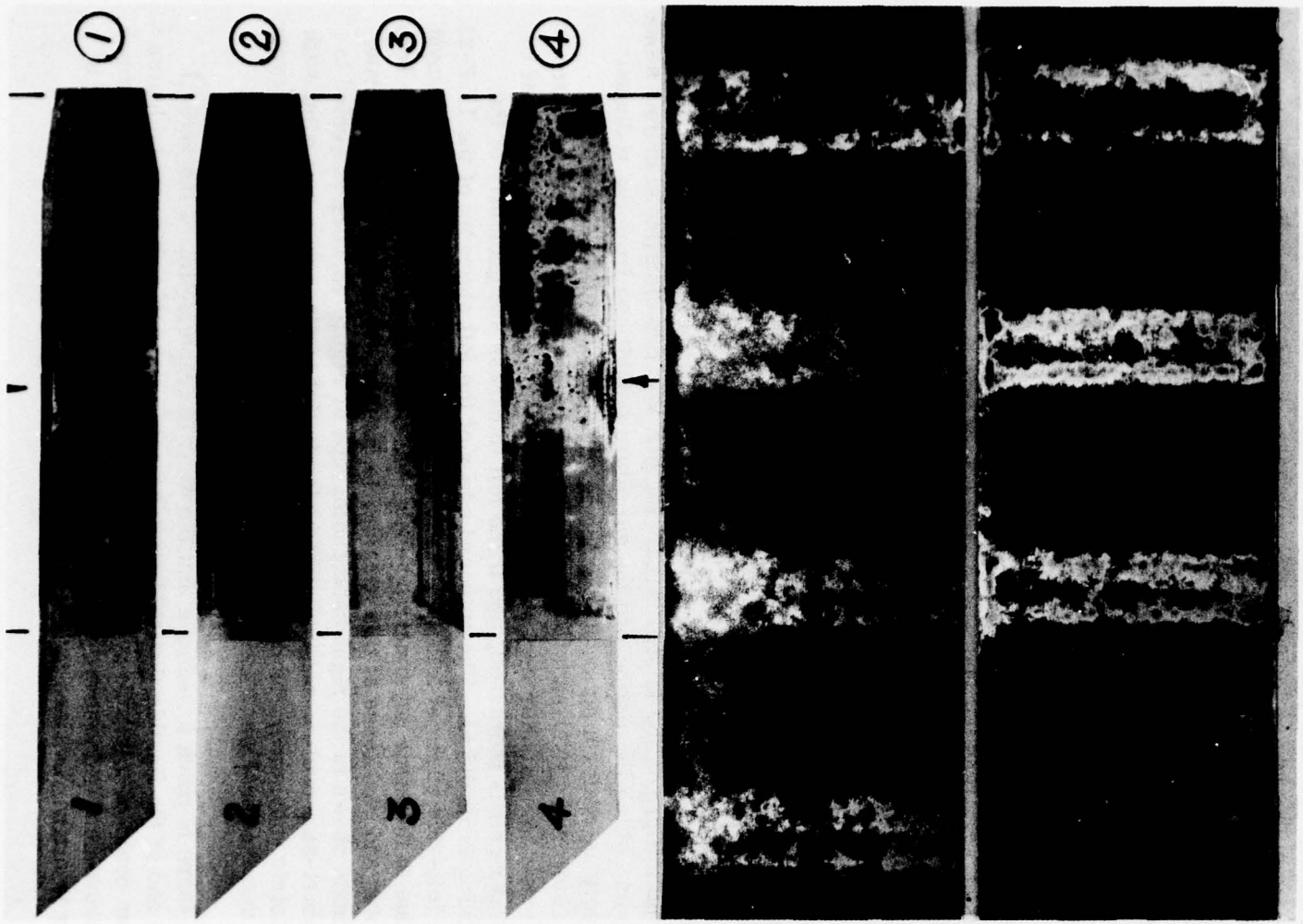

FIGURE 88. TYPICAL SURFACE-WEAR OF JOURNAL FOIL-BEARINGS (STEEL FOILS AND ORGANICALLY BONDED MoS_2 COATING).-APPEARANCE FOLLOWING OPERATION WITH HIGH UNBALANCE, WITH PROLONGED DWELLING AT CRITICAL SPEEDS AND MULTIPLE STARTS AND STOPS.-BEARING LLF-1J (LEFT): FOUR FOILS; TWO PER BEARING (WITH INNER FOILS REMOVED FOR SINGLE-ELEMENT OPERATION).-BEARING LLF-2J (RIGHT): TWO FOILS; ONE PER BEARING

8.0 DISCUSSION AND SUMMARY OF RESULTS

The tasks undertaken and successfully completed in the course of this investigation were balanced in emphasis and scope, and complementary in purpose. The innovative design of resilient thrust and journal bearings was followed by convincing demonstrations of their performance under exacting conditions, both individually and jointly as a unified rotor-support system.

The thrust-bearing configurations merit particular attention as important additions to the family of foil bearings, especially since the development of reliable, axial supports has been lagging in comparison with journal foil-bearings. In fact, with the exception of one isolated example [48, 50, 51], apparently no thrust foil-bearing of known utility have been developed in the past.

On the other hand, while design data for rigid spiral-groove thrust bearings has been readily available for many years [57 to 62], and much effort was devoted to various analytical refinements [63, 64], the possibility of exploiting the superior load capacity of the grooved configuration within the framework of a fully flexible bearing has apparently not been explored and put to good use.

The approach taken was necessarily venturesome, but tempered with caution. The first thrust-bearing design (LLF-1T) was sturdier, more conservative, and required a greater number, yet simple and readily available components. The motivation of the writer was to approach with caution what neither he nor others have attempted before. One could say that the intent was to make the thrust bearing more flexible "in stages", which lead logically to the evolution of the spider-spring support of the LLF-2T thrust-bearing.

The aim of the design was to provide progressively more simplicity in construction, fabrication and assembly. The retention of high load-capacity by flexible, spiral-groove thrust bearings could only be accomplished if the membrane remained sensibly parallel to the runner, and the compliant supports of membranes were designed exiguously to fulfill this requirement, at least approximately.

The thrust-bearing debutantes are presented in homemade togs, and the analytical haute couture of tribology will undoubtedly deprecate the absence of sophisticated software, glove-fitted to an exquisite mathematical model. But those concerned with useful wear will surmise from the content of this report and the account given of bearings, membranes and spider springs as they exist, that greater sophistication may lead quickly to a point of diminishing returns, and that complexity at the expense of uneven weighting and omission of salient effects may not aid us in design and application.

It is difficult to make meaningful, quantitative comparisons, and the problem is inherent in the limitation of what could be measured without discarding bearing development and making the entire activity subordinate to highly specialized

instrumentation. The foregoing remark applies in particular to the determination of clearance topography, possibly in a manner analogous to that described in references [20] or [31], a task quite incompatible and far too difficult to accomplish within the framework of the present test apparatus. The method of determination of $\tilde{h}$, and the possible relation this quantity may have to the mean value of clearance $\bar{h}$, and ultimately to the perfectly uniform clearance h_o of an idealized, parallel-surface thrust bearing, was discussed in Section 2.3. While comparisons of $\tilde{h}$ and h_o at low loads are not very meaningful, because of initial membrane distortion, results indicate that these quantities become commensurate with increasing load, particularly if the initial membrane distortion is slight.

The published data relevant to rigid, spiral-groove thrust bearings applies to optimized designs only [61]. In particular, the present thrust bearings were designed for an optimum groove depth $\Delta = 3h_o = 45\ \mu m$, so that correlation is necessarily limited to $\tilde{h} \approx h_o = 15\ \mu m$, assuming that $\tilde{h}$ and $\bar{h}$ do not differ greatly from h_o. A tabulation is furnished, which contains values of $\tilde{h}$ and h_o within a range sufficiently close to the design point to warrant order-of-magnitude comparisons. In the region of interest, the linear relationship $\bar{F} \approx 0.0246\ \Lambda$ applies to a twelve-groove bearing and $Ri/R_o = 0.4$ [61]. For the present thrust bearings, and $\mu = 1.89 \times 10^{-9}$ N.sec/cm^2, this reduces to $h_o \approx 7.0\ (N/F)^{1/2}\ \mu m$, where N is in rps and F in newtons.

The tabulation identifies the figure relevant to the data, specifies N, F, $\tilde{h}$ and h_o, and gives the percent deviation referred to the theoretical value h_o.

Fig. No.	N	F	$\tilde{h}$	h_o	$100\ (\tilde{h} - h_o)/h_o$
-	(rps)	(N)	(μm)	(μm)	(%)
37	450	101.0	17.5	14.8	+18
42	450	89.1	17.0	15.7	+8
50	400	86.7	14.0	15.0	-7
	400	86.7	17.5	15.0	+17
52	400	81.9	13.5	15.5	-13
	400	81.9	16.5	15.5	+6
53	450	96.3	14.5	15.1	-4
	450	96.3	17.0	15.1	+13
60	720	127.6	25.5	16.6	+54
62	720	127.6	26.5	16.6	+60
65	750	145.0	15.0	15.9	-6

The correlation of $\tilde{h}$ and h_o in the vicinity of the design point ($h_o = 1/3\,\Delta = 15\,\mu m$) is surprisingly good, except in Figure 60 and Figure 62. Yet the acquisition of data relevant to Figure 60 and Figure 62 must be considered even more reliable than results obtained in the early part of the investigation. It is not proposed to engage in a lengthy discussion in regard to this correlation and speculate on the multiplicity of possible causes of agreement and disagreement. If one considers the smallness of $\tilde{h}$ in the absolute sense, and the fact that deviations may have been of the same order of magnitude as the quantities measured, the correlation of $\tilde{h}$ and h_o is reasonably good. Unfortunately, the writer has no numerical data at his disposal, which would allow comparisons of variations of F with $\tilde{h}$ at constant N, when h_o/Δ is not optimum.

Similar considerations apply to comparisons of data relevant to friction-torque measurements. The dimensionless torque of the optimized thrust bearing is nearly constant with the bearing number Λ[61], and for $\overline{R_i/R_o = 0.4}$:

$$\overline{M} = 6M/P\,\pi(R_o^2 + R_i^2) \cdot \Lambda \cdot h_o \approx 0.7$$

A cross-correlation of operating points in Figures 50, 52 and 53, at which $\tilde{h} \approx 15\mu m$, with corresponding data of friction moments in Figures 55 and 57, shows that the measured values of friction torque were larger than the calculated moments for $h_o = 15\mu m$. Specifically, $1.17 < (M/M_{CAL}) < 1.39$, which suggests that the mean clearance was smaller than $h_o = 15\mu m$ (i.e., $\tilde{h} > \bar{h} \approx h_o$). The measured moment contained an extraneous contribution, due to air friction acting on the anti-rotation pins protruding into the rotating clearance-groove, Figure 22, and on the stator surfaces exposed to air set in motion by the runner, Figure 11. It is estimated, however, that the error due to the spurious torque was less than +10%, and that the measured moment was approximately 30% larger than the calculated value at the design point. This implies also that the mean clearance $\bar{h}$ was less than the measured quantity $\tilde{h}$, since the comparison is for $\tilde{h} = h_o = 15\mu m$.

It was not expected that the performance of the flexible thrust bearings would match that of an ideal, spiral-groove prototype with perfectly parallel surfaces. It was a foregone conclusion that a flexible thrust bearing would support a given load at a clearance smaller than the theoretically predicted value. A commensurate clearance reduction would also occur in rigid spiral-groove bearings, because of thermal distortion, imperfections of manufacture and assembly, and a variety of factors excluded in the ideal model. On the other hand, since rigid spiral-groove bearings can in principle support an equal load at a larger clearance than other bearings of commensurate dimensions, which generate pressure by means of surfaces converging in the direction of rotation provided on sectors and shoes, it is reasonable to assume that this superiority also applies to the flexible derivatives of the rigid progenitors. Moreover, approximate but simple design tools have been provided to control the film shape, that is the parallelism of surfaces required for efficient pressure generation in a spirally-grooved thrust bearing. It should be noted at this point that no planned and purposeful method is provided to control the film shape of tapered-land, flexible thrust-bearings derived

from their rigid precursors, and that the relation, therefore, between the two-dimensional and nonsymmetrical pressure fields and clearance topographies of such bearings is casual and incidental.

The writer is of the opinion that if further development of flexible, spiral-groove thrust bearings is pursued vigorously and with competence, the effort required to incorporate such bearings in various types of high-speed turbomachinery will be greatly reduced. Because of the inherently superior load capacity of the spiral-groove configuration and the means provided herewith to exploit it within the framework of a resilient structure, the present thrust bearings go far toward the elimination of the weakest link in flexible rotor-support systems.

Turning now to the second part of this investigation, which focused on radial foil-bearing and culminated in the union of journal and thrust bearings in a fully flexible rotor-support system, it is well to recall at this point the speed limitations imposed on thrust-bearing tests by the instability of externally-pressurized journal bearing. As previously stated in Section 6.0, a rotor speed of $N_c \approx 33,000$ rpm could not be exceeded with these journal bearing, despite the fact that much effort was expended in endeavoring to extend the stable speed range. Furthermore, the stability of the pressurized journal bearings was so marginal in the vicinity of the critical speed that the apparently destabilizing influence of the thrust bearing necessitated a reduction of test speeds to and below 27,000 rpm. This provided also a very appropriate and timely reminder that the onset of instability in both self-acting and externally-pressurized air bearings of the rigid kind is a violent event; the amplitude of motion increases very rapidly and almost discontinuously upon crossing the threshold speed and leads to bearing destruction. This threshold cannot be crossed, and even if stable regions were to exist at higher speeds, they cannot be reached within the confines of bearing clearance. Otherwise stated, even if limit-orbits several times the size of a clearance circle were to exist in theory, they could not be attained within the confines of the bearing surface, and if other stable regions were to exist at higher speeds, they could not be reached.

An entirely different situation arises when such rigid journal-bearings are replaced with foil bearings, as in the course of the present experimental study. The reader will recall that changes in the rotating assembly were very minor, and that the rotors used with externally-pressurized and with foil journal-bearings had nearly identical masses and moments of inertia (see Sections 5.0 and 6.0). If instability occurred, as in the case of the LFF-1J bearings, the journal trajectories were limited in size and of the same order of magnitude as the largest resonant orbits. Not only could such unstable trajectories be accommodated within the confines of flexible bearing surfaces, but the unstable speed-range could be dwelled in and traversed with impurity. Furthermore, as can be observed in many amplitude scans of response presented in the preceding sections, the trajectories of unstable motion frequently contracted with increasing speed (e.g., in Figure 68 with $N > 630$ rps, or in Figure 79 with $N > 500$ rps). The results presented in Sections 6.1 and 6.2 indicate that the dynamic performance of the LLF-1J bearings was improved by a reduction of effective clearance. The

performance characteristics of this simple bearing can be further enhanced through judicious choice of parameters, such as foil and coil thickness for example.

The LLF-2J journal foil-bearings with a quasi-octagonal backing provided an excellent rotor-support. No regions of instability were detected within the experimental speed range, and resonant amplitudes were well damped and relatively small. The method of fabrication of foil elements, which comprise quasi-polygonal supports with radiused vertices integral with sections of plane foil, is extremely simple and inexpensive, Figure 31. Since foils can be both plated and etched, the thickness of plane and preformed sections can be varied independently. No welding is required [53, 55]. A simple bending tool, provided with several radii, Figure 31, will accommodate foils independently of thickness and allow an almost unlimited choice of vertex spacings and angles of bend. The quasi-polygonal support, Figure 89, is not prone to buckling, a mode of failure characteristic of foil bearings with corrugated elements [53], and the rounded-vertex construction avoids the initiation and propagation of cracks in fabrication and operation, a disadvantage inherent in the method of sharply creasing the foil element [56]. The nonlinear (hardening) stiffness characteristic of the foil element has the advantage of providing means for a light preload, while resisting displacement at an increasing rate when journal excursions become large. At the same time, the excellent damping reduces the amplitudes excited by unduly large unbalance to magnitudes that would be accommodated even in small clearances of rigid air-bearings, Figure 84.

The reader is reminded that the performance data presented in the form of oscilloscope records of trajectories, waveforms and scans of amplitude response were almost invariably acquired in the presence of excessive and most unfavorably disposed unbalance. Despite this self-imposed handicap, and also because of it, the support worthiness of these resilient thrust and journal bearings has been convincingly demonstrated; not only individually, but also jointly as a unified rotor-support system.

This is not to imply that the rapid progress made in the reduction of these new concepts to working prototypes is sufficient, and that further development is almost superfluous. (To do so would be as unrealistic as to delude oneself that numerical design-data and computer simulation can largely supersede various stages of experimentation and testing in development, and provide a direct transition from paper to hardware.) On the contrary, further improvements and modifications of design are both feasible and desirable.

In addition to refinements and improvements of present designs, there exists a wide range of complementary requirements and prerequisites in the application of foil bearings to various types of rotating machines. These requirements (and problems) grow exponentially when operating conditions are associated with elevated temperatures and steep temperature gradients, particularly if the dynamic loads are equally severe, and if the bearings are to survive large numbers of starts and stops. Applications to machines operating under such hostile conditions will require tenaciously adhering, protective and lubricating coatings and their testing in actual foil bearings and under realistic conditions. No claim is made by the writer of having solved these and other equally important problems, and

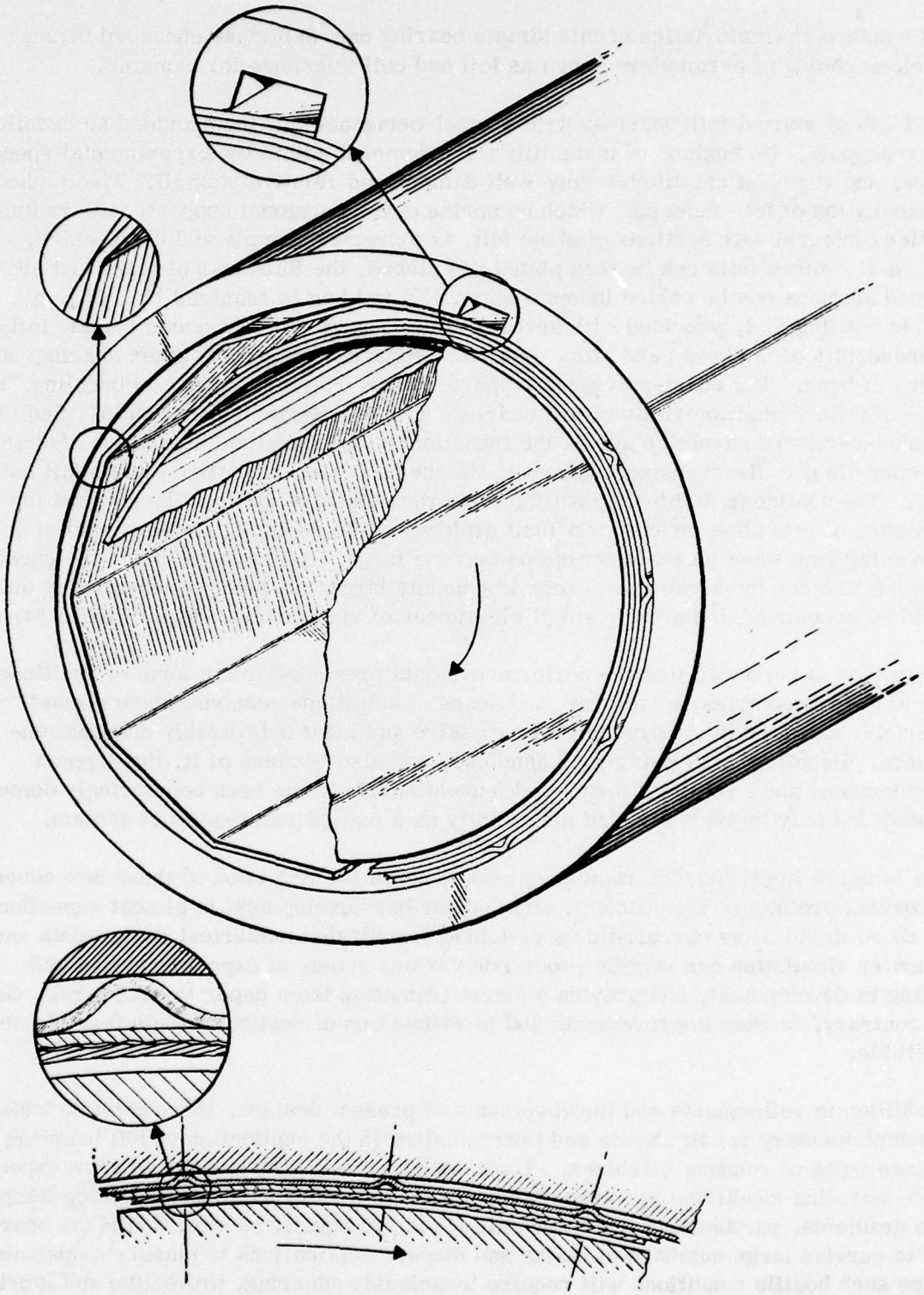

FIGURE 89. SCHEMATIC DRAWING OF JOURNAL FOIL-BEARING LLF-2J. STRUCTURE BEFORE AND AFTER INSERTION OF JOURNAL IS DEPICTED. DETAILS ILLUSTRATE ROUNDED VERTICES AND RETAINING GROOVE

it would be naive to suggest that oilless and refractory bearings require only a little more alchemy.

For many applications, however, the present state of development has progressed sufficiently far to reduce future work to manageable proportions, and to allow for the early incorporation of these thrust and journal bearings in hardware.

9.0 REFERENCES

1. Higginson, G.R., "The Theoretical Effects of Elastic Deformation of the Bearing Liner on Journal Bearing Performance," Proceedings of the Symposium of Elastohydrodynamic Lubrication, Institution of Mechanical Engineers, Vol. 180, Part 3B, 1965, p. 31.

2. Hooke, C.J., Brighton, D.K., and O'Donoghue, J.P., "The Effect of Elastic Distortion on the Performance of Thin Shell Bearings," Proc. Inst. Mech. Engrs., Vol. 181, Part 3B, 1966/7, p. 63.

3. Brighton, D.K., Hooke, C.J., and O'Donoghue, J.P., "A Theoretical and Experimental Investigation into the Effect of Elastic Distortion on the Performance of Journal Bearings," Proc. Inst. Mech. Engrs., Vol. 182, Part 3N, 1967/8, p. 192.

4. Oh, K.P., and Huebner, K.H., "Solution of the Elastohydrodynamic Finite Journal Bearing Problem," Journal of Lubrication Technology, Trans. ASME, Vol. 95, Ser. F, No. 3, 1973, p. 342.

5. Oh, K.P., and Huebner, K.H., "A Theoretical Analysis of a Compliant Shell Air Bearing," ASME Paper No. 76-Lub-5, October 5/7, 1976.

6. Dowson, E., Higginson, G.R., and Whitaker, A.V., "Elastohydrodynamic Lubrication: A Survey of Isothermal Solutions," Journal of Mechanical Engineering Science, Vol. 4, No. 2, 1962, p. 121.

7. Johnson, K.L., "Regimes of Elastohydrodynamic Lubrication," Journal of Mechanical Engineering Science, Vol. 12, No. 1, 1970, p. 9.

8. Cameron, A., and Gohar, R., "Theoretical and Experimental Studies of Oil Film in Lubricated Point Contact," Proceedings of the Royal Society (Great Britain), Ser. A, Vol. 291, 1966, p. 520.

9. Lund, J.W., "The Stability of an Elastic Rotor in Journal Bearings with Flexible, Damped Supports," Journal of Applied Mechanics, Trans. ASME, Vol. 87, Ser. E, No. 4, 1965, p. 911.

10. Glienicke, J., and Dabrowski, K., "Untersuchungen zur Beseitigung von Rotorschwingungen durch federnde und dämpfende Stützung der Lager-Literaturrecherche (Examination of Methods for the Elimination of Rotor Vibrations by Means of Flexible and Damped Bearing Supports - A Literature Survey)," Forschungs-Ber. 253/1 H.99 der Forschungsvereinigung Verbrennungskraftmachinen, Frankfurt/M, W. Germany, 1969.

11. Ream, L.W., "Performance of Gas-Lubricated Nonconforming Pivoted-Pad Journal Bearings and a Flexibly Mounted Thrust Bearing," Technical Memorandum NASA TM X-2765; NASA Lewis Research Center, Cleveland, Ohio, 1973.

12. Anderson, W.J., "Analysis of an All-Metallic Resilient Pad Gas-Lubricated Thrust Bearing," Journal of Lubrication Technology, Trans. ASME, Vol. 97, Ser. F, No. 2, 1975, p. 296.

13. Etsion, I., "A Cantilever Mounted Resilient Pad Gas Thrust Bearing," Journal of Lubrication Technology, Trans. ASME, Vol. 99, Ser. F, No. 1, 1977, p. 89.

14. Marsh, H., "The Stability of Self-Acting Gas Journal Bearings with Noncircular Members and Additional Elements of Flexibility," Journal of Lubrication Technology, Trans. ASME, Vol. 91, Ser. F, No. 1, 1969, p. 113.

15. Powell, J.W., and Tempest, M.C., "A Study of High Speed Machines with Rubber Stabilized Air Bearings," Journal of Lubrication Technology, Trans. ASME, Vol. 90, Ser. F, No. 4, 1968, p. 701.

16. Shapiro, W., Colsher, R., and Kramberger, F., "Development of Compliant-Mounted Gas Bearings for High-Speed Turbomachine," Trans. SAE, Vol. 84, Sec. 4, Paper No. 751071, 1975, p. 2989.

17. Rightmire, G., Castelli, V., and Fuller, D.D., "An Experimental Investigation of a Tilting Pad, Compliant Surface, Thrust Bearing," Journal of Lubrication Technology, Trans. ASME, Vol. 98, Ser. F, No. 1, 1976, p. 95.

18. Benjamin, M.K., and Castelli, V., "A Theoretical Investigation of Compliant Surface Journal Bearings," Journal of Lubrication Technology, Trans. ASME, Vol. 93, Ser. F, No. 1, 1971, p. 191.

19. Conway, H.D., and Lee, H.C., "The Analysis of the Lubrication of a Flexible Journal Bearing," Journal of Lubrication Technology, Trans. ASME, Vol. 97, Ser. F, No. 4, 1975, p. 599.

20. Field, G.J., and Nau, B.S., "An Optical Interference Method of Studying the Lubrication of a Compliant Bearing," Journal of Lubrication Technology, Trans. ASME, Vol. 98, Ser. F, No. 4, 1976, pp. 486-490.

21. Hooke, C.J., and O'Donoghue, J.P., "Elastohydrodynamic Lubrication of Soft, Highly Deformed Contacts," Journal of Mechanical Engineering Science, Vol. 14, No. 1, 1972, p. 34.

22. Blok, H., and van Rossum, J.J., "The Foil Bearing-A New Departure in Hydrodynamic Lubrication," Lubrication Engineering, Vol. 9, No. 6, 1953, p. 316.

23. Patent Specification 296,132 (Great Britain), August 27, 1928 - "Improvements in and Relating to Journal Bearings," Pollock, A.A., assigned to the British Thomson-Houston Company, Ltd., London, Great Britain.

24. Baumeister, H.K., "Nominal Clearance of Foil Bearings," IBM Journal of Research and Development, Vol. 7, N. 2, 1963, p. 153.

25. Langlois, W.E., "The Lightly Loaded Foil Bearing at Zero Angle of Wrap," IBM Journal of Research and Development, Vol. 7, No. 2, 1963, p. 112.

26. Barlow, E.J., "Derivation of Governing Equations for Self-Acting Foil Bearings," Ampex Corporation, Research Report RR65-1, 1965.

27. Eshel, A., "Analytical Study of the Self-Acting Foil Bearing," Doctoral Thesis, Department of Mechanical Engineering, Columbia University, 1966.

28. Eshel, A. and Elrod, H.G., Jr., "Stiffness Effects on the Infinitely Wide Foil Bearing," Journal of Lubrication Technology, Trans. ASME, Vol. 89, Ser. F, No. 1, 1967, p. 92.

29. Eshel, A., and Licht, L., "Foil Bearing Design Manual," Ampex Corporation, Research Report RR71-18, Contract No. Nonr-N00014-71-C-0001, Office of Naval Research, Fluid Dynamics Branch, Arlington, Virgina, 1971.

30. Barlow, E.J., "Self-Acting Foil Bearing of Infinite Width," Journal of Lubrication Technology, Trans. ASME, Vol. 89, Ser. F, No. 3, 1967, p. 341.

31. Licht, L., "An Experimental Study of Elastohydrodynamic Lubrication of Foil Bearings - Part I: Displacement in the Central Zone and Part II: Displacement in the Edge Zone," Journal of Lubrication Technology, Vol. 90, Ser. F, No. 1, 1968, p. 199.

32. Hayashi, K., "Studies of Self-Acting Foil Bearing," Doctoral Thesis, Department of Mechanical Engineering, University of Kyoto, Japan, 1973.

33. Ma, J.T.S., "Investigation of Self-Acting Foil Bearings," Journal of Basic Engineering, Trans. ASME, Vol. 87, Ser. D, No. 4, 1965, p. 837.

34. Licht, L., "On the Velocity of Propagation of a Disturbance Along a Foil," Journal of Applied Mechanics, Trans, ASME, Vol. 36, Ser. E, No. 2, 1969, p. 364.

35. Eshel, A., and Wildman, M., "Dynamic Behavior of a Foil in the Presence of a Lubricating Film," Journal of Applied Mechanics, Trans. ASME, Vol. 35, Ser. E, No. 2, 1968, p. 242.

36. Barnum, T.B., and Elrod, H.G., Jr., "A Theoretical Study of the Dynamic Behavior of Foil Bearings," Journal of Lubrication Technology, Trans. ASME, Vol. 93, Ser. F, No. 1, 1971, p. 133.

37. Licht, L., "An Experimental Study of High-Speed Rotors Supported by Air-Lubricated Foil Bearings - Part I: Rotation in Pressurized and Self-Acting Foil Bearings, and Part II: Response to Impact and Periodic Excitation," Journal of Lubrication Technology, Trans. ASME, Vol. 91, Ser. F, No. 3, 1969, p. 477 and p. 494.

38. Licht, L., "The Dynamic Characteristics of a Turborotor Simulator Supported on Gas-Lubricated Foil Bearings - Part I: Response to Rotating Imbalance and Unidirectional Excitation, and Part II: Operation with Heating and Thermal Gradients," Journal of Lubrication Technology, Trans. ASME, Vol. 92, Ser. F, No. 4, 1970, p. 630 and p. 650.

39. Licht, L., "The Dynamic Characteristics of a Turborotor Simulator Supported on Gas-Lubricated Foil Bearings - Part III: Rotation in Foil Bearings of Reduced Length, with Starting and Stopping Unaided by External Pressurization," Journal of Lubrication Technology, Trans. ASME, Vol. 94, Ser. F, No. 3, 1972, p. 211.

40. Licht, L., Branger, M., and Anderson, W.J., "Gas-Lubricated Foil Bearings for High Speed Turboalternator - Construction and Performance," Journal of Lubrication Technology, Trans. ASME, Vol. 96, Ser. F, No. 2, 1974, p. 215.

41. Eshel, A., "Dynamic Analysis of a Three Foil Rotor System in Zero Gravity Environment," Journal of Lubrication Technology, Trans. ASME, Vol. 92, Ser. F, No. 4, 1970, p. 617.

42. Levy, S.B., and Coogan, C.H., Jr., "Flexible Membrane Hydrostatic Air Bearing," Journal of Lubrication Technology, Trans. ASME, Vol. 90, Ser. F, No. 1, 1968, p. 184.

43. U.S. Patent No. 835,739, November 13, 1906 - "Spring Neck-Bearing," Sundberg, P. T.

44. U.S. Patent No. 1,048,166, December 24, 1912 - "Bearing," Hoyt, M. L.

45. U.S. Patent No. 1,384,173, July 12, 1921 - "Flexible Bushing," Wikander, O. R., assigned to the SKF Ball Bearing Company, Hartford, Connecticut.

46. U.S. Patent No. 3,215,480, November 2, 1965 - "Hydrodynamic Foil Bearings with Bearing Foil Retaining Means," Marley, D. J.

47. U.S. Patent No. 3,382,014, May 7, 1968 - "Self-Acting Foil Bearings," Marley, D.J., assigned to the Garrett Corporation, Los Angeles, California.

48. U.S. Patent No. 3,375,046, March 26, 1968 - "Foil Thrust Bearing Arrangement," Marley, D.J., assigned to the Garrett Corporation, Los Angeles, California.

49. U.S. Patent No. 3,434,761, March 25, 1969 - "Hydrodynamic Shaft Bearing," Marley, D.J., assigned to the Garrett Corporation, Los Angeles, California.

50. Barnett, M.A., and Silver, A., "Application of Air Bearings to High-Speed Turbomachinery," SAE Paper No. 700720, September 1970.

51. Heuer, D. F., and Collins, R.A., "Dynamic and Environmental Evaluation of Compliant Foil Gas-Lubricated Bearings," Technical Report AFAPL-TR-73-56, Air Force Aero Propulsion Laboratory, Wright-Patterson Air Force Base, Ohio, 1973.

52. Oh, K. P., and Rohde, S. M., "A Theoretical Investigation of the Multileaf Journal Bearing," Journal of Applied Mechanics, Trans. ASME, Vol. 47, Ser. E, No. 2, 1976.

53. Walowit, J.A., Murray, S. F., McCabe, J. T., Arwas, E. B., and Moyer, T., "Gas Lubricated Foil Bearing Technology Development for Propulsion and Power Systems," Technical Report AFAPL-TR-73-92, Air Force Aero Propulsion Laboratory, Wright-Patterson Air Force Base, Ohio, 1973.

54. U.S. Patent No. 3,809,443, May 7, 1974 - "Hydrodynamic Foil Bearings," Cherubim, J.L., assigned to Mechanical Technology Incorporated, Latham, N.Y.

55. Gray, S., Sparks, N., and McCormick, J., "The Application of Gas-and-Oil-Lubricated Foil Bearings for the ERDA/Chrysler Automotive Gas Turbine Engine," ASME Paper No. 76-GT-115, March 21/25, 1976.

56. Licht, L., and Branger, M., "Motion of a Small High-Speed Rotor in 3 Types of Foil Bearings," Journal of Lubrication Technology, Trans. ASME, Vol. 97, Ser. E, No. 2, 1975, p. 270.

57. Whipple, R.T.P., "Herringbone Pattern Thrust Bearing," AERE T/M 29, Harwell, Great Britain, 1949.

58. Wordsworth, D.V., "The Viscosity Plate Thrust Bearing," AERE E/R 2217, Harwell Great Britain, 1952.

59. Malanoski, S.B., and Pan, C.T.H, "The Static and Dynamic Characteristics of the Spiral-Grooved Thrust Bearing," Journal of Basic Engineering, Trans. ASME, Vol. 87, Ser. D, No. 3, 1965, p. 547.

60. Muijderman, E.A., "Spiral-Groove Bearings," Doctoral Thesis, Technological University, Delft, The Netherlands, 1964 (Springer Verlag New York, Inc., New York, N.Y.).

61. "Design of Gas Bearings," RPI-MTI Design Notes, 1966.

62. Pan, C.T.H., and Sternlicht, B., "Thermal Distortion of Spiral-Groove Gas-Lubricated Thrust Bearing due to Self-Heating," Journal of Lubrication Technology, Trans. ASME, Vol. 89, Ser. F, No. 2, 1967, p. 197.

63. Elrod, H.G., Jr., "A Generalized Narrow-Groove Theory for the Gas-Lubricated Herringbone Thrust Bearing," Gas Bearing Symposium, Paper No. 18, University of Southampton, Great Britain, 1969.

64. Gupta, P.K., Coleman, R.L., and Pan, C.T.H., "Ambient Edge Correction for the Locally Incompressible Narrow-Groove Theory," Journal of Lubrication Technology, Trans. ASME, Vol. 96, Ser. F, No. 2, 1974, p. 284.

65. Gu, A., Pan, C.T.H., and Badgley, R.H., "Dynamic Stability of a Gimbaled Spiral-Groove Thrust Bearing," Journal of Lubrication Technology, Trans. ASME, Vol. 95, Ser. F, No. 2, 1973, p. 222.

66. Drescher, H., "Special Features of Air Bearings and Their Effect on Practical Application," First International Symposium on Gas-Lubricated Bearings, Office of Naval Research ACR-49, 1959, p. 319.

67. Feldman, S., "Unbalance Tolerances and Criteria," Proceedings, General Electric Balancing Seminar, Vol. IV, 1958.

68. Tondl, A., "Some Problems of Rotor Dynamics," Chapman and Hall, London, 1965.

69. Tondl, A., "Notes on the Problem of Self-Excited Vibrations and Nonlinear Resonances of Rotors Supported in Several Journal Bearings," Wear, Vol. 8, No. 5, 1965, p. 349.

70. Tondl, A., and Licht, L., "Nonlinear Resonances of Rotors and Their Identification," Acta Technica CSAV (Czechoslovak Academy of Science), No. 1, 1976, p. 74.

APPENDIX A

DESIGN CALCULATION OF FLEXIBLE THRUST BEARINGS

Rigid, parallel-surface thrust bearings of the spiral-groove type have been the subject of numerous investigations [57 to 65]. Given a bearing area bounded by circles of radii R_i and R_o, the spiral-groove bearing can support a considerably greater load at the same speed and minimum clearance than inclined-surface and step bearings.

If the clearance topographies of a rigid and of a flexible-surface bearing were identical, the pressure fields and load capacities would be also identical. Furthermore, if a spiral-groove pattern were generated on a flexible membrane (or on the rigid runner), and if the membrane were mounted on a compliant support of distributed stiffness designed to maintain parallelism of bearing surfaces for a known, or prescribed pressure distribution, then the flexible bearing would support a load equal to that carried by the rigid prototype.

The support with a continuously varying stiffness is approximated here by concentric arrays of discrete spring-elements, the stiffness of the arrays being proportional to pressure loads acting on concentric annuli of the bearing surface, as shown in Figure A-1.

If the mean pressure field is known from results of numerical analyses (within limits of assumptions made), stiffness can be selected to produce a sensibly uniform clearance at the design point. A useful and convenient simplification is to assume that springs are linear and that the mean pressure varies linearly with the radius, as indicated in Figure A-1(b). The error associated with the triangular pressure-profile is not significant in comparison with actual deviations due to imperfections of geometry, dissymmetry, misalignment, runout and thermal distortion, all of which occur in real bearings.

Referring to Figure A-1, let the bearing area be divided into n annuli, each annulus supporting a load component f_n, so that $F = \Sigma f_n$.

With the assumption of a triangular pressure profile, that total load is given by the integral:

$$F = 2\pi\Delta p_g \cdot \left(\int_{R_i}^{R_g} \frac{R^2 - R.R_i}{R_g - R_i} \cdot dR + \int_{R_g}^{R_o} \frac{R.R_o - R^2}{R_o - R_g} \cdot dR \right)$$

$$= \frac{1}{3} \Delta p_g \left[(R_o^2 - R_i^2) + R_g (R_o - R_i) \right], \qquad (1)$$

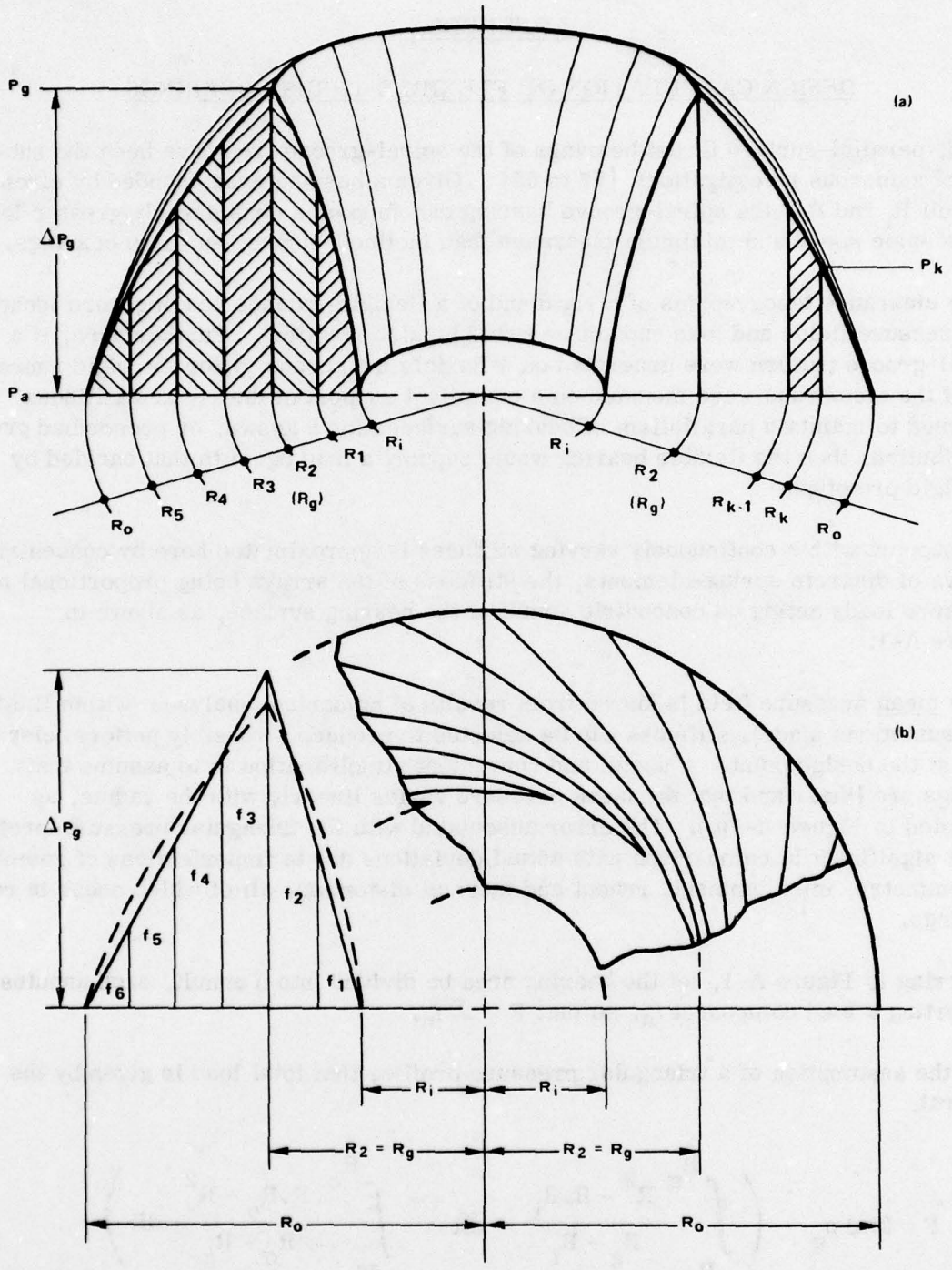

FIGURE A-1. SCHEMATIC DIAGRAM OF PRESSURE LOADING OF SPIRAL-GROOVE THRUST BEARING

so that the pressure rise corresponding to the applied load F is:

$$\Delta p_g = 3F \Big/ \left[(R_o^2 - R_i^2) + R_g (R_o - R_i) \right] \cdot \pi . \tag{2}$$

The load component f_n supported by the n-th annulus, bounded by circles of radii R_n and R_{n+1}, is given by the following expressions:

$$f_n = 2\pi \Delta p_g \int_{R_n}^{R_{n+1}} \frac{R^2 - R_i R}{R_g - R_i} \cdot dR$$

$$= \frac{1}{3} \pi \Delta p_g \cdot \frac{2 (R_{n+1}^3 - R_n^3) - 3 R_i (R_{n+1}^2 - R_n^2)}{R_g - R_i} \tag{3}$$

for $R_i < R < R_g$, and

$$f_n = 2\pi \Delta p_g \int_{R_n}^{R_{n+1}} \frac{R_o R - R^2}{R_o - R_g} \cdot dR$$

$$= \frac{1}{3} \pi \Delta p_g \cdot \frac{3 R_o (R_{n+1}^2 - R_n^2) - 2 (R_{n+1}^3 - R_n^3)}{R_o - R_g} \tag{4}$$

for $R_g < R < R_o$.

In the present designs of both thrust bearings (referred to in the text as LLF-1T and LLF-2T), their areas are subdivided into six annuli (n = 6), bounded by circles of radii R_i, R_1, $R_2 = R_g$, R_3, R_4, R_5 and R_o, Figure A-1.

In the thrust bearing LLF-1T, three (m = 3) simply supported plate-springs constitute an array of flexible elements in each of the six (n = 6) annuli. In the thrust bearing LLF-2T, twelve (m = 12), nearly rectangular strips (Figure 24) represent an array of flexible elements in each of the six (n = 6) annuli.

Simplicity and ease of manufacture, coupled with the need of maintaining reasonably good parallelism, dictated the choice of controlling the stiffness of the circular elements by varying the radius (a) and of controlling the stiffness of the rectangular elements through the width (b).

For the simply supported, circular plate-spring, the stiffness is given by the expression:

$$k_m = \frac{f_n/m}{\delta} = \frac{1}{m} \cdot \frac{4\pi E}{3\,(1-\upsilon)\,(3+\upsilon)} \cdot \frac{t_s^3}{a_n^2}\,, \tag{5}$$

and for a rectangular spring element by the expression:

$$k_m = \frac{f_n/m}{\delta} = \frac{\alpha}{m} \cdot \frac{E\,b}{1-\upsilon^2} \cdot \left(\frac{t_s}{l_s}\right)^3, \tag{6}$$

in which α is a constant, related to end (boundary) conditions of the rectangular element ($\alpha = 4$ for simple supports and $\alpha = 16$ for built-in ends). For the case at hand, the ends may not be fully constrained, and to make allowance for rotation the value of $\alpha = 10$ was arbitrarily assumed for each array of twelve elements.

Referring to the expressions (5) and (6), it is noted that the error in stiffness:

$$\frac{d\,k_m}{k_m} = \left\{ \begin{array}{l} 2\left|\frac{da}{a}\right| + 3\left|\frac{dt_s}{t_s}\right| \\ \left|\frac{db}{b}\right| + 3\left|\frac{dt_s}{t_s}\right| + 3\left|\frac{dl_s}{l_s}\right| \end{array} \right\} \tag{7}$$

is strongly influenced by dimensions of spring elements other than the controlling dimensions (a and b). The high uniformity of thickness of the circular plate-springs, contour-etched from precision shim-stock, is useful in ensuring parallel stacking of the support elements of the thrust bearing LLF-1T, Figure 11. In the case of the rectangular elements of the spider spring of the thrust bearing LLF-2T, Figure 24, their width and stiffness is determined in the course of contour-etching of the spider spring. A second etching operation (of depth, on one surface only) reduces the thickness of elements from the initial value of the spider disc t_p to the required value t_s. Although average values of deviations of thickness from the mean $\bar{t}_s$ were of the

order of 1% and maximum deviations of the order of 9%, the deviations of thickness of 72 elements was quite random and thus conducive to smoothing of differences in deflection. Inspection data of a (very acceptable) steel spider-spring of overall thickness t_p = 171/169 μm are tabulated below.

THICKNESS t_s (μm)

NUMBER OF ELEMENT	NUMBER OF ARRAY 1	2	3	4	5	6
1	50	53	48	47	48	46
2	50	50	53	50	50	52
3	50	51	52	52	53	55
4	46	47	46	50	46	52
5	54	53	53	50	50	51
6	54	53	50	51	50	48
7	52	47	46	49	50	53
8	53	54	52	51	52	52
9	49	50	49	54	50	50
10	50	53	50	48	48	47
11	48	50	49	50	52	50
12	52	50	52	51	52	50

$\bar{t}_s$ = 50.4

Ave. Deviation = 0.8%

Max. Deviation = 8.7%

The width of the spring elements, the controlling dimension, remained within the specified tolerance of ±0.1 mm (see Figure 24). Average values, based on twelve width measurements of each annular array of this spider spring, are given below (nominal dimensions in brackets):

b_1 = 1.37 (1.3)

b_2 = 4.68 (4.6)

b_3 = 6.37 (6.3)

b_4 = 5.25 (5.2)

b_5 = 3.57 (3.5)

b_6 = 1.35 (1.3)

} mm

In this case, the average error is of the order of 0.05 to 0.08 mm. For b_1, the average deviation from nominal is largest, approximately 5.4%.

It is reasonable to assume that the error made in assuming the average pressure to vary linearly with the radius is not inconsistently large with various sources of discrepancies related to these bearings. Theoretical refinements would be futile if lost among imperfections related to manufacture, assembly and operation of real bearings.

The following data apply to the design of both thrust bearings:

Inside radius:	$R_i = 1.60$ cm (16 mm)
Outside radius:	$R_o = 4.00$ cm (40 mm)
Design speed:	$N = 36,000$ rpm (600 rps); $\omega = 3.77 \times 10^3$ rad/sec
Design clearance:	$h_o = 15\ \mu$m (1.5×10^{-3} cm)
Uniform deflection at design load:	$\delta = 5h = 75\ \mu$m (7.5×10^{-3} cm)
Viscosity:	$\mu = 1.86 \times 10^{-9}$ N. sec/ cm^2
Ambient pressure:	$p_a = 10.0$ N/cm^2
Number of grooves:	$N_g = 12$

To determine the optimal dimensions of a parallel-clearance, spiral-groove bearing [61], the magnitude of the bearing number is calculated first:

$$\Lambda = \frac{3\mu\omega\ (R_o^2 - R_i^2)}{p_a\ h_o^2} = \frac{(3)\ (1.86 \times 10^{-9})\ (3.77 \times 10^3)\ (13.44)}{(10)\ (2.25 \times 10^{-6})} = 12.57$$

In the range $0 < \Lambda < 25$, the dimensionless load of a bearing with a very large number of grooves varies linearly with :

$$\overline{F}_\infty = F_\infty / \pi p_a\ (R_o^2 - R_i^2) = 0.029\Lambda. \qquad (8)$$

A correction must be applied to account for the effects due the finite number of grooves. For $N_g = 12$ and $R_i/R_o = 0.4$, a load reduction of approximately 16% is predicted, since

$$\overline{F} \approx \overline{F}_\infty / 1.18.$$

The corrected theoretical load is then given approximately by:

$$\overline{F} = 0.0246\Lambda, \qquad (9)$$

or

$$F = 0.0246\Lambda \times \pi \times p_a \times (R_o^2 - R_i^2) = 130.6 \text{ N}^*.$$

*Design calculations of support stiffness were based on F = 13 Kg·f = 127.5 N, a value smaller by 2.35%.

The optimum configuration of the spiral-groove bearing was determined and resulting dimensions were rounded off, or changed by sensibly small amounts to conform with requirements of design and fabrication. The following, near-optimum dimensions were determined:

Radius at groove terminals:	$R_g = R_2 = 2.4$ cm (24 mm)
Angle subtended by ridge:	$\theta_r = 12°$
Angle subtended by groove:	$\theta_g = 18°$
Spiral angles:	$\beta = 17.5°$
Groove depth:	$\Delta = 3h = 45\ \mu m$ (0.045 mm)

Using expressions (2) through (6), the following values were obtained:

Pressure rise: $\Delta p_g = p_g - p_a = 6.343\ N/cm^2$

Loads supported on annuli 1 through 6:

$$\left.\begin{aligned} f_1 &= 7.440 \\ f_2 &= 26.570 \\ f_3 &= 36.135 \\ f_4 &= 29.759 \\ f_5 &= 20.193 \\ f_6 &= 7.440 \end{aligned}\right\} \text{ N}$$

$$F = \Sigma f_n = 127.5\ N$$

The effective diameters of plate springs ($t_s = 0.13$ mm) to produce a deflection $\delta = 5h = 75\ \mu m$ at the design load were:

Number of annuli: n = 6
Number of plate springs per annulus: m = 3
Material: Spring steel ($E \approx 19.62 \times 10^6\ N/cm^2$)

$$\left.\begin{aligned} d_1 &= 9.72 (9.7) \\ d_2 &= 5.90 (5.9) \\ d_3 &= 4.86 (4.9) \\ d_4 &= 4.41 (4.4) \\ d_5 &= 5.14 (5.1) \\ d_6 &= 9.72 (9.7) \end{aligned}\right\} \text{ mm}$$

The plate springs were simply supported on edges of holes and the dimensions within brackets are standard reamers determining the hole size. The controlling widths of elements of the spider spring (t_s = 50 μm = 0.005 cm) to produce a deflection δ = 5h = 75 μm at the design load were:

Number of annuli: n = 6
Number of plate springs per annulus: m = 12

Material: Copper-beryllium ($E \approx 12.5 \times 10^6$ N/cm^2)

b_1 = 1.29 (1.3)
b_2 = 4.61 (4.6)
b_3 = 6.27 (6.3)
b_4 = 5.18 (5.2)
b_5 = 3.51 (3.5)
b_6 = 1.29 (1.3)

} mm

The dimensions within parentheses are those specified in the drawing of the spider spring in Figure 24 to a tolerance of $\pm$ 0.1 mm. The average thickness $\bar{t}_s$ of flexure elements of the spiders springs used in the course of experiments was in the range $40 < \bar{t}_s < 72$ μm.

1. Report No.	2. Government Accession No.	3. Recipient's Catalog No.
NASA CR-2940		

4. Title and Subtitle
FOIL BEARINGS FOR AXIAL AND RADIAL SUPPORT OF HIGH SPEED ROTORS - DESIGN, DEVELOPMENT, AND DETERMINATION OF OPERATING CHARACTERISTICS

5. Report Date
Jan[illegible]78

6. Performing Organization Code

7. Author(s)
L. Licht

8. Performing Organization Report No.
None

10. Work Unit No.

9. Performing Organization Name and Address
L. Licht, ~~Engineering Consultant~~
123 N. El Camino Real, No. 18
San Mateo, Ca~~lifornia 94401~~

17 p.

11. Contract or Grant No.
~~ONR Contract~~ N00014-76-C-0191
NASA Purchase Request C-75012-C

13. Type of Report and Period Covered
Contractor Report

12. Sponsoring Agency Name and Address
Department of the Navy and National Aeronautics and Space Administration
Office of Naval Research Washington, D. C. 20546
Arlington, Virginia 22217

14. Sponsoring Agency Code

15. Supplementary Notes
Final report. Project Managers, Stanley W. Doroff, Office of Naval Research, Arlington, Virginia 22217, and William J. Anderson, Fluid System Components Division, NASA Lewis Research Center, Cleveland, Ohio 44135

16. Abstract

Flexible-surface thrust and journal foil-bearings of novel design were fabricated, and their performance was convincingly demonstrated, both individually and jointly as a unified rotor-support system. A versatile rig was constructed and instrumented, and experimental results are copiously documented with graphs and oscilloscopic data of trajectories, waveforms, and scans of amplitude response. The thrust bearings combine advantages of surface compliance with the superior load capacity of the spiral-groove configuration. The flexible supports provide means of deliberate control of clearance topography, in contrast to bearings in which the formation of the lubricating wedge is casual and incidental. At speeds of 40 000 to 45 000 rpm and a mean clearance of the order of 15 to 20 μm (600 to 800 μin), the resilient, air-lubricated, spiral-groove thrust bearings comfortably support a load of 127 N (29 lb; 13 kgf), equivalent to 3.0 N/cm^2 (4.5 lb/in^2, 0.31 kgf/cm^2). The construction of journal foil-bearings is extremely simple. In one design, a coiled ribbon of plane foil and a retaining cartridge constitute the only components. In another design, the plane foil and a retaining cartridge constitute the only components. In another design, the plane foil is integral with a section preformed to an open octagon with rounded vertices. A radical departure from operational characteristics of rigid gas bearings is achieved. Amplitudes of motion are strongly attenuated, because of substantial damping by friction between foil layers and viscous dissipation in interstitial clearances. Unstable regions, if present, can be dwelled in and traversed with impunity. Trajectories remain bounded and small, and their envelopes diminish with speed. Journal bearings with polygonal sections, endowed with particularly favorable characteristics, provided stable and highly damped supports at speeds up to 50 000 rpm. An asymmetric rotor, weighing 19.0 N (4.3 lb; 1.95 kgf) and supported in journal foil-bearings, was subjected to an angular excitation (pitching) by a total unbalance of 42.5 μm-N (6180 μin-oz; 0.433 cm-gf), while an axial load of 127 N (29 lb; 13 kgf) was applied via the flexible thrust bearing at 45 000 rpm. Repeated and prolonged operation under such highly adverse conditions fully substantiated the support worthiness of the foil-bearing system.

micrometers micro in. sq. cm sq. in.

17. Key Words (Suggested by Author(s))	18. Distribution Statement
Gas bearings Compliant bearings Turbomachinery	Unclassified - unlimited STAR Category 37

19. Security Classif. (of this report)	20. Security Classif. (of this page)	21. No. of Pages	22. Price*
Unclassified	Unclassified	100	A08

*For sale by the National Technical Information Service, Springfield, Virginia 22161

NASA-Langley, 1978

S/C 392 126